Master's thesis

NTNU
Norwegian University of Science and Technology
Faculty of Information Technology and Electrical Engineering
Department of Energy and Process Engineering

Dan Remi Antonsen

Increased solar energy utilization in Norwegian agriculture

A case study on the milk barn at Mære Agricultural School

Master's thesis in Energy and Environmental Engineering
Supervisor: Hans Martin Mathisen
July 2020

NTNU
Norwegian University of Science and Technology

Dan Remi Antonsen

Increased solar energy utilization in Norwegian agriculture

A case study on the milk barn at Mære Agricultural School

Master's thesis in Energy and Environmental Engineering
Supervisor: Hans Martin Mathisen
July 2020

Norwegian University of Science and Technology
Faculty of Information Technology and Electrical Engineering
Department of Energy and Process Engineering

NTNU
Norwegian University of
Science and Technology

Preface

This master thesis was finished in the late spring of 2020 and was a continuation of the project work that began in the latter half of 2019. It marks the end of the 5-year master's degree program Energy and Environmental Engineering at the Norwegian University of Science and Technology in Trondheim. This thesis was written at the Department of Energy and Process Engineering, and it is worth 30 ECTS credits.

To begin with, I would like to acknowledge the excellent guidance and encouragement I got from my supervisor Hans Martin Mathisen. I would also like to thank the administration at Mære Agricultural School, especially Tove Irene Hatling Jystad, for always providing me with the data, measurements and relevant information I needed, even during the Covid-19 pandemic. Without their help, this master thesis would not have been possible. I would also like to express my gratitude towards Håvard Lutdal at NTE for providing me with information regarding the power grid and the existing photovoltaic system at the boarding house at Mære Agricultural School.

Lastly, I would also like to thank my sister and father for helping me with my English.

Dan Remi Antonsen

Trondheim, July 4th, 2020

Sammendrag

Dette studiets hovedmål er å utforske potensialet en økt utnyttelse av solenergi vil kunne ha for reduksjon i klimagassutslipp relatert til strømforbruk i norsk landbruk. For å kunne undersøke dette potensialet er det designet flere solcelleløsninger og solvarmeanlegg for et melkefjøs lokalisert ved Mære landbruksskole i Trøndelag fylke. Systemene er deretter gjenskapt i en programvare for simulering av resultater knyttet til løsningene. Den potensielle reduksjonen i forbruket av kjøpt elektrisitet er deretter multiplisert med flere forskjellige utslippsfaktorer for å estimere den mulige nedgangen i klimagassutslipp.

Etter at systemløsningene er gjenskapt i simuleringsprogramvaren Polysun, er resultatene fra de forskjellige modellene sammenlignet med hverandre basert på et sett med forhåndsbestemte indikatorer for systemytelse. I tillegg er det utført en kort parametrisk studie av både solcelle- og solvarmeanleggene. Resultatene fra studien antyder at solcelleanleggene er følsomme for antagelser rundt helningsvinkelen og antatte energitap, mens resultatene fra solvarmeanleggene er sterkt påvirket av rørdimensjonene i solkretsen, helningsvinkelen til solfangerne og kompleksiteten i systemoppsettet.

Solcelleanleggene er designet for å dekke omtrent 30 % av det årlige strømforbruket, men den endelige dekningsgraden på sitt høyeste ble 26,9 % (53 831,9 kWh). Av de ulike foreslåtte systemløsningene er det mest effektive solcelleanlegget i stand til å redusere klimagassutslippene fra 997 til 13 091,4 kg CO_2-ekvivalenter, avhengig av den gjeldende utslippsfaktoren til elektrisitetsblandingen. Selv om det opprinnelig ikke var gode løsninger for solvarmeanleggene, ble de i stand til å redusere strømforbruket til varmtvannsanlegget i fjøset etter at resultatene fra den parametriske studien ble brukt for å optimalisere systemløsningene. De nye solvarmeanleggene resulterte i en reduksjon i strømforbruket fra 1 113 til 3 123 kWh, noe som tilsvarer fra 21 til 759,5 kg CO_2-ekvivalenter. Bare ett av solvarmeanleggene klarte å oppnå den planlagte soldekningsgraden på 50 %.

Sett i en større nasjonal sammenheng med utgangspunkt i de totalt 7 600 melkegårdene i Norge, hadde disse installert både det beste foreslåtte solcelleanlegget og solvarmeanlegget, ville det i beste fall være mulig å redusere dagens klimagassutslipp relatert til strømforbruk i norsk landbruk med om lag 105 266 tonn CO_2-ekvivalenter. Dette utgjør i så fall ¼ av utslippene fra strømbruk i jordbruk, skogbruk og fiskeri i Norge i 2017.

Abstract

This study's main objective is to study the potential an increased utilization of solar energy could have on greenhouse gas emissions related to electricity consumption in Norwegian agriculture. To be able to investigate this potential, several photovoltaic system solutions and solar water-heating system solutions were designed for an existing milk barn located at Mære Agricultural School in Trøndelag-county. The solutions are then recreated in a simulation software. The potential reduction in consumed imported electricity is then multiplied with several different emission factors to estimate the possible decline in greenhouse gas emissions.

After the system solutions are created in the simulation software Polysun, the results from the different models are compared against each other based on a set of predetermined indicators for system performance. Also, a short parametric study is performed on both the photovoltaic system solutions and the solar water-heating systems. The results from the study indicate that the photovoltaic systems are sensitive towards assumptions made on factors such as the inclination angle and potential energy losses, while the results from the solar water-heating systems were strongly affected by the pipe dimensions in the solar circuit, inclination angle of the solar collectors and the complexity of the system layout.

The photovoltaic system solutions are designed to cover about 30 % of the annual electricity consumption, but the resulting coverage ratio was at highest 26.9 % (53 831.9 kWh). Based on the proposed system solutions, the most competent photovoltaic system is able to reduce the amount of greenhouse gas emissions somewhere between 997 to 13 091.4 kg CO_2 equivalents, depending on the emission factors of the currently used electricity mix. The solar water-heating systems, though not initially efficient solutions, became capable enough to reduce the electricity consumption of the hot water system in the barn after the results from the parametric study was used to optimize the system solutions. These new solar water-heating systems resulted in a reduction in electricity consumption by 1 113 to 3 123 kWh, which is equal to about 21 to 759.5 kg CO_2 equivalents. The simulation results shows that only one of the system solutions are able to reach the planned solar fraction of 50 %.

In conclusion, if all 7 600 milk farms in Norway choose to implement both the best case photovoltaic system solution and solar water-heating system solution, it might reduce the current greenhouse gas emissions related to electricity consumption in Norwegian agriculture around 105 266 tons of CO_2 equivalents, similar to ¼ of the emissions from electricity usage in agriculture, forestry and fisheries in 2017.

Table of contents

List of figures

List of tables

Nomenclature

γ_s:	*Inclination angle of the sun [°]*	C_t:	*Net cash outflow in period t [NOK]*
α_1:	*First order heat loss coefficient [W/m²K]*	C_{tot}:	*Minimum required total battery storage capacity [kWh]*
α_2:	*Second order heat loss coefficient [W/m²K²]*	DC:	*Direct current*
AC:	*Alternating current*	DHW:	*Domestic Hot Water*
A_{PV}:	*Surface area of photovoltaic module [m²]*	d_{min}:	*Minimum distance between PV modules [m]*
A_{SC}:	*Surface area of solar collectors [m²]*	DoD:	*Depth of Discharge*
b:	*Width of photovoltaic module [m]*	DTC:	*Differential Temperature Control*
β:	*Inclination angle of photovoltaic module [°]*	E_d:	*Average daily energy consumption [kWh]*
$\beta_{battery}$:	*Capacity of desired battery product [Ah]*	E_{el}:	*Electricity consumption [kWh]*
β_{PV}:	*Temperature coefficient for PV efficiency [%/°C]*	ETC:	*Evacuated Tube Collector*
β_{system}:	*The required battery capacity for the storage system [Ah]*	E_F:	*Fuel consumption [kWh]*
B_t:	*Net cash inflow in period t [NOK]*	E_{Year}:	*Annual energy consumption [kWh]*
C_B:	*Required battery storage capacity when accounting for battery inefficiency [kWh]*	f_a:	*Azimuth angle correction factor [-]*
C_{DoD}:	*Required battery storage capacity when accounting for DoD [kWh]*	f_b:	*Inclination angle correction factor [-]*
$CdTe$:	*Cadmium Telluride*	f_{el}:	*Electricity emission factor [g CO_2 equivalents per kWh]*
CHS:	*Chemical Heat Storage*	F_{el,CO_2}:	*CO_2 emissions related to electricity consumption*
$CIGS$:	*Copper Indium Gallium Selenide*	f_F:	*Fuel emission factor [g CO_2 equivalents per kWh]*
$C_{I,CC}$:	*Required battery storage capacity when accounting for inverter and charge controller inefficiencies [kWh]*	FF:	*Fill Factor [-]*
CO_2:	*Carbon dioxide*	F_{F,CO_2}:	*CO_2 emissions related to fuel consumption*
COP:	*Coefficient of Performance*	FPC:	*Flat-Plate Collector*
c_p:	*Specific heat of water [J/kg·K]*	G:	*Global solar irradiance [W/m²]*
CPC:	*Compound Parabolic Collector*	I_0:	*Initial Investment Cost [NOK]*
CR:	*Coverage Ratio [-]*	I_E:	*Estimated global solar irradiance at a specific azimuth and inclination angle [W/m²]*
C_S:	*Number of shaded cells in photovoltaic module*	I_{MPP}:	*Current at maximum power point [A]*
C_T:	*Number of cells in photovoltaic module*	$I_{n,p}$:	*Maximum current from parallel connected modules [A]*

I_{Opt}: *Global solar irradiance at optimal azimuth and inclination angle [W/m^2]*

I_S: *Solar irradiance over a year [kWh/m^2]*

I_{SC}: *Short-circuit current [A]*

$I_{SC,STC}$: *Short-circuit current at Standard Test Conditions [A]*

$I_{SC,oper}$: *Short-circuit current at the given operating temperature [A]*

IT: *Insulated-Terra*

k: *Thermal conductivity [W/mK]*

k_θ: *Incident angle modifier [-]*

L: *Length of pipe [m]*

LHS: *Latent Heat Storage*

LID: *Light-Induced Degradation*

$MLPE$: *Module-Level Power Electronics*

$Mono-Si$: *Monocrystalline Silicon*

$MPPT$: *Maximum Power Point Tracker*

m_w: *Mass of water [kg]*

n: *Number of time periods*

n_b: *Number of coherent days' worth of battery storage*

η_b: *Battery efficiency [-]*

$n_{b,p}$: *Number of batteries in parallel*

$n_{b,s}$: *Number of batteries in series*

$n_{b,tot}$: *Total number of batteries*

η_{CC}: *Charge controller efficiency [-]*

$n.d.$: *No date available*

η_I: *Inverter efficiency [-]*

η_o: *Max. conversion factor of solar collector [-]*

n_p: *Number of modules in parallel*

n_{PM}: *Required number of photovoltaic modules*

η_{PV}: *Efficiency of photovoltaic modules [-]*

NPV: *Net Present Value [NOK]*

$\eta_{PV,STC}$: *Efficiency of photovoltaic modules at STC [-]*

n_s: *Number of modules in series*

$\eta_{SC,CR}$: *Coverage rate of solar collectors [-]*

$\overline{\eta_{SC}}$: *Average efficiency of solar collector [-]*

NTE: *Nord-Trøndelags Elektrisitetsverk*

P: *Measured constant*

P_{Demand}: *Demanded installed peak power [W_p]*

P_{In}: *Solar input on photovoltaic modules [W]*

P_{Max}: *Peak power [W_p]*

P_{MPP1}: *Maximum Power Point with no shading [W]*

P_{MPP2}: *Maximum Power Point with partial shading [W]*

$P_{n,p}$: *Maximum peak power of photovoltaic modules in parallel [W_p]*

$P_{n,s}$: *Maximum peak power of photovoltaic modules in series [W_p]*

$Poly-Si$: *Polycrystalline Silicon*

P_{tot}: *Total installed peak power [W_p]*

PV: *Photovoltaic*

PWM: *Pulse Width Modulation*

Q_{EN}: *Annual energy need of DHW and space-heating [kWh]*

$Q_{Pipe,Loss}$: *Heat loss from pipes [kWh]*

Q_S: *Thermal Energy Storage capacity [J]*

Q_{Yield}: *Estimated specific annual energy yield for solar collectors [kWh/m^2]*

r: *Discount rate [-]*

r_1: *Inner pipe radius [m]*

r_2: *Outer pipe radius [m]*

SHS: *Sensible Heat Storage*

STC: *Standard Test Conditions*

T_a: *Ambient air temperature [K]*

T_C: *Temperature of photovoltaic cell [^{o}C]*

$TC_{I_{SC}}$: *Short-circuit current temperature coefficient [%/^{o}C]*

TCM:	*Thermo-Chemical Materials*	TT:	*Terra-Terra*
$TC_{V_{oc}}$:	*Open-circuit voltage temperature coefficient [%/°C]*	$V_{battery}$:	*Nominal battery voltage [V]*
TES:	*Thermal Energy Storage*	V_{MPP}:	*Voltage at maximum power point [V]*
T_M:	*Temperature Multiplier*	$V_{n,s}$:	*Maximum voltage across modules in series [V]*
T_m:	*Average fluid temperature [K]*	V_{OC}:	*Open-circuit voltage [V]*
TN:	*Terra-Neutral*	$V_{OC,oper}$:	*Open-circuit voltage at the given operation temperature [V]*
T_{oper}:	*Operation temperature [°C]*	$V_{OC,STC}$:	*Open-circuit voltage at Standard Test Conditions [V]*
$T_{Peak-Hour}$:	*Number of average daily peak sun-hours [h]*	V_{system}:	*Nominal system voltage [V]*
Δt_s:	*Storage temperature range [K]*	Θ:	*Incident angle of solar radiation [°]*
T_{STC}:	*Temperature at Standard Test Conditions [°C]*		

1 Introduction

1.1 Background

The Norwegian government pledged in 2016, under the Paris agreement, to reduce the country's greenhouse gas emissions with 40 % by 2030, compared to 1990. According to (Øvrebø, 2020), the total greenhouse gas emissions were about 51.5 million tons of CO_2 equivalents in 1990, and this suggests that the annual emission level must be below 30.9 million tons CO_2 equivalents by 2030. To compare, the greenhouse gas emissions in 2018 were about 52 million tons CO_2 equivalents, according to (Øvrebø, 2020), indicating that we are still far from reaching the goal. To be able to accomplish the greenhouse gas emission goal set by the Norwegian government, all Norwegian sectors have to do their part in reducing their greenhouse gas emissions.

(Miljøstatus, 2019) explains that the Norwegian agriculture sector was responsible for 8.6 % of the country's total greenhouse gas emissions in 2018. This amount is equal to approximately 4.5 million tons of CO_2 equivalents, and the majority of these emissions were methane gas and nitrous oxide gas from livestock and manure. According to (Miljøstatus, 2019), the greenhouse gas emissions linked to energy consumption for space heating and both fuel-driven and electric machinery in Norwegian agriculture are not included in the account for greenhouse gas emissions in the agricultural sector but rather the Norwegian energy sector.

(Miljødirektoratet, 2019) observed that the total greenhouse gas emissions associated with energy use in agriculture, forestry and fisheries, in 2017, were about 0.4 million tons of CO_2 equivalents. If the greenhouse gas emissions are assumed to be approximately the same in 2018, then the actual greenhouse gas emissions related to agriculture would be somewhere between 4.5 to 4.9 million tons of CO_2 equivalents.

Even if the direct greenhouse gas emissions in the farming agriculture sector are relatively marginal compared to methane and nitrous oxide gases, the reduction of these emissions is still the main focus of this master thesis.

1.2 Objective

The main objective of this master thesis is to study the effect a potential increase in solar energy utilization could have on the greenhouse gas emissions from Norwegian agriculture. The first step towards accomplishing this goal will be to design a photovoltaic system and solar water-heating system for the milk barn at Mære Agricultural School. The second step will be to determine, through extensive simulations, the amount of energy consumption that it is possible to replace with renewable solar energy.

By generalizing the results from the simulations and by mapping out other agricultural buildings with similar energy consumption as the milk barn, it is possible to estimate the total effect it could have if more buildings installed similar active solar systems.

Due to time restrictions, the main focus of this master thesis is the photovoltaic systems, and while the solar water-heating systems will still be described and simulated, it will not be as detailed as the photovoltaic system and will function more as a feasibility study.

This paper is a continuation of the project work conducted in the latter half of 2019.

1.3 Outline

Chapter 2 to 4 & Chapter 6 to 7 contains a comprehensive literature review of relevant theory about energy consumption in Norwegian agriculture, weather and solar conditions effect on solar energy harvesting, and components in photovoltaic systems and solar water-heating systems. The literature study is a continuation of the research performed during the project work in the latter half of 2019. In Chapter 6 & 7, the basic concept behind photovoltaics and solar collectors are briefly explained, before delving deeper into each system's relevant components.

At the end of each of the subchapters in Chapter 6: *Designing a photovoltaic system*, an appropriate system component for the milk barn is suggested. These suggestions are based on the literature review and actually existing products. The focus of Chapter 7: *Designing a solar water-heating system* is to gather information regarding solar water-heating systems, making it possible to perform a feasibility study on its potential for the milk barn.

In Chapter 5: *The milk barn at Mære Agricultural School*, the milk barn at the school is described, with special consideration given to the energy consumption, energy systems, technical equipment, hot water demand and the already existing photovoltaic systems at the school.

In Chapter 8: *Methodology*, the method for determining the system performances of the solar energy systems is presented, as well as how the results from the simulations will be generalized.

In Chapter 9: *Polysun simulations*, the simulation software Polysun is described, and the relevant parameters from the literature review and the main features of the simulation models are also presented.

In Chapter 10: *Results*, the results from the simulations are presented in an orderly fashion, and the potential effect on the total agricultural greenhouse gas emission is also explained.

In Chapter 11: *Discussion*, the results from the previous chapters are discussed, and a relatively short parametric study is also performed.

In Chapter 12: *Conclusion*, the most suitable energy system solution for the milk barn with consideration to the main purpose of this master thesis is presented.

In Chapter 13: *Further work*, the potential next steps for the results presented in this paper are presented.

In Chapter 14: *References*, an extensive list of all references used during the writing of this master thesis is presented.

In Chapter 15: *Attachments*, an extensive list with all the attachments relevant for this study is presented.

2 Energy usage and CO_2 emissions in agriculture

It could be argued that agriculture is one of the most important industries worldwide. Among other things, it is responsible for providing and maintaining food security in a world where the population is continuously growing. According to (Chena et al., 2020), the usage of new technologies and more modern machinery have increased in farming during the last decades.

This would suggest that the energy consumption related to agriculture should have increased, but as stated by (Eurostat, 2019), the energy consumption in European agriculture has actually been reduced. This can possibly be contributed to several factors, such as phasing out of small-scale farms and more energy-efficient equipment. According to (Eurostat, 2019), the consumption was reduced by 15.4 % from 1997 to 2017. This corresponds to a decrease in greenhouse gas emissions from the original amount of 29 million tons of CO_2 equivalents in 1997 to 25 million tons of CO_2 equivalents in 2017.

(Eurostat, 2019) also presents an overview of the evolution of the fuel share in EU agriculture from 1997 to 2017 (See Figure 1). In 1997, the percentage of renewable energy and biofuels was about 4 %, and this percentage increased to 10 % by 2017. During the same period, oil and petroleum products have remained dominant, with an estimated share of 53 % in 2017.

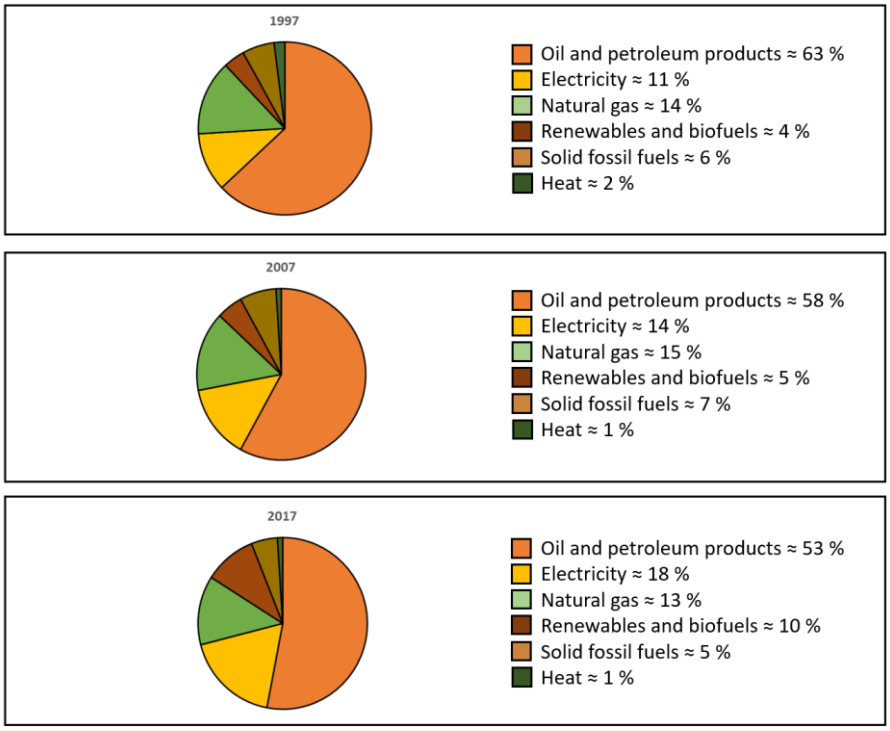

Figure 1: Approximate evolution of fuel types utilized in EU-agriculture, EU-28, 1997-2017. Source: Based on values from (Eurostat, 2019)

According to (Saunders et al., 2006), all energy consumption in agriculture can generally be broken into either direct or indirect energy usage. All usage is considered direct if it is linked to the farming operations, while it is considered indirect if it is related to producing the tools and equipment used during these farming operations. An example of direct energy usage is the fuel used to make the tractor run, while an example of indirect energy usage is the energy consumed when producing the tractor. Figure 2 shows some of the inputs into farming operations that are considered direct and indirect.

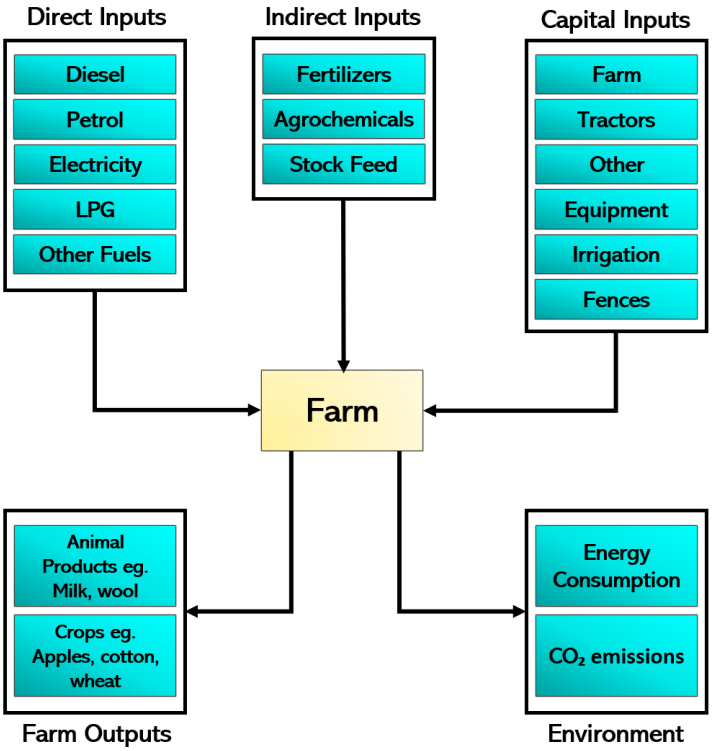

Figure 2: Direct and indirect inputs related to farming operations.
Source: Based on (Chen et al., 2015; Saunders et al., 2006)

In the next subchapter energy consumption and greenhouse gas emissions related to Norwegian farms will be presented. Unfortunately, both values are seldom provided by Norwegian sources, and to be able to study both greenhouse gas emissions and energy consumption, some emission factors will be presented in Table 1 and Table 2. The purpose is to use these factors later to calculate the energy consumption from greenhouse gas emissions and vice versa.

(Miljødirektoratet, 2019) provides the following equation for converting energy consumption into CO_2 equivalents:

$$F_{el,CO_2} = E_{el} \cdot f_{el} \cdot \frac{ton}{10^6 g} \quad \textbf{[2.1]}$$

Where F_{el,CO_2} is the CO_2 emissions related to the electricity consumption [ton CO_2 equivalents], E_{el} is the electricity consumption [kWh], and f_{el} is the electricity emission factor [g CO_2 equivalents/kWh]. Equation 2.1 can also be changed to portray fuel consumption:

$$F_{F,CO_2} = E_F \cdot f_F \cdot \frac{ton}{10^6 g} \quad \textbf{[2.2]}$$

Where F_{F,CO_2} is the CO_2 emissions related to the fuel consumption [ton CO_2 equivalents], E_F is the energy consumption from burning the fuel [kWh], and f_F is the fuel emission factor [g CO_2 equivalents/kWh].

Table 1: Emission factors for the Norwegian, Nordic and European electricity mix.

Electricity mix	Emission factor: [g CO_2/kWh]	Source:
Norway 2018	18.9	(NVE, 2019)
Nordic 2017	61.5	(NPRO, 2018)
European 2016	295.8	(EEA, 2018)

Table 2: Emission factors for different fuel types.
Source: (Andersson & Sand, 2018)

Fuel type:	Emission factor [g CO_2 equivalents per kWh]
Propane	243
Heating oil (petroleum)	289
Wood chips	18
Pellets	19
Diesel	267

2.1 Norwegian agriculture

As explained by (Bondelaget, 2017), Norwegian agriculture is characterized by small farms, located across the whole country. Its structural development is regulated by the state, and this is accomplished through legislation and economic instruments. According to (Orlund, 2018), around 3 % of the total landmass area in Norway is agriculture land. These cultivation areas are located all across Norway in almost every municipality. Table 3 shows the development in the number of farms in Norway from 2005 to 2016, and it also shows the number of milk producers and amount of milk production. According to (Melk.no, 2019), there were around 7 600 milk farms in Norway at the beginning of 2019. Of these 7 600 farms, about 1 500 were located in Trøndelag, 1 200 in Rogaland and 1 000 in Oppland. A considerable challenge for the farmers in Norwegian agriculture is the long winter season, which, as stated by (Orlund, 2018), results in a much lower yield compared to other countries in Europe.

Table 3: Facts on Norwegian agriculture.
Source: (Orlund, 2018)

	2005	2016	Change 2005 – 2016
Number of farms	53 000	41 200	- 22 %
Agricultural land (10^{10} m²)	1.03	0.98	- 5 %
10 000 m² per farm	19.5	23.8	+ 21 %
Milk production in million litre	1 526	1 510	- 1 %
Milk producers	15 800	8 400	- 47 %

According to (Lien et al., 2018), the energy consumption in Norwegian farming agriculture was 3.37 TWh in 2016, and they also assumed that the energy usage would increase by 0.2 % every year towards 2035. If their assumption is correct, then the energy consumption would be 3.390 TWh in 2019. (SSB, n.d.) lists some of the electricity consumptions in Norwegian agriculture, excluding the electricity usage for greenhouses, and discovered that the total usage was about 0.98 TWh in 2014. If it is assumed that this electricity consumption also increases with 0.2 % every year, then the electricity consumption in Norwegian agriculture, excluding greenhouses, would be 0.988 TWh in 2019.

If the Norwegian electric mix for 2019 is used with Equation 2.1, then the estimated greenhouse gas emissions for the electricity consumption was about 18 673.2 tons of CO_2 equivalent in 2019. If the Nordic electricity mix was used instead, then the greenhouse gas emissions would be 60 762 tons of CO_2 equivalents.

In 2017, a more comprehensive and detailed study on the energy consumption of agriculture in Trøndelag-county was conducted by (Andersson & Sand, 2018). The purpose of the study was to determine the energy consumption associated with more energy-intensive farm types, specifically milk, pig, chicken and egg production.

According to (Andersson & Sand, 2018), milking farms ordinarily use diesel and electricity in their production cycle. They explain that the reason for this is that the process of milking and feeding requires several large pieces of equipment, which all demands considerable quantities of electricity. (Andersson & Sand, 2018) states that milk production is also characterized by little demand for heating, unlike the pig farms, which require considerable amounts of electricity for equipment and also have a high heating demand.

(Andersson & Sand, 2018) explains that chicken farms have the highest utilization of fossil fuels for covering heating needs, but that they have a limited diesel and electricity need. Egg production farms only require heat while the chicken is still in its growth phase but require little energy after this. Table 4 presents the energy consumption for the different production farms in Trøndelag. The greenhouse gas emissions displayed on the far right are only estimations performed by (Andersson & Sand, 2018). Figure 3 shows the percentage share of the energy consumption and CO_2 emissions related to the different farm types.

Table 4: Energy consumption and estimated CO_2 emissions for different farm types in Trøndelag. Source: (Andersson & Sand, 2018)

Farm type	Electricity [GWh]	Heat [GWh]	Diesel [GWh]	Sum energy [GWh]	CO_2 emissions [Tons]
Milk	82.6	0.0	72.7	155.3	22 708
Piglets	6.2	13.6	6.9	41.0	2 423
Hogs	10.8	3.5			
Chicken	4.2	37.7	2.7	41.9	8 428
Egg	2.5	0.5	0.0	3.0	50
Total	**106.1**	**55.3**	**82.3**	**241.2**	**33 609**

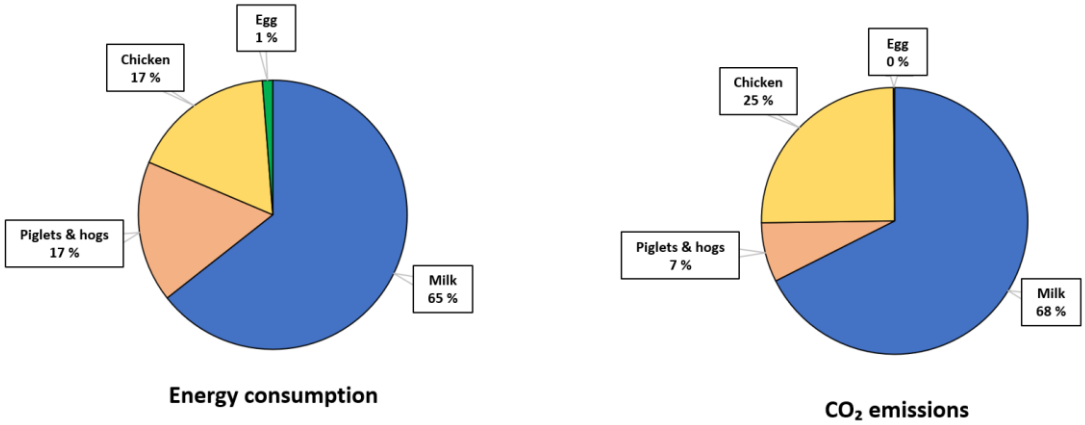

Figure 3: The energy and emission percentage share of the different farm types. Source: Based on values from (Andersson & Sand, 2018)

According to (Andersson & Sand, 2018), greenhouse gas emissions from Norwegian agriculture were about 4.5 million tons of CO_2 equivalents in 2016. They concluded that 16.1 % of the total Norwegian agriculture domain is located in Trøndelag, based on other sources, and assumes that the greenhouse gas emissions are proportional to the agricultural area. If this assumption is correct, then Trøndelag is accountable for about 724 500 tons of the total CO_2 equivalents. If it also is assumed that the estimates in Table 4 are somewhat correct, then 4.64 % of the CO_2 emissions are due to energy consumption.

3 Renewable energy in agriculture

According to (Bondelaget, n.d.), there are great opportunities for both producing and utilizing renewable energy in Norwegian agriculture. The renewable energy produced at the farms can be either used on-site or supplied to society through the power grid or in the shape of fuel. (Reynolds & Wenzlau, 2012) lists several possibilities such as utilizing active solar energy through either solar collectors or photovoltaics, utilization of kinetic energy from small or cooperatively owned wind or water turbines and utilizing free solar energy through careful building design meant to maximize the use of natural daylight.

In addition to the renewable energy sources mentioned above by (Reynolds & Wenzlau, 2012), (Chel & Kaushik, 2011) states that other renewable energy sources in agriculture are biomass, biofuels and geothermal heat.

All of these renewable energy sources and their role in agriculture are briefly explained in the subchapters below.

3.1 Solar energy

According to (Norsk Solenergiforening, n.d.-a), the earth annually receives about 15 000 times more energy from the sun then what is consumed. There are several benefits associated with harvesting solar energy. Among other things, the sun is a free, sustainable and environmentally friendly energy source, and it is possible to utilize this energy both passively, through dark surfaces and large windows, or actively, through solar collectors or photovoltaics.

As stated by (SEIA, 2018), photovoltaics and solar collectors work very differently. Photovoltaics convert sunlight into electricity, while solar collectors harvest thermal energy from the solar irradiance and use it to heat water or provide cooling.

Some benefits and drawbacks with the utilization of solar energy in agriculture are stated by (Union of Concerned Scientists, 2008) and (Renewable Resources Co, 2016). According to them, solar energy offers the opportunity to save money, reduce pollution and greenhouse gas emissions, and increases the buildings self-reliance. The drawback, on the other hand, is that solar energy systems often have a high initial investment cost, and the profitability of the installed system therefore heavily depends on the actual placement of the solar energy system.

Active solar energy utilization in the form of solar collectors and photovoltaics is the main focus of this master thesis.

3.2 Wind energy

Wind is a free and abundant, as well as a clean, renewable energy source, similar to the sun. It is also, according to (Energy.Gov, n.d.-a), one of the fastest-growing energy sources in the world today. Electricity is generated by having wind flow through turbines, converting the kinetic energy of the wind into usable electricity. For optimal energy production, the wind turbines should be located in areas that experience large amounts of wind.

Benefits and drawbacks with wind energy are presented by (EnergyInformative, 2015) and (Energy.Gov, n.d.-a). Advantages with wind systems are that they are cost-effective, sustainable, have a vast electricity generation potential, and can be built on already existing farms. Unfortunately, wind turbines can sometimes create significant noise, and not everyone finds them aesthetically pleasing. The turbines can also sometimes cause harm to local wildlife.

(Herbert et al., 2009) declares that wind turbines can be a beneficial addition to structures that previously have installed photovoltaic systems, as wind is often available through all the seasons, whereas solar energy is not.

According to (AWEA, n.d.), farmers in some countries have the opportunity to lease their land to wind companies for a stable income, especially as turbines do not restrict farming operations.

3.3 Geothermal energy

According to (Energy.Gov, n.d.-b), geothermal energy is clean and sustainable energy, obtained in the form of relatively constant temperatures in the ground. This thermal energy can be withdrawn without using significant amounts of fossil fuels, with equipment such as heat pumps.

As explained by (Energy.Gov, n.d.-b), the benefit of geothermal energy is that it is available all through the year. The system also has a minimal visual impact on the environment, but as a result, are often better suited for new buildings, as (Herbert et al., 2009) states, due to the extensive excavation involved. The most prominent drawback with geothermal systems is their high investment costs.

(Nguyen et al., 2015) explains that geothermal energy has the potential to reduce the required energy and fuel consumption associated with greenhouse heating. The thermal energy can also be used for agro-industrial processes and soil heating.

3.4 Hydro energy

Hydro energy is the conversion of hydropower into electricity, and as (USGS, n.d.) states, hydropower is one of the most widely used renewable energy sources in the world. (WVIC, n.d.) explains that similar to energy based on wind, electricity is generated by having water flow through a turbine, converting the kinetic energy into mechanical energy. This mechanic energy is then transformed into electricity by a generator.

According to (USGS, n.d.), the benefits of hydro energy is that no fuel is needed, leading to minimal pollution, the operation and maintenance cost is relatively low, and the technology has been proven reliable over time. Some of the drawbacks, as stated by (USGS, n.d.), are the high investment costs, intervention in nature, and sometimes changes in the water quality. (Osborn et al., 2017) explains that three components have been identified for harnessing hydro energy in agriculture. These first are on-farm pressurized irrigation systems, while the second and third are conduit drops on irrigation ditches and existing agricultural dams. As (Osborn et al., 2017) mentions, one example of on-farm pressurized irrigation systems is micro-hydropower plants.

(Clean Green Energy Zone, 2016) states that the benefits of micro-hydropower plants are, among other things, their reliability and relatively high efficiency. They also do not require reservoirs, and it is possible to integrate the solution into the local power grid.

3.5 Bioenergy

Briefly explained, bioenergy is all form of renewable energy obtained from biological sources. According to (USDA, n.d.), these sources include wood, grass, corn, soybeans, forest or agricultural residues.

As explained by (EESI, n.d.), bioenergy is often a common term including both energies from biomass and biofuels. (Klimasmart Landbruk, 2017) further elaborates by mentioning the farms' opportunity to produce and use the biomass on-site, for generating thermal and electric energy, as well as supply biomass to society, increasing the overall use of renewables. (McFarland, 2017) mentions some benefits with biomass, such as their high availability, relatively low cost, and the opportunity to reduce the amount of garbage on landfills, as waste is considered as biomass.

According to (Lehman & Selin, 2008), biofuels are manufactured from biomass, and similar to biomass, biofuels are relatively cost-effective and environmentally friendly. (EIA, 2019) further explains that biofuels can be combined with other fossil fuels to produce cleaner and more environmentally friendly fuels than just pure gasoline and diesel.

(McFarland, 2017) also provides a few drawbacks associated with biofuels, as they are often not as efficient as traditional fossil fuels. Also, even if bioenergy is considered carbon-neutral, it is not entirely clean energy, as the usage of human and animal waste increase the amount of methane gas in the atmosphere. Overreliance of bioenergy can also lead to deforestation.

4 Harvesting of solar energy

Solar energy is radiation from the sun, and when harnessed through the means of solar collectors or photovoltaics, can generate either heat or electricity. All solar radiation is split into diffuse and direct radiation from the sun.

(DSG, 2010) explains that diffuse radiation is the share of solar radiation that reaches the surface of the earth, after first having been separated from the direct solar beam, by either molecules or particles in the atmosphere (See Figure 4). Direct radiation, on the other hand, is the amount of solar radiation that directly hits the surface of the earth.

The sum of these two radiation types is also known as global solar irradiance.

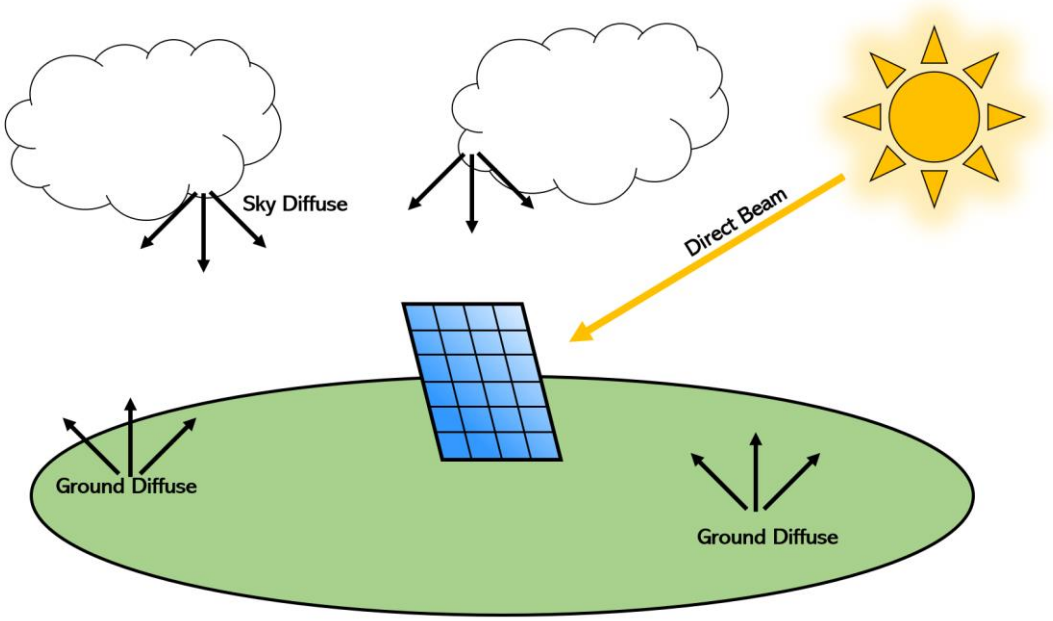

Figure 4: Types of irradiance.
Source: Based on a figure by (Brown, 2018a)

Figure 5 is based on an estimate from (Zijdemans, 2014), and the illustration shows the expected amount of global solar irradiance, on a surface located in the south of Norway and angled directly towards the sun, at different sky conditions. As further explained by (Zijdemans, 2014), during sunny days, the global solar irradiance will primarily consist of direct radiation, while on cloudy days, the consistency will mainly be diffuse radiation.

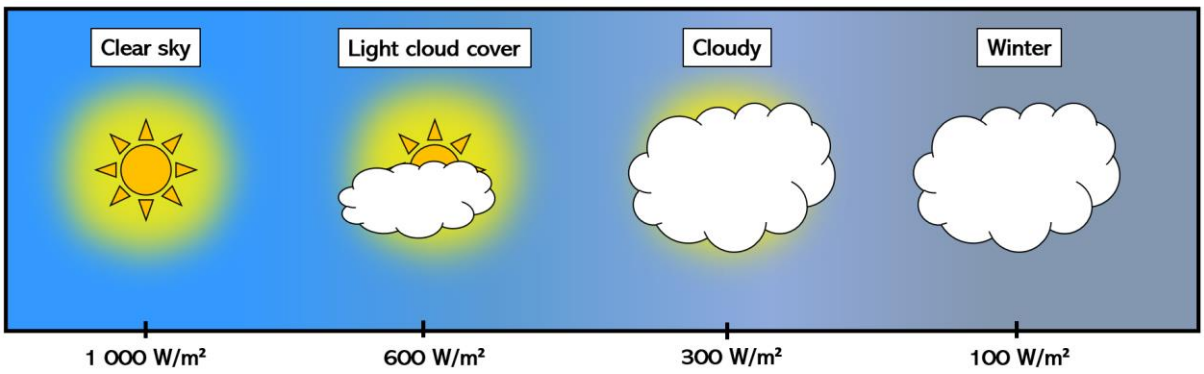

Figure 5: The expected amount of global solar irradiance during different sky conditions. Source: Based on a figure by (Zijdemans, 2014)

4.1 Influence of orientation and inclination angle

As stated by (DSG, 2010), several factors determine the amount of solar energy that it is possible to harvest. These factors include the location of the solar harvesting system, the system solution, and conditions such as shading, orientation and inclination angle.

The angle corresponding to the orientation of the system is known as the azimuth angle. (Honsberg & Bowden, n.d.-b) explains this angle to be the compass direction in which the sunlight is received. An azimuth angle of 0^o corresponds to due south, while 90^o and 180^o correspond to due east and north, respectively.

The inclination angle is the angle between the equatorial plane of the earth and the surface plane of the solar collector or photovoltaic module. According to (Zijdemans, 2014), we differentiate between optimal and recommended inclination angle. The optimal angle is the fixed inclination angle that would result in the highest amount of radiated energy during the year, while the recommended inclination angle is the angle that would contribute more solar energy during periods when it can be used. As explained by (Zijdemans, 2014), this is because the optimal angle may lead to excess electricity or heat production during periods where it is simply not necessary, but deficit production during periods when the additional energy is needed.

Both the azimuth angle and the inclination angle can be seen in Figure 6.

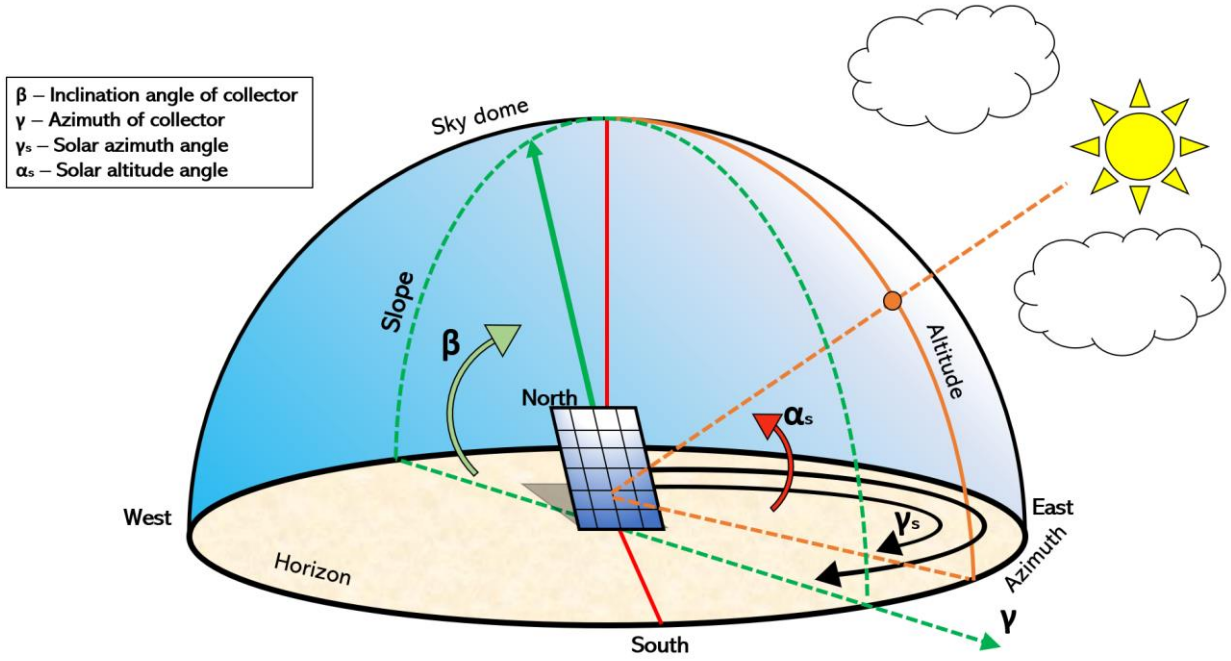

Figure 6: Azimuth and inclination angle of a thermal collector or photovoltaic module. Source: Based on a figure by (Brownson, n.d.).

To be able to optimize the solar energy system, the azimuth and inclination angle should be chosen wisely. This is further confirmed by (Sørensen et al., 2017), who states that if the majority of energy consumption takes place during winter, then the harvesting system should have a much steeper inclination angle, as the sun is lower on the horizon. The azimuth angle should be decided based on the time of day with the highest energy consumption.

As an example, consider a solar energy system located in the northern hemisphere. If the majority of energy consumption takes place before noon, then the azimuth angle should be somewhere between - 90^o (East) and 0^o (South), as this is the orientation of the sun in the morning.

If the optimal global solar irradiance is known, at a particular location, then it is possible to estimate the global solar irradiance for a specific azimuth and inclination angle, by using the correction factors, introduced in Table 5, with the following equation:

$$I_E = I_{Opt} \cdot f_a \cdot f_b \qquad \textbf{[4.1]}$$

Where I_E is the estimate of the global solar irradiance at a specific azimuth and inclination angle [W/m^2], I_{Opt} is the global solar irradiance at the optimal azimuth and inclination angle (at the same location) [W/m^2], and f_a and f_b is the correction factor of the azimuth and inclination angle, respectively.

Table 5: Typical correction factors for different azimuth and inclination angles. Source: (Zijdemans, 2014)

Azimuth angle [°]	Correction factor f_a [−]	Inclination angle [°]	Correction factor f_b [−]
		0	0.81
80 (South-West)	0.74	10	0.89
60 (South-West)	0.87	20	0.95
40 (South-West)	0.94	30	0.98
20 (South-West)	0.98	40	1
0 (South)	1	50	0.99
20 (South-East)	0.96	60	0.97
40 (South-East)	0.90	70	0.92
60 (South-East)	0.75	80	0.85
70 (South-East)	0.70	90	0.78

4.2 Global solar irradiance and climate in Norway

(Norsk Solenergiforening, n.d.-b) estimates that Norway annually gets approximately 1 500 times more energy from the sun than what is consumed. According to them, the annual amount of solar energy on a horizontal plane in Norway is commonly between 700 and 1 000 kWh/m^2. These numbers are heavily dependent on the actual system's location in the country. Table 6 provided by (Zijdemans, 2014), reinforces the quantities presented by (Norsk Solenergiforening, n.d.-b), as they are within the range of 700 to 1 000 kWh/m^2.

Table 6 also shows the annual radiated energy for large Norwegian cities such as Oslo, Bergen and Trondheim, and it also shows the optimal inclination angle at all of these locations.

Table 6: The amount of solar energy during a year for different inclination angles and cities. Source: (Zijdemans, 2014)

City	Radiated energy [kWh/m²·year]				Optimal angle
	0° (Horizontal)	25°	90° (Vertical)	At optimal angle	
Oslo	846	982	746	1 001	40°
Flekkefjord	871	996	732	1 014	38°
Bergen	819	927	674	939	34°
Trondheim	825	983	792	1 023	44°
Tromsø	705	841	692	880	45°

As indicated by Table 6 and Figure 7, the cities and locations in Norway have some differences in the average daily amount of radiated solar energy. A probable cause for the variations in average daily solar radiation is the fact that the Norwegian environment consists of areas with several distinct climates. According to (Climates to travel, n.d.), the Norwegian environment consists of maritime climates, continental climates, mountain climates and Baltic climate.

As explained by (Climates to travel, n.d.), Norway's mainland climate is more temperate than what the country's northern position first would indicate, and this is probably because of the ocean currents delivering heat to mainland Norway.

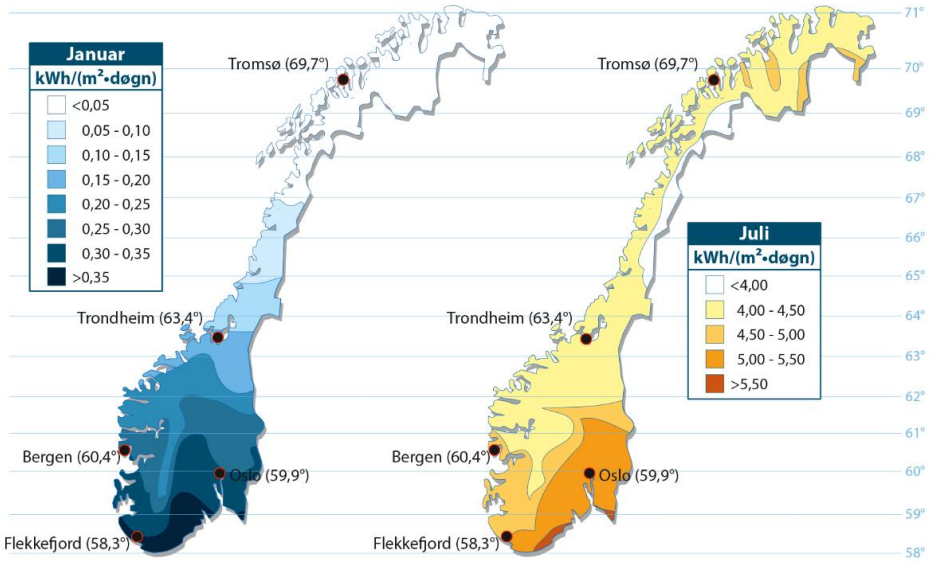

Figure 7: The daily average global solar radiation for Norway during January and July. Source: Used with permission from (Zijdemans, 2014), see Attachment A.10

4.3 Conditions for solar harvesting at Mære Agricultural School

(European Commission, 2020) can be used to map out the average monthly global solar irradiance on a horizontal plane located at Mære Agricultural School. The monthly average values, obtained through the tool, can be seen in Figure 8, and the included monthly global solar irradiance are from the period 2013 to 2016, as newer results are unavailable in the tool. Based on the average results in the figure, it is possible to assume that May is the month with the highest potential for solar harvesting.

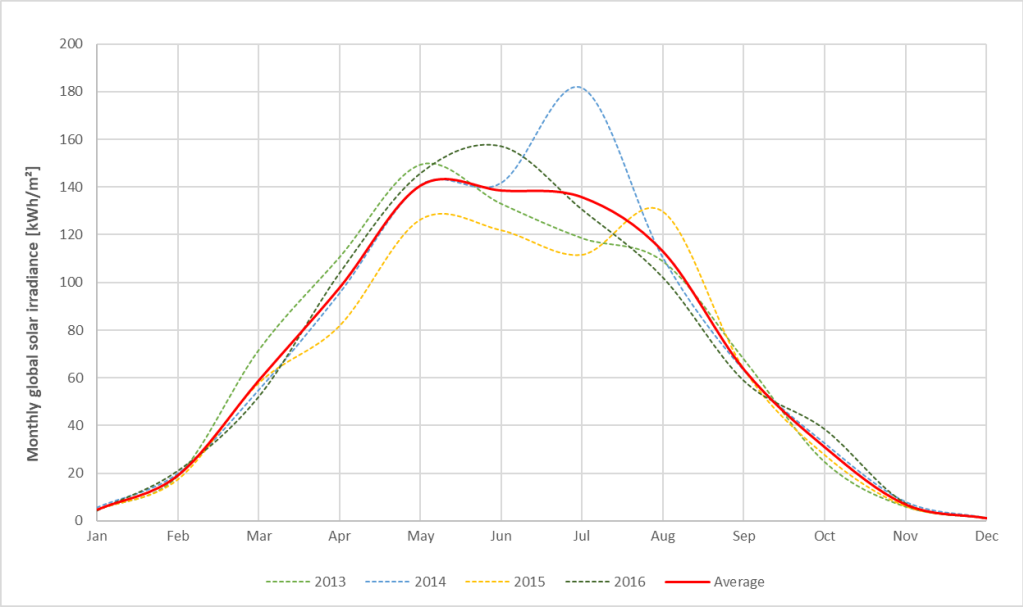

Figure 8: Average monthly global solar irradiance on a horizontal plane at Mære Agricultural School. Source: Based on values from (European Commission, 2020)

Another indicator of the solar conditions at Mære is the average number of peak sun-hours the area experience annually. Peak sun-hours is explained by (Honsberg & Bowden, n.d.-a) to be the number of hours each year where the average global irradiance is 1 000 W/m^2. It should be noted that peak sun-hours are determined by taking the total daily, monthly or annual global solar irradiance and dividing the total value on 1000 W/m^2. The result is the number of hours with equivalent global irradiance to 1000 W/m^2.

Table 7 displays the average monthly and the total number of peak sun-hours at Mære from 2013 to 2016. The table also includes peak sun-hours for global solar irradiance hitting a horizontal plane and a plane with an inclination angle of 26º, which is the angle of the south-facing roof of the milk barn.

Table 7: The average monthly and total amount of peak sun-hours for Mære.
Source: (European Commission, 2020)

Months	Jan	Feb	Mar	Apr	May	Jun	Jul	Aug	Sept	Oct	Nov	Dec	Total
Horizontal plane	4.9	19.3	59.1	98.0	140.7	138.5	135.6	112.8	63.4	30.9	7.0	1.3	811.6
Inclination angle of 26°	14.4	37.7	90.6	121.6	156.1	145.4	146.3	135.4	89.6	57.6	16.1	2.7	1 013.6

(European Commission, 2020) also makes it possible to determine the optimal inclination angle for each month (see Figure 9). The red line in Figure 9 indicates the fixed inclination angle of the south-facing roof on the milk barn.

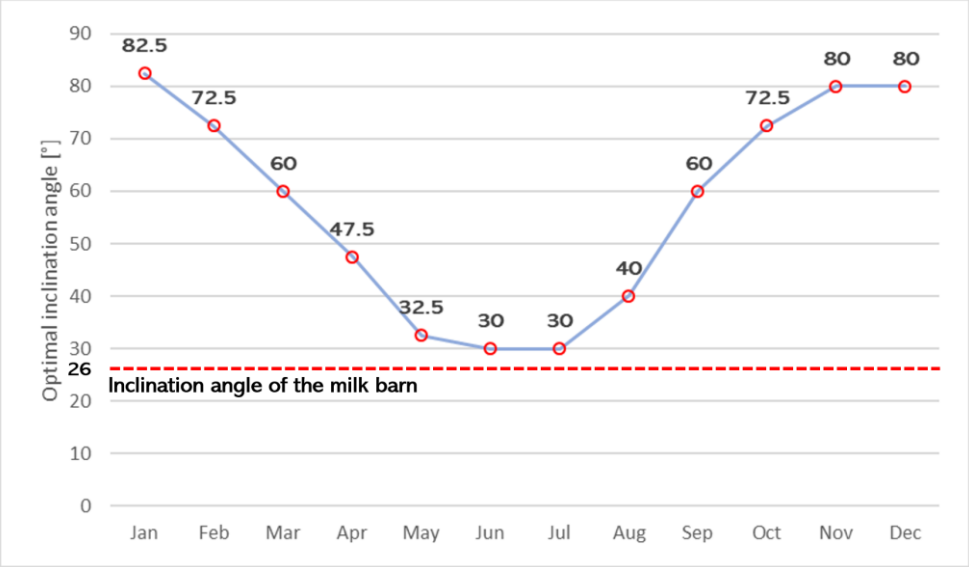

Figure 9: Optimal inclination angle during the year for Mære.
Source: Based on values from (European Commission, 2020)

The last thing to point out is the climate at Mære. As explained by (Dannevig, 2019), Trøndelag experiences vast differences in local climates all over the county. As an example, the north-west region of Trøndelag is characterized by a maritime climate, while the south-east region is characterized by a continental climate. According to (Climate-Data.org, n.d.), Mære experiences a Continental Subarctic Climate, which is further explained by (Britannica, 2009) to be a climate dominated by long and cold winters, and with few sunny days during the year.

The outdoor temperature at Mære Agricultural School has been mapped out by the Norwegian Institute for Bioeconomy (NIBIO), as they have installed several temperature sensors at farms located all over Norway. Their measurements for 2019 can be seen in Figure 10.

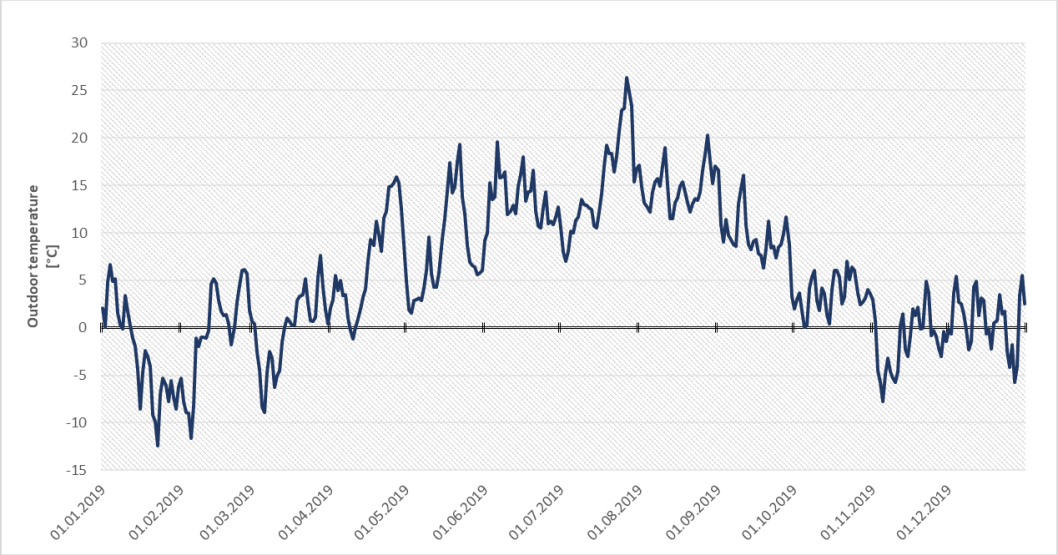

Figure 10: The daily average outdoor temperature at Mære Agricultural School in 2019. Source: Based on measurements from NIBIO

5 The milk barn at Mære Agricultural School

This chapter consists of information gathered during the project work in the latter half of 2019, with some additions of new information. Most of the text has been reworked and rewritten for this master thesis, but in some sections, the wording may be similar to the project work.

According to the administration at Mære Agricultural School, the milk barn was built during the period 2015 to 2016 and stood finished in May 2016. About 134 animals inhabit the barn, and the animal stock consists of calves, heifer and cows. The location of the milk barn, in regard to the rest of the school, can be seen in Figure 11. Google maps estimate that there are about 300 meters from the milk barn to the remaining buildings of the school.

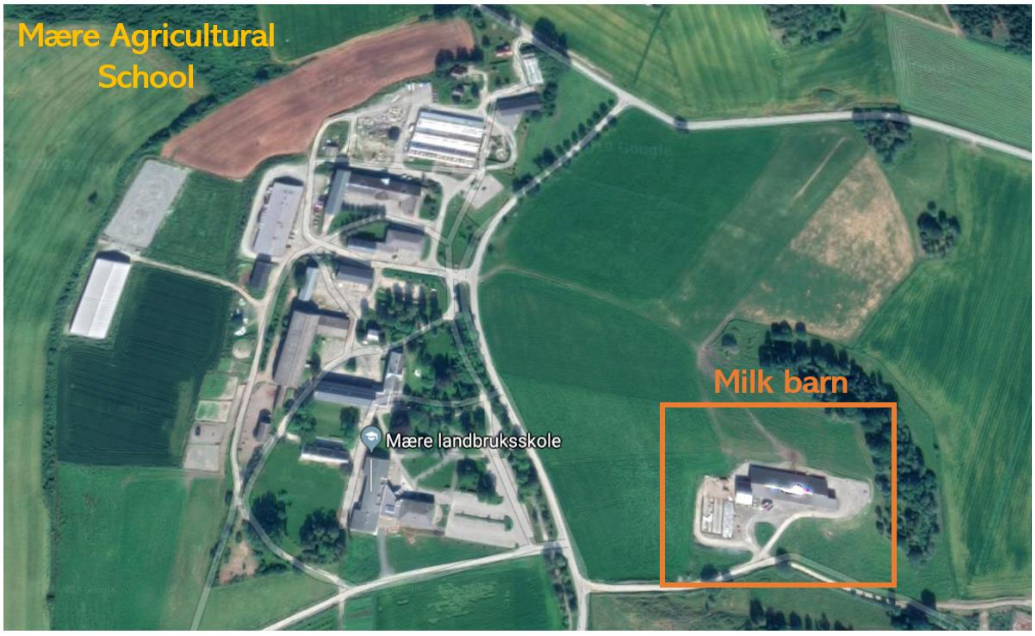

Figure 11: Satellite picture of Mære Agricultural School and the milk barn.
Source: Retrieved from Google Maps

It should be noted that the design and building phase of the milk barn was not completely hassle-free, as an old church from the latter half of 1100 is located near the milk barn. According to (Steinkjer Kommune, 2015), the church is automatically protected by the Norwegian Cultural Heritage Act due to its age. This Norwegian Act also puts comprehensive restrictions on all neighboring buildings. Therefore, all changes done on the facade or outfacing parts of the construction must be approved by the Norwegian antiquities' organization.

5.1 Mære Agricultural School

Mære Agricultural School is located in Trøndelag-county, in Steinkjer municipality. (Steinkjerleksikonet, n.d.) explains that the school was built in 1895 as an educational institution centered around teaching agriculture and housewife duties. In 1916, the housewife part of the school was moved to Stjørdal, and the school primarily started focusing on teaching students about agriculture. In 1990, Mære Agriculture School was implemented into the Norwegian high-school system.

Today, the school consists of several different buildings with various functions. All the main buildings at the school are displayed in Figure 12.

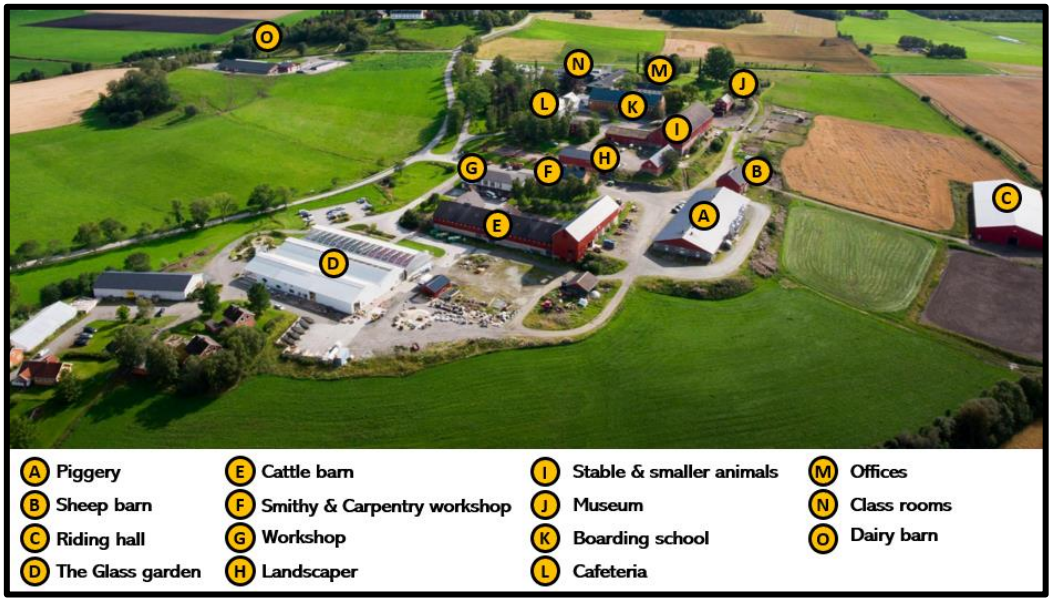

Figure 12: Buildings located at Mære Agricultural School.
Photo: Mære landbruksskole.
Published with permission from Mære Agricultural School (see Attachment A.11)

5.1.1 Energy consumption at Mære Agricultural School

According to NTE (see Attachment A.4), the total energy consumption at Mære Agricultural School was around 3.4 GWh in 2018. As they state, this annual consumption has been relatively stable during the last ten years, as can be seen in Figure 13. The trendline suggests that the overall energy consumption at the school is steadily decreasing.

The annual energy consumption is separated into electricity, bio, propane/oil and heat storage, and can be seen in Table 8.

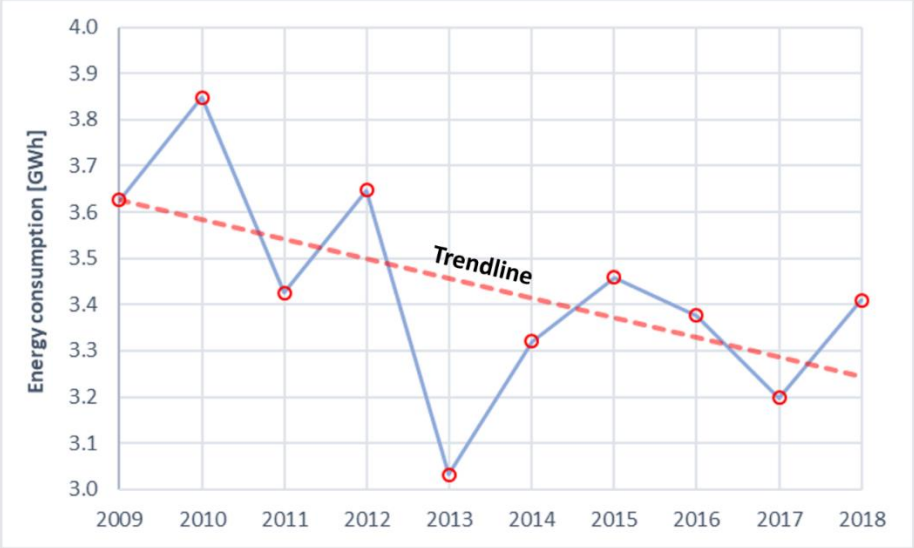

Figure 13: Annual total energy consumption at Mære Agricultural School. Source: NTE (see Attachment A.4)

Table 8: Annual energy consumption at Mære Agricultural School (separated into type of energy source). Source: NTE (see Attachment A.4)

Year	Electricity [kWh]	Bio [kWh]	Propane/Oil [kWh]	Heat storage Out [kWh]	Total energy consumption [kWh]
2009	2 267 473	361 600	996 648		3 625 721
2010	2 202 448	541 560	1 103 980		3 847 988
2011	1 952 029	470 296	667 536	335 274	3 425 135
2012	2 202 359	518 168	612 480	313 878	3 646 885
2013	1 725 846	465 224	602 388	238 994	3 032 452
2014	1 993 120	438 920	728 172	160 697	3 320 909
2015	2 300 669	318 560	445 716	393 526	3 458 471
2016	2 507 164	219 560		649 948	3 376 672
2017	2 318 725			879 916	3 198 641
2018	2 445 680			963 203	3 408 883

The table above shows that both bio and propane/oil, as an energy source, was phased out by 2017 and replaced with an increased share of heat from the local heat storage. The table also shows that electricity consumption at the school has remained relatively stable during the period from 2015 to 2018.

5.2 Building description of the milk barn

The milk barn at Mære Agricultural School is split into two distinctly separate sections. The livestock inhabits one of the sections, while the other section is meant for long periods of occupancy by people. The livestock section is known as the "Cold barn", as the building structures are uninsulated and there is also no form of space-heating. In the other part the building, the walls are insulated, and the areas are heated by a hydronic floor heating system.

The floor plan of the building can be seen in Figure 14, while Figure 15 displays 3D illustrations of the building.

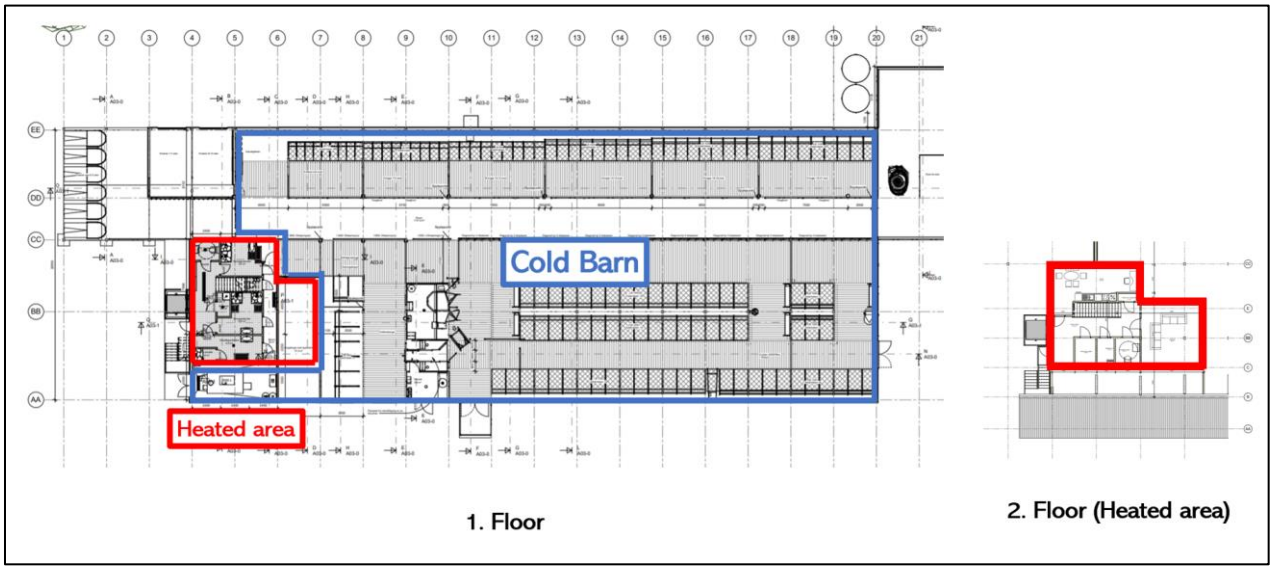

Figure 14: Schematic of 1st and 2nd floor at Mære milk barn.
Source: Mære landbruksskole.
Published with permission from Mære Agricultural School (see Attachment A.11)

The "Cold barn" consists of only one floor, while the heated section of the barn has two. In addition to livestock, there are also several large pieces of technical equipment inside the "Cold barn". These pieces of equipment include machines for mixing food for the animals, delivering the food, cow milking, and a robot for cleaning after the animals. The technical room is also found in the "Cold barn".

The 1st floor of the heated zone consists primarily of wardrobes with showers, while the 2nd floor has two meeting rooms and three bathrooms.

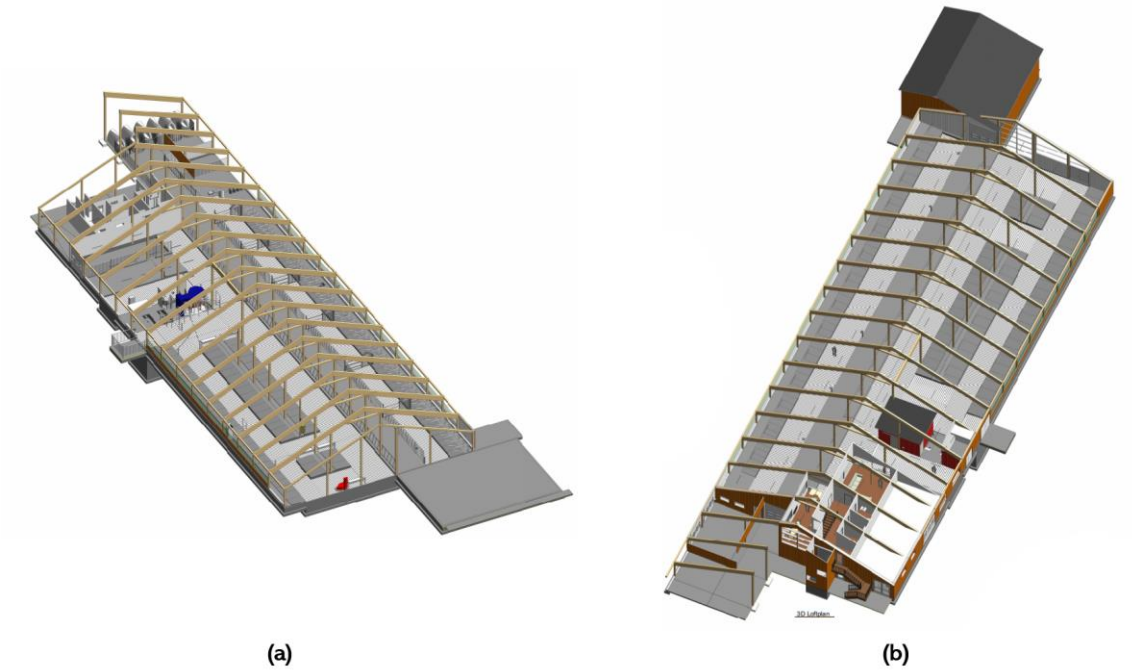

Figure 15: 3D-illustration of the *(a)* 1st floor and *(b)* 2nd floor at the milk barn.
Source: Mære landbruksskole.
Published with permission from Mære Agricultural School (see Attachment A.11)

The total 1st floor area of the milk barn is about 1 305 m^2, while the 2nd floor has around 82 m^2. The building has a length of 53 m and a width of 22.6 m. It also has a height of 8.8 m at its highest point and 3.2 m at its lowest. The roof surface area is approximately 1 337 m^2, equally divided between the south- and north-facing roof.

5.3 Existing energy systems at the milk barn

5.3.1 Hot water system

The hot water system found in the milk barn is displayed in Figure 16. The heat pump that is seen on the left side of the figure is an air-to-water heat pump of the type aroTHERM VWL 85/2 A-230V (see Attachment A.12). The pump preheats the water inside the 300-litre storage tank before it is either sent to the floor heating system or transferred to the water heater. In addition to the heat pump, an electric heating element is connected to the middle of the storage tank. The storage tank also utilizes heat recovery from a 6000-litre storage tank for milk, extracting water at the base of the tank and returning it at the center of the storage tank.

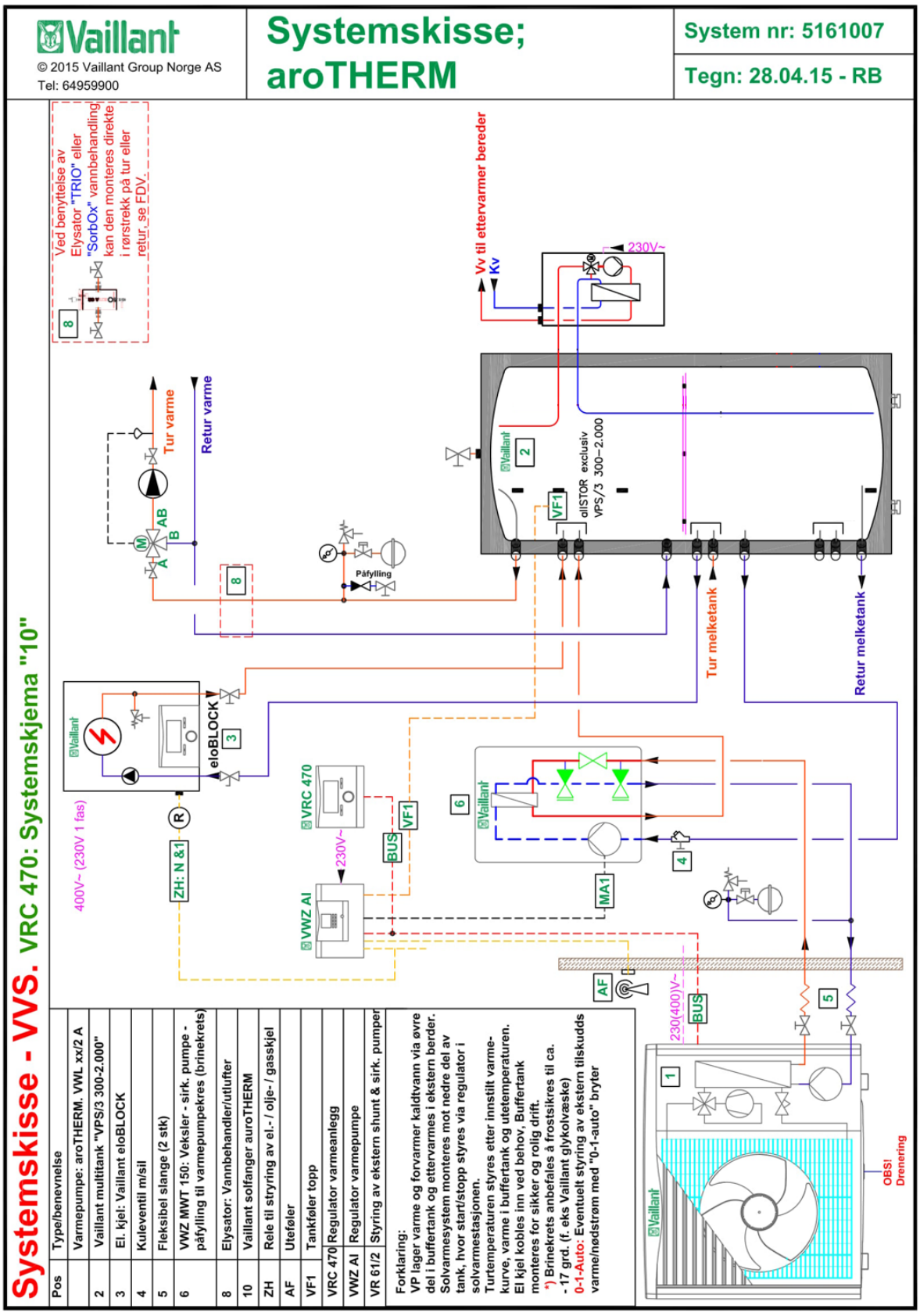

Figure 16: The existing hot water system at the milk barn.
Source: Mære landbruksskole.
Published with permission from Mære Agricultural School (see Attachment A.11)

Figure 17: The electric boiler, storage tank and water heater at the milk barn. Photos: Dan Remi Antonsen.

5.3.2 Electrical equipment inside the barn

As already mentioned, numerous large pieces of equipment are found inside the milk barn. The most prominent of which are the milking robot, feeding machine, feed mixer, feed hoppers and the cleaning robot. Table 9 displays the estimated operation hours for the equipment during the day, as well as the installed effect. The number of operation hours was determined through correspondence, but the established power of the machines was estimated based on similar products from the same supplier.

Table 9: The effect and operation hours of large pieces of electric equipment inside the milk barn. Source: Mære Agricultural School

Electric equipment	Installed effect [kW]	Operation hours [h/day]
Milking robot - DeLaval VMS 2015	3.30	18.3
DeLaval robotskrape RS250	0.255	6
K2 FeedRobot	9.2	1
TKS FeedMixer	22	4
TKS Feed Hopper 1	3	4
TKS Feed Hopper 2	3	4

5.4 Energy consumption at the milk barn

Unlike most of the other buildings located at Mære Agricultural School, the milk barn is not connected to the local heating network. As the majority of the machines and tools inside the barn are electric, it assumed that the energy consumption at the milk barn is entirely based on electricity.

The annual electricity consumption at the milk barn is presented in Table 10. Based on the values for 2018, the milk barn was responsible for 5.89 % of the total energy consumption of the school that year. The milk barn was not finished before May 2016, explaining the low electricity consumption that year.

Table 10: Annual electricity consumption at the milk barn in the period 2016-2019. Source: Attachment A.4 & NTE

Year	2016	2017	2018	2019
Annual energy consumption [kWh]	123 040	179 101	200 647	199 672

The estimated energy consumption related to the necessary heating of water for space heating and domestic hot water was calculated in the report on the opportunities for renewable energy on Mære Agricultural School (see Attachment A.1). The estimated water consumption by livestock can be seen in Table 11, and the corresponding energy need can be seen in Table 12. The second table also shows the estimated energy consumption related to space-heating in the heated section of the milk barn, as well as energy-savings by the utilization of the air-to-water heat pump and heat recovery from the milk tank.

If the estimated energy consumption for water heating is removed from the annual electricity consumption, then the results suggest that the remaining consumption of about 170 000 kWh is due to the electricity demand of the lighting and the remaining pieces of electrical equipment.

Table 11: Estimated amount of necessary water for the livestock.
Source: Attachment A.1

Type of animal	Age	Number of animals	Liters per animal/day	Liters per day	Liters per year
Calves	1 – 7 weeks	9	5	45	16 425
Calves	8 – 12 weeks	9	10	90	32 850
Calves	4 – 6 months	9	15	135	49 275
Heifer	7 – 9 months	9	20	180	65 700
Heifer	10 – 12 months	9	30	270	98 550
Heifer	13 – 15 months	9	35	315	114 975
Heifer	16 – 18 months	9	60	540	197 100
Heifer	19 – 21 months	9	70	630	229 950
Heifer	21 – 24 months	9	80	720	262 800
Cows	-	55	100	5500	2 007 500
Sum		136		8 425	3 075 125

Table 12: Calculated net energy need for heating of water.
Source: Attachment A.1

	Specific heat capacity [kJ/kg·K]	Amount of water [L]	Temperature difference [K]	Annual energy Consumption [kWh]
Drinking water – Animals	4.18	3 075 125	10	35 706
Tap water – Milking robot	4.18	98 550	75	8 582
Tap water – Tank storage rom	4.18	9 490	75	826
Tap water – Sanitary rom	4.18	29 200	75	2 543
Heating service area (151 m²)				16 610
Total energy need for heating of water				**64 267**
Heat recovery – Milk tank (Deduction)	4.18	200 000	75	- 17 417
Heat pump air-to-water				- 16 000
Net energy need for water heating				**30 850**

5.4.1 Current energy costs

In Norway, the general electricity cost includes both electricity and grid importing charges. Table 13 shows the monthly and total electricity cost for the milk barn in the period from 2018 to 2019. By dividing the total monthly electricity costs with monthly usage, it is possible to determine the average monthly expense per kWh imported. These values are presented to the right in the table.

Table 13: The monthly and total electricity and grid costs for the milk barn in 2018 and 2019. Source: NTE

	2018				2019			
	Electricity cost [NOK]	Grid cost [NOK]	Total cost [NOK]	Average cost [NOK/kWh]	Electricity cost [NOK]	Grid cost [NOK]	Total cost [NOK]	Average cost [NOK/kWh]
January	6 633.06	11 048.17	17 681.23	0.786	8 363.61	11 506.27	1 9869.88	0.990
February	6 393.61	9 533.89	15 927.50	0.799	7 777.00	10 525.94	1 8302.94	0.979
March	7 861.33	10 214.33	18 075.66	0.826	8 396.69	11 340.34	1 9737.03	0.949
April	5 186.15	9 046.00	14 232.15	0.879	6 215.14	8 674.35	1 4889.49	0.951
May	3 766.50	3 571.35	7 337.85	0.572	5 312.82	3 700.98	9 013.80	0.665
June	4 102.12	3 424.63	7 526.75	0.613	4 162.18	3 361.04	7 523.22	0.621
July	5 008.44	3 533.14	8 541.58	0.674	4 699.58	3 574.98	8 274.56	0.638
August	4 340.71	3 555.42	7 896.13	0.619	5 220.42	3 691.60	8 912.02	0.660
September	5 219.99	3 872.95	9 092.94	0.637	5 317.71	3 828.49	9 146.20	0.643
October	6 024.15	9 496.14	15 520.29	0.887	6 033.61	7 521.86	13 555.47	0.867
November	8 823.15	10 347.96	19 171.11	1.052	8 379.20	10 463.62	18 842.82	0.896
December	4 278.62	10 683.68	14 962.30	0.765	7 899.59	10 476.39	18 375.98	0.857
Total	67 637.83	88 327.66	155 965.49	0.777	77 777.55	88 665.86	166 443.41	0.834

5.5 Existing photovoltaic systems at Mære Agricultural School

There are currently two existing photovoltaic systems already installed at Mære Agricultural School (see Attachment A.2 & A.3). One of these systems is installed on the roof of the boarding house (Figure 12 K), while the second system is installed on the roof of the cattle barn (Figure 12 E). The photovoltaic system on the boarding house consists of 216 photovoltaic modules, with an individual peak power of 270 W_p, which results in a total system power of 58.3 kW_p. In comparison, the photovoltaic system at the cattle barn consists of 120 photovoltaic modules, with a total installed system power of 34.8 kW_p. All excess energy produced from both photovoltaic systems is delivered to the grid.

The photovoltaic system at the boarding house is further elaborated in the subchapter below.

5.5.1 The photovoltaic system on the boarding house

As previously mentioned, the photovoltaic system consists of 216 modules (58.32 kW_p), each with an inclination angle of 43° and an azimuth angle of 0° (facing directly south). The photovoltaic modules are connected to four SolarEdge string inverters. All of these inverters have 3 MC4 pair inputs, meaning that a maximum of three strings can be attached to each of the inverters.

Figure 18 displays the monthly electricity production of the system, while Figure 19 shows the daily.

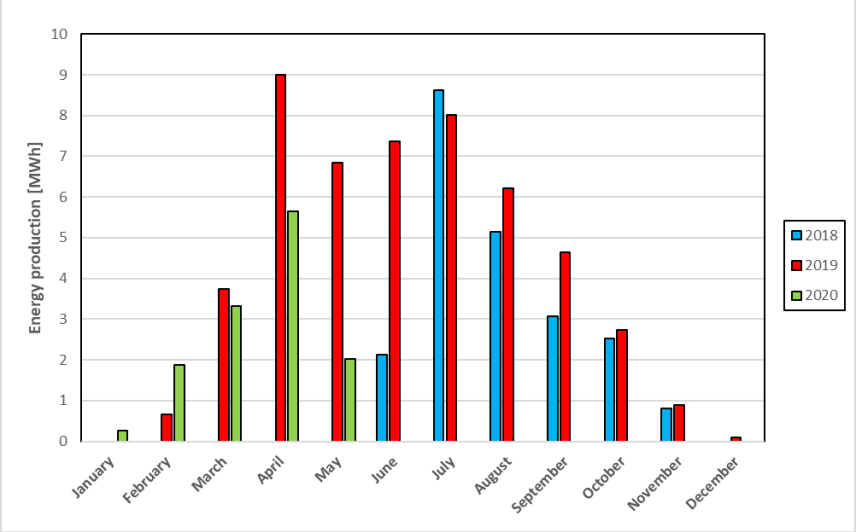

Figure 18: Monthly energy production (as of 11.05.2020).
Source: NTE & SolarEdge

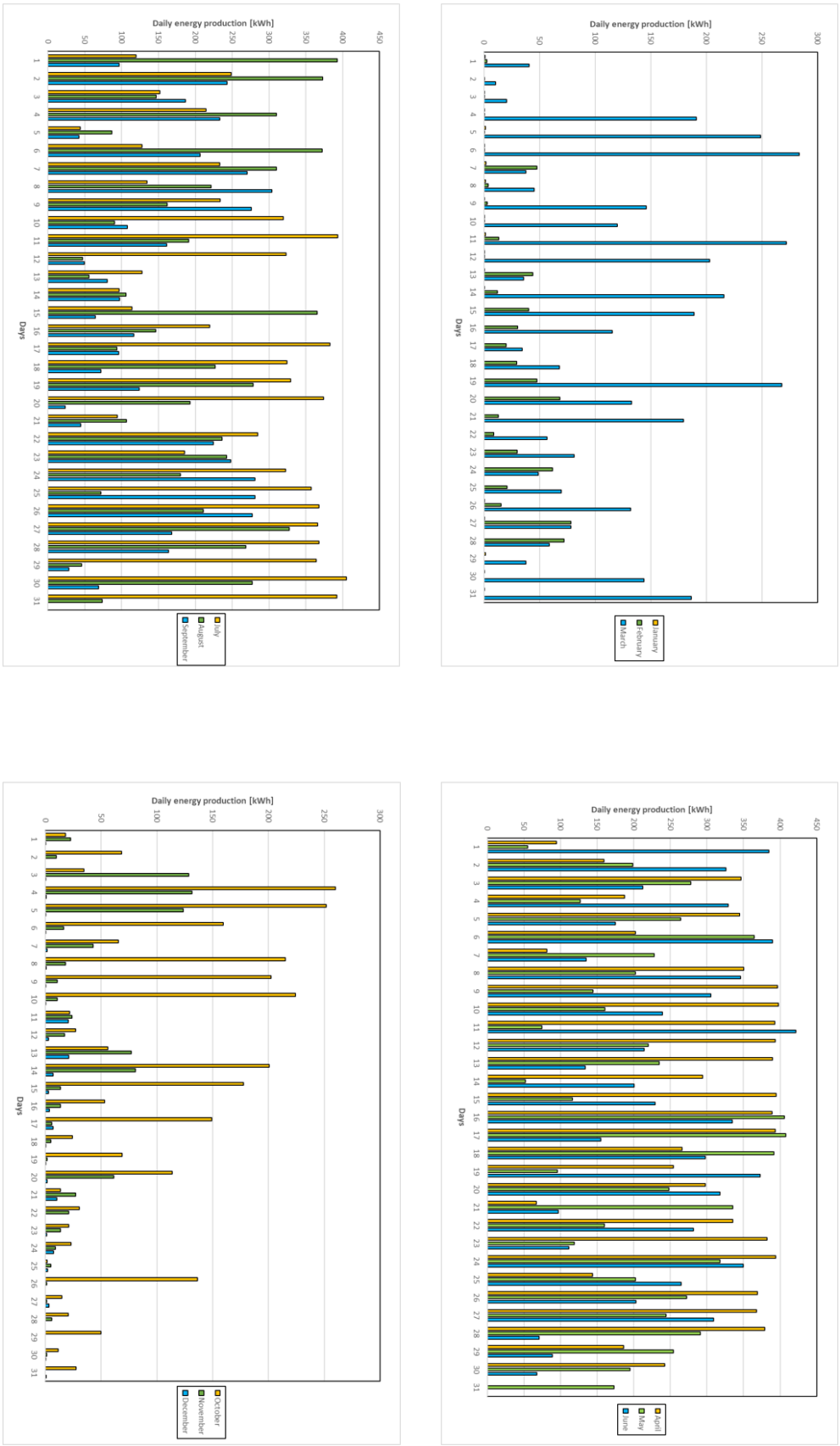

Figure 19: Daily energy production in 2018.
Source: NTE

6 Designing a photovoltaic system

According to (Norsk Solenergiforening, n.d.-c), photovoltaic modules have traditionally been used to generate electricity onsite on cabins and cottages in Norway. These traditional systems were usually very modest and ordinarily not attached to the Norwegian power grid. (Norsk Solenergiforening, n.d.-c) also explains that even though this was the tradition, photovoltaic systems have become much more common on the envelope surface of both commercial and residential buildings in Norway. And unlike the modest photovoltaic systems utilized on cabins, these systems are often connected to the grid, presenting the owner with the opportunity to export surplus electricity production.

Numerous significant factors have to be considered when designing photovoltaic systems from scratch. This is due to, as (Pearsall, 2017) explains, the fact that photovoltaic systems can have abundant different system configurations, and in the center of all this is the photovoltaic modules. In addition to these modules, each system also consists of several large and small components, often known under the commonly used term Balance-of-System components (BOS).

The necessary BOS components vary strongly with the photovoltaic system type. (EnergyInformative, n.d.-a) presents the three main types of photovoltaic systems, as well as benefits and the necessary BOS components. The three main system types are:

- Grid-tied systems
- Stand-alone systems
- Hybrid systems

All of the required BOS components can be seen in Table 14, and Figure 20 shows how the different system components operate together in a hybrid photovoltaic system.

Table 14: Necessary Balance-of-System components for each type of photovoltaic system. Source: (EnergyInformative, n.d.-a)

	Grid-tied photovoltaic system	Stand-alone photovoltaic system	Hybrid photovoltaic system
Balance-of-System components	• Grid-Tie Inverter (GTI) • Power Meter	• Solar Charge Controller • Battery Bank • DC Disconnect (*Additional*) • Off-Grid Inverter • Back-up Generator (*Optional*)	• Solar Charge Controller • Battery Bank • DC Disconnect (*Additional*) • Battery-Based Grid-Tie Inverter • Power Meter

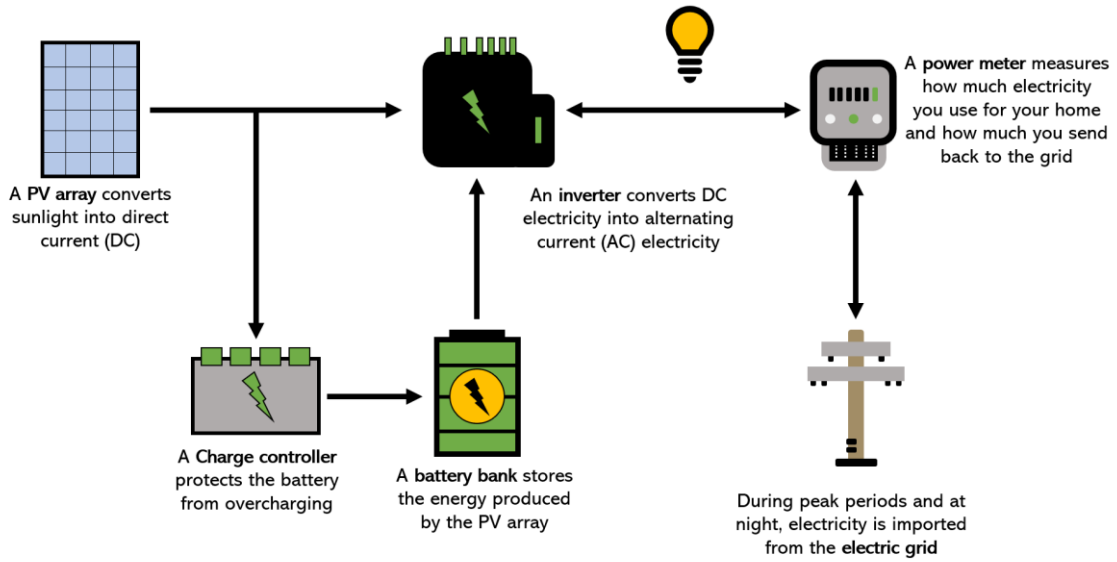

Figure 20: Illustration of a hybrid photovoltaic system and the relationship of its individual components. Source: Based on a figure from (Vekony, 2019)

The main characteristics of each photovoltaic system type are that grid-tied systems are connected to the local power grid, while stand-alone systems are not. Since the latter is not attached to any power grid, batteries are sometimes utilized to store the excess energy generation. Hybrid systems are photovoltaic systems that are connected to the power grid and also attached to battery storage.

In the following subchapters, the technology and characteristics for all of the necessary system components for designing a photovoltaic system will be presented. A suitable system component for the photovoltaic system at the milk barn will also be chosen at the end of each subchapter. The main focus is a grid-tied system, but information and components regarding battery storages will be also be presented.

6.1 Photovoltaic modules

As previously alluded to, a photovoltaic module is the main component of any photovoltaic system. This system component is responsible for converting sunlight into Direct current (DC) electricity in a process known as the photovoltaic effect. According to (Afework et al., 2018), the conversion process takes place in photovoltaic cells, and all photovoltaic modules consist of several arrays of these cells. A common framework of a photovoltaic cell is depicted in Figure 21. As can be seen in the figure, a cell is built up with several different layers of material, where each layer fulfills a specific purpose. Arguably, the most crucial layer in any photovoltaic cell is the semiconductor layer, as this is where the conversion takes place.

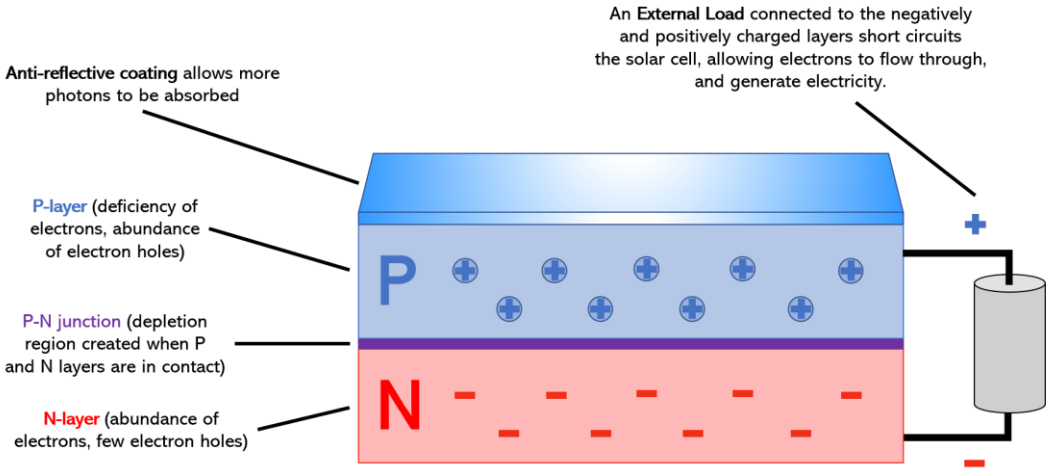

Figure 21: Framework of a photovoltaic (PV) cell.
Source: Based on a figure by (Sheir.org, n.d.)

6.1.1 Photovoltaic cell parameters

The amount of electricity a photovoltaic cell, and therefore module, can convert from sunlight is dependent on several characteristics of the photovoltaic cells. (Smets et al., 2016) states that the parameters that affect the performance the most are the Peak power (P_{Max}), Short-circuit current (I_{SC}), Open-circuit voltage (V_{OC}) and the fill factor of the cell. The size of these characteristics in the photovoltaic cell is commonly determined under Standard Test Conditions (STC).

Standard Test Conditions (STC)

As explained by (Dutta, 2018), Standard Test Conditions are fixed conditions, applied to photovoltaic modules after they have been produced, to determine the performance of the photovoltaic modules. The idea behind using the same circumstances for all of the photovoltaic modules is that it becomes more straightforward when comparing the performance of various module products from different manufacturers.

The Standard Test Conditions are:

- Irradiance = 1000 W/m^2
- Module temperature = 25 ºC
- Air mass = 1.5

Peak power (P_{Max})

According to (Skaugen & Romundstad, 2017), peak power is the obtained power of the photovoltaic module when examined under STC. It is commonly considered as the highest possible output from the photovoltaic module.

In practice, photovoltaic modules rarely produce power that is equivalent to the modules peak power, as stated by (Skaugen & Romundstad, 2017). The main reason behind this is external factors such as time of day, weather and geographical location. In addition to these factors, the generated power is also dependent on the module's inclination angle, surface temperature and efficiency.

According to (Smets et al., 2016), peak power is usually provided by the manufacturer of the photovoltaic module, but this is not always the case. If it is not provided, then it is possible to calculate the peak power by the following equation:

$$P_{Max} = I_{MPP} \cdot V_{MPP} \quad \textbf{[6.1]}$$

Where P_{Max} is the peak power [W_p], I_{MPP} is the current at the maximum power point [A], and V_{MPP} is the voltage at the same point [V]. The maximum power point is the point on the IV curve that results in the highest power output (see Figure 22).

Based on the information provided by (Honsberg & Bowden, n.d.-d), the IV curve can in brief terms be explained as a graphical illustration of the current-voltage relationship in a photovoltaic cell.

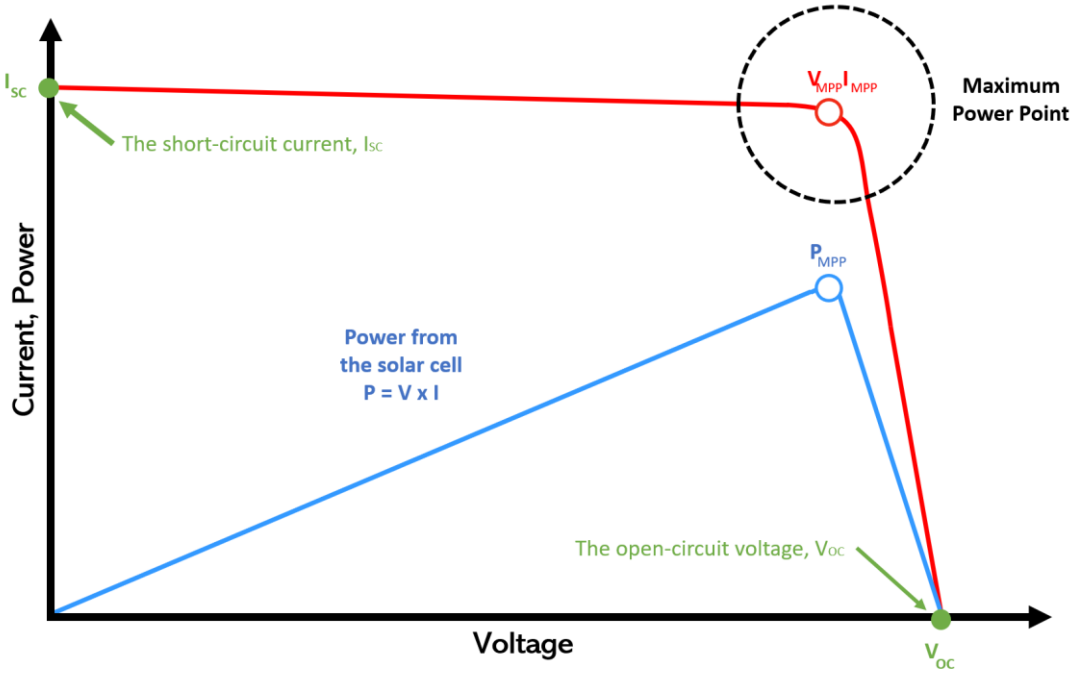

Figure 22: IV Curve.
Source: Based on a figure by (Honsberg & Bowden, n.d.-d)

Short-circuit current (I_{SC}) & open-circuit voltage (V_{OC})

According to (Honsberg & Bowden, n.d.-f), the short-circuit current is the electrical current going through the photovoltaic cell when the voltage across the photovoltaic cell is 0 V, and it is also the highest possible current running through the photovoltaic cell.

While, as explained by (Honsberg & Bowden, n.d.-e), the open-circuit voltage is the highest possible voltage achievable in a photovoltaic cell. This voltage level is achieved when the photovoltaic module is open-circuit, and the current flowing through the photovoltaic cell is 0 A.

The relationship between the short-circuit current and the open-circuit voltage can be seen in the graph in Figure 22.

Fill Factor (FF)

A photovoltaic cell's Fill Factor (FF) is a measure of the quality of that cell, as stated by (Smets et al., 2016). It can be mathematically represented as the ratio between the peak power (P_{Max}) of the photovoltaic cell and the product of the short-circuit current (I_{SC}) and open-circuit voltage (V_{OC}), as seen in the equation below:

$$FF = \frac{P_{MAX}}{I_{SC} \cdot V_{OC}} = \frac{I_{MPP} \cdot V_{MPP}}{I_{SC} \cdot V_{OC}} \quad \textbf{[6.2]}$$

FF can also be expressed graphically as the ratio between square A ($I_{MPP} \cdot V_{MPP}$) and B ($I_{SC} \cdot V_{OC}$), which is why (Honsberg & Bowden, n.d.-c) states that FF is a measure of the "squareness" of the photovoltaic cells. Both square A and B are seen in Figure 23.

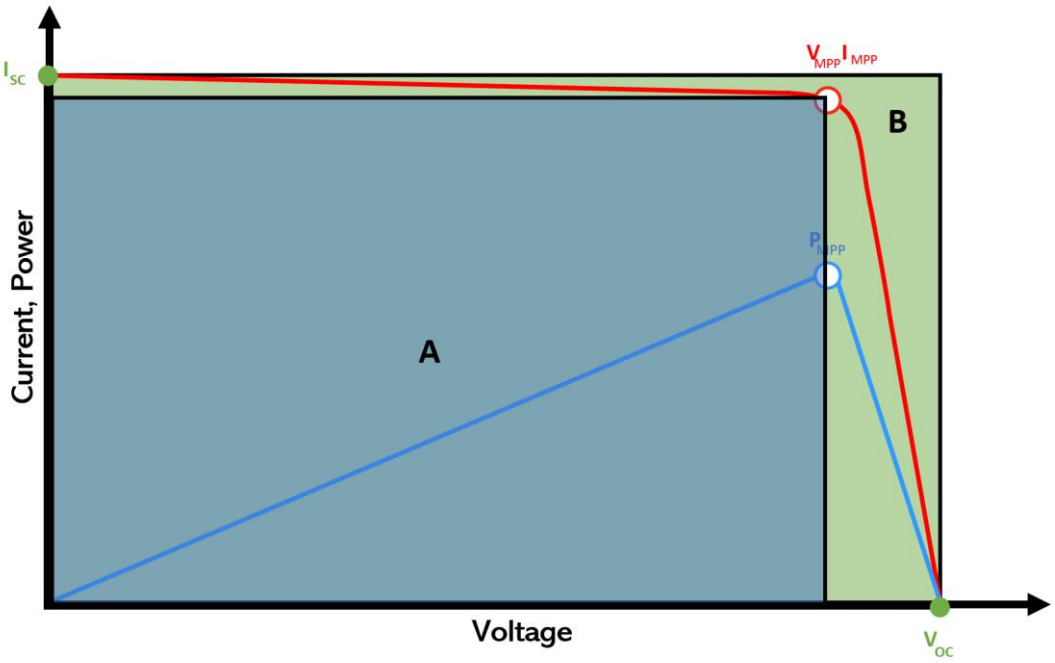

Figure 23: Example of a photovoltaic cell with a high Fill Factor.
Source: Based on a figure by (Honsberg & Bowden, n.d.-c)

Conversion efficiency

According to (Honsberg & Bowden, n.d.-g), the conversion efficiency is defined as the ratio between the maximum possible generated power and the incident power, or simply put, the ratio between the output electricity of the photovoltaic module and the input solar energy from the sun. Of all the parameters associated with photovoltaic modules, this is the parameter that is most frequently used when comparing the performance of different modules.

The conversion efficiency can be calculated with the following equation:

$$\eta_{PV} = \frac{P_{Max}}{P_{In}} \quad \textbf{[6.3]}$$

Where P_{Max} is the Peak Power [W_P], which can be calculated with Equation 6.1**,** and P_{In} is the solar input power on the surface of the photovoltaic modules [W].

The solar input power can also be expressed as:

$$P_{In} = I_S \cdot A_{PV} \quad \textbf{[6.4]}$$

Where I_S is the solar irradiance hitting the surface of the photovoltaic module [kWh/m^2], and A_{PV} is the surface area of the photovoltaic module [m^2].

Equation 6.3 can also be combined with Equation 6.1, 6.2 and 6.4 to make the following equation:

$$\eta_{PV} = \frac{I_{MPP} \cdot V_{MPP}}{I_S \cdot A_{PV}} = \frac{I_{SC} \cdot V_{OC} \cdot FF}{I_S \cdot A_{PV}} \quad \textbf{[6.5]}$$

As shown above, there are several ways to calculate the conversion efficiency based on measurements with STC on the photovoltaic modules. It is often not necessary to calculate these values, as the conversion efficiency is almost always presented with the other properties by the manufacturer.

6.1.2 Available technologies for photovoltaic modules

The majority of the technologies and module products available on the market can be separated into either crystalline silicon or thin-film technology products. The products each have their benefits and drawbacks. It is therefore necessary to consider factors and limitations specific to the building and desired system characteristics before choosing a product.

According to (Glunz et al., 2012), crystalline silicon modules have been the dominant type of photovoltaic modules since it was first introduced in the 1950s. Crystalline silicon modules are subdivided into either Monocrystalline silicon (Mono-Si), Polycrystalline silicon (Poly-Si) or ribbon silicon modules. Of these three, Mono-Si and Poly-Si cells are usually the most common.

(Breeze, 2016) explains that Mono-Si cells are constructed from pure silicon crystals, while Poly-Si cells are assembled from fragments of several different silicon crystals. (Sendy, n.d.-b) states that Mono-Si cells have the highest efficiency of the bunch at around 22 %, while Poly-Si cells usually have a conversion efficiency between 14 to 16 %. Both products based on Mono-Si and Poly-Si usually last somewhere around 25 years.

According to (Breeze, 2016), photovoltaic cells based on thin-film technology are the main competitor to crystalline silicon cells. The main reason for this is that the process of manufacturing thin-film cells is both more manageable and more affordable than it is for crystalline silicon cells. The major drawback with thin-film products, on the other hand, is that they have lower efficiencies compared to crystalline silicon cells. The three most common thin-film technologies are amorphous silicon, CdTe and CIGS, with CdTe as the main alternative, as it is more efficient than amorphous silicon and more affordable to manufacture than CIGS. (Sendy, n.d.-b) estimates that the commercialized thin-film products have an efficiency of around 10 to 15 %.

6.1.3 Connection principles

When designing a photovoltaic system, the electrical characteristics of the photovoltaic modules must either be below or match the maximum inputs of the inverters and, if used, charge controllers. As explained by (Rogers, 2018), this concern especially applies to the maximum voltage across the photovoltaic system, as a too high system voltage may irreparably damage system components.

(Pop, n.d.) suggests that the maximum voltage for a grid-tie inverter should be minimum 75 V and maximum 750 V. For hybrid systems, the maximum voltage should be able to handle back-up loads and the DC power delivered from the modules simultaneously. There are of course inverters designed to handle larger system voltages than 750 V.

The consideration of maximum system voltage should come early in the design process, as one possible way to reduce or increase this voltage is by connecting photovoltaic modules in series and parallels. According to (Brown, 2019), the process of wiring together photovoltaic modules is known in the solar industry as "stringing", and two or more modules connected in a series is known as a "string".

The benefits and drawbacks with series and parallel connections are described in the subchapters below.

Series

(Solar Reviews, 2018) explains that the connection between photovoltaic modules is called a series when each of the photovoltaic modules only connects to the next module, basically creating a line. Figure 24 shows the wiring principle for photovoltaic modules in a series. One can consider photovoltaic modules somewhat similar to batteries in the way that the photovoltaic modules have to be wired from the positive terminal of the first module to the negative terminal of the second.

Photovoltaic modules are usually connected in series to keep the maximum electric current through the system constant, no matter the number of photovoltaic modules added to the series. According to (UnderstandSolar, 2017), the benefit of using series connections is that a more modest wiring-thickness is required, resulting in smaller expenses. The main drawback is that the current running through the series will only be as high as the current running through the most unfavorable module.

What this essentially means is that if one module is shaded, soiled or damaged, then this will affect the production of the entire photovoltaic series.

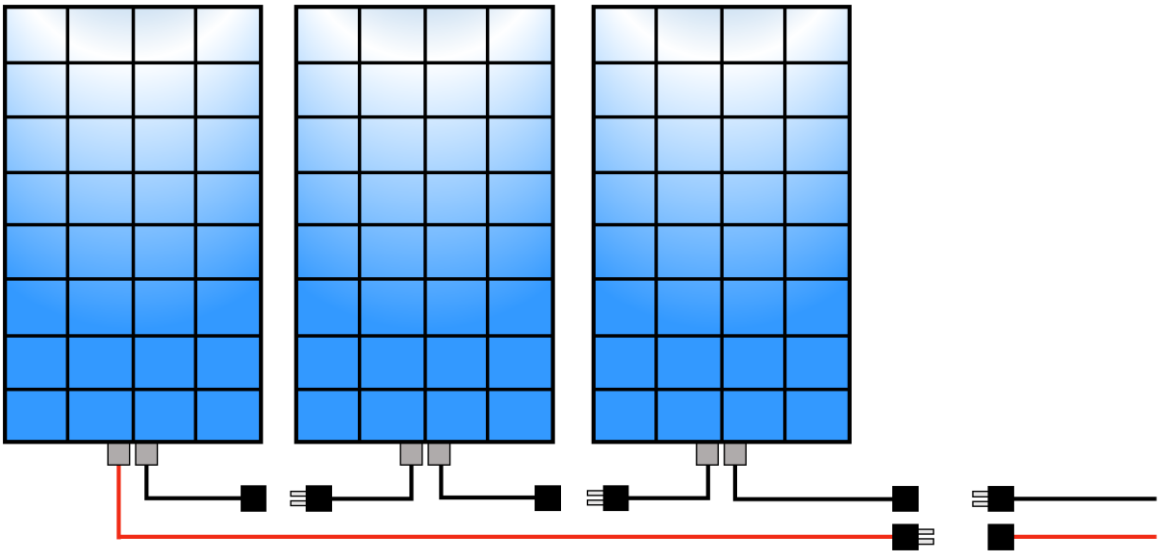

Figure 24: Photovoltaic modules connected in series.
Source: Based on a figure by (Parked In Paradise, 2020)

(Rossing, 2011) provides the following equations for calculating the maximum voltage, current and power in a photovoltaic system where the modules are wired in series:

$$V_{n,s} \approx n_s \cdot V_{OC} \quad \textbf{[6.6]}$$

Where $V_{n,s}$ is the maximum voltage across the photovoltaic modules in the series [V], n_s is the number of modules in the series, and V_{OC} is the open-circuit voltage of each individual module [V/module]. It should be noted that the equations presented above and below require that all photovoltaic modules are the same type and product. Meaning that the open-circuit voltage, peak power and short-circuit current are the same for all photovoltaic modules in the system.

As previously mentioned, the maximum current for the whole series is equal to the short-circuit current of one of the photovoltaic modules.

The maximum peak power of the photovoltaic system can be calculated with:

$$P_{n,s} \approx n_s \cdot P_{Max} \quad \textbf{[6.7]}$$

Where $P_{n,s}$ is the maximum peak power of the photovoltaic modules in series [W_p], and P_{Max} is the peak power of a single photovoltaic module in series [W_p/module].

Parallel

According to (Brown, 2019), the process of wiring photovoltaic modules in parallels is a little more complicated than for an ordinary series connection. In a photovoltaic system where the photovoltaic modules are attached in parallel, all of the positive terminals of the modules are wired together, and all the negative terminals are wired together (see Figure 25).

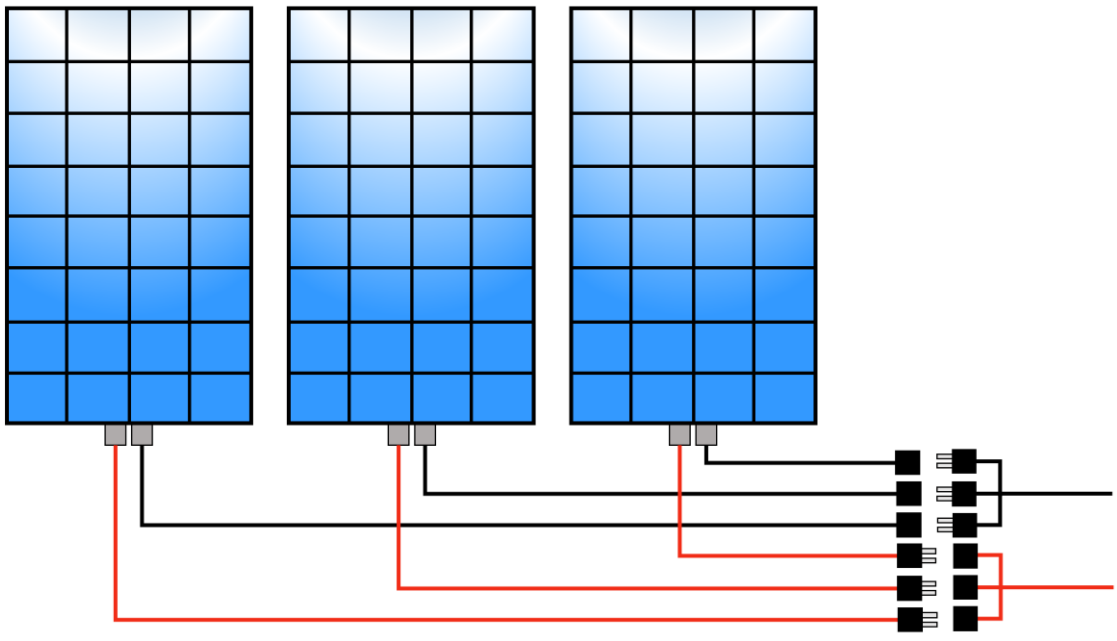

Figure 25: Photovoltaic modules connected in parallel.
Source: Based on a figure by (Parked In Paradise, 2020)

As explained by (UnderstandSolar, 2017), a benefit with parallel-connected photovoltaic modules is that no matter how many strings are attached in parallel, the system voltage remains the same as if it was only one photovoltaic module. The electrical current, on the other hand, increases with each additional parallel module.

In addition to the advantage described above, (Brown, 2019) suggests that the main benefit with parallel-connected photovoltaic modules is that even if some of the photovoltaic modules are partially shaded, the electricity production from the remaining modules remains mostly unaffected. (UnderstandSolar, 2017) explains that one of the principal drawbacks with parallel connections are the need for thicker cables for handling the increased electric current.

(Rossing, 2011) also provides equations for calculating maximum peak power, current and voltage in parallel-connected photovoltaic systems:

$$I_{n,p} \approx n_p \cdot I_{SC} \quad \textbf{[6.8]}$$

Where $I_{n,p}$ is the maximum current through the parallel-connected photovoltaic system [A], n_p is the number of modules wired in parallel, and I_{SC} is the short-circuit current for each of the photovoltaic modules [A/module]. For the parallel-connected photovoltaic system, the maximum voltage across the system is equal to the open-circuit voltage of one photovoltaic module.

The following equation is used for determining the maximum peak power of the parallel-connected photovoltaic system:

$$P_{n,p} \approx n_p \cdot P_{Max} \quad \textbf{[6.9]}$$

Where $P_{n,p}$ is the maximal installed peak power delivered by all the photovoltaic modules in parallel [W_p], and P_{Max} is the peak power of one single photovoltaic module used in the system [W_p/module].

Series-parallel connection

According to (Renogy, n.d.), a series-parallel connection is a connection principle, which utilizes both of the previously introduced connection types. Larger photovoltaic systems may obtain electric currents and voltages, which are significantly higher than the designed limits for both the charge controller and the inverters. This connection principle introduces creative approaches to avoid going above these limits. The number of photovoltaic modules in the parallel series must be equal. If they are not, the result is large losses of power.

The following formula can be used to determine the maximum peak power of the system:

$$P_{tot} \approx n_s \cdot n_p \cdot P_{Max} \quad \textbf{[6.10]}$$

Where P_{tot} is the total installed peak power of the system [W_P], and as previously mentioned, n_s is the number of photovoltaic modules in series, n_p is the number of photovoltaic modules in parallel, and P_{Max} is the peak power of one single photovoltaic module used in the system [W_p/module]. Equation 6.6 and 6.8 can be used to determine the maximum voltage and current through the system, respectively.

A series-parallel connected system can be seen in Figure 26.

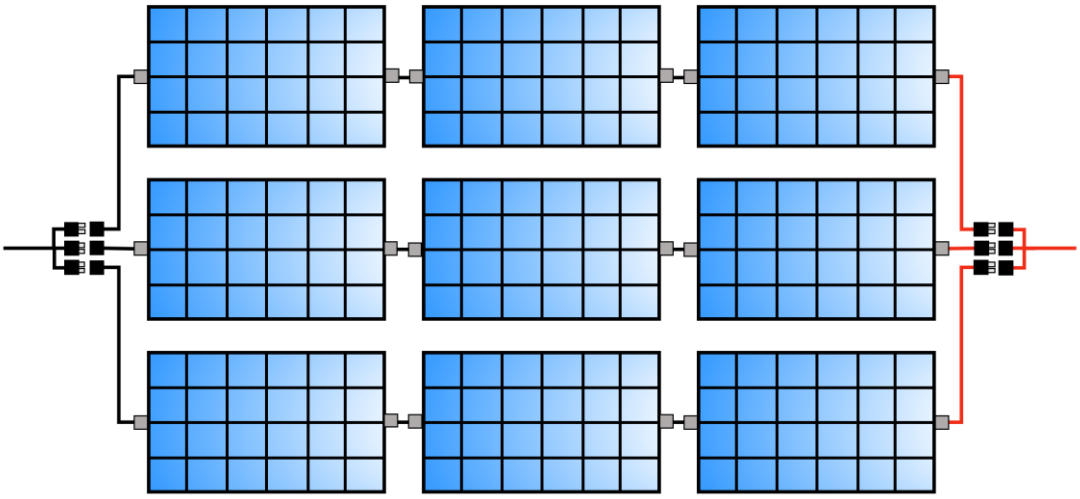

Figure 26: Series-parallel connected photovoltaic modules.
Source: Based on a figure by (Brown, 2019)

6.1.4 The cost of PV Modules

There are several different photovoltaic modules on the market, and the cost of these products varies considerably with the peak power, efficiency, utilized technology and the manufacturer. (Schachinger, 2020) maps the monthly EU spot prices of photovoltaic modules, and in February 2020 the average consumer should expect to pay 0.26 €/W_p (or 2.51 NOK/W_p) for general mainstream crystalline modules, and 0.34 €/W_p (or 3.72 NOK/W_p) for all black modules with a peak power between 200 to 340 Wp. It should be noted that these prices are tax-free and for customs-cleared photovoltaic modules.

There is little information available on labor charges related to the installation of photovoltaic modules, but (EnergyInformative, n.d.-b) estimates that the total expense associated with installing a complete photovoltaic system is roughly 10 % of the total photovoltaic system component costs. If the price of the complete system is 100 000 NOK, then one should be expected to pay an additional 10 000 NOK in labor expenses, resulting in a total system cost of 110 000 NOK.

Enova

According to (Enova, 2020b), it is possible to receive 10 000 NOK in support for privately installing photovoltaic systems, with additional 1 250 NOK per kW_p up to 15 kW_p. What this means is that it is possible to reduce the total cost of the photovoltaic modules with a maximum of 28 750 NOK.

It should be noted that the constant rate of 10 000 NOK is going to be reduced to 7 500 NOK from July 1st, 2020.

6.1.5 Determining the required area for photovoltaic modules

The following simplified approach and equations are based on information provided by (SunPower, n.d.). There are several steps one must go through when determining the necessary ground, facade or roof area for photovoltaic modules, and the first step is usually to determine:

- How much energy does the building consume on an average yearly basis?
- How much surface area is available for the photovoltaic modules?
- What are the solar conditions and peak sun-hours at the desired location?
- What are the peak power and relative efficiency of the photovoltaic modules considered?

The next step is to estimate how much of the annual energy demand that should be covered with a photovoltaic system. Depending on the size of the annual consumption and the available surface area, the coverage rate could be either very high or low.

When the designer has decided on a coverage rate, the following equation can be used to determine the necessary installed power to cover such a demand:

$$P_{Demand} = \frac{CR \cdot \frac{E_{Year}}{365\ days} \cdot 1000 \frac{W}{kW}}{T_{Peak-hour}} \quad \textbf{[6.11]}$$

Where P_{Demand} is the necessary amount of power that must be installed to cover the desired energy consumption [W_p], CR is the planned coverage ratio [-], E_{Year} is the annual energy consumption of the building [kWh], and $T_{Peak-hour}$ is the number of average daily sun peak-hours [h].

The necessary number of solar modules can then be calculated with:

$$n_{PM} = \frac{P_{Demand}}{P_{Max}} \quad \textbf{[6.12]}$$

Where n_{PM} is the required number of photovoltaic modules to cover the CR percent of the annual energy consumption, and P_{Max} is the peak power of the chosen photovoltaic modules.

Photovoltaic modules infrequently experience conditions where they can produce electricity at peak power for longer periods, and there are also energy losses linked to different components in the photovoltaic systems. A safety factor can therefore be introduced to Equation 6.11 to increase the likelihood of covering enough energy demand.

6.1.6 Photovoltaic modules for the milk barn

The following information is provided for the milk barn at Mære Agricultural School:

- The annual energy demand was 200 647 kWh in 2019.
- The available roof surface area is about 1340 m^2, with 670 m^2 facing south.
- The annual peak sun-hours at Mære, with an inclination angle of 26^o, is on average 1 013.6 hours, with a daily average of 2.77 or 2 hours and 47 minutes.

The peak sun-hours was roughly estimated for Mære, at an inclination angle of 26^o, by using the interactive tools provided by (European Commission, 2020).

By using the information presented above in combination with Equation 6.11, the necessary electricity production per daily peak sun-hour, to cover 100 % of the annual energy consumption, is 198 454 W.

Photovoltaic module products

The extensive photovoltaic module database provided by (ENF Solar, 2020) was used to find relevant photovoltaic modules for the milk barn. Table 15 shows several photovoltaic modules, and their respective performance, technology, short-circuit current, open-circuit voltage, efficiency, peak power and temperature coefficient for P_{Max}.

Equation 6.12 was used to find the number of photovoltaic modules necessary to cover 15, 30, 50 or 100 % of the annual energy demand. The number of modules was then multiplied with the dimensions of the different products presented in Table 15 to try to determine the necessary roof surface area. The results of these calculations can be seen in Figure 27. The required number of photovoltaic modules for each of the coverage ratios and products are presented in Table 16.

Table 15: Possible photovoltaic module products.
Source: (ENF Solar, 2020)

Products	Manufacturer	Panel Dimensions (H/W/D) [mm]	Technology	Panel Efficiency [%]	Maximum Power Pmax [Wp]	Open-circuit Voltage [V]	Short-circuit Current [A]	Temperature Coefficient of Pmax [%/°C]
PERC 300W 60 CELLS	Yuhuan Sunpro Power Co., Ltd.	1640x992x35	Monocrystalline	18.3	300	39.9	9.64	-0.4
TP330PP-72	Topsky Electronics Technology (HK) Co., Ltd.	1956x992x40	Polycrystalline	17.0	330	49.9	9.14	-0.4
AE M6-60	AE Solar	1650x992x35	PERC[1]	18.6	305	39.6	9.66	-0.4
Soluxtec Das Modul Poly Serie	Soluxtec GmbH	1640x991x35	Polycrystalline	17.6	285	38.8	9.42	-0.4
FSM 360W	Future Science and Technology Co., Ltd.	1960x992x40	Monocrystalline	18.6	360	46.7	9.89	-
HC 400W Mono	Powitt Solar Co., Ltd.	2024x1004x40	Monocrystalline	19.7	400	49.8	10.36	-0.4
TTN-250P60	Zhejiang TTN Electric Co., Ltd.	1640x992x40	Polycrystalline	15.4	250	37.6	8.90	-0.4

[1]PERC stands for Passivated Emitter and Rear Cell

The red line in the figure indicates the maximum available south-facing roof area (670 m^2). As the graph clearly shows, it is not possible to cover 100 % of the energy demand with photovoltaic modules, as there is not enough south-facing roof area available.

In this master thesis, the focus will be to try to cover about 30 % of the annual energy consumption with solar energy.

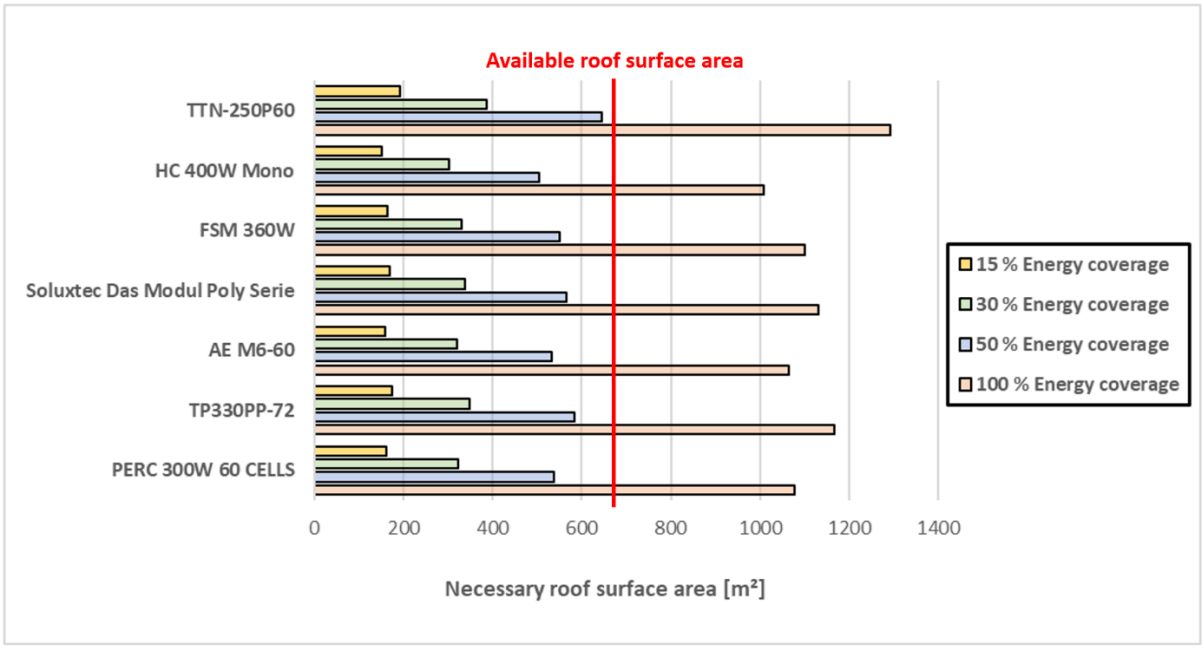

Figure 27: Necessary south-facing roof area to cover 15, 30, 50 or 100% of the annual energy demand.

Table 16: Required number of modules to cover 15, 30, 50 or 100 % of the average annual energy consumption.

	PERC 300W 60 CELLS	TP330PP-72	AE M6-60	Soluxtec Das Modul Poly Serie	FSM 360W	HC 400W Mono	TTN-250P60	Average
Number of modules for 100 %	662	601	651	696	551	496	794	**635.9**
Number of modules for 50 %	331	301	325	348	276	248	397	**318.0**
Number of modules for 30 %	198	180	195	209	165	149	238	**190.6**
Number of modules for 15 %	99	90	98	104	83	74	119	**95.3**

The PERC 300W 60 CELLS photovoltaic modules are chosen for the milk barn. This photovoltaic module was preferred based on its implemented technology (Mono-Si), relatively high efficiency, and low open-circuit voltage. For aesthetic symmetry on the roof of the building, ten rows of photovoltaic modules should be placed horizontally along the width of the roof. Unfortunately, it is not possible to have 198 photovoltaic modules equally divided into ten rows. The number of photovoltaic modules is therefore increased from 198 to 200, with 20 modules on each row (see Figure 28). These photovoltaic modules will account for 325.4 m^2 of the available roof area.

The installed peak power of the photovoltaic system, independent on the connection method, is 60 kW_p.

The optimal connection method for these 200 photovoltaic modules will be discussed in Chapter 6.2.3: *Choosing solar inverters for the milk barn*. The reason for this is that the remaining Balance-of-System components have limitations related to the DC voltage and current delivered from the photovoltaic modules.

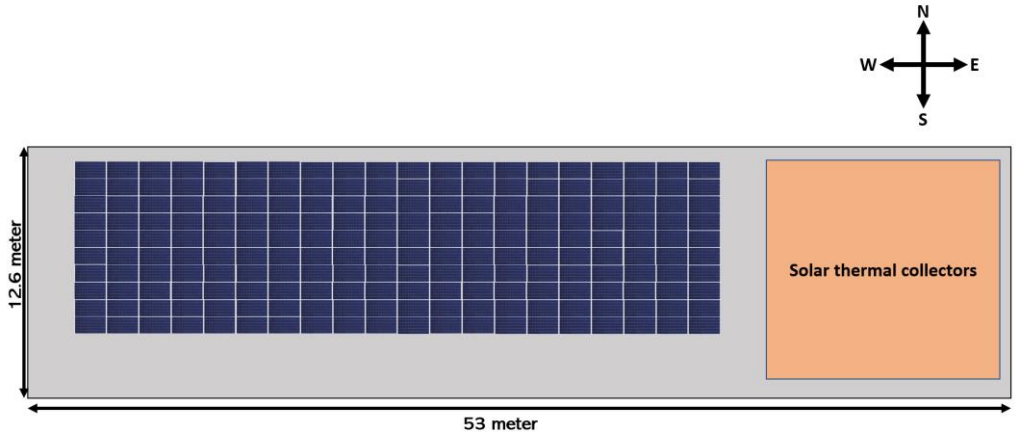

Figure 28: Illustration of the possible photovoltaic module layout on the south-facing roof.

Cost of photovoltaic modules for the milk barn

If the information presented in Chapter 6.1.4: *The cost of PV Modules* is combined with the information on the photovoltaic module system described above, then it is possible to estimate the cost of all these photovoltaic modules. Based on the information in Chapter 6.1.4: *The cost of PV Modules*, and the fact that PERC 300W 60 CELLS photovoltaic modules are all black, an investor should expect a price of about 3.72 NOK/W_p with a total charge of 223 200 NOK (excluding tax).

6.2 Solar inverter

The central objective of solar inverters is to convert the DC electricity produced by the photovoltaic modules into usable Alternating Current (AC). As such, the inverters are a necessary component in any photovoltaic system, since household appliances and technical equipment run on AC.

(Norton et al., 2011) explains that the performance of the inverters depends on the inverters point of work, threshold of operation, output waveform, harmonic distortion, frequency, MPPT tracker(s) and the transformer. Based on the inverters output waveform, there are mainly three available inverter types. These are inverters with sine wave, modified sine wave or square wave output.

The difference between the output waveforms can be seen in Figure 29.

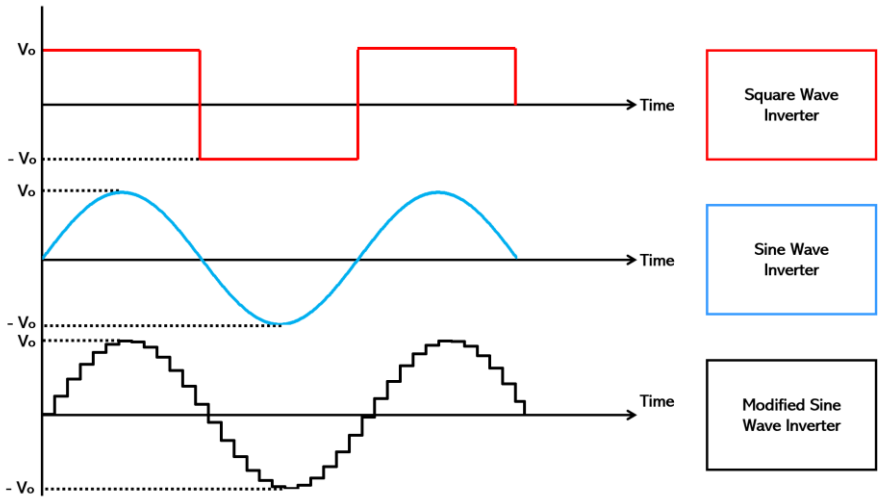

Figure 29: The three main output waveforms available from inverters.
Source: Based on a figure by (Kansagara, 2018)

According to (Norton et al., 2011), the advantage with sine wave inverters is that most pieces of electrical equipment that are available, commercially, are intended for sine wave operation. The modified sine wave inverters are also able to operate a vast number of electric appliances, but square wave inverters can generally only operate quite simplistic types of equipment.

Briefly explained by (Detjen, 2018), Maximum Power Point Tracker (MPPT) is a technology found in most modern solar inverters. The purpose of MPPT is to optimize the power output during unfavorable solar conditions.

6.2.1 Solar inverter products

According to (EnergySage, 2020b), there are three main kinds of inverter products available for photovoltaic systems on the market. These products are:

- String inverters
- Power optimizers
- Micro-inverters

(EnergySage, 2020b) explains that power optimizers and micro-inverters are also known as Module-Level Power Electronics (MLPEs). These are further defined by (Brown, 2018b) to be devices that are incorporated into the photovoltaic system to achieve higher performance during normal and certain unfavorable conditions, as well as providing other system benefits.

String inverters

String inverters are also known as centralized inverters and are, according to (EnergySage, 2020b), the far more commonly installed inverter product. As a result, the vast majority of products available on the market today are string inverters. They are also more affordable than micro-inverters. (Zipp, 2013) lists several benefits with string inverters, and among the beneficial properties listed are their reliability, accessibility and high efficiency. They are therefore well-suited for residential and small commercial systems.

According to (EnergySage, 2020b), special consideration must be given to the surrounding area as the main drawback with string inverters are the effect the photovoltaic module with least favorable conditions has on the remaining photovoltaic modules. This effect can be considered as a bottleneck, where the production of each photovoltaic module can only be as high as the production at the most shaded, soiled or damaged photovoltaic module.

An illustration of a single string inverter installed in a photovoltaic system is shown in Figure 30.

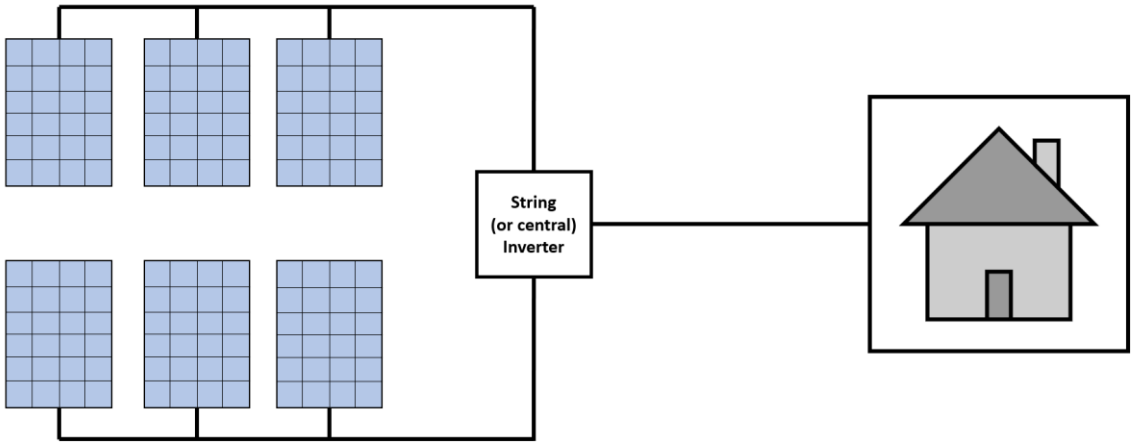

Figure 30: Photovoltaic modules attached to a string inverter.
Source: Based on a figure by (Solar Tribune, n.d.)

String inverters + Power optimizers

As stated by (EnergySage, 2020b), power optimizers are additional pieces of equipment that can be installed with string inverters in photovoltaic systems. The required number of power optimizers in a photovoltaic system varies with the type of optimizer, as some power optimizers can be attached to more than one photovoltaic module. At most, one power optimizer for each of the photovoltaic modules (see Figure 31). Unlike the string inverter which converts DC electric energy into AC, power optimizers "conditions" the DC electricity and sends it to the string inverter. Power optimizers can therefore be seen as DC to DC converters.

(EnergySage, 2020b) further explains that power optimizers increase the performance of the string inverter(s) in the photovoltaic system and that they also lessen the bottleneck effect that partial shading or soiling can have on the total electricity production. Installing power optimizers with a string inverter can be considered a compromise between only having string inverters or micro-inverters, as it is less costly than micro-inverters, but also not as effective.

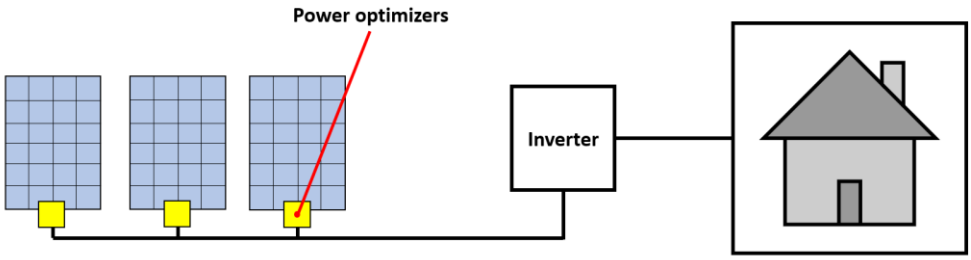

Figure 31: String inverter combined with power optimizers.
Source: Based on a figure by (Solar Tribune, n.d.)

Micro-inverters

According to (EnergySage, 2020b), micro-inverters, similar to power optimizers, are installed at the actual location of the photovoltaic modules (see Figure 32). But, unlike power optimizers, which as mentioned can be seen as DC to DC converters, micro-inverters convert DC electricity into AC. (EnergySage, 2020b) states that the most prominent advantage with micro-inverters is their ability to cancel out the negative impacts of partial shading. Since the DC into AC conversion happens at each photovoltaic module, the bottleneck difficulty does not take place. In principle, this means that the electricity production at each photovoltaic module becomes almost independent of the other modules.

(Sendy, n.d.-a) states that an additional benefit with micro-inverters is that they usually arrive with preinstalled monitoring software, making it possible to observe the production of every single photovoltaic module. By utilizing monitoring software, it is also easier to determine technical errors with the photovoltaic modules. It should be noted that this additional feature is also often included with power optimizers.

According to (EnergySage, 2020b), the single most prominent drawback with micro-inverters is that they are expensive. Since several of them are required for one system, the total cost of these micro-inverters quickly becomes very steep.

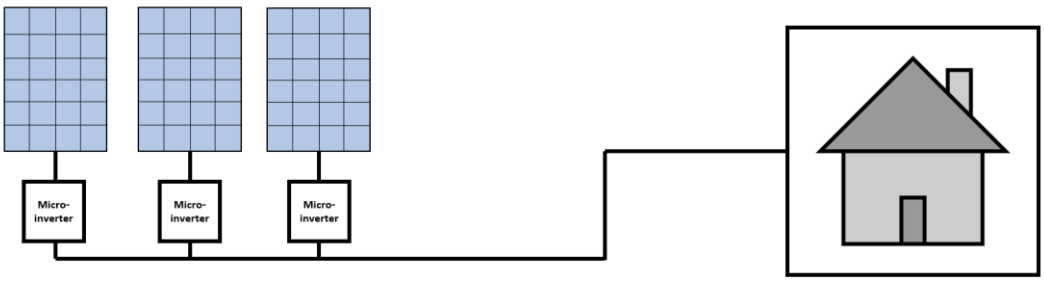

Figure 32: Micro-inverters.
Source: Based on a figure by (Solar Tribune, n.d.)

6.2.2 Factors determining the location of the string inverter(s)

According to (Contrino, n.d.), a usual rule of thumb is to install string inverters as close to the existing grid equipment as possible. The general location can be both inside and outside the building, but it should be easily accessible for maintenance. Also, the string inverter should not be located in direct sunlight and should therefore either be installed indoors or at a shaded location outside.

(SolarEdge, n.d.) explains that there should be at least a 20 cm clearance above and below the string inverter. Also, there should be 10 cm available space to the left and right of the inverter, but if two inverters are placed next to each other, the distance should be minimum 20 cm (see Figure 33). The distances can also be enlarged, allowing for easier access to the inverter fans during maintenance.

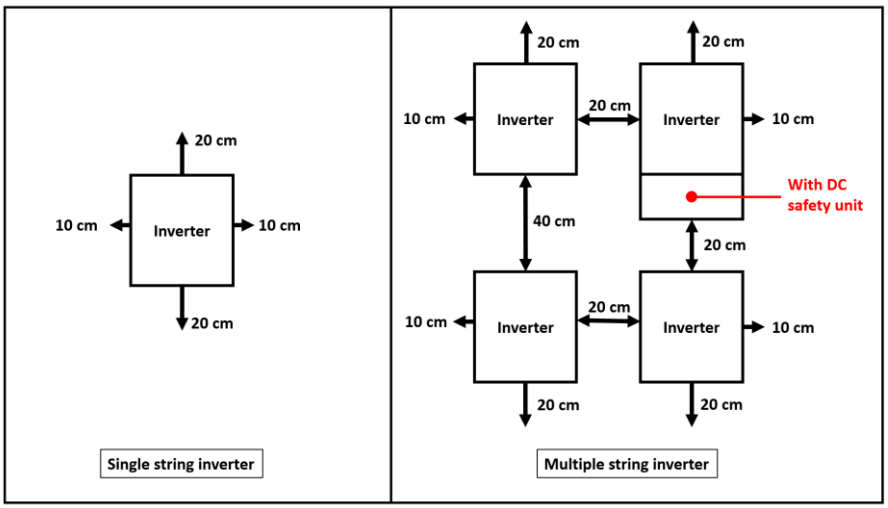

Figure 33: Recommended string inverter clearance when installing one or multiple string inverters.
Source: Based on a figure from (SolarEdge, n.d.)

According to (Contrino, n.d.), a final important consideration is the installed height of the string inverter. The inverter should be installed at a reasonable height above ground level, to avoid damaging the inverter during a flood or rising water level incident.

6.2.3 Choosing solar inverters for the milk barn

It is crucial to consider the electrical characteristics of the photovoltaic modules when choosing an inverter system solution for the milk barn. The properties associated with the PERC 300W 60 CELLS photovoltaic modules were presented in Table 15 in Chapter 6.1.6: *Photovoltaic modules for the milk barn*.

What was not mentioned in Chapter 6.1.6: *Photovoltaic modules for the milk barn*, was that the open-circuit voltage and short-circuit current is highly dependent on the operating temperature of the photovoltaic module. What this means is that even if the open-circuit voltage for the photovoltaic module is 39.9 V during STC, it can actually be much higher, which is also the case for the short-circuit current.

The solar inverters have to be able to handle these voltage and current levels during high and low operating temperatures. Because if they are not, the inverter may be damaged and has to be replaced by a new, adding to additional costs and unnecessary photovoltaic system problems.

The datasheet for the various photovoltaic modules often contains temperature coefficients for both the open-circuit voltage and short-circuit current, and these coefficients indicate that the open-circuit voltage increases with decreasing operating temperature, while the short-circuit current increases with increasing operating temperature.

(Brown, 2019) provides the following formula for calculating the open-circuit voltage at different operating temperatures:

$$V_{OC,oper} = \left(1 - \left(\left(T_{STC} - T_{oper}\right) \cdot \frac{TC_{V_{OC}}}{100}\right)\right) \cdot V_{OC,STC} \qquad \textbf{[6.13]}$$

Where $V_{OC,oper}$ is the open-circuit voltage of the photovoltaic module [V] at operation temperature T_{oper} [^{o}C], T_{STC} is the standard test condition temperature [^{o}C], $TC_{V_{OC}}$ is the open-circuit voltage temperature coefficient of the module [%/^{o}C], and $V_{OC,STC}$ is the open-circuit voltage at standard test conditions [V].

The information presented by (Brown, 2019) can also be used to determine the short-circuit current at different operating temperatures:

$$I_{SC,oper} = \left(1 - \left(\left(T_{STC} - T_{oper}\right) \cdot \frac{TC_{I_{SC}}}{100}\right)\right) \cdot I_{SC,STC} \qquad \textbf{[6.14]}$$

Where $I_{SC,oper}$ is the short-circuit current of the photovoltaic module [A] at an operating temperature of T_{oper} [^{o}C], $TC_{I_{SC}}$ is the short-circuit current temperature coefficient of the module [%/^{o}C], and $I_{SC,STC}$ is the short-circuit current at standard test conditions [A].

As the simulation software used in this master thesis uses an operating temperature limit of -10 and 70 ^{o}C, the maximum open-circuit voltage and short-circuit current will be calculated for these values. The results of using Equation 6.13 and 6.14 with these operating temperatures can be seen in Table 17. If the maximum DC voltage input into the string inverter is 1000 V, then the maximum number of photovoltaic modules in series should not exceed 22, when accounting for operating temperature.

Table 17: Maximum short-circuit current and open-circuit voltage.

	Short-circuit current [A] (Operating temperature 70°C)	Open-circuit voltage [V] (Operating temperature -10°C)
PERC 300W 60 CELLS	11.787	43.940

Due to the size of the photovoltaic system, it would be difficult to find a single string inverter which meets the electric conditions required to convert DC electricity from 200 photovoltaic modules into AC. Three different solar inverter system will therefore be introduced to the photovoltaic system at the milk barn, and later compared using the simulation software Polysun.

System 1: Delta Solar Solution and SMA Solar Technology

According to (Delta Solar Solutions, 2020), the company known as Delta Solar Solution was founded in 1971. They specialize in solar inverters for residential, commercial and large-scale photovoltaic systems. Their main headquarter is located in Taiwan, but they also manufacture solar inverters for China, Europe, Japan, Singapore, Thailand and the U.S.

A suitable photovoltaic string inverter for the photovoltaic modules at the milk barn is the M50A Grid PV Inverter (see Figure 34). The inverter is manufactured by Delta Solar Solutions and is according to them (see Attachment A.6), a perfect fit for large-scale photovoltaic systems built in the agriculture sector. Unfortunately, due to restrictions with the string inverter, specifically regarding the maximum input current of 50 A per MPP Tracker, the single string inverter is not enough to convert all the DC power, delivered from the photovoltaic modules, into AC power.

The M50A Grid PV Inverter is a relatively large string inverter, and it is therefore possible to attach 176 PERC 300 W 60 CELL photovoltaic modules at most. Figure 35 shows how the photovoltaic modules should be connected to the string inverter, with four strings of 22 modules in each MPP Tracker.

Delta Solar Solution
M50A Grid PV Inverter

SMA
Sunny Tripower 4.0

Figure 34: The two string inverters utilized in system solution 1.
Source: Attachment A.6 & (Europe - Solar Store, 2020b)

Ordinarily, the additional string inverter should be chosen from the same manufacturer, as there is no guarantee that the two different components will work together, but in this case, the more modest string inverters produced by Delta Solar Solutions are not able to handle the 70 °C short-circuit current of 11.787 A per string. The additional string inverter is therefore provided by the German company SMA, with the specific product being the Sunny Tripower 4.0 (see Figure 34).

According to Attachment A.6, the product has two MPP Trackers, which can handle short-circuit currents up towards 18 A. For this system solution, two strings will be attached to the inverter, one in each MPP Tracker. As shown in Figure 35, both series will consist of 12 photovoltaic modules each.

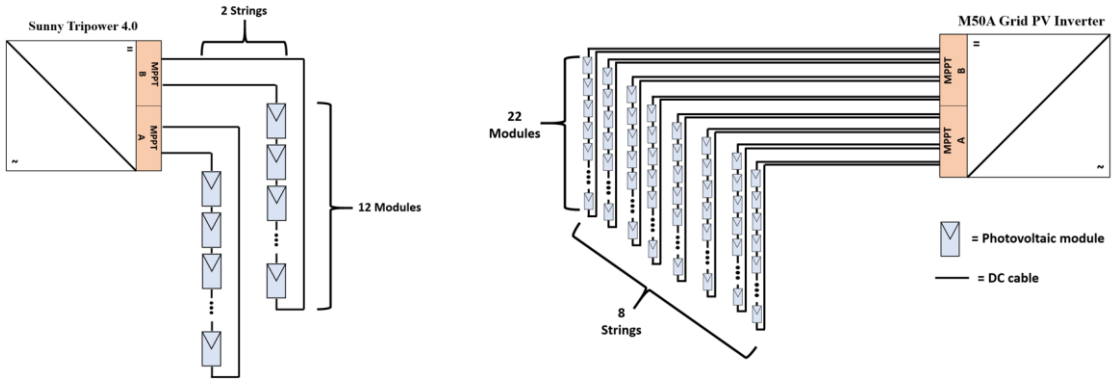

Figure 35: A schematic of the number of photovoltaic modules and strings inserted into each inverter.

Based on the information provided in Chapter 6.2.2: *Factors determining the location of the string inverter(s)*, the string inverters should be installed inside the technical room of the milk barn. This location will protect the string inverters from direct sunlight and harsh weather conditions from the outside, and it will also be easy to perform regular maintenance.

Their actual placement inside the technical room should be carefully considered, but a possible option is presented in Figure 36.

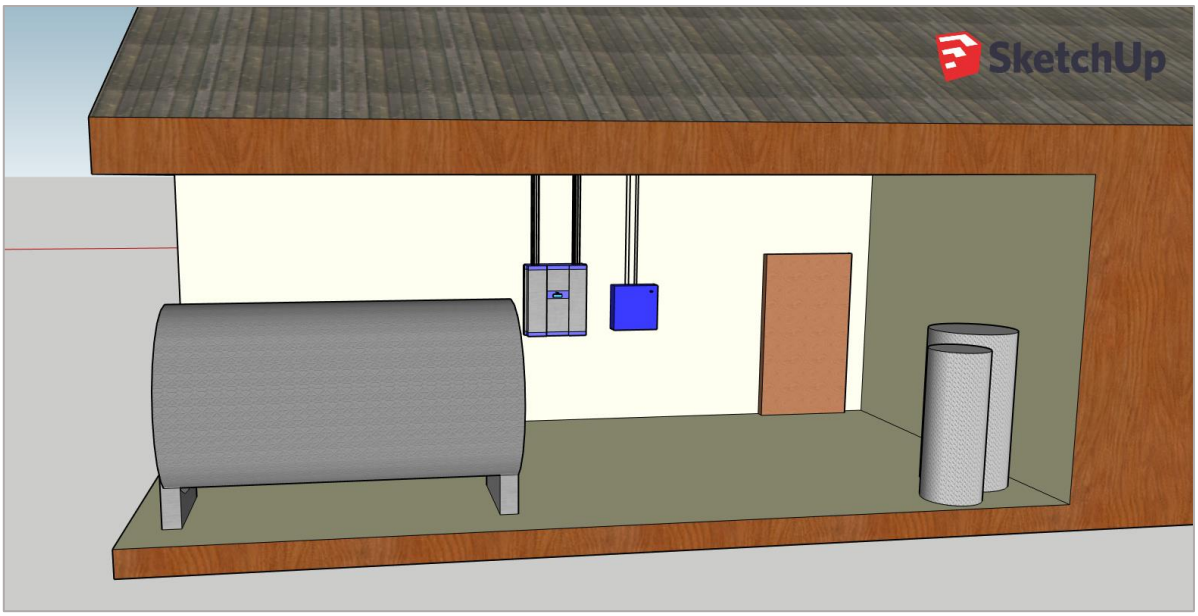

Figure 36: The location of the string inverters inside the technical room.

The cost of the two string inverters varies somewhat with the supplier contacted to order the product, but according to (RenuGen, 2020) & (Europe - Solar Store, 2020b), the M50A Grid PV Inverter costs 38 830 NOK, and the SMA Sunny Tripower 4.0 inverter costs 11 700 NOK, respectively.

System 2: SMA Sunny Tripower 10.0 PV Inverter

In addition to the Sunny Tripower 4.0 Inverter introduced for the previous system solution, SMA also manufactures inverter models meant for larger photovoltaic systems, such as the 10.0 model (see Attachment A.7). The exterior design is quite similar to the 4.0, but it can handle a more substantial amount of inputted DC power.

The 10.0 model has two MPP Trackers, Tracker A and B, where input A can handle two strings, while B can only handle one. The maximum inputted DC voltage for the inverter is 1000 V, and the maximum short-circuit currents for Tracker A is 30 A and 18 A for Tracker B, while the highest DC input power for the 10.0 inverter model is 15 kWp.

As the total peak power of the photovoltaic modules is 60 kWp, a total of four string inverters are necessary to convert sufficient DC power, with a total of 50 photovoltaic modules attached to each inverter.

To be able to take full advantage of the MPP Trackers in the Sunny Tripower 10.0, the string inputted into Tracker B should consist of as many photovoltaic modules as possible, as the electricity generation of the two other inputs into Tracker A is dependent on each other. The string inputted into B should therefore have 22 photovoltaic modules, while the two strings attached to input A should have 14 modules each.

The layout of this system can be seen in Figure 37.

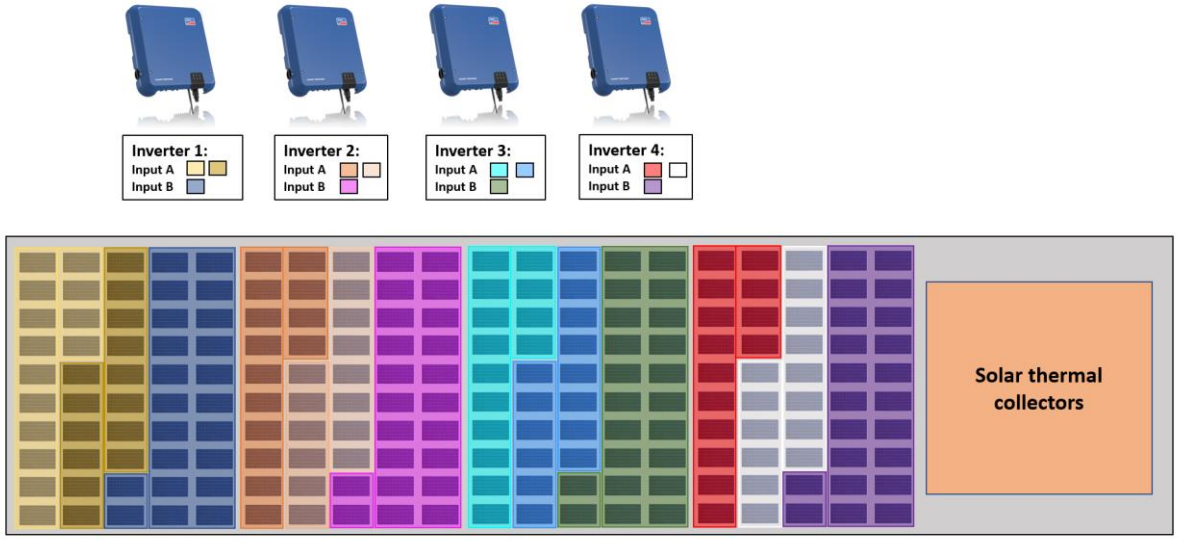

Figure 37: Illustration of the layout of the four string inverters and their corresponding inputs.

Similar as for the first system solution, the cost of Sunny Tripower 10.0 PV Inverter can be found on websites that specialize in selling photovoltaic system components. According to (Europe - Solar Store, 2020c), the cost of a single Sunny Tripower 10.0 PV Inverter is about 18 850 NOK, making the total cost of four inverters approximately 75 400 NOK.

System 3: Altenergy Power (AP) Systems YC1000 3-Phase Micro-inverter

There are only a couple of manufacturers that specialize in producing micro-inverters for the inverter market. According to (APSystems, 2020), the American company Altenergy Power Systems were founded in Silicon Valley, California in 2010, and the company is today the world's third-largest merchant of Module Level Power Electronics (MLPE). As mentioned in a previous chapter, both micro-inverters and power optimizers are commonly known as MLPEs.

One micro-inverter model manufactured by AP Systems is the YC1000 3-Phase Micro-inverter, and this inverter can be attached to either 3 or 4 photovoltaic modules, depending on the preferences of the buyer. The wiring schematic for the micro-inverters connected to four photovoltaic modules can be seen in Figure 38. A slight disadvantage with these micro-inverters is that a maximum amount of 12 micro-inverters can be utilized in each electrical circuit.

Five circuits should, therefore, be installed in the photovoltaic system. Each would consist of 10 micro-inverters connected to a total of 40 photovoltaic modules. The micro-inverters have a maximum input current of 14.8 A from each photovoltaic module, and the maximum DC input voltage is 60 V.

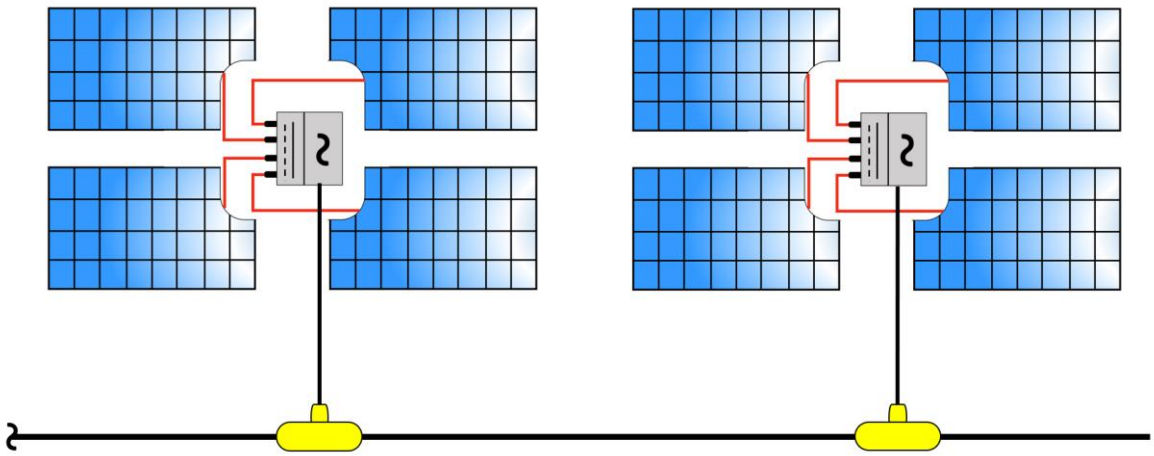

Figure 38: Wiring schematic for YC1000 3-Phase Micro-inverters.
Source: Based on a figure in Attachment A.8

As stated in the literature review, and also by studying micro-inverter products on the Internet, the general cost of micro-inverter systems is far more expensive than regular string inverter and power optimizer systems. The main reason is that the micro-inverter system requires numerous micro-inverters, often one for each photovoltaic module. There is little, if any, information about the cost of the YC1000 3-Phase Micro-inverter for the European market. According to (A1 Solar Store, 2020), the YC1000 3-Phase Micro-inverter, made for the American market (277/480V), cost about 3 065 NOK per micro-inverter.

It will be assumed that the product for the European market costs about the same.

6.3 Power meter

Power meters, also more commonly known as utility meters, are briefly explained by (Vekony, 2019) to be devices that measure the electricity consumption in the building. A power meter can also be combined with a grid-tied photovoltaic system, monitoring both the amount of electric energy consumed in the building and also help to determine the amount of surplus generated electricity exported to the power grid. The reason for this is, as (O'Neill, 2018) explains, that some power meters are bi-directional, meaning that they can measure both the electricity exported to the grid, as well as the electricity imported from the power grid.

(Bushong, 2015) mentions that a benefit with power meters is that they make it easier to observe and analyze the performance of the photovoltaic system, giving the system owner an advantage, as it will be quicker to discover photovoltaic system malfunctions.

According to (Bushong, 2015), most solar inverters come installed with internal power meters, but that these meters are often not revenue-grade, meaning that the accuracy of the meters usually is below 2 %. (Bushong, 2015) therefore suggests that an external power meter should be installed along the AC cable between the solar inverter and the main distribution panel, to get more accurate readings.

6.3.1 Smart power meters

In addition to traditional power meters, a concept known as smart power meters has been developed for monitoring. According to (Infinite Energy, 2019), smart meters can be installed inside the switchboard of the building. Here, the "smart power meter" monitors the amount of electricity that is being imported from, and exported to, the power grid. The meter then sends and extracts information from the solar inverter, through a data cable connection, presenting all relevant system data on one single monitoring platform in real-time.

An additional benefit with these meters, (Infinite Energy, 2019) points out, is that they give an increased data overview, which can assist the system owner in finding potential ways to save energy and reduce the utility bill.

6.4 The Norwegian power grid

As explained by (Statnett, 2018), all generated electricity must be used the same second that it is produced. It is therefore crucial that there is always a balance between the amount of electric energy consumed and the amount generated. In Norway, the state-owned company Statnett is responsible for providing this energy balance.

The power grid could be considered the backbone of the Norwegian power system, as it functions as the link between the electricity producer and the consumers and it is therefore deemed a crucial infrastructure in any modern society.

According to (Olje- og energidepartementet, n.d.), the Norwegian power grid consists of three network levels. These levels are:

- The transmission network
- The regional network
- The distribution network

The transmission network is briefly explained by (Olje- og energidepartementet, n.d.). According to them, the transmission network, which is also known as the central network, connects the energy producers with the consumers in a nationwide grid system. The transmission network consists of several international interconnections, and in Norway the network has a high voltage level, commonly between 300 to 420 kV. In some parts of the country, the transmission lines may have a voltage level of 132 kV.

According to (Olje- og energidepartementet, n.d.), the regional network usually works as an interconnection between the central transmission network and the distribution network, where the voltage level in the interconnection network is between 33 kV to 132 kV.

The last network level is the distribution network. This network-level consists of local power grids, which usually deliver power to the smaller end-users. According to (Olje- og energidepartementet, n.d.), the distribution network has a voltage level of up to 22 kV, but there is a distinction made between high-voltage and low-voltage distribution networks. The separation is at 1 kV, and the low-voltage distribution grid is usually 230 V or 400 V for delivering electricity for general consumption.

An illustration of the three grid networks and their voltage level can be seen in Figure 39.

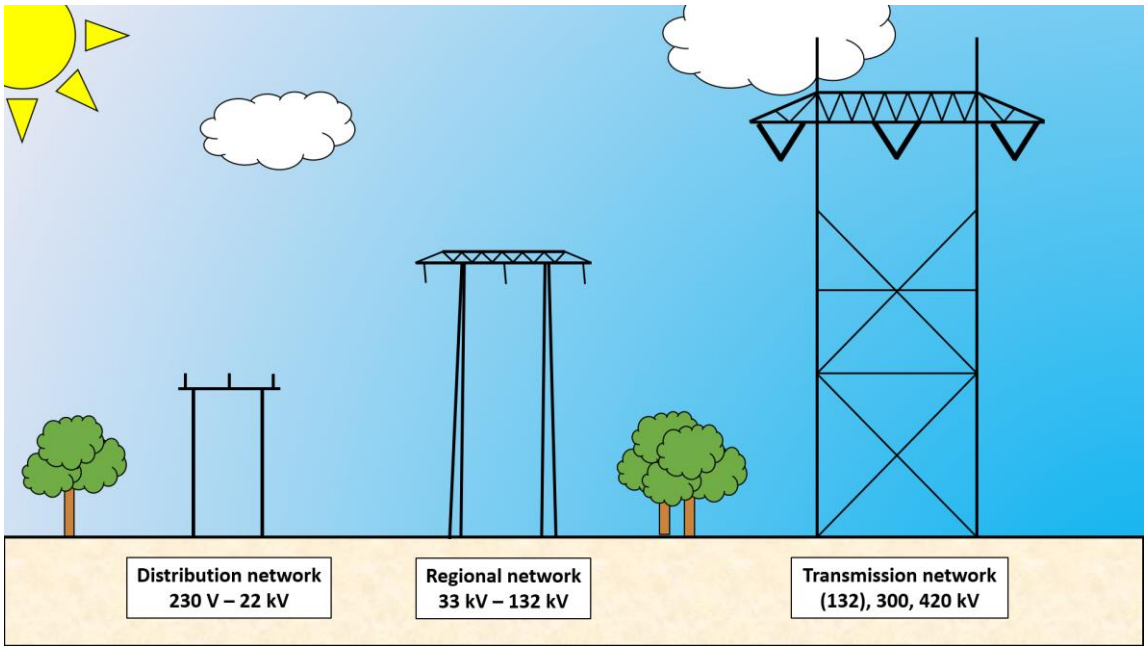

Figure 39: The different Norwegian grid levels and their corresponding voltages.
Source: Based on a figure by (NVE, 2018)

6.4.1 Types of low voltage distribution networks

According to (Rosvold, 2018), low voltage distribution networks are divided into three system types:

- Insulated-Terra (IT)
- Terra-Terra (TT)
- Terra-Neutral (TN)

These three system types are named after their relationship with the ground.

(Rosvold, 2018) explains that in IT systems, the distribution transformer's neutral point is insulated from the ground, while it is grounded in TT systems. In TN systems, the neutral point of the distribution transformer is passed on to the consumer. The IT and TT systems only have access to a voltage of 230 V, while the TN systems have access to two voltage levels, 230 V and 400 V.

The voltage level of 230 V is commonly used to power ordinary electrical household appliances and lighting, while 400 V is more ordinarily used to power and operate larger pieces of equipment. (Rosvold, 2018) states that all new electrical installations in Norway are built as TN systems, and at the same time, older IT systems are being converted into TN.

6.4.2 Nord-Trøndelag Elektrisitetsverk (NTE)

According to (NTE, 2020), NTE is the Norwegian power company responsible for producing and supplying power to consumers located in Trøndelag. Their main office is located in Steinkjer in Trøndelag-county, and according to (Rosvold, 2019), NTE's power plants have an average annual power production of about 3 900 GWh.

In 2019, NTE and TrønderEnergi jointly established the company Tensio AS, with the sole purpose to manage the network services in Trøndelag.

The Plus Customer Scheme

(Tensio, 2020) explains that NTE and Tensio AS provides some of their customers, known as Plus Customers, the opportunity to export excess generated electricity from privately owned energy systems to the power grid. This agreement does not only apply for owners of photovoltaic systems but also owners of wind turbines and small hydropower plants.

According to (Tensio, 2020), all network costumers can, in principle, be upgraded to take advantage of their Plus Customer Scheme. The most crucial requirement is that the customer establishes a privately-owned energy production system. Tensio AS has set an upper export limit of 100 kWh of excess production each hour, where all exported energy above this limit will come with an additional grid cost.

These following requirements are demanded from their customers for them to be allowed to use the Plus Customer Scheme:

- The customer must have installed an automatic power meter.
- The power generating system must be connected to the grid by an approved electrician.
- The production plant must not reduce the voltage quality of the distribution network.
- An agreement on the payment of exported excess production must be made between the electricity provider and the owner of the production plant.

(Tensio, 2020) also explains that all Plus Customers must pay for the production system equipment and installer themselves. Also, the grid company may expect the customers to pay for additional construction fees, or part of the expenses related to the process of strengthening the network due to increased power flow. The grid company covers the costs of the necessary measuring devices, and the customer does not need to pay a grid fee for the electricity exported to the grid, only the electricity imported.

Mære Agricultural School

Through e-mail correspondence with NTE, it was discovered that the majority of the buildings at Mære Agricultural School was connected to the old IT network (230 V), but that the greenhouse at the school is connected to the TN network (400 V). It was also believed by the correspondent from NTE that the new milk barn is connected to the TN network.

Based on the information presented above, it is not unlikely that this is the case, as the barn contain several large pieces of equipment, as well as the fact that the building is relatively new compared to the other buildings at the school.

Mære Agricultural School already has an arrangement with the grid company and NTE for the existing photovoltaic systems at the school. The understanding is that NTE buys the excess energy production from the school with a price based on the hourly electricity spot price. The money earned by selling and exporting excess power during the month is automatically subtracted from the monthly electricity and grid costs for the building.

6.5 Battery bank

Photovoltaic systems may experience prolonged periods during the day where the photovoltaic modules generate more electric energy than the appliances and equipment consume. The excess electricity can either be exported to the power grid or stored on batteries, with the purpose to be of later use.

According to (Spiers, 2012), batteries are commonly more employed in stand-alone photovoltaic systems, but they may also be installed in grid-tied systems, basically transforming it into a hybrid photovoltaic system.

(Spiers, 2012) also emphasizes that batteries have three primary uses in photovoltaic systems. Their main purpose is of course to store quantities of electric energy for later usage, but storage batteries can also sometimes stop large voltage fluctuations, as these could potentially damage the system. In addition to the two previous usages, storage batteries can also function as a buffer store to reduce the mismatch between available power from photovoltaic modules and power demand from the load.

In this master thesis, the main focus will be on the batteries ability to store electric energy.

6.5.1 Battery types

According to (EnergySage, 2020a), various significant battery specifications should be examined and assessed before choosing a potential battery storage solution for the photovoltaic system. These specifications are:

- Capacity: The total amount of electricity that can be stored in the battery.
- Power ratings: The highest amount of electric energy that the battery can deliver.
- Depth of Discharge (DoD): Specifies the amount of the battery's capacity that one can utilize.
- Round-trip efficiency: The amount of energy that can be used compared to the amount of energy it took to store it.
- Warranty: The amount of time the manufacturer will guarantee that the battery will last.

(Wholesale Solar, 2018) lists some of the most commonly used battery types in photovoltaic systems on the market today. These include flooded lead-acid (FLA), sealed lead-acid (SLA) and lithium-ion batteries. According to (EnergySage, 2020a), lithium-ion batteries are more expensive and have a higher Depth of Discharge than traditional lead-acid batteries. Of these three types, (Vekony, 2020) estimates that lithium-ion batteries have a technical lifespan between 11 to 15 years, while the lead-acid batteries last between 5 to 7.5 years.

As photovoltaic systems often last about 25 years, the owner should expect to replace the batteries at least once during the lifespan of the photovoltaic system.

6.5.2 Attaching battery storage to a grid-tied photovoltaic system

According to (Taylor-Parker, 2019), there are primarily three ways to attach battery storage to grid-tied photovoltaic systems. These three methods are:

- AC coupling
- DC coupling
- Storage-ready Inverter

The first two can be employed on already existing photovoltaic systems, as well as new, but the third is primarily used on new photovoltaic systems.

AC coupling

The basic premise of grid-tied photovoltaic systems is that they implement inverters meant for grid connection (Grid-tie inverters), and as a result, require a continuous link to the power grid to operate. According to (Taylor-Parker, 2019), the reason for this is that the grid-tie inverters continually sense both the voltage and frequency of the power grid, and should these parameters exceed a predetermined range, then the inverter will shut off. In these cases, an AC coupling may be a sound solution for attaching battery storage.

The complete AC coupling process is explained by (Taylor-Parker, 2019). In brief, the battery storage is added to the photovoltaic system by pairing an off-grid inverter with the grid-tie inverter, as mentioned in the introduction, and then connecting the battery storage with the off-grid inverter (see Figure 40). The off-grid inverter will then function as a second power source, tricking the grid-tie inverter into not shutting down. The photovoltaic system will then be able to charge the batteries, and also provide electricity to equipment and household appliances during periods with a power outage.

(Taylor-Parker, 2019) also mentions that the basic guideline for sizing the off-grid inverter is to use an inverter with at least 25 % higher nameplate capacity than the grid-tie inverter.

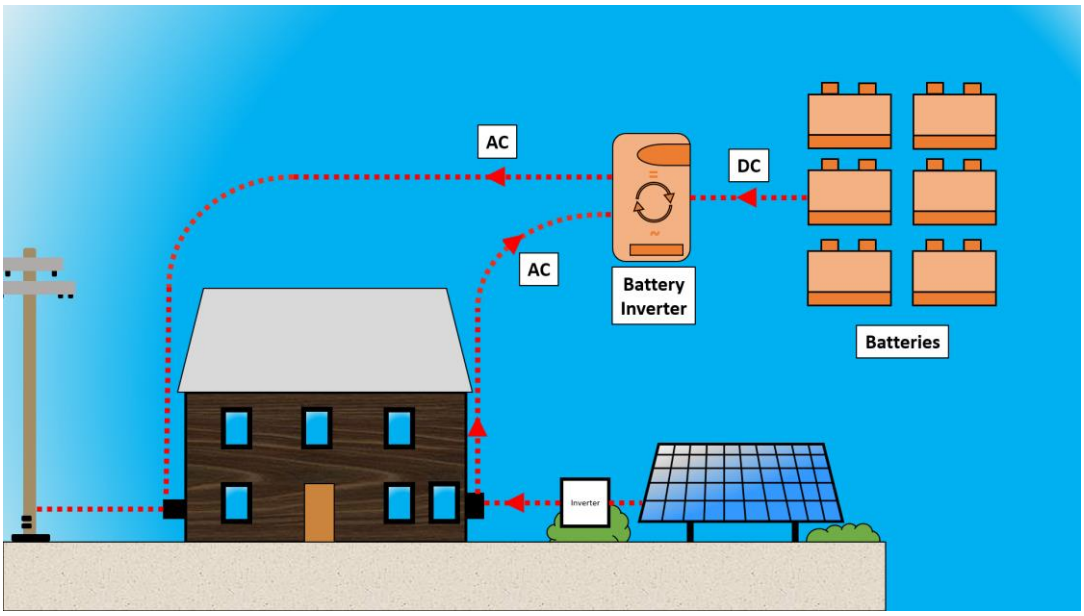

Figure 40: A grid-tied photovoltaic system attached to a battery storage through an AC coupling. Source: Based on a figure by (Taylor-Parker, 2019)

In addition to the information presented above, (Taylor-Parker, 2019) also lists several benefits and drawbacks of the AC coupling. One of the advantages of AC coupling is that it is one of the simplest methods to employ when planning to connect battery storage during the retrofitting of an existing system, and especially if the system already has installed micro-inverters. A drawback with AC coupling is that the sizing of the battery storage must be done carefully and correctly, as an undersized inverter or battery bank can result in lower photovoltaic system performance.

DC coupling

According to (Taylor-Parker, 2019), DC coupling is primarily done on stand-alone photovoltaic systems, but can also be used on grid-tied systems. For this method, the photovoltaic modules are directly connected to the battery bank through a charge controller and battery inverter.

A schematic illustration of a DC coupling can be seen in Figure 41.

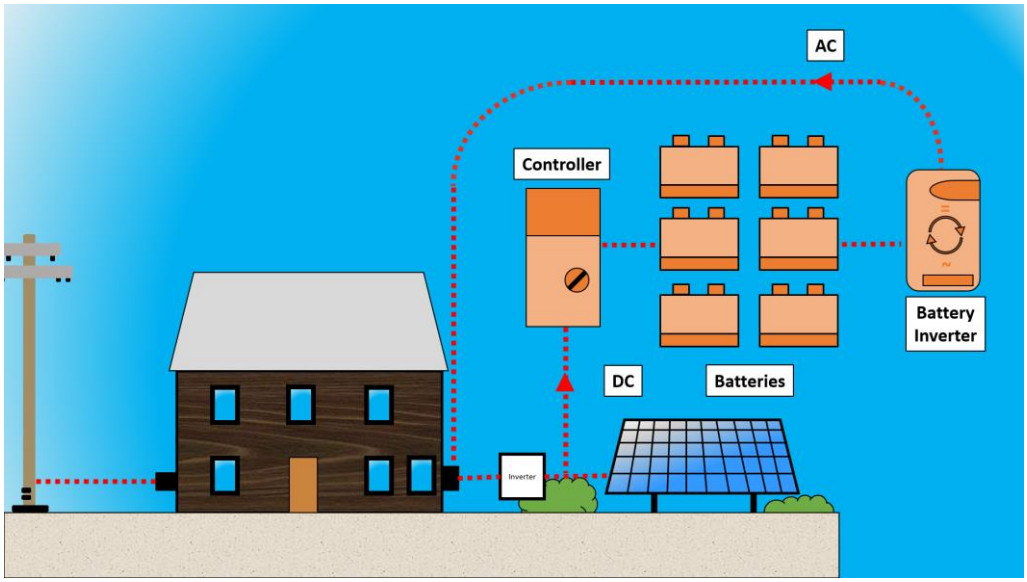

Figure 41: A grid-tied photovoltaic system attached to a battery storage through an DC coupling. Source: Based on a figure by (Taylor-Parker, 2019)

(Taylor-Parker, 2019) also mentions that the solar charge controller must be manually switched ON, for the batteries in the system to charge. If the switch is turned to OFF, then the storage batteries will stop charging and start sending the generated electricity to the household appliances or the power grid instead.

(Taylor-Parker, 2019) explains that the benefits with DC coupling compared to AC coupling is that the method generally works for a broader range of off-grid inverters and battery storage sizes. The main problem with DC coupling is that the switch on the charge controller has to be flipped manually for the batteries to start charging. The system will still provide backup power, but the batteries won't recharge until the solar charge controller switch is turned to ON.

Additional benefits and drawbacks with AC and DC coupling are provided by (Naked Solar, 2020) and can be seen in Table 18.

Table 18: Benefits and drawbacks with AC and DC coupling.
Source: (Naked Solar, 2020)

	AC coupling	DC coupling
Benefits	• **Increased power:** The system gets the combined power from batteries and inverters • **Increased freedom:** The batteries and the inverter does not need to be near each other • **Increased component independency:** Problems and faults with the batteries will not affect the photovoltaic modules and vice versa	• **Increased efficiency:** Has 1-3 % more efficient power transfer than AC coupling • **More affordable:** A DC coupling system is often more affordable as it only requires a single inverter
Drawbacks	• **Decreased efficiency:** Has 1-3 % less efficient power transfer compared to DC coupling • **Costly:** A AC coupling system can be expensive as it requires more than one inverter	• **Increased limitations:** Has limited access to power • **Increased component dependency:** Any problems with the inverter can render the batteries useless • **Decreased freedom:** The batteries in the system must be installed close to the inverter

Storage-ready Inverter

As explained by (Taylor-Parker, 2019), some string inverters have been specially manufactured with hybrid photovoltaic systems in mind. These inverters are often a more superior solution than just employing either AC or DC couplings. The major drawback with the storage-ready inverters is that they are far more expensive than traditional inverters and can therefore be a very costly solution.

Figure 42 shows an illustration of a photovoltaic system that uses a Storage-Ready inverter.

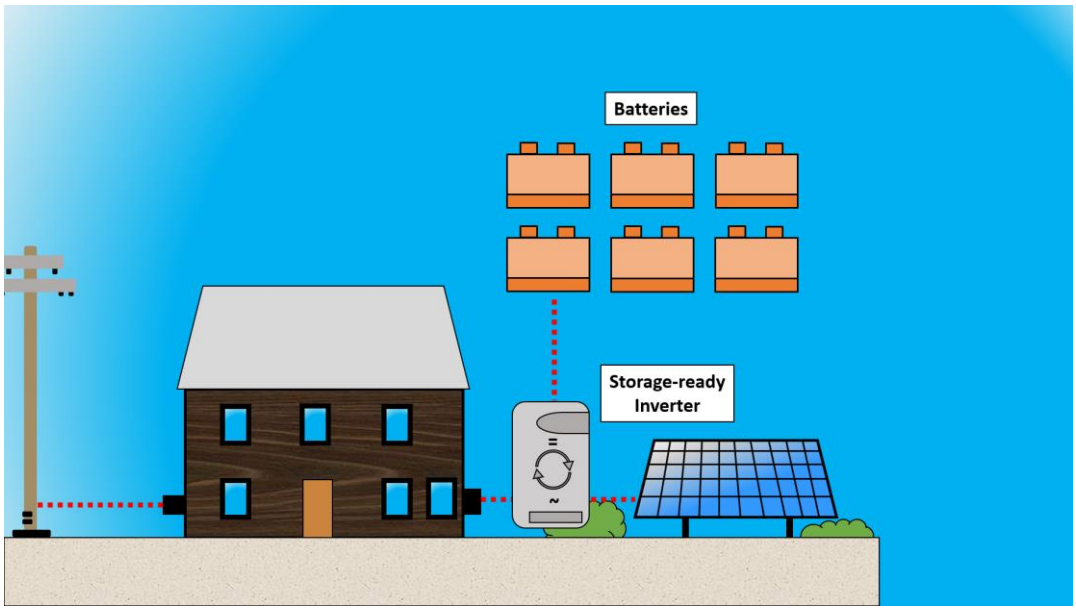

Figure 42: A grid-tied photovoltaic system attached to a battery storage with a storage-ready inverter. Source: Based on a figure by (Taylor-Parker, 2019)

6.5.3 Calculating the necessary size of a battery storage system

There are several possible approaches for determining the required size of battery storages. These approaches may vary from estimates based on simplifications, to complex analysis of real factors that affect the capacity of the batteries. (Wholesale Solar, 2018) provides a method that utilizes simplifications and assumptions, but at the same time considers a couple of external factors, such as ambient temperature. The complete Wholesale Solar approach can be seen in Attachment A.9, and it will be the method used in this master thesis for determining the battery sizes.

The first step in determining the required battery storage size is to map out the average daily energy consumption for the building. When this is obtained, the value should be multiplied with the inefficiency factor of the battery type, and the number of coherent days' worth of energy the battery should be able to store. These values are provided by (Wholesale Solar, 2018), who states that the efficiency factor is commonly 80 % for lead-acid batteries and 95 % for lithium-ion batteries. The equation for adding the inefficiency factor is:

$$C_B = \frac{n_b \cdot E_D}{\eta_{battery}} \qquad \textbf{[6.15]}$$

Here, C_B is the necessary storage capacity [kWh], when the inefficiency of the batteries have been considered, n_b is the number of coherent days the batteries should be able to provide back-up energy, E_D is the average daily energy consumption [kWh], and $\eta_{battery}$ is the efficiency of the battery type.

The next step is to take the Depth of Discharge into account. According to (Wholesale Solar, 2018), the Depth of Discharge is ordinarily 50 % for lead-acid batteries and 80 % for lithium-ion batteries. The equation for incorporating the Depth of Discharge is:

$$C_{DoD} = C_B \cdot \frac{1}{DoD} \quad \textbf{[6.16]}$$

In the equation above, C_{DoD} is the necessary battery capacity when both the inefficiency of the batteries and the Depth of Discharge is accounted for [kWh], C_B is calculated with Equation 6.15, and DoD is the Depth of Discharge [-].

In the fourth step, the inefficiencies of the inverter and the charge controller are incorporated into the calculations. (Wholesale Solar, 2018) estimates that these two components usually have a combined efficiency of between 90 to 95 %. The following equation can then be used to account for these inefficiencies:

$$C_{I,CC} = \frac{C_{DoD}}{\eta_I \cdot \eta_{CC}} \quad \textbf{[6.17]}$$

Where $C_{I,CC}$ is the necessary battery capacity when both the inverter and charge controller is taken into consideration [kWh], C_{DoD} is the capacity requirement calculated with Equation 6.16, η_I is the efficiency of the inverter, and η_{CC} is the efficiency of the charge controller. It should be noted that these efficiencies are rarely constant but are treated as such in these equations.

The fifth step is to account for the effect of ambient temperature in the planned battery storage location, as also the temperature affects the capacity of the batteries. Several temperature multipliers are provided by Wholesale Solar (see Attachment A.9) and can also be seen in Table 19.

The ambient temperature can be accounted for by using the following equation:

$$C_{tot} = T_M \cdot C_{I,CC} \quad \textbf{[6.18]}$$

Where C_{tot} is the minimum total capacity necessary to store n days' worth of energy [kWh], T_M is the temperature multiplier, here provided by Wholesale Solar, and $C_{I,CC}$ is the capacity calculated with Equation 6.17.

Table 19: Temperature multipliers for calculating battery capacity at different ambient temperatures. Source: Attachment A.9

Ambient temperature [°C]	Multiplier
26.7	1.00
21.2	1.04
15.6	1.11
10.0	1.19
4.4	1.30
-1.1	1.40
-6.7	1.59

The calculated minimum capacity of the required battery bank, obtained by using the equations above, should have the unit kWh. One thing to consider is that some battery manufacturers frequently promote their battery storages rated in ampere-hours (Ah). It is possible to convert the calculated value into ampere-hours by dividing it in the nominal system voltage (usually 12, 24 or 48 V). According to (Wholesale Solar, 2018), a nominal system voltage of 24 or 48 V are ordinarily used for larger photovoltaic systems, as they require larger battery capacities and also large inverters.

The next step of the sizing is to choose an actual battery for the photovoltaic system. The minimum capacity, calculated above into Ah, should then be divided on the ampere-hour rating of the preferred battery product. The result is the required number of batteries that has to be connected in parallel to obtain the desired minimum capacity. The equation for calculating the necessary amount of battery units connected in parallel is:

$$n_{b,p} = \frac{B_{system}}{B_{battery}} \quad \textbf{[6.19]}$$

Where $n_{b,p}$ is the number of batteries in parallel, B_{system} is the calculated required battery capacity for the storage system [Ah], and $B_{battery}$ is the capacity of the desired battery product [Ah].

The number of required parallel connections have been calculated, but it remains to determine the required number of batteries in series. The required amount can be determined by dividing the nominal system voltage by the battery voltage and then round upwards to the closest whole number. The following equation can be used to determine the necessary amount of batteries in series:

$$n_{b,s} = \frac{V_{system}}{V_{battery}} \quad \textbf{[6.20]}$$

Where $n_{b,s}$ is the necessary number of batteries connected in series, V_{system} is the nominal system voltage [V] and $V_{battery}$ is the nominal battery voltage [V].

In the last step of the battery sizing procedure, the required number of battery units in parallel is multiplied with the calculated number of units in series (see Equation 6.21). The result is the required total amount of batteries for the photovoltaic system ($n_{b,tot}$).

$$n_{b,tot} = n_{b,s} \cdot n_{b,p} \quad \textbf{[6.21]}$$

6.5.4 Designing a battery storage solution for the milk barn

Before calculating the necessary capacity of a battery bank system for the milk barn, the potential for batteries should be determined first. The photovoltaic modules, introduced in Chapter 6.1.6: *Photovoltaic modules for the milk barn*, is expected to have an inclination angle of 26^{o} and an azimuth angle of 0^{o}. If it is also assumed that the modules have a constant efficiency of 18.3 %, then (European Commission, 2020) can be used to determine the average hourly electricity production each month. The results of these estimations can be seen in Figure 43, were also the average hourly energy consumption is included.

As mentioned, the daily average energy consumption at the milk barn was included in Figure 43. This was achieved by going through all of the energy consumption data for these months, creating an hourly average. The standard deviation was also calculated and is included in the figure. By comparing the estimated hourly electricity production and calculated hourly consumption, it is possible to predict the hourly surplus generation for a worst-case, average-case and best-case scenario (see Table 20). Best-case is when the building's energy consumption is equal to the average usage minus the calculated standard deviation, meaning that the energy usage is as low as possible, while the worst-case scenario is when the standard deviation is added to the consumption, resulting in max hourly energy consumption.

The months of November and December are not included in the figure due to limited measurements.

Table 20: Estimated daily surplus energy production based on measured energy consumption in 2019. Source: (European Commission, 2020) & Mære Agricultural School

Month	Estimated daily energy production [kWh]	Average daily energy consumption [kWh]	Estimated daily surplus production - *Low daily energy consumption* [kWh]	Estimated daily surplus production - *Average daily energy consumption* [kWh]	Estimated daily surplus production - *High daily energy consumption* [kWh]
January	21.6	647.5	No surplus	No surplus	No surplus
February	82.5	667.9	No surplus	No surplus	No surplus
March	174.2	671.9	3.5	No surplus	No surplus
April	248.5	574.3	39.3	15.8	No surplus
May	302.5	426.6	96.6	74.3	52.8
June	294.0	391.6	108.0	68.0	41.6
July	287.9	418.3	88.1	61.7	39.6
August	245.3	436.6	58.5	43.2	29.8
September	163.8	474.3	29.4	4.3	No surplus
October	95.0	503.7	No surplus	No surplus	No surplus

The table above implies that one should anticipate a total annual surplus electricity production of 5 036.2, 8 198.2 and 12 948.7 kWh, for the worst-, average- and best-case scenario, respectively.

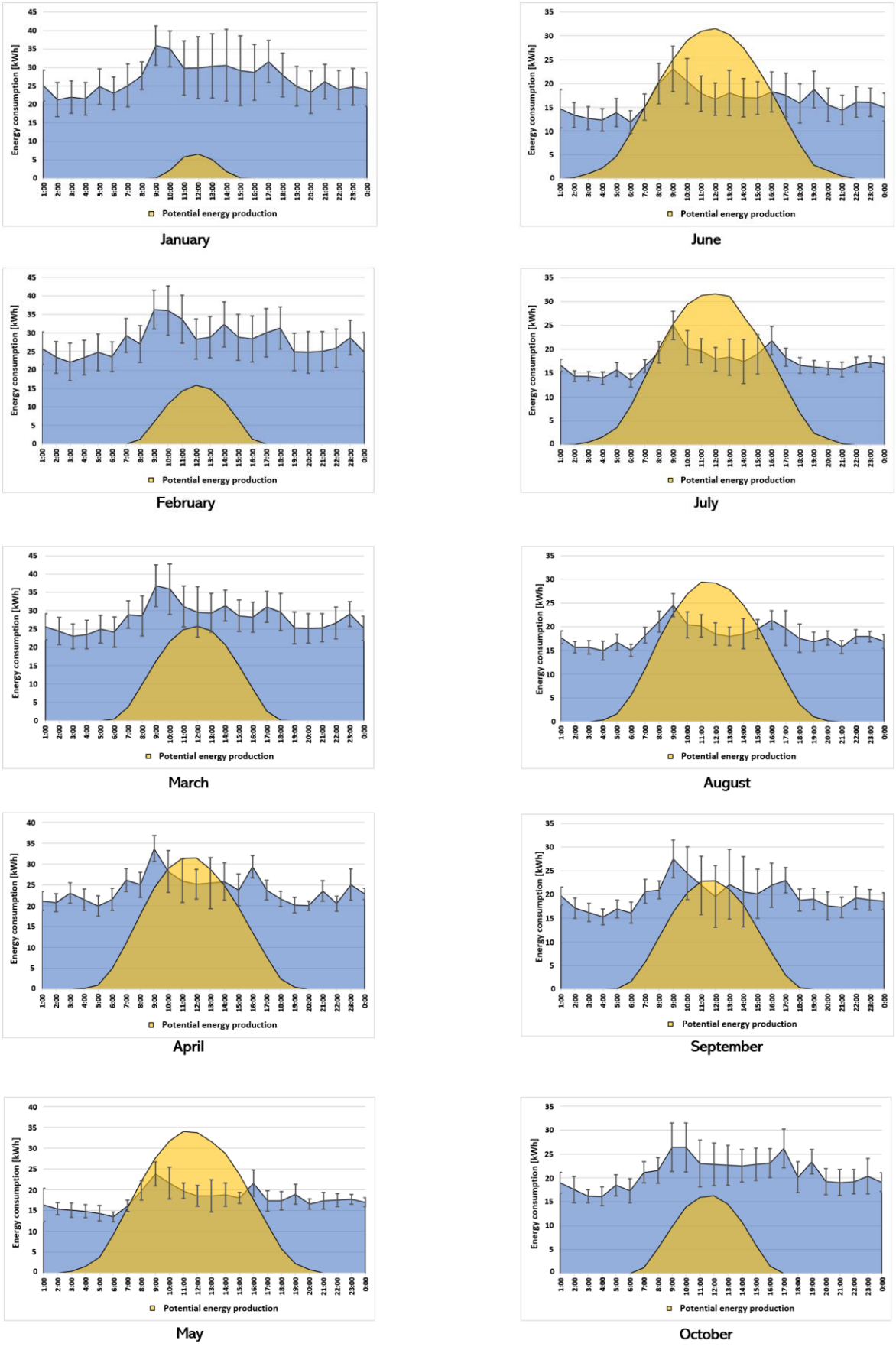

Figure 43: Energy consumption vs. potential energy production at the Milk barn. Source: (European Commission, 2020) & Mære Agricultural School

Determining the necessary amount of batteries for the milk barn

If the energy consumption for the milk barn in 2019 is taken as the basis (199 672 kWh), then the average daily energy consumption is about 547 kWh. By applying the information and equations provided in this chapter, the required minimum battery capacity for either one, two- or three-days' worth of energy storage can be calculated. Table 21 shows these calculated battery capacities when it is assumed that the inverter and the charge controller have a combined efficiency of 95 % and that the ambient temperature for the batteries will be 16 ^{o}C, resulting in a temperature multiplier of 1.11.

Table 21: Calculated battery capacity required for storing n days' worth of back-up power.

Battery type:	Number of days with back-up power	C_B [kWh]	C_{DoD} [kWh]	$C_{I,CC}$ [kWh]	C_{tot} [kWh]
Lead-Acid	One	684	1 368	1 516	**1 683**
	Two	1 368	2 736	3 032	**3 366**
	Three	2 051	4 102	4 545	**5 045**
Lithium-ion	One	576	720	798	**886**
	Two	1 152	1 440	1 596	**1 772**
	Three	1 727	2 159	2 392	**2 655**

The photovoltaic system presented in Chapter 6.1.6 & 6.2.3 has a much higher nominal system voltage than the standard 48 V. To attempt to determine how much a battery storage solution for the milk barn could be expected to cost, it will be assumed in this subchapter that the nominal system voltage is 48 V, even with the 200 photovoltaic modules and the average daily energy consumption of 547 kWh.

For the lithium-ion batteries, presented in Table 21, the required total capacity becomes 18 459, 36 917 or 55 313 Ah for one, two- or three-days' worth of autonomy, and 35 063, 70 125 or 105 105 Ah for lead-acid batteries. Table 22 shows several battery products provided by Wholesale Solar. The products consist of different technologies, ampere-hour ratings and battery voltages, and the corresponding cost for a single battery is also provided in the table.

Table 23 shows the required total number of batteries in series and parallel, as well as the total cost, for all of the products introduced in Table 22, but only for one day's worth of autonomy.

Table 22: Available battery products based on technology, nominal voltage, ampere-hour and cost. Source: (Wholesale Solar, 2020a; Wholesale Solar, 2020c; Wholesale Solar, 2020d)

Manufacturer	Product type	Technology	Nominal Voltage [V]	Ampere-hour rating [Ah]	Round-trip efficiency [%]	Dimensions (H x W x D) [mm]	Weight [kg]	Warranty	Cost
Discover Battery AES	3.1kWhr	Lithium-ion	24	110	> 95	330 x 338 x 274	40	10 years	33 300 NOK
	7.4kWhr		48	130	> 95	470 x 338 x 373	87	10 years	66 400 NOK
SimpliPhi PHI	2.7 kWh		24	151	98	286 x 279 x 241	27.4	10 years	25 550 NOK
	3.8 kWh		48	75	98	343 x 356 x 203	35.5	10 years	30 200 NOK
Solar-One HUP	SO-6-85-27	Flooded Lead-acid	24	1 375	Not Specified	2 032 x 286 x 635	1 000	10 years	90 300 NOK
	SO-6-85-27		48	1 375		4 064 x 286 x 635	2 000	10 years	180 650 NOK
	SO-6-100-33		48	1 990		4 064 x 343 x 711	2 812	10 years	254 300 NOK
	SO-6-85-21		48	1 055		4 064 x 222 x 635	1 600	10 years	148 650 NOK
	SO-6-125-33		48	2 490		4 064 x 342 x 838	3 081	10 years	299 300 NOK
Outback Power	EnergyCell 1000XLC	Sealed Lead-acid	48	972	Not Specified	1 710 x 1 125 x 555	2 007	10 years	228 160 NOK

Table 23: Required number of batteries for storing one day's worth of autonomy.

Manufacturer	Product type	Technology	Nominal Voltage [V]	Ampere-hour rating [Ah]	Necessary total capacity [Ah]	Nominal system voltage [V]	Number of batteries in series	Number of batteries in parallel	Total number of batteries	Total cost
Discover Battery AES	3.1kWhr	Lithium-ion	24	110	18 459	48	2	168	**336**	11 188 800 NOK
Discover Battery AES	7.4kWhr	Lithium-ion	48	130	18 459	48	1	142	**142**	9 428 800 NOK
SimpliPhi PHI	2.7 kWh	Lithium-ion	24	151	18 459	48	2	123	**246**	6 285 300 NOK
SimpliPhi PHI	3.8 kWh	Lithium-ion	48	75	18 459	48	1	247	**247**	7 459 400 NOK
Solar-One HUP	SO-6-85-27	Flooded Lead-acid	24	1 375	35 063	48	2	26	**52**	4 695 600 NOK
Solar-One HUP	SO-6-85-27	Flooded Lead-acid	48	1 375	35 063	48	1	26	**26**	4 696 900 NOK
Solar-One HUP	SO-6-100-33	Flooded Lead-acid	48	1 990	35 063	48	1	18	**18**	4 577 400 NOK
Solar-One HUP	SO-6-85-21	Flooded Lead-acid	48	1 055	35 063	48	1	34	**34**	5 054 100 NOK
Solar-One HUP	SO-6-125-33	Flooded Lead-acid	48	2 490	35 063	48	1	15	**15**	4 489 500 NOK
Outback Power	EnergyCell 1000XLC	Sealed Lead-ac	48	972	35 063	48	1	37	**37**	8 441 920 NOK

In addition to the traditional batteries produced for nominal system voltages of 24 and 48 V, there have also been manufactured battery units for nominal system voltages of 400 V. One such battery product is manufactured and distributed by LG Chem, and according to (Europe - Solar Store, 2020a), the lithium-ion product RESU 10H has an ampere-hour rating of 63 Ah and a cost of 55 150 NOK per battery unit.

If it is now assumed that the nominal system voltage of the photovoltaic system is 400 V, then the required battery capacity can be calculated to be 2 215 Ah for one day's worth of autonomy. The battery storage system would then only need one battery unit in series and 36 units in parallel, resulting in a total of 36 batteries. The total cost of all these batteries is 1 985 400 NOK, which is considerably more affordable than the other battery options presented in Table 23.

Due to the expensive nature of battery storage systems, as well as the option to become a Plus Customer to NTE, battery storages will not be considered suitable for the photovoltaic system for the milk barn. One of the most crucial components for any photovoltaic system attached to batteries, the charge controller, will still be explained in the following subchapter, but no product will be chosen for the actual photovoltaic system.

6.6 Charge controller

As mentioned in the subchapter above, charge controllers are an additional photovoltaic system component traditionally found in stand-alone or hybrid photovoltaic systems that utilize battery storage.

(altE Store, n.d.) explains that the primary function of charge controllers is to manage the produced electricity going into the battery storage from the photovoltaic system. The charge controller controls the power flow, ensuring that the batteries do not overcharge during periods with energy production. Charge controllers also obstruct the power flow from returning to the photovoltaic system during the night, which would drain the batteries.

According to (altE Store, n.d.), the additional features of charge controllers are:

- Its ability to disconnect depleted batteries from the load system until the batteries are sufficiently recharged.
- Its ability to turn lights that are connected to the load system ON or OFF, based on if it is dusk or dawn.
- Its ability to display the voltage level of the batteries, state of charge and the amount of electricity coming from the photovoltaic modules.

Charge controllers are not always required for battery storage in photovoltaic systems, but as (Qazi, 2017) mentions, systems without charge controllers run the risk over overcharging their batteries, reducing both the batteries lifespan and their performance.

6.6.1 Type of charge controllers

Based on the information provided by (altE Store, n.d.), there are principally two charge controller products available on the market. The main difference between these two products is the technology implemented into the charge controller. The products are known as Pulse Width Modulation (PWM) and Maximum Power Point Tracking (MPPT).

PWM charge controller

According to (Marsh, 2019), charge controllers based on Pulse Width Modulation are the most conventional type of charge controller available on the market. These controllers operate by slowly diminishing the amount of power going into the battery storage as it nears its maximum capacity. Then when the battery is fully charged, the PWM controller continues to supply small amounts of power steadily to the battery storage to keep it topped off.

(Marsh, 2019) also explains that PWM charge controllers require the battery storage and the photovoltaic system to have matching system voltages. Traditionally, PWM charge controllers are not suitable for larger photovoltaic systems, as it is challenging to deliver matching voltages in these systems. PWM controllers are therefore more suited for smaller photovoltaic systems where both the photovoltaic system and the storage system have relatively low voltages.

MPPT charge controller

MPPT charge controllers, unlike its PWM counterpart, are an excellent fit for larger photovoltaic systems. As explained by (Marsh, 2019), the main difference between the PWM and the MPPT charge controllers is that the MPPT controllers coordinate their power input to collect the maximum power available from the photovoltaic system, and it also adjusts the output power from the system to match the batteries. Similarly, to PWM charge controllers, the MPPT charge controllers decrease the amount of energy flowing into the battery storage as it approaches full capacity.

According to (Marsh, 2019), MPPT charge controllers are more complex than regular PWM charge controllers, and as a result, is by far the more expensive option. But, as stated by (Qazi, 2017), MPPT charge controllers have a faster charge time, higher performance and offer overall better battery management compared to regular PWM charge controllers and can sometimes be worth the additional expense.

6.6.2 The charge cycle of modern charge controllers

The charge cycles of most modern charge controllers are fully explained by (Qazi, 2017). Each cycle usually consists of three steps or phases. The different voltage levels described in each of the steps below apply for a 12 V battery and are in this part only used as an example.

- The first stage is known as the bulk stage, and in this stage, the battery voltage rises until it approaches a voltage level between 14.4 to 14.6 V, which is known as the bulk level. While the battery voltage rises to this level, it draws a maximum current from the photovoltaic system. When the bulk level is reached, the battery is about 80 to 90 % fully charged.
- The next stage is known as the absorption stage. Here, the battery voltage is kept at the bulk level, while the amount of current into the battery is gradually reduced. This stage usually lasts approximately one to three hours.
- The final step in the charging cycle is known as the float stage. In this stage, the voltage is slowly reduced until it reaches a float level of about 13.4 to 13.7 V. When the voltage reaches this level, it is almost 100 % charged. The charge rate at this level must not exceed the self-discharge rate, as this will result in overcharging.

6.6.3 The cost of charge controllers

Similar to inverters and batteries for photovoltaic systems, there is no standard cost associated with charge controllers. The price depends on the manufacturer of the equipment, technology used, nominal battery bank voltage and also the maximum output current. Table 24 displays several different charge controller products sold by Wholesale Solar.

As mentioned in Chapter 6.5.4: *Designing a battery storage solution for the milk barn*, no charge controller will be chosen for the photovoltaic system designed for the milk barn at Mære Agricultural School, as there will be no batteries attached to the system.

Table 24: Costs of several different charge controller products.
Source: (Wholesale Solar, 2020b)

Manufacturer	Product type	Technology	Nominal Battery voltage [V]	Max. output current [A]	Dimensions (H x W x D) [mm]	Weight [kg]	Warranty	Cost
Outback power	FlexMax 80	MPPT	12/24/36/48/60	80	413 x 146 x 114	6.8	5 years	5 270 NOK
Morningstar	SunSaver-10L-12V	PWM	12	10	152 x 55 x 34	0.5	5 years	790 NOK
Magnum Energy	PT-100	MPPT	12/24/48	100	394 x 216 x 102	6.2	5 years	9 160 NOK
Morningstar	Tristar MPPT TS-60	MPPT	12/24/48	60	291 x 130 x 142	4.2	5 years	6 130 NOK
Schneider	Conext XW 60-150	MPPT	12/24/36/48/60	60	368 x 146 x 138	4.8	5 years	5 930 NOK
Morningstar	Tristar TS-45	PWM	12/24/48	45	260 x 127 x 71	1.6	-	1 800 NOK
Morningstar	Tristar TS-60M	PWM	12/24/48	60	260 x 127 x 71	1.6	-	3 840 NOK

6.7 Energy losses in photovoltaic systems

During the planning and designing of a photovoltaic system, considerable care and attention should be given to the system components, to reduce the chance of mismatching, and to the actual placement and orientation of the photovoltaic modules. This is important because photovoltaic modules already have a relatively low performance, and it is essential to reduce the possible energy losses as much as possible.

(Ekici & Kopru, 2017) explains that all energy losses in photovoltaic systems are either due to environmental factors or due to the components. (Ekici & Kopru, 2017) mentions that environmental factors can be shading from nearby obstructions, soiling or snow covering the photovoltaic modules, while factors contributed to components can be due to inefficiencies of the photovoltaic modules, cables and inverters.

6.7.1 Photovoltaic system component losses

Module nameplate rating losses

Module nameplate rating losses is explained by (Aurora Solar, 2019) to be energy losses related to inadequate or faulty listed information concerning the stated performance of the photovoltaic modules at Standard Test Conditions, compared to the actual performance of the photovoltaic modules. A comprehensive study on the evolution of these losses was performed by (Lopez-Garcia & Sample, 2018). During their research, they studied reports on 992 photovoltaic modules selected from the period 1982 to 2014. They found that the average P_{Max} divergence, based on the literature, was about -3.15 %.

According to (Aurora Solar, 2019), these losses have declined considerably, and new photovoltaic modules usually have an accurate description in the datasheet, making the losses closer to 0 %.

Mismatch losses

Mismatch losses are explained by (Koirala et al., 2014) to be losses that occur due to a mismatch between the produced electricity by two or more photovoltaic modules connected inside an array. One of the causes for mismatch can be partial shading of the photovoltaic modules. According to (Aurora Solar, 2019), industry research suggests that mismatch losses usually range from 0.01 to 3 %. They state that they always assume a mismatch loss of 0 % when either micro-inverters or power optimizers are installed in the photovoltaic system.

Light-Induced Degradation

(Aurora Solar, 2019) explains that Light-Induced Degradation (LID) is a phenomenon where the photovoltaic modules continuous exposure to sunlight, for a few days after installation, permanently reduces the efficiency of the new photovoltaic modules. LID affects some module types more than others, and according to (Lindroos & Savin, 2016), most of the crystalline silicon modules are affected by it. (Sopori et al., 2012) studied the effect of LID on crystalline silicon cells, and they observed that the energy losses due to LID were about 0.5 %.

(Aurora Solar, 2019) on the other hand, states that the energy loss due to LID is about 1.5 % for most of the monocrystalline modules and 0.5 % for most polycrystalline modules.

Thermal losses

According to (Aurora Solar, 2019), when the photovoltaic cell temperature increases, the efficiency of the cell drops. Most crystalline silicon modules usually have a temperature coefficient between -0.30 to -0.45 %/^{o}C, and the temperature coefficient shows the estimated decline in photovoltaic module efficiency for each increase in temperature.

(Sabri & Benzirar, 2014) provides the following equation for calculating the effect of increasing temperature on the efficiency of the photovoltaic module:

$$\eta_{PV} = \eta_{PV,STC} \cdot \left(1 + \frac{\beta_{PV}}{100} \cdot (T_C - T_{STC})\right) \quad \textbf{[6.22]}$$

Where η_{PV} is the efficiency of the photovoltaic module, $\eta_{PV,STC}$ is the efficiency of the photovoltaic module at Standard Test Conditions, T_C is the cell temperature [°C], T_{STC} is the temperature at Standard Test Conditions [°C], and β_{PV} is the module's efficiency temperature coefficient [%/°C].

Cable losses

According to (PVPerformance, n.d.), cable losses are energy losses, which can mostly be contributed to the ohmic resistance inside the cables that interconnect the photovoltaic components and strings. (Aurora Solar, 2019) explains that these losses usually are about 2 %, which is further reinforced by (Ekici & Kopru, 2017), who also suggests that the cable losses regularly are about 2 %.

Inverter losses

The efficiency of the inverter principally describes how well the inverter converts DC electricity into AC. As stated by (Mertens, 2014), the inverter efficiency varies based on the amount of capacity connected to the inverter, and also the size of the inverter compared to the size of the photovoltaic module system. According to (Mertens, 2014), energy losses related to the DC-AC power conversion is between 5-10 % for high-quality sine wave inverters.

6.7.2 Losses due to environmental factors

Shading

It is difficult to estimate potential energy losses due to shading, as numerous factors determine the effect of the shading. According to (Deline, 2010), the impact shading has on the photovoltaic system depends on which type of photovoltaic module that is utilized (fill factor, bypass diode placement, etc.), the severity of the shading and also the string configuration.

(Masters, 2004) calculated that a complete shading of one single cell in a 36-cell photovoltaic module has the potential to reduce the power with over 75 %. Careful consideration should therefore be given to the actual location of the photovoltaic system to avoid complete or even partial shading altogether. One possible solution is to install bypass diodes at every cell in the photovoltaic module, but as (Masters, 2004) points out, few manufacturers do this as it is highly impracticable, though they do sometimes install bypass diodes around photovoltaic modules to protect the arrays from the effect of partial shading.

It is possible to calculate potential energy loss due to partial shading on a photovoltaic array, where each of the photovoltaic cells are connected to a bypass diode. The following equation is provided by (Mertens, 2014), and is a simplification that can be used when bypass diodes are included in the photovoltaic module:

$$\frac{P_{MPP2} - P_{MPP1}}{P_{MPP1}} \approx \frac{(C_T - C_S) \cdot I_{MPP} \cdot V_{MPP} - C_T \cdot I_{MPP} \cdot V_{MPP}}{C_T \cdot I_{MPP} \cdot V_{MPP}} = -\frac{C_S}{C_T} \qquad \textbf{[6.23]}$$

Where P_{MPP1} is the Maximum Power Point if no cells are shaded [W], P_{MPP2} is the maximum power point during partial shading [W], C_T is the total number of cells in the module, and C_S is the number of shaded cells.

If a total number of 36 cells are used, and only one of the cells is shaded, then by using Equation 6.23, the energy loss should be about 2.78 %, which is a significant reduction from a 75 % loss for a module without bypass diodes, introduced by (Masters, 2004).

Figure 44 illustrates the potential effect partial shading may have on the performance of a single photovoltaic module with 36 cells, and without bypass diodes.

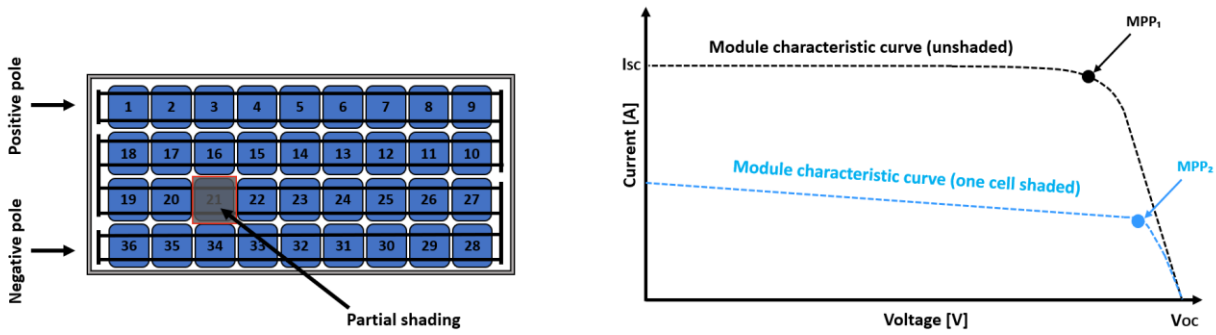

Figure 44: The effect of one shaded cell on the power of the photovoltaic module.
Source: Based on a figure by (Mertens, 2014)

In addition to shading from trees and nearby buildings, the photovoltaic modules can also shade each other. The phenomenon is commonly known as self-shading and is according to (Mertens, 2014) a consequence of poor photovoltaic system design (see Figure 45).

Self-shading is not a problem with building-integrated modules, but rather photovoltaic modules with fixed tilt angles, located near each other, on a relatively flat area. (Mertens, 2014) states that the minimum distance between the photovoltaic modules can be determined with the following formula:

$$d_{min} = b \cdot \frac{Sin(\gamma_s + \beta)}{Sin(\gamma_s)} \qquad \textbf{[6.24]}$$

Where d_{min} is the minimum distance between the photovoltaic modules [m], b is the width of the photovoltaic module [m], γ_s is the angle of the sun [°], and β is the fixed inclination angle of the photovoltaic module [°] (see Figure 45).

According to (Mertens, 2014), if the goal is to avoid self-shading at all costs, then γ_s should be chosen based on the actual inclination angle of the sun on the 21st of December (Northern-Hemisphere). Unfortunately, this is often not possible due to limitation with the available installation area.

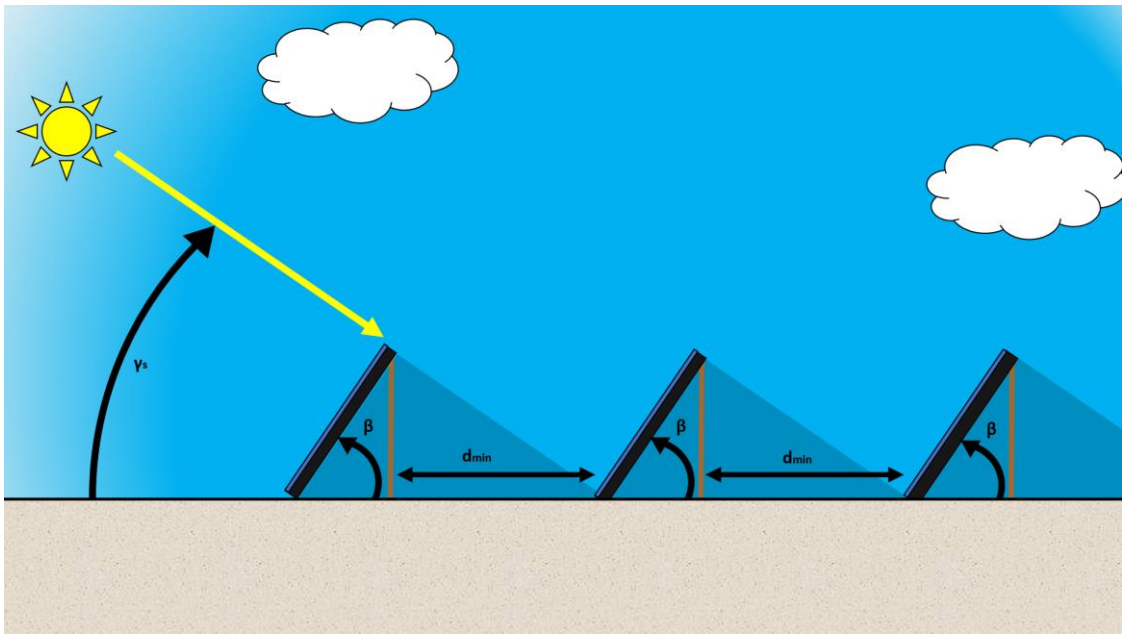

Figure 45: Self-shading of photovoltaic modules.
Source: Based on a figure by (Mertens, 2014)

Snow

Several studies have been made on the effect of snow accumulation on photovoltaic modules. (Pawluk et al., 2019) presents and summarizes the findings of several of these studies. The source also provides information regarding the inclination angle of the photovoltaic modules, the annual amount of snow, system location, and if snow sliding obstructions were installed for the photovoltaic modules.

Out of the studies presented by (Pawluk et al., 2019), three were done on locations with similar winter conditions as Norway. Two of these investigations were conducted on a photovoltaic system located in the city of Truckee, in the county of California.

The first study was conducted in 2010 by (Powers et al., 2010), while the second was performed the following year by (Townsend & Powers, 2011). The studies were conducted on photovoltaic modules with inclination angles of 0, 24 and 39°. (Powers et al., 2010) observed that the electricity production of the photovoltaic modules was reduced by 18, 15 and 12 %, respectively, compared to regularly cleaned photovoltaic modules during the same conditions and inclination angles.

In 2011, (Townsend & Powers, 2011) witnessed an increased production loss of 26 %, 17 % and 13 %, compared to the year before. They reasoned that the rise in production losses was due to an increase in the amount of snowfall from the previous year.

The last study was conducted by (Heidari et al., 2015), and was performed on a photovoltaic system installed in the city of Calumet in Michigan, USA. The study began in October 2013 and lasted for one whole year. The photovoltaic modules were adjusted, in pairs, to have the same inclination angle. The tilt angles used in the research were 0, 15, 30 and 45^{o}, and one module in each pair was installed with snow sliding obstruction. The observed annual electricity production losses for the photovoltaic modules, with and without snow sliding obstruction, are presented in Table 25.

Table 25: Estimated generation losses due to snow in Michigan, USA. Source: (Heidari et al., 2015)

Tilt angle [^{o}]	Without snow sliding obstruction	With snow sliding obstruction
0	34 %	
15	12 %	34 %
30	10 %	29 %
45	5 %	31 %

Soiling

Soiling, similar to snow accumulation during winter, shades the photovoltaic modules, resulting in lower photovoltaic system performance. According to (Maghami et al., 2016), shading due to soiling can be classified into two categories, which are Soft and Hard shading. Soft shading is shading that occurs due to air pollution, while Hard shading is shading due to dust accumulation on the modules, which blocks out the sunlight.

A figure provided by (Maghami et al., 2016) shows the dust intensity level for Norway is about two. Unfortunately, few studies have been conducted on dust and soiling on Norwegian photovoltaic systems. A possible approximation is therefore to examine studies performed on several photovoltaic systems in countries with the same dust intensity classification as Norway.

Spain is one of these countries, but with a higher level of annual dust. In Málaga, Spain, (Zorrilla-Casanova et al., 2011) studied the effect of dust accumulation on photovoltaic modules, installed with a tilt angle of 30^{o}. During their research, they observed that the average photovoltaic system loss, due to dust deposition, were about 4.4 %.

A similar study, based on the same location and inclination angle, was performed by (Piliougine et al., 2008). In their research, they observed that the losses in the photovoltaic system due to dust accumulation were about 6 %. Both studies also noted that the photovoltaic system losses increased during lengthy periods with little to no rainfall. (Zorrilla-Casanova et al., 2011) observed a monthly system loss of 15 % during dry months with unfavorable weather conditions, and (Piliougine et al., 2008) noted a system loss of 16 % for similar conditions.

Special care, as well as routine cleaning, should be given to photovoltaic modules mounted near areas meant for farming or construction sites, as the dust accumulation related to specific tasks performed on these locations may considerably reduce the performance of the modules.

All of the different types of losses presented in the subchapters above are summarized in Figure 46.

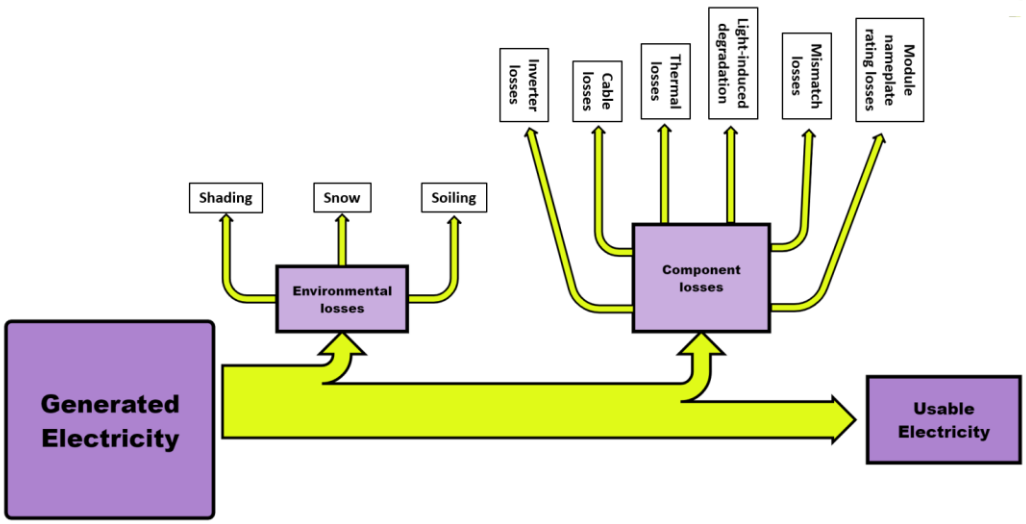

Figure 46: Energy losses that occur in photovoltaic systems.
Source: Created with Sankeyflowshow.com

6.8 Estimated total cost of the photovoltaic systems

By combining the costs of the photovoltaic modules and the different inverter systems, presented in Chapter 6.1.6 & 6.2.3, it is possible to estimate the total investment cost of the photovoltaic system. All the relevant expenses from these chapters are displayed in Table 26.

The installation cost is added to the investment cost by assuming it is 10 % of the total component costs (see Chapter 6.1.4: *The cost of PV Modules*).

It should be mentioned that these investment costs are only estimates and do not include expenses related to cables, plugs and other electrical components, which are all required for installing a complete photovoltaic system.

Table 26: Total estimated investment cost of photovoltaic systems.

Photovoltaic system cost						
	Inverter system 1		*Inverter system 2*		*Inverter system 3*	
Photovoltaic modules	200 x PERC 300 60 CELLS	223 200 NOK	200 x PERC 300 60 CELLS	223 200 NOK	200 x PERC 300 60 CELLS	223 200 NOK
Inverters	Delta Solar M50A Grid PV Inverter	38 830 NOK	4 x Sunny Tripower 10.0 PV Inverter	75 400 NOK	50 x APSystems YC1000 3-Phase Micro-inverter	153 250 NOK
	Sunny Tripower 4.0 PV Inverter	11 700 NOK				
Total system cost:		273 730 NOK		298 600 NOK		376 450 NOK
Installation cost: (assumed 10 % of total system cost)		27 373 NOK		29 860 NOK		37 645 NOK
Total cost:		301 103 NOK		328 460 NOK		414 095 NOK

7 Designing a solar water-heating system

Photovoltaic systems are not the only way to utilize solar energy, as solar energy can also be utilized through the use of solar collectors. In this master thesis, these systems will be referred to as solar water-heating systems. (Greenmatch, 2019) explains that these systems convert solar radiation into useable thermal energy, with the intention of heating water for domestic and commercial purposes. Solar water-heating systems can be used to heat domestic hot water and also water meant for hydronic space-heating.

According to (Evangelisti et al., 2019), these types of water-heating systems have gained a considerable amount of attention during the last decade. This is primarily due to the high system performance, but also due to the solar water-heating system's ability to deliver low-cost domestic and industrial heating. (Streicher, 2016) mentions that the solar thermal energy market is, to a great extent, dominated by China, while the European market share has been considerably lessened since 2008. According to (Streicher, 2016), this reduction has been caused by the fact that even though the investment cost for solar thermal systems have been relatively steady over the years, the European prices for photovoltaic systems has simultaneously decreased, making them more affordable.

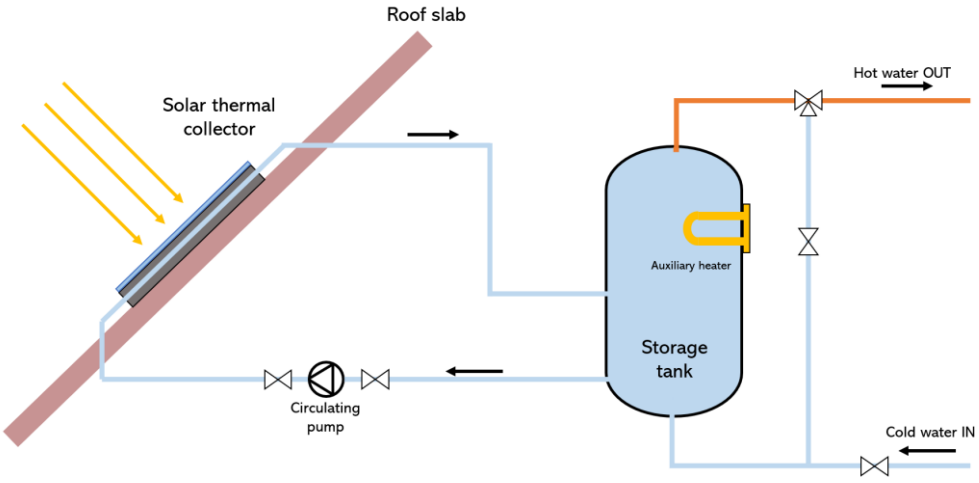

Figure 47: A direct (open-loop) solar water-heating system.
Source: Based on a figure by (Kalogirou, 2014b)

(Kalogirou, 2014b) explains that there are currently two central types of solar water-heating systems available today, and that these systems are commonly differentiated based on how the water inside the storage tank is heated with the thermal energy from the solar collectors. According to (Kalogirou, 2014b), if the water inside the storage tank is directly heated through the solar collectors, indicating no separation between the solar circuit and the storage tank, then the solar water-heating system is known as a direct or open-loop system (see Figure 47).

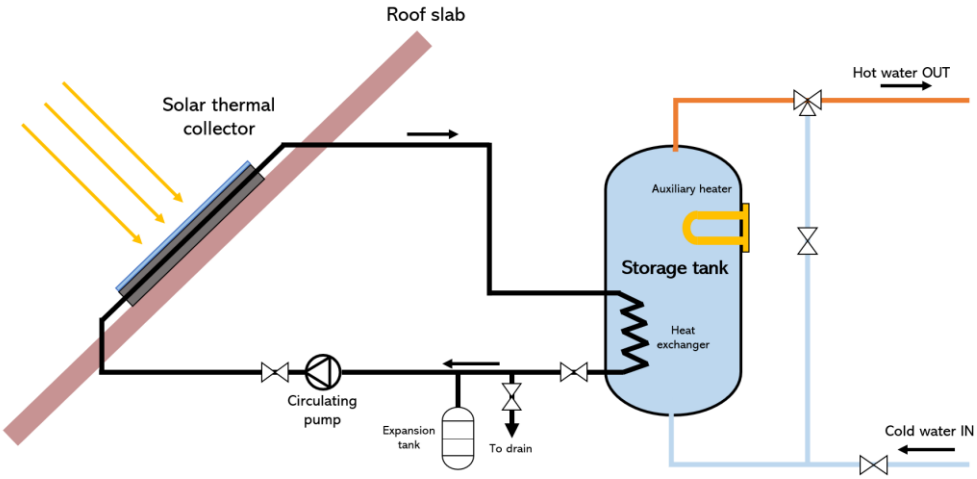

Figure 48: A indirect (closed-loop) solar water-heating system.
Source: Based on a figure by (Kalogirou, 2014b)

(Kalogirou, 2014b) explains that if the water inside the storage tank is heated with solar energy through a heat exchanger, then the solar water-heating system is known as an indirect or closed-loop system (see Figure 48). According to (Kalogirou, 2014b), if the solar circuit is a closed-loop, then the most commonly used heat transfer fluid is a mixture of water and ethylene glycol. This is to hinder the fluid from freezing in the circuit, making the closed-loop system a suitable solution for areas which experience longer periods with low ambient outdoor temperatures. Due to the nature of an open-loop system, the only possible heat transfer fluid is pure water, making the system unsuitable for colder areas.

Solar water-heating systems are, in addition to being categorized into direct- and indirect systems, classified based on how the heat transfer fluid is transported through the solar circuit. According to (Kalogirou, 2014b), the heating system is known as passive if the circulation of the heat transfer fluid occurs due to natural convection, but if the fluid is pumped through the circuit by a circulation pump, then the system is known as an active system.

Now that the different classifications have been introduced, it is crucial to get an overview of the various components in a solar water-heating system. According to (EnergySage, 2019), these system components are:

- Solar collectors
- Storage tank
- Heat exchanger (if indirect system)
- Controller system(s)
- Auxiliary heat source

The structure of this chapter is very similar to Chapter 6: *Designing a photovoltaic system*, where relevant literature for some of the components are introduced first, and in some cases, appropriate parameters for the simulation model for the milk barn will also be determined. As the main purpose of this chapter is not to design a solar water-heating system for the milk barn, but rather to gather the necessary information to perform a feasibility study on the possibility of such a system at the milk barn, this chapter will not be as detailed as the previous chapter.

7.1 Solar thermal collectors

The solar collector could be considered as one of the most vital elements in any solar energy system planned for water-heating. (Kalogirou, 2014a) explains that solar collectors are in essence heat exchangers that convert solar radiation into thermal energy (usable heat). The energy is then "collected" or absorbed by the heat transfer fluid running through pipes inside the solar collector, carrying the usable heat to the storage tank.

Even though the concept of utilizing solar energy to heat water with a solar collector may sound relatively new, the technology has existed for over 100 years, as can be seen in Figure 49, which shows an advertisement for solar-water heaters dated as far back as 1896 and 1902. Solar collectors are not only used to heat water intended for either tap or a combination of tap water and space-heating, as explained by (Streicher, 2016). They can also be used for heating of swimming pools, district heating, process heating and thermal cooling, as well as electricity production in solar thermal power plants.

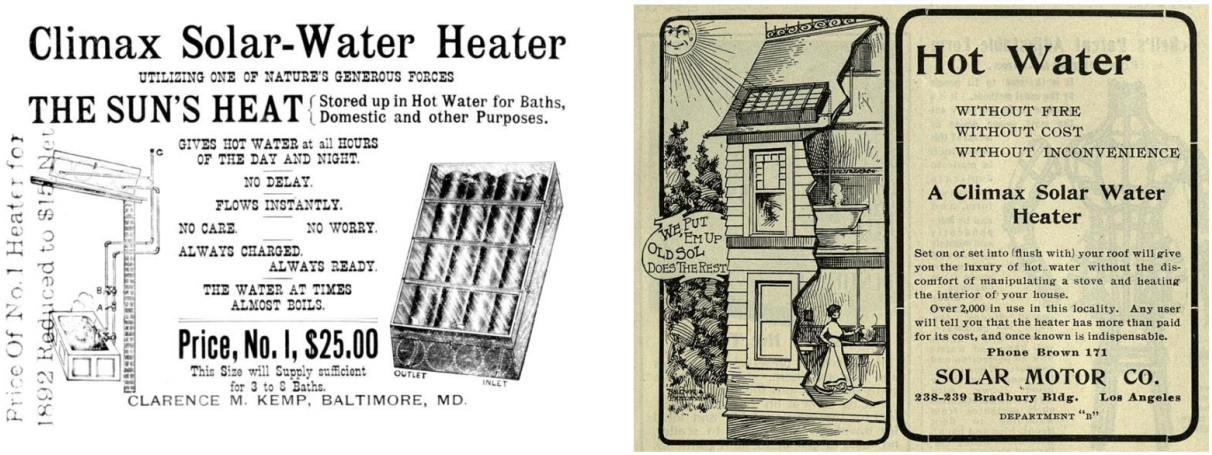

Figure 49: Advertisements for a Solar-Water Heater dated back to 1896 (left) & 1902 (right).
Source: (Perlin, 2013; Streicher, 2016)

Unlike the older simpler models that existed 100 years ago, there are several different solar collectors available today, where the technology ranges from simple to complex. According to (Evangelisti et al., 2019), non-concentrating solar collectors are the primary collectors used for heating of domestic hot water and water intended for space-heating, in both residential and commercial buildings. Concentrating solar collectors, on the other hand, are typically used in larger solar power plants.

Figure 50 shows some of the solar collectors mentioned by (Evangelisti et al., 2019).

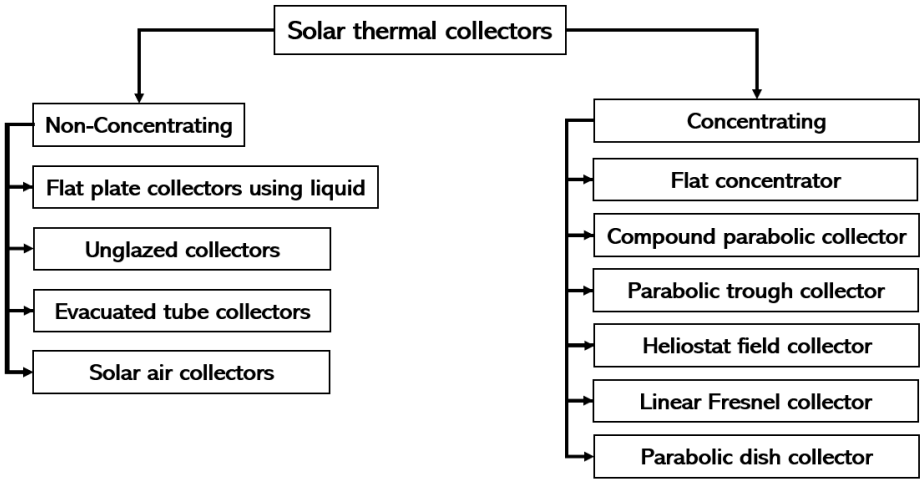

Figure 50: Various solar collectors.
Source: Based on a figure by (Evangelisti et al., 2019)

Both (Kalogirou, 2004), and to some degree (Kalogirou, 2014b), mentions that flat-plate collectors, evacuated tube collectors and compound parabolic collectors are frequently used in modern indirect solar water-heating systems, as can be seen in Table 27. Due to the aesthetic limitations of the milk barn (see Chapter 5: *The milk barn at Mære Agricultural School*), compound parabolic collectors will not be considered in the feasibility study.

Table 27: System types, circulation types and thermal collectors for solar water-heating systems. Source: (Kalogirou, 2004; Kalogirou, 2014b)

Solar water-heating		
System type	**Circulation type**	**Solar collector**
Thermosiphon systems	Passive	FPC
Integrated collector storage	Passive	CPC
Direct circulation	Active	FPC, CPC, ETC
Indirect water-heating systems	Active	FPC, CPC, ETC
Air systems	Active	FPC

7.1.1 Flat-plate collector

Flat-plate collectors (FPC) are according to (Evangelisti et al., 2019) one of the most studied technologies for solar energy to produce domestic hot water. The construction of the FPC is further described by (Kalogirou, 2014a), who explains that the solar radiation passes through a transparent cover on the surface of the FPC, hitting the dark absorber surface within. The FPCs are structured to have as low conduction loss as possible. This is achieved by insulating all the sides, as well as the surface beneath the absorber plate.

Figure 51 shows the different energy gains and losses associated with the FPC. It should be noted that the arrow signifying the thermal power output, represents the energy carried from the solar collector to the storage tank (not including heat loss in the pipes).

According to (Zijdemans, 2014), the main benefits with FPCs are their robust construction and long technical lifespan, usually lasting between 30 to 50 years. Another advantage with FPCs is that snow typically slides off the surface of the solar collector easily, thereby helping to avoid snow accumulation. FPCs also have a wider assortment of colors and forms, compared to other solar collector types, making it possible to choose aesthetically pleasing products.

One of the most prominent shortcomings of the FPCs, according to (Zijdemans, 2014), is the lower performance compared to evacuated tube collectors. FPCs are also usually installed in a permanently fixed position, meaning that special care should be given to both the orientation and inclination of the solar collectors, to ensure optimal harvesting of solar energy. According to (Kalogirou, 2014a), if the solar collector system is placed in the Northern Hemisphere, the collectors should be facing directly south, and the optimal inclination angle is usually equal to the latitude of the location, with variations of roughly 10 to 15º.

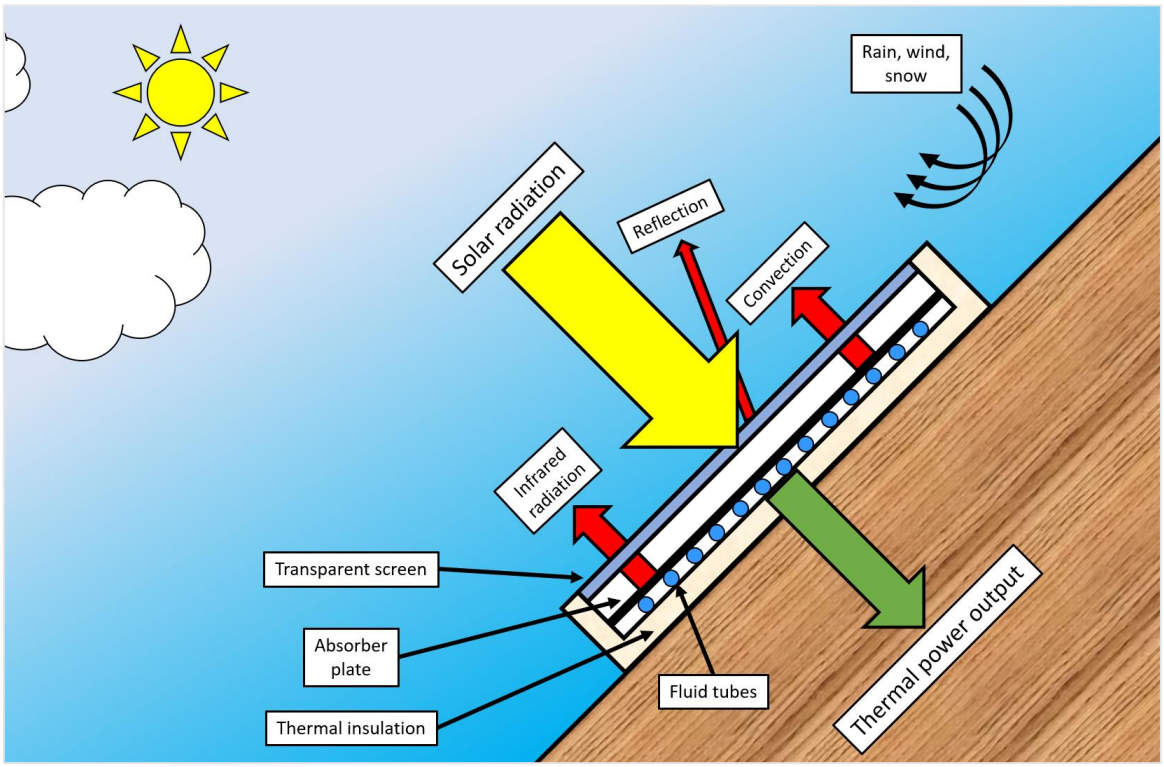

Figure 51: A schematic of a flat-plate collector and the heat transfer phenomena. Source: Based on a figure by (Evangelisti et al., 2019)

7.1.2 Evacuated tube collector

According to (Kalogirou, 2014a), conventional flat-plate collectors are usually developed for sunny and warm climates, which results in a low performance during periods with unfavorable solar conditions and cold ambient temperatures. Evacuated tube collectors (ETC), on the other hand, work differently than flat-plate collectors and are according to (Kalogirou, 2014a) usually a better option for colder climates.

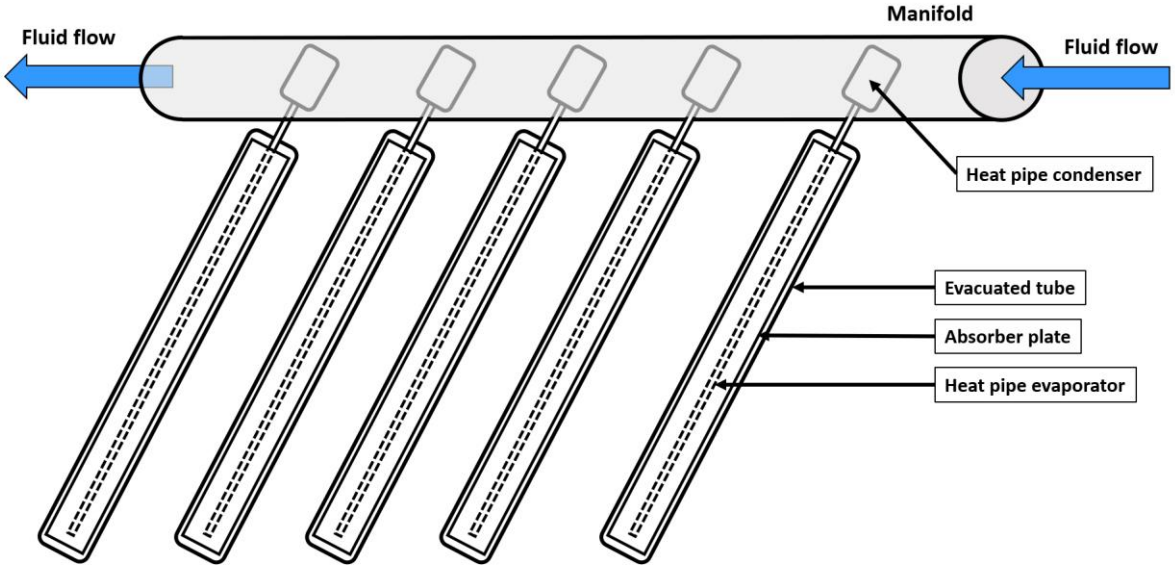

Figure 52: A schematic of an evacuated tube collector.
Source: Based on a figure by (Kalogirou, 2014a)

The traditional structure of an ETC can be observed in Figure 52. According to (Kalogirou, 2014a), ETCs consists of several heat pipes encapsulated inside vacuum-sealed tubes connected to the same manifold. Each of the sealed pipes is attached to a black copper fin (absorber), and also has a metal tip (condenser) attached to the sealed top. The metal tip reaches above the evacuated tube, and functions as a heat exchanger within the manifold. Lastly, inside the heat-pipe is a small amount of fluid, which regularly experience an evaporation-condensing cycle.

The evaporation-condensing cycle is explained by (Kalogirou, 2014a) to be a cycle where the solar energy from the sun evaporates the fluid in the evacuated tubes, and the lower density of the vapor makes it rise to the heat sink region of the pipe. At the heat sink region, the evaporated fluid delivers its latent thermal energy to the fluid running through the manifold and condenses back into liquid form. The fluid then returns back to the bottom of the tubes, before the process is repeated.

It has already been mentioned that ETCs have a relatively high performance compared to other solar collectors. According to (Kalogirou, 2014a), ETCs can also operate at higher temperatures than FPCs. The major drawbacks with ETCs, at least according to (Zijdemans, 2014), are steep investment costs and lower sturdiness compared to FPCs.

7.1.3 Performance of solar collectors

According to (Kalogirou, 2014a), the performance of a solar collector is defined as the ratio between the amount of solar radiation that is converted into useful thermal energy and the total amount of solar radiation hitting the collector surface. According to (Streicher, 2016), this performance is heavily dependent on the optical and thermal characteristics of the materials utilized in the solar collector, as well as the actual design of the collectors.

(Fan et al., 2009) provides the following equation for determining the performance of a solar collector:

$$\eta_{SC} = \eta_o \cdot k_\theta - a_1 \cdot \frac{T_m - T_a}{G} - a_2 \cdot \frac{(T_m - T_a)^2}{G} \quad \textbf{[7.1]}$$

Where η_o is the conversion factor of the collector [-], a_1 and a_2 are the first and second order heat loss coefficients of the collector in [W/m^{2}K] and [W/m^{2}K^2], respectively. T_m is the average temperature of the fluid running through the collector [K], T_a is the ambient air temperature [K], and G is the global solar irradiance in [W/m^2]. The parameter k_θ is the incident angle modifier of the solar collector, which can be calculated with:

$$k_\theta = 1 - \tan^P\left(\frac{\theta}{2}\right) \quad \textbf{[7.2]}$$

Where θ is the incident angle of the solar radiation [°], and P is a constant which has to be determined through measurements.

An explanation of the heat loss coefficients is provided by (Streicher, 2016), who explains that:

- a_1 is the overall heat transfer coefficient related to $T_m = T_a$
- a_2 is a quadratic term used as a black-box approach for the nonlinear radiation losses and the temperature dependency of the heat transfer coefficient

Both of these coefficients, as well as the conversion factor, are usually provided by the manufacturer of the solar collectors.

Figure 53 displays how the performance of the solar collector decreases for increasing temperature differences between T_m and T_a. The amount of solar radiation that is lost at optimal conditions is known as optical losses or reflection losses. The remaining radiation losses that occur due to the decreasing performance of the solar collector ($\Delta T > 0$) are known as thermal losses (heat losses). Figure 54 depicts the typical performance curve, as well as areas of application, for a swimming pool absorber, flat-plate collector and evacuated tube collector, at a global irradiance of 1000 W/m^{2}K.

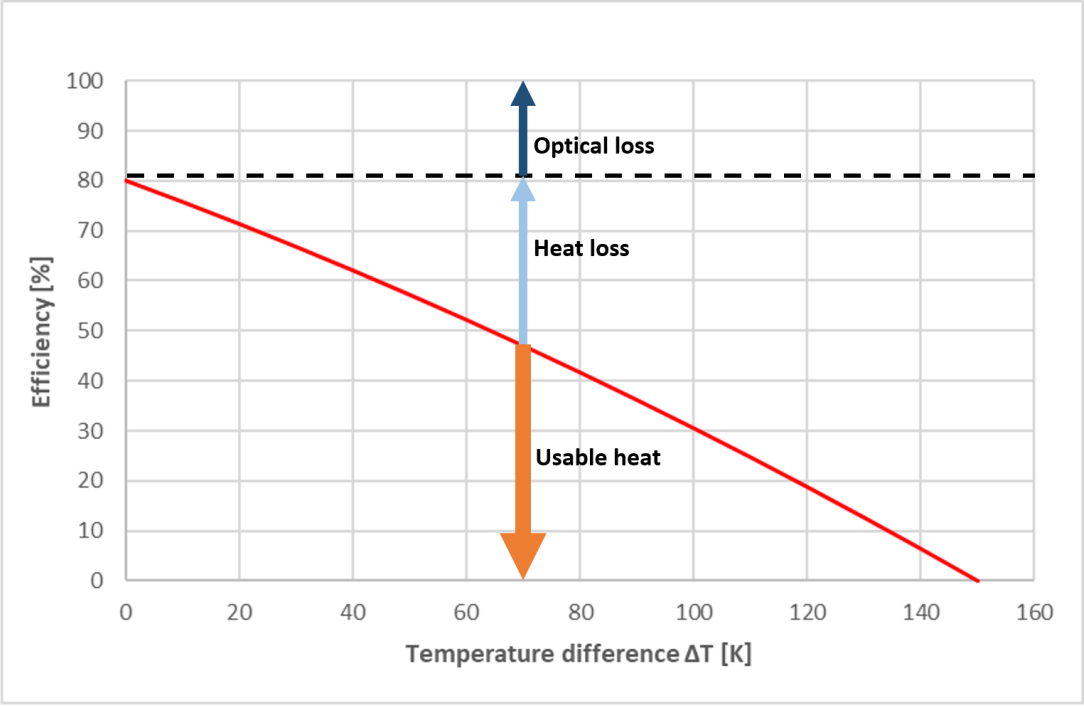

Figure 53: Decreasing performance of a solar collector due to increasing ΔT.
Source: Based on a figure by (Zijdemans, 2014)

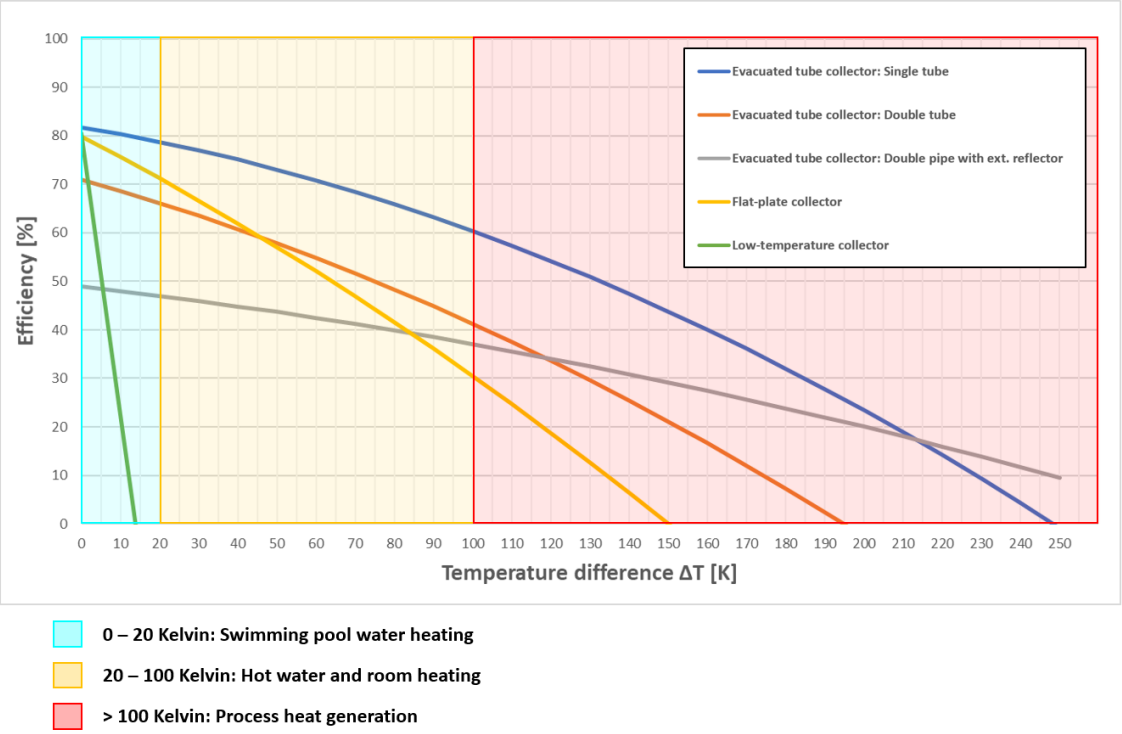

Figure 54: Performance curves and application areas for three different types of solar collectors. Source: Based on a figure by (DSG, 2010) and information by (Zijdemans, 2014)

7.1.4 Calculating the required solar collector area

The first step towards designing a solar water-heating system, at least according to (Zijdemans, 2014), is to map out the current energy need related to water-heating for the building. After this demand is identified, it is necessary to decide on a solar coverage ratio. This ratio indicates how much of the mapped hot water energy demand that the solar water-heating system should be able to cover. (Zijdemans, 2014) explains that this ratio is on average 50 to 60 % for the average Norwegian household if the sole purpose is to provide heat for domestic hot water. If the system is meant for both domestic hot water and space heating (combi-system), then the usual coverage ratio is 50 % for the DHW and between 10 to 30 % for the hydronic space-heating.

The next step is to calculate the amount of thermal energy the solar collectors can deliver to the system per square meter. It is therefore necessary to decide on the inclination and azimuth angle of the solar collectors. In addition to the aforementioned angles, several factors related to the type of solar collector should also be determined for a more accurate calculation of the energy yield.

The following two simplified equations, which are provided by (Zijdemans, 2014), are only suggested for smaller solar water-heating systems. The first equation is:

$$Q_{Yield} = I_{Opt} \cdot \overline{\eta_{SC}} \cdot f_A \cdot f_B \quad \textbf{[7.3]}$$

Where Q_{Yield} is the estimated specific annual energy yield of the solar collectors [kWh/m^2], I_{Opt} is the total amount of solar irradiance at the optimal solar inclination angle [kWh/m^2], $\overline{\eta_{SC}}$ is the average efficiency of the desired solar collectors [-], and f_A and f_B is the correction factor for the azimuth and inclination angle [-], respectively (introduced in Chapter 4.1: *Influence of orientation and inclination angle*).

When the annual estimated energy yield is calculated with Equation 7.3, then the following equation can be used to determine the required solar collector absorption area:

$$A_{SC} = \frac{Q_{EN} \cdot \eta_{SC,CR}}{Q_{Yield}} \quad \textbf{[7.4]}$$

Where A_{SC} is the required solar collector absorption area [m^2], Q_{EN} is the annual energy need of domestic hot water and space-heating in the building [kWh], and $\eta_{SC,CR}$ is the solar coverage ratio [-].

7.1.5 Cost of solar collectors

Similar to the photovoltaic modules introduced in Chapter 6.1: *Photovoltaic modules*, the cost of solar collectors are also heavily dependent on the utilized technology, manufacturer, expected performance, and additional features. Unfortunately, there are few, if any, standardized costs available for solar collectors. Various investment costs were therefore mapped out based on products found on the Internet.

Table 28 shows a couple of these solar collector products, and also displays some relevant features with them.

Table 28: Solar collector products found on Alibaba.com.
Source: Products from (Alibaba.com, 2020)

Manufacturer	Model	System type	Technology	Aperture area [m²]	Absorption area [m²]	Working environment	Weight [kg]	Warranty	Cost
Sidite Energy Co., Ltd	SP-F	Pressurized	Flat-plate	1.824	-	-	40	5 years	880 – 1 200 NOK
Sidite Energy Co., Ltd	SC-HP-30	Pressurized	Vacuum tube	2.82	2.42	-	25.7	5 years	3 120 – 3 360 NOK
Sidite Energy Co., Ltd	FP-GV2.0 (Black Chrome)	Pressurized	Flat-Plate	-	1.90	-40 to 140 °C	45	5 years	1 075 NOK
Haining Vision Solar Water Heater CO., Ltd	VFC-A	-	Flat-Plate	-	1.85	Down to -40 °C	35	10 years	975 – 1 460 NOK
Haining Vision Solar Water Heater CO., Ltd	VHC-5830	Pressurized	Vacuum tube	2.82	-	-40 to 260 °C	-	10 years	4 880 NOK
Haining Vision Solar Water Heater CO., Ltd	VUC-5818A-30	-	Vacuum tube	2.82	-	Down to -40 °C	-	15 years	1 952 NOK
Changzhou SKI Solar Energy Co., Ltd	SKI-CF	Pressurized	Flat-Plate	1.84	1.73	Down to -40 °C	35	3 years	1 350 – 1 760 NOK

Based on the costs above, one should expect to pay between 1 000 to 5 000 NOK for a single solar collector. The products displayed above are all manufactured in China, so one should also expect to pay a steep additional charge for having it shipped to Norway.

Enova

According to (Enova, 2020c), it is possible to receive 10 000 NOK in support for privately installing a solar thermal system, with an additional 200 NOK per m^2 for up to 25 m^2. What this means is that it is possible to reduce the total cost of solar collectors by a maximum of 15 000 NOK.

Similar to the Enova support scheme for photovoltaic modules, the fixed rate of 10 000 NOK is going to be reduced to 5 000 NOK from July 1st, 2020.

7.1.6 Solar collectors for the milk barn

As mentioned in Chapter 5.4: *Energy consumption at the milk barn*, the milk barn has an estimated total annual energy need of 28 561 kWh for the heating of tap water and water intended for space-heating. As the existing system on Mære already is a combi-system, the intention is to cover 50 % of the total hot water energy need. The solar collectors on the milk barn should therefore be dimensioned to cover about 14 280.5 kWh, annually. The potential heat recovery from the milk tank will be excluded in the calculations, as well as the simulation model, as it is challenging to implement into the software.

The simplified equations for determining the required solar collector area (Equation 7.3 & 7.4), were only recommended for smaller solar heating systems, but they will still be used in this master thesis as a basis for determining the required solar collector area for the milk barn.

The final result will be compared with the planned energy coverage, to estimate the possible error of such an assumption.

The expected annual energy yield for potential solar collectors on the milk barn can be found by using an azimuth angle correction factor of 1, as the collectors are assumed to be south-face, and an inclination angle correction factor of 0.96, as the roof on the milk barn has a tilt angle of 26º. The correction factors are found in Table 5.

According to (European Commission, 2020), the annual specific energy yield at an optimal angle at the location of the milk barn is about 1 082.47 kWh/m^2.

If Figure 54 is used to estimate the average solar collector efficiency for flat-plate and evacuated tube collectors, in the application area of 20-100 K hot water and room heating, and an average temperature difference of 60 K is assumed, then the estimated efficiency is 0.55 and 0.62 for the flat-plate and evacuated tube collector, respectively.

By using Equation 7.3, the expected energy yield for a flat-plate and evacuated tube collector at Mære Agricultural School, facing directly south and having an inclination angle of 26º, is 571.54 kWh/m^2 per year and 644.29 kWh/m^2 per year, respectively.

The next step is to use Equation 7.4 to determine the required solar collector area for both collector types. If the plan for the solar water-heating system is to cover 14 280.5 kWh annually, then the required solar collector area should be 24.99 m^2 for the flat-plate collectors and 22.16 m^2 for the evacuated tube collectors.

It should be noted that this is the required absorption area, not the gross area.

7.2 Thermal energy storage

After the solar collectors, the next central component in any solar water-heating system is the Thermal Energy Storage (TES). As explained by (Kalogirou, 2014b), this component is crucial in these systems as most areas experience darkness, or lack of sunlight, roughly half of the year. TES makes it possible to operate solar water-heating systems continuously during the year by storing heat from periods with surplus thermal energy generation.

According to (Kalogirou, 2014b), the two central functions of TES are:

- To improve the utilization of the collected solar energy. Primarily by storing the excess thermal energy from periods with a large amount of solar radiation to periods with low amounts.
- To improve the efficiency of the system by preventing the heat transfer fluid, which runs through the solar collectors, to reach a too high temperature.

(Sarbu & Sebarchievici, 2018) explains that there are several possible ways to classify TES. These classifications are primarily based on the characteristics and features of the storage component, such as the:

- Capacity (Storage process, medium and size of the system)
- Power (Charge and discharge speed)
- Efficiency (System losses)
- Storage period (hours, days or months)
- Charge and discharge time
- Cost (Capital and operation cost)

Even though there are several possible classifications, the three main categories for TES are Sensible Heat Storage, Latent Heat Storage, and Chemical Heat Storage (see Figure 55). The most common characteristics for these three TES systems, such as capacity, power, efficiency and storage period, are all summarized in Table 29.

Sensible Heat Storage (SHS) is explained by (Sarbu & Sebarchievici, 2018) to be both the most manageable and also generally the most utilized heat storage principle. Briefly described, SHS revolves around accumulating thermal energy into a solid or liquid medium whose temperature will therefore begin to rise.

A graphical illustration of SHS can be seen in Figure 56a.

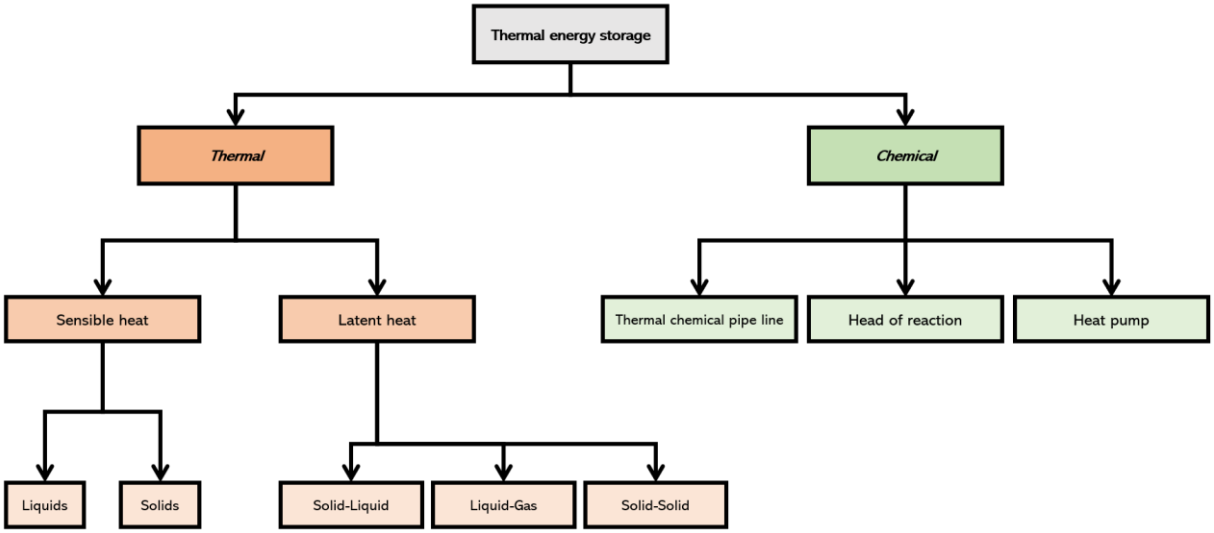

Figure 55: Different types of thermal energy storages.
Source: Based on a figure by (Sarbu & Sebarchievici, 2018)

Table 29: Typical parameters for different types of thermal energy storage systems.
Source: (Hauer, 2011)

Thermal Energy Storage System	Capacity [kWh/t]	Power [MW]	Efficiency [%]	Storage Period
Sensible (hot water)	10 – 50	0.001 – 10.0	50 – 90	Day – Year
Phase-change material (PCM)	50 – 150	0.001 – 1.0	75 – 90	Hour – Week
Chemical reactions	120 – 250	0.01 – 1.0	75 – 100	Hour - Day

The concept of Latent Heat Storage (LHS) (also known as Phase-Changing Materials) is also explained by (Sarbu & Sebarchievici, 2018). The principal idea is to get materials to absorb or release thermal energy by changing its physical state. LHS makes it possible to store heat at a relatively constant temperature.

Figure 56b shows a graphical illustration of the LHS principle.

According to (Sarbu & Sebarchievici, 2018), the main benefit of LHS compared to SHS, is its capacity for storing heat at almost a constant temperature. Table 29 also suggests that LHS have a higher efficiency than SHS.

The last type of TES, Chemical Heat Storage (CHS), is also described by (Sarbu & Sebarchievici, 2018). The storing process of CHS is more complicated than the other two, but the primary approach is to utilize Thermo-Chemical Materials (TCM) to store and release thermal energy in a reversible endothermic and exothermic reaction process (see Figure 56c).

A more detailed breakdown of the process is provided by (Sarbu & Sebarchievici, 2018). First, thermal energy is applied to a material A in a charging process. The employed heat leads material A to split into two separate substances, B & C, respectively. The two materials are then stored and kept separate until a discharge process is necessary. B & C are then mixed back together at the appropriate pressure and temperature conditions, releasing the stored thermal energy.

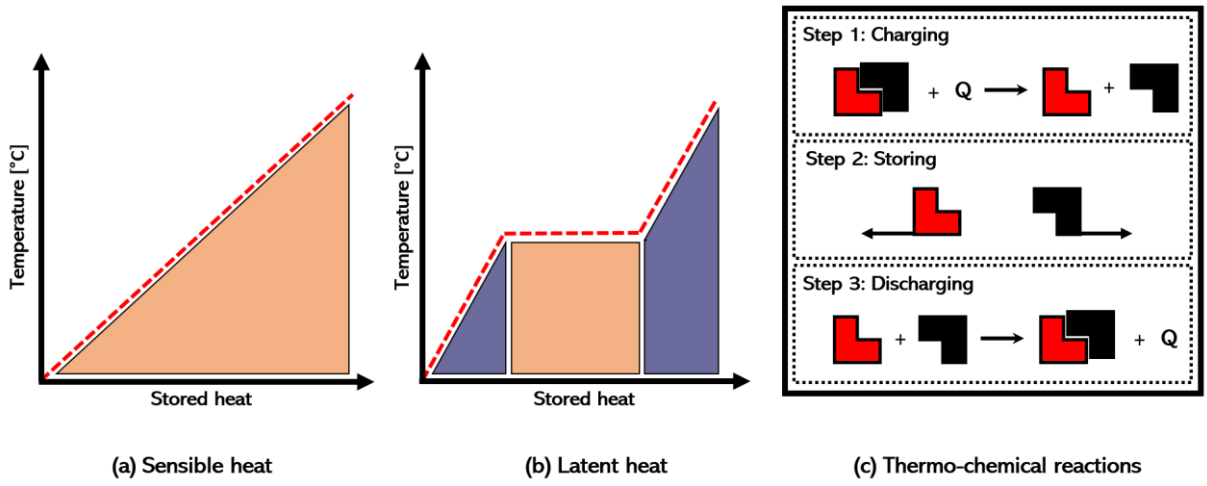

Figure 56: Three different types of thermal energy storage.
Source: Based on a figure by (Sarbu & Sebarchievici, 2018)

For this master thesis, the focus of the feasibility study will be on thermal energy storage that utilizes sensible heat storage, intended for short-term storage and with water as the storage material.

7.2.1 Thermal stratification and temperature requirements

Thermal stratification

Thermal stratification is a phenomenon that should be accounted for when designing solar water-heating systems. According to (Eyecular, n.d.), water density is dependent on the water temperature, where hot water has a lower density than cold water, which results in the water being divided into thermal layers in the storage tank, with layers of hot water being stored above the cold water layers.

The phenomenon of water being stored in layers due to different temperatures is known as thermal stratification.

The importance of including thermal stratification into the design considerations is due to its effect on the performance of the solar water-heating system. According to (Fan & Furbo, 2009), if the storage tank experiences a high degree of thermal stratification, then the performance of the solar heating system is increased due to the lower return temperature to the solar collectors, which makes it possible to collect more solar energy and increase the number of operating hours.

(Fan & Furbo, 2009) further explains that a higher degree of thermal stratification also results in lower demand for auxiliary heating, as the temperature in the top of the storage tank will be close to the desired temperature load.

According to (Han et al., 2009), three methods can be utilized to achieve thermal stratification in the storage tank. These methods are:

1. Heating the vertical surfaces of the storage tank, as this will result in thermal boundary layers which will draw the heated fluid upwards in the tank.
2. Carefully placing the heat exchanger between the solar circuit and the storage tank (if closed-loop).
3. Directly inputting the fluid running from the solar collectors into suitable heights in the storage tank (if open-loop).

If (Han et al., 2009) is to be believed, then thermal stratification may increase the efficiency of the storage tank with up to 6 %, and also improve the performance of the solar water-heating system with up to 20 %, compared to utilizing a storage tank where the water is thoroughly mixed (uniform temperature).

Both these types of storage tanks can be seen in Figure 57.

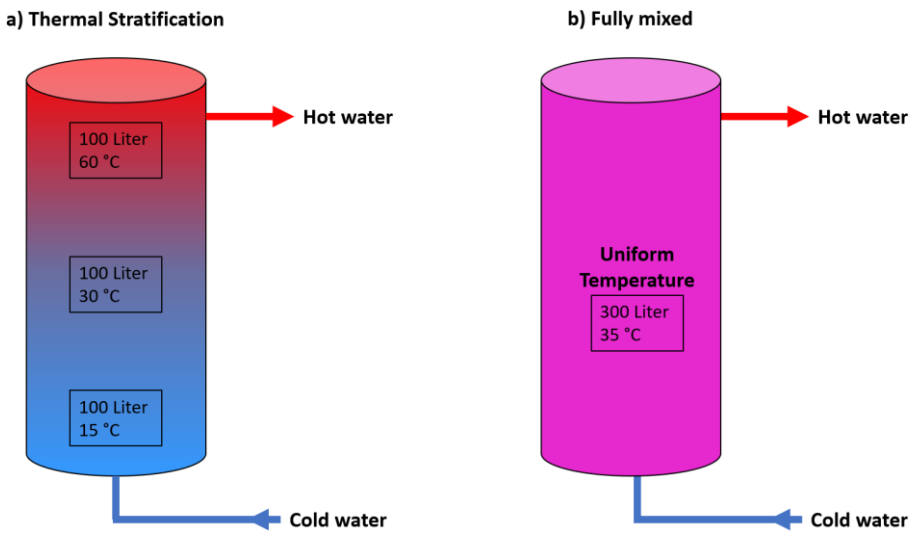

Figure 57: Thermal energy storage tanks with a) Thermal Stratification, and b) Uniform temperature. Source: Based on a figure by (DSG, 2010)

According to (Sarbu & Sebarchievici, 2018), it is possible to determine the storage capacity of a thoroughly mixed thermal energy storage by using the following equation:

$$Q_s = m_w \cdot c_p \cdot \Delta t_s \qquad \textbf{[7.5]}$$

Where Q_s is the total thermal energy capacity of the storage [J] at a temperature range of Δt_s [K], c_p is the specific heat of water [J/kg·K], and m_w is the mass of water [kg].

Temperature requirements

In addition to thermal stratification, another factor that it is crucial to consider when designing a domestic hot water system is the actual temperature of the hot water. As stated by (Zijdemans, 2014), the tap water temperature should be high enough so that the users are satisfied, but also have no risk of burning (scolding) the user.

The water temperature inside the storage tank must also be high enough so that it poses no risk of forming legionella.

According to (Zijdemans, 2014), the three main factors that affect the choice of hot tap water temperature are:

1. Low enough temperature from the mixing valve to avoid scolding.
2. High enough water temperature to cover the demand of the consumer.
3. High enough temperature to avoid legionella growth in the storage tank and the pipes.

The highest temperature allowed before the user should expect scolding is dependent on the age and health of the occupant(s). Table 30 shows the average temperature requirements necessary to cover consumer demands. According to (Byggteknisk forskrift, 2017), water fixtures in buildings containing residents that should not be expected to be able to change the water temperature themselves, should be installed with additional safety devices, preventing the hot tap water temperature from rising above 38 ^{o}C.

For average occupancy, the water fixtures should not deliver water with a higher temperature than 55 ^{o}C.

Table 30: The required temperatures for different hot water activities.
Source: (Zijdemans, 2014)

Activity	Common temperature requirements
Bathing, showering and hand washing	38 – 40 °C
Dishwashing and rinsing by hands	40 – 50 °C
Laundry and rinsing by hands	40 – 50 °C
Floor cleaning	45 – 55 °C

According to (Zijdemans, 2014), legionella can grow naturally in humid areas, but is not considered very dangerous to healthy, young people unless it reaches very high concentrations, while other occupants, such as people with impaired immune systems, older residents or people who smoke, will be more vulnerable to lower intensities of legionella.

(Zijdemans, 2014) lists the following circumstances that influence the growth of legionella in storage tanks:

- The bacteria propagate in the water when the temperature is between 20 to 50 ^{o}C, though they favor 30-43 ^{o}C.
- The bacteria is dependent on a pH value between 3 to 10, but usually prefer a value between 6 and 7.
- The concentration of Sodium salts in the water must be below 1.5 % for legionella to grow.
- A high degree of Calcium and Magnesium in the water will increase legionella growth, with Iron and Zinc having a similar effect.
- Legionella needs oxygen to survive, and the minimum oxygen content in water for legionella to thrive is 2.2 mg/L.

(Zijdemans, 2014) also lists a couple of methods to reduce the risk of legionella. These methods are also recommended by the Norwegian National Institute of Public Health. An excerpt of some of these methods are:

- Not laying the cold water pipelines in heated zones of the building, and avoid having the temperature of the cold water, sent out from the mixing valve, below 20 ^{o}C after 2 minutes of continuous consumption.
- All water inside the storage tank must be heated to a minimum temperature of 70 ^{o}C, regularly. This also applies to the water below the electric heating element.
- The temperature of the water sent out from the mixing valve attached to the storage tank should not decrease to below 55 ^{o}C for more than 20 minutes a day.
- If a storage tank is used as a preheater, then the water inside the tank should be increased to a minimum of 70 ^{o}C, at least once a week during periods with lower water consumption.

7.2.2 Charging with solar energy and auxiliary heating

There are several possible ways to connect and attach solar circuits to storage tanks. An overview of some of these circuits is provided by (DSG, 2010), and can be seen in Figure 58. The letter S in the figure symbolizes the placement of the temperature sensor. (DSG, 2010) also presents various ways to attach an auxiliary heat source to the storage tank (see Figure 59). In this figure, the abbreviation AH stands for Auxiliary heater.

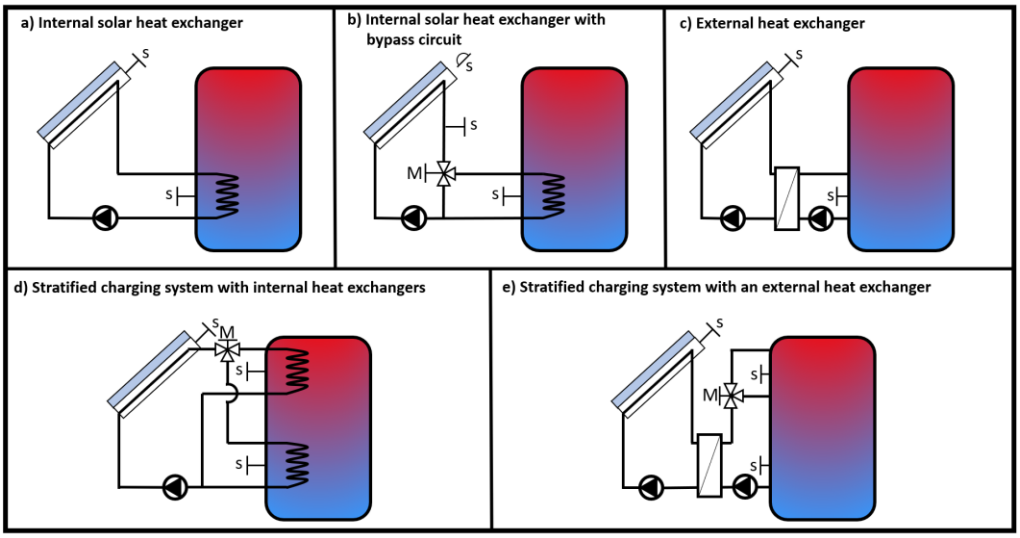

Figure 58: Types of store charging with solar energy.
Source: Based on a figure by (DSG, 2010)

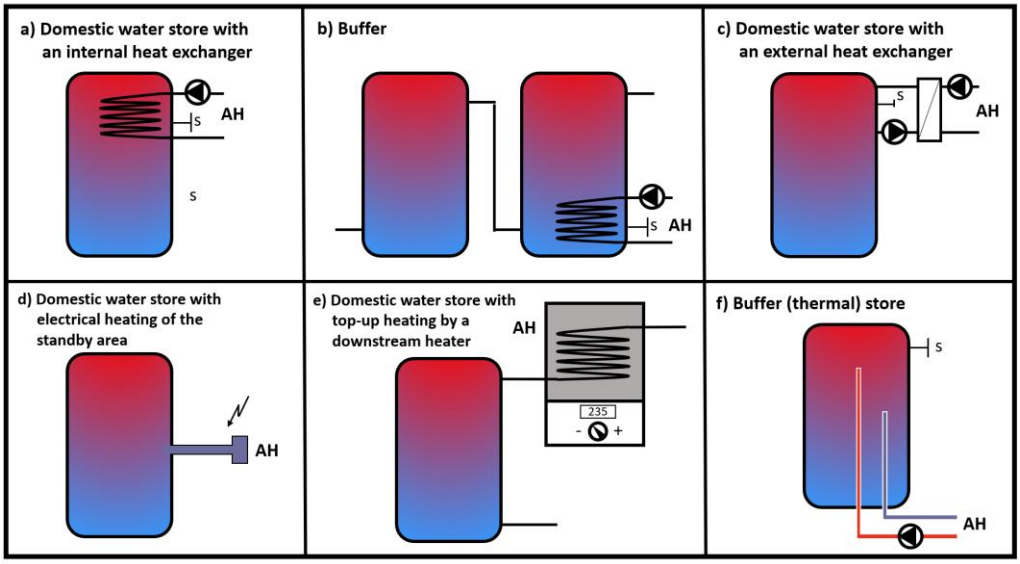

Figure 59: Types of store charging with auxiliary heating.
Source: Based on a figure by (DSG, 2010)

Discharging stored energy

In the previous subchapter, the focus was on charging TES with either solar energy or auxiliary heaters. The storage tanks must also be able to discharge the thermal energy, and according to (DSG, 2010), there are several different methods to accomplish this, some of which can be seen in Figure 60.

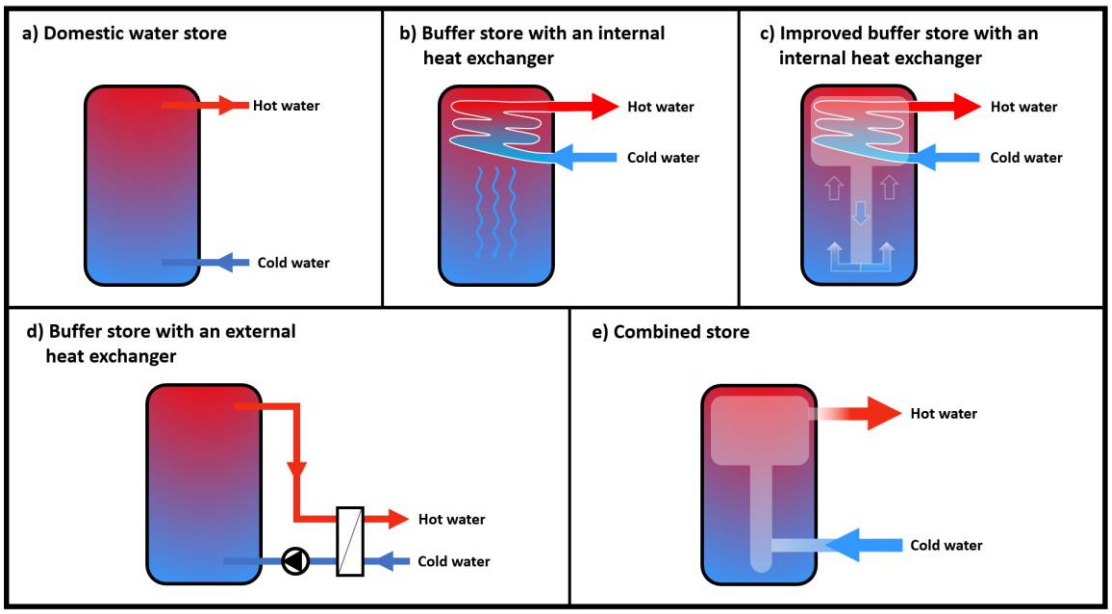

Figure 60: Methods for discharging stored energy.
Source: Based on a figure by (DSG, 2010)

The different charging and discharging arrangements presented in Figure 58, Figure 59 and Figure 60 can be combined to create several different hot water system solutions. According to (DSG, 2010), the most basic solar water-heating system for heating of domestic hot water can be seen in Figure 61.

The figure shows a closed-loop solar system (indirect), with an internal heat exchanger, that utilizes a circulation pump to force circulation to the solar collectors. The storage tank is also connected to an auxiliary heater through an additional internal heat exchanger.

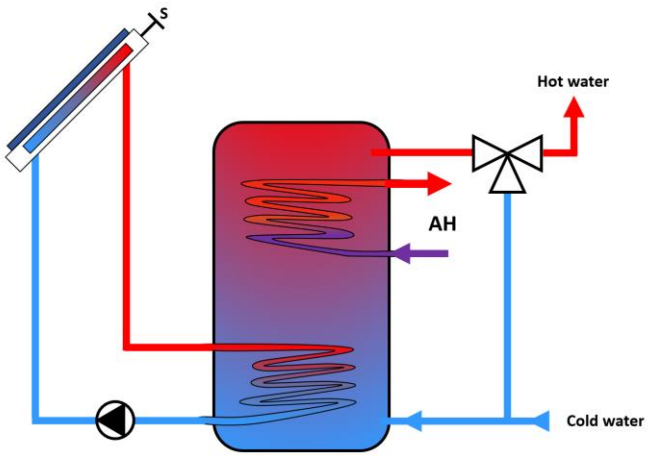

Figure 61: Standard solar water-heating system for domestic hot water.
Source: Based on a figure by (DSG, 2010)

7.2.3 Sizing storage tanks for solar energy

It is vital to take special care when sizing the storage tank for the solar water-heating system. As (Zijdemans, 2014) points out, an oversized storage tank may result in long periods where the water has to be heated with an auxiliary heat source before reaching appropriate temperatures. On the other hand, the storage tank can also be dimensioned too small, resulting in inefficient use of solar collectors, as the storage tank cannot store the full amount of solar energy due to its limited capacity.

(Zijdemans, 2014) provides simplified assumptions to more easily determine the required storage tank size in solar water-heating systems. The assumptions vary based on if the storage tank should be able to store energy intended for only hot tap water or be able to cover a part of the space-heating demand as well.

According to (Zijdemans, 2014), for solar water-heating systems that are only meant for hot tap water, the storage tank size should be between 1.2 to 1.5 times the daily amount of consumed hot water. If the hot tap water consumption is not known, then the sizing of the storage tank is usually based on previous experience, often about 50 to 75 liters per m^2 of solar collector surface area. If the solar water-heating system is a combi-system (tap water + space-heating), then (Zijdemans, 2014) suggest using 75–125 liters per m^2 of solar collector surface area.

(Zijdemans, 2014) lastly mentions that simulation software is necessary to determine a more accurate sizing of the storage tank.

7.2.4 Cost of sensible heat storage

(IRENA, 2013) suggests that the price of SHS is heavily dependent on the size of the storage tank, application and also utilized insulation technology, and that one should expect to pay between 1 to 100 NOK per kWh capacity. A similar estimate is provided by (Glatzmaier, 2011), who suspects that an investor should expect to pay 70 NOK per kWh of capacity for a high-temperature stainless steel tank, and 30 NOK per kWh if the storage tank is a low-temperature carbon steel unit. In addition to the cost of the storage tank itself, (Glatzmaier, 2011) also suggests that one should expect an additional charge of 130 NOK per kWh for storage tank supports, site work, storage medium, electrical equipment and instrumentation, as well as necessary piping, valves and fittings.

Enova

In addition to supporting investments in photovoltaic modules and solar collectors, (Enova, 2020a) also economically contribute with the installing of a storage tank inside a building. They will support the purchase with up towards 5 000 NOK, depending on the investment cost of the unit. To be able to receive the maximum amount of support, the total investment cost of the storage tank has to be equal or above 20 000 NOK.

7.2.5 Sizing the required storage tank for the milk barn

The annual water consumption at the milk barn is estimated by the administration of the school to be about 3 212 365 liters. Of the hot water consumption, 3 075 125 liters is drinking water for the livestock, while the remaining 127 240 liters are hot tap water and water intended for hydronic space-heating. According to technical specifications provided by Mære Agricultural School, the existing storage unit has a volume of 300 L, while the attached water heater has a size of 250 L. This suggests that the drinking water meant for the cattle is not heated in the hot water system in the milk barn.

If solar collectors are implemented into the existing hot water system, then the current storage tank has to be replaced with a larger unit to be able to store the additional amounts of solar energy. If the ratio of 75 to 125 liters per m^2 of solar collector area is used to determine the size, then the minimum storage tank should be roughly 1 662 liters, while the maximum should be 3 123.75 liters.

Due to the wide variations in volume, based on the simplified assumptions, three cases will be implemented into the simulation software. The first case is a 1500 liters volume tank, while the second and third case is storage tanks with a volume of 2000 and 3000 liters, respectively.

The 3000-liter storage tank is the reference case in this master thesis.

7.3 Solar circuit

According to (Zijdemans, 2014), liquid-based solar water-heating systems are usually relatively simple and consists only of a few elements. Both solar collectors and thermal energy storage have been introduced in the previous subchapters, and in this subchapter, the main focus is on the components in the solar circuit.

(Zijdemans, 2014) explains that the solar circuit is defined as a collective term for pipelines and components linking the solar collectors to the thermal energy storage. The most central pieces of equipment in the solar circuit are:

- Pipes
- Circulation pump
- Check valve
- Filters
- Expansion and drain-back vessels
- Controllers and monitors
- Heat transfer fluid

7.3.1 Pipes

The pipes in the solar circuit are responsible for transporting the heat transfer fluid between the solar collectors and the thermal energy storage. According to (Zijdemans, 2014), the most frequently used pipe types are corrugated stainless steel pipes and copper pipes, and the heat transfer fluid should be carried through the pipelines with as little friction, impact, and heat loss as possible.

The reason for this, as stated by (Zijdemans, 2014), is that heat loss from the pipes represents a significant proportion of the total heat loss of the solar water-heating system and should therefore be reduced as much as possible.

(Smith, 2018) provides the following equation for calculating the heat loss from the pipelines:

$$Q_{pipe,loss} = 2 \cdot \pi \cdot k \cdot L \cdot \frac{T_m - T_a}{\ln\left(\frac{r_2}{r_1}\right)} \quad \textbf{[7.6]}$$

Where $Q_{pipe,loss}$ is the heat loss from the pipe [W], k is the thermal conductivity of the pipe material [W/m·K], L is the length of the pipe [m], T_m is the temperature of the heat transfer fluid inside the pipe [K], T_a is the ambient air temperature surrounding the pipe [K], and r_1 and r_2 is the inner and outer radius of the pipe [mm], respectively.

(Zijdemans, 2014) suggests several possible methods for reducing the heat losses related to the pipes. One suggestion is to have the pipelines be as short as possible. The thickness of the pipelines can also be increased to reduce the losses. If this increased thickness is due to additional insulation, the result will be a lower thermal conductivity, which would reduce the heat losses even further.

Sizing pipes to and from solar collectors

According to (Solar365, n.d.), to be able to dimension the pipelines going to and from the solar collectors, it is vital to consider the amount of flow expected to run through the pipes. If the diameter is too small, then the friction increases, resulting in a slower flow and necessitates a bigger circulation pump. On the other hand, if the pipe diameter is too large, then the system installation costs may become unnecessary high.

Table 31 shows estimations on the required pipe diameters for different volume flows.

Table 31: Pipe diameter with recommended maximum flow.
Source: (Solar365, n.d.)

Pipe diameter	12.7 mm (0.5 inch)	19.1 mm (0.75 inch)	25.4 mm (1 inch)	31.8 mm (1.25 inches)	38.1 mm (1.5 inches)	50.8 mm (2 inches)	63.5 mm (2.5 inches)	76.2 mm (3 inches)
Recommended maximum flow	340.7 L/h	608.5 L/h	1 817.0 L/h	3 179.8 L/h	4 996.7 L/h	10 220.6 L/h	19 305.6 L/h	29 526.2 L/h

7.3.2 Circulation pump

(Zijdemans, 2014) describes the circulation pump as the heart of any solar water-heating system, and this is probably an accurate description, as it is responsible for pumping the heat transfer fluid to the solar collectors and back to the storage tank. If the pump stagnates, then the solution will stop running, and if the stagnation is due to faulty equipment, it is possible that the heat transfer fluid starts to boil and evaporate, potentially damaging the system. This can be avoided by installing appropriate safety equipment in the solar circuit.

According to (Zijdemans, 2014), one way to reduce the risk of overheating is to install a circulation pump with a high starting torque, decreasing the probability of unintentional stagnation. The pump should also be able to handle the frequent start and stop cycles for solar water-heating systems and also be able to manage the high fluid temperatures running through the pipelines.

7.3.3 Check valve

According to (Zijdemans, 2014), during periods where there are little to no available sunlight, the temperature of the water inside the storage unit may rise above the temperature of the heat transfer fluid in the solar collectors. During these situations, it is possible that the system involuntarily starts to circulate in reverse, removing the heat from thermal energy storage and carrying it to the solar collectors, trying to achieve a sort of heat balance. A check valve can be used to prevent this backward circulation from ever happening.

The concept of check valves is further explained by (Menon, 2015), who states that check valves are usually in a closed position, only opening for fluid running the correct way through it. If the pressure downstream of the valve surpasses the pressure upstream, then the check valve will close, hindering the fluid from returning through the check valve.

Some of the available check valve types can be seen in Figure 62.

The principal distinctions between the check valve types presented in the figure below are the permitted ratio range between the length of the pipeline and the diameter of the pipe. According to (Menon, 2015), swing check valves can have a length/diameter ratio of upwards to 50, while lift check valves allow for a maximum ratio of 600.

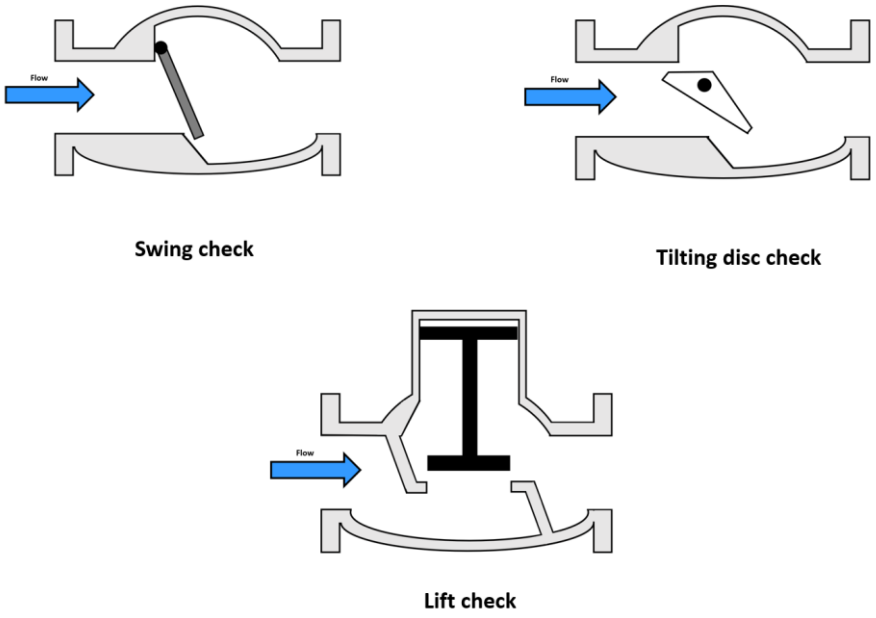

Figure 62: Different types of check valves.
Source: Based on figures by (Menon, 2015)

7.3.4 Filters

Briefly mentioned by (Zijdemans, 2014), filters are solar circuit equipment that catches and collects particles inside of the circuit. The filters have to be manually removed and systematically cleaned to avoid blocking of the circulation flow. By installing throttling valves on both sides of the filters, the fluid flow can be restricted during maintenance.

According to (DSG, 2010), if no proper filtering is employed in the solar circuit, then this can over time impair functions of the circulation pump, safety valves and mixing valves.

7.3.5 Expansion and drain-back vessels

According to (Viridian Solar, n.d.), expansion vessels are additional equipment used in pressurized closed-loop solar energy systems. In these systems, the solar circuit is entirely filled with heat transfer fluid, and as the fluid's density is dependent on its temperature, an expansion vessel becomes necessary to avoid having the liquid expand to a larger volume, which could possibly harm the pipes and components.

This necessity is further pointed out by (Zijdemans, 2014), who states that since the circuit is already full of liquid, the expanded volume must have somewhere to move.

Drain-back vessels are a little different than expansion vessels, as these additional pieces of equipment are installed in non-pressurized systems, where the solar circuit is not completely packed with a heat transfer medium. Non-pressurized solar water-heating systems that utilize a drain-back vessel are known as a drain-back system, are according to (Viridian Solar, n.d.) a suitable addition to solar water-heating systems located in colder climates. The reason for this is that during periods where there are unfavorable solar conditions or the circulation pump has stagnated, the heat transfer fluid "rests" inside the drain-back vessel.

(Viridian Solar, n.d.) also explains that to have the fluid rest during pump stagnation, the drain-back vessel has to be located at a height below the solar collectors, but also at a point higher than the circuit's circulation pump. It is also preferred to have the vessel installed at a location where the temperature of the resting fluid does not reach the freezing point.

A drain-back system during both operation and stagnation can be seen in Figure 66.

7.3.6 Control and monitoring

Subjects relevant for this section will be further elaborated in Chapter 7.4: *Controllers for solar water-heating systems*. Briefly explained, the central purpose of controllers in solar circuits is to operate the circulation pump during periods where the solar collectors generate thermal energy. As (Zijdemans, 2014) points out, this means periods where the temperature in the solar collector is higher than in the thermal energy storage.

According to (Zijdemans, 2014), there also exist more advanced control systems, such as velocity regulated circulation pumps, which serves to provide a predetermined supply temperature to the thermal energy storage. If some of the solar collectors have different orientations, then the solar water-heating system could be divided into several separate solar circuits.

In this case, the control system must be able to control several pumps at the same time, or the controllers have to be able to communicate with each other.

7.3.7 Heat transfer fluid

The heat transfer fluid in the solar circuit is usually referred to as the solar liquid, and if the circulation pump is the heart of every solar water-heating system, then the heat transfer fluid is the blood. The main purpose of the solar liquid is to absorb the heat generated at the solar collectors and carry it to the storage tank. (DSG, 2010) explains that the temperature of the solar liquid may vary from -15 to 350 ^{o}C, depending on the solar conditions at the system location, which means that in worst-case scenarios, the heat transfer fluid may freeze or evaporate. It is therefore necessary to choose a heat transfer fluid that is appropriate for the individual solar water-heating system.

According to (Zijdemans, 2014), the most common heat transfer fluid in pressurized systems is a glycol-water mixture. He also lists the following benefits of using this fluid as the solar liquid:

- It can handle high temperatures without taking permanent damage.
- It has a low freezing temperature and a relatively high specific heat capacity.
- It doesn't affect the environment negatively when released into nature.
- It is neither poisonous for humans nor corrosive for the solar energy system.

(Zijdemans, 2014) also provides estimations on freezing temperatures for different concentrations of propylene glycol in a water mixture. These temperatures and their corresponding mixture concentrations can be seen in Table 32.

Table 32: Freezing temperatures for propylene glycol-water mixtures.
Source: (Zijdemans, 2014)

Share of propylene glycol [mass %]	Freezing point [^{o}C]
0	0
10	-3
20	-7
30	-12
36	-18
40	-20
43	-23
48	-29
52	-34
55	-40
58	-46
60	-51

Unfortunately, there are not only benefits with using such mixtures. (Guyer, 2019) explains that these mixtures have a lower heat capacity compared to pure water, and they also have a higher fluid viscosity, resulting in a higher circulation pump energy demand to push the fluid through the circuit. In addition to the previous drawback, there is also a possibility of the glycol mixture deteriorating, which can result in an internal blockage of the heat transfer fluid or permanent damage to the solar circuit. Lastly, it becomes more necessary than ever to have a heat exchanger between the solar circuit and the thermal energy storage, to avoid having the solar liquid mix with the drinking water. This additional heat exchanger will reduce the efficiency of the heat transfer.

7.4 Controllers for solar water-heating systems

Control systems in solar water-heating systems are responsible for managing the operation of the circulation pump in the solar circuits, and poor system performance is often, at least according to (DSG, 2010), contributed to faulty controller systems. (Kalogirou, 2014b) suggests avoiding very complicated control systems to lower the risk of experiencing difficulties with the solar water-heating system.

(Kalogirou, 2014b) also explains that control systems should be able to handle all of the operating modes of the solar water-heating system. These modes include heat collection and rejection, power failure, freeze protection and auxiliary heating.

7.4.1 Differential Temperature Controller

According to (Kalogirou, 2014b), the most common solar circuit controller is the Differential Temperature Controller (DTC). This controller measures and compares the temperature from a minimum of two separate temperature sensors. In this case, one is located at the solar collector, while the other is placed inside the thermal energy storage. If the temperature of the fluid inside the collectors exceeds the temperature inside the storage unit, the controller signals the circulation pump to start.

Figure 63 shows a DTC system for a solar water-heating system.

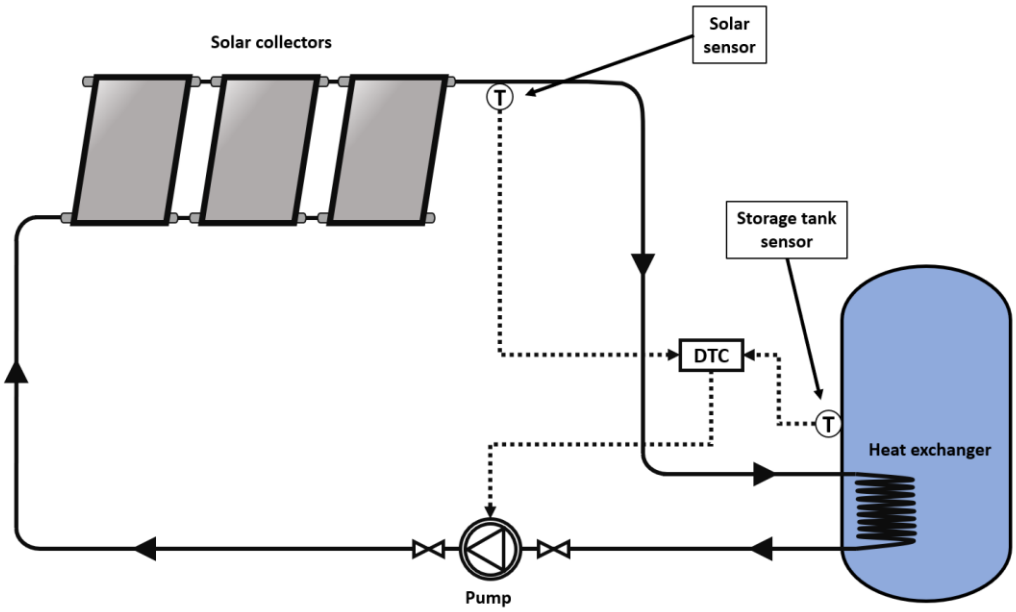

Figure 63: A solar water-heating system with a differential temperature controller. Source: Based on a figure by (Kalogirou, 2014b)

Potential difficulties with DTC systems

According to (Kalogirou, 2014b), there may be some difficulties with DTC systems if they are not correctly configurated. The most significant being the phenomenon known as short cycling. Here, the temperature differences for the start-up and shut-off on the circulation pump is too close to each other, resulting in the pump frequently starting and stopping. Periods with short cycling should be avoided, or at least minimized as much as possible, as it may do damage the circulation pump.

(Kalogirou, 2014b) explains that short cycling is influenced by factors such as solar radiation intensity, the flow rate of the pump, the thermal mass of the solar collectors and fluid inlet temperature into the solar collectors, and that the traditional way to avoid short cycling is to use broad temperature differences for the start-up and shut-off control. The biggest drawback with this solution is that the solar water-heating system could now require large amounts of solar radiation to start the circulation pump, which may result in potentially extensive production losses, especially during periods with moderate amounts of solar radiation.

Considerations when placing sensors

The placing of the various temperature sensors plays a significant role in the performance of the solar water-heating system, as they measure the temperature conditions and sends the information to the controller. According to (Kalogirou, 2014b), it is imperative that the sensors have sufficient thermal contact with the solar collector plate or the pipes, as this will affect the accuracy of its measurements.

For solar collectors, the temperature sensor can be placed either inside of the collector or at the outlet pipe. According to (Kalogirou, 2014b), there are benefits and drawbacks with both of these options, as it is more challenging to install temperature sensors inside the solar collectors, but that it would present more accurate readings, instead of simply placing it at the beginning of the outlet pipe.

If the sensors are going to be placed at the outlet, then there are two possible ways to install the temperature sensor, both of which are presented in Figure 64.

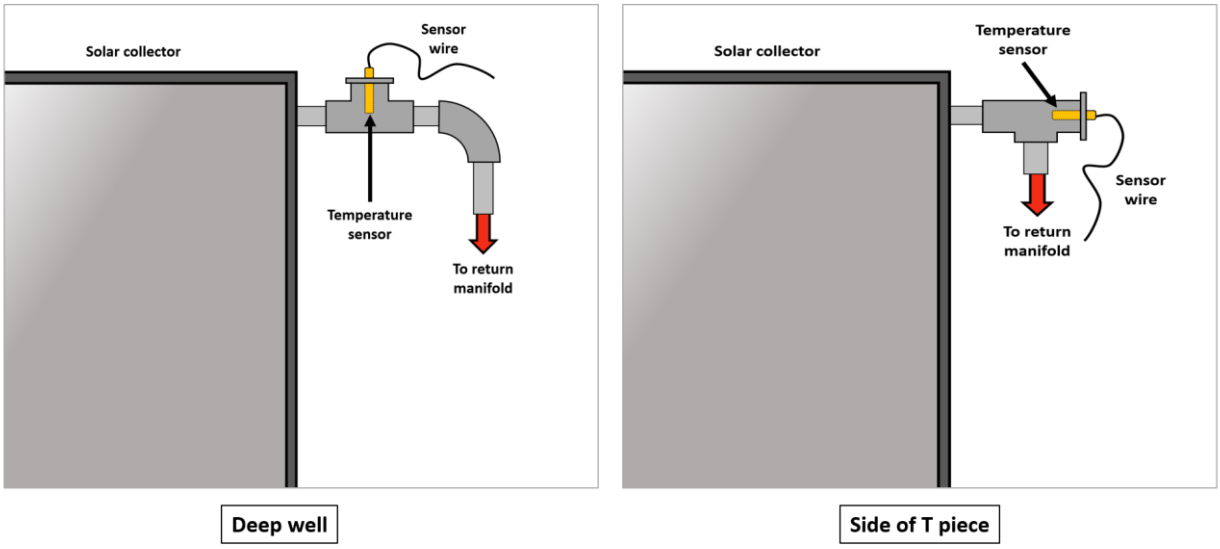

Figure 64: Potential placement of temperature sensors at a solar collector outlet.
Source: Based on figures by (Kalogirou, 2014b)

The sensor inside the storage tank is ordinarily located close to the bottom of the tank, but according to (Kalogirou, 2014b), the optimal placement of the temperature sensors is at one-third of the height of the storage tank. If an internal heat exchanger is utilized inside the storage tank, then the temperature sensor should be installed above the exchanger.

If the solar water-heating system is expected to experience long periods with low ambient temperatures and does not utilize anti-freeze fluid in the solar circuit, then it may become necessary to place a freeze protection sensor inside the collector. (Kalogirou, 2014b) states that this sensor should be placed at a location where it has the opportunity to detect the coldest temperature of the fluid running through the collectors. There are two locations at the solar collector that fits this description. The first is at the back of the absorber plate inside the solar collector, while the other is at the inlet pipe to the collectors.

Figure 65 shows illustrations of other possible placements of temperature sensors for DTC configurations.

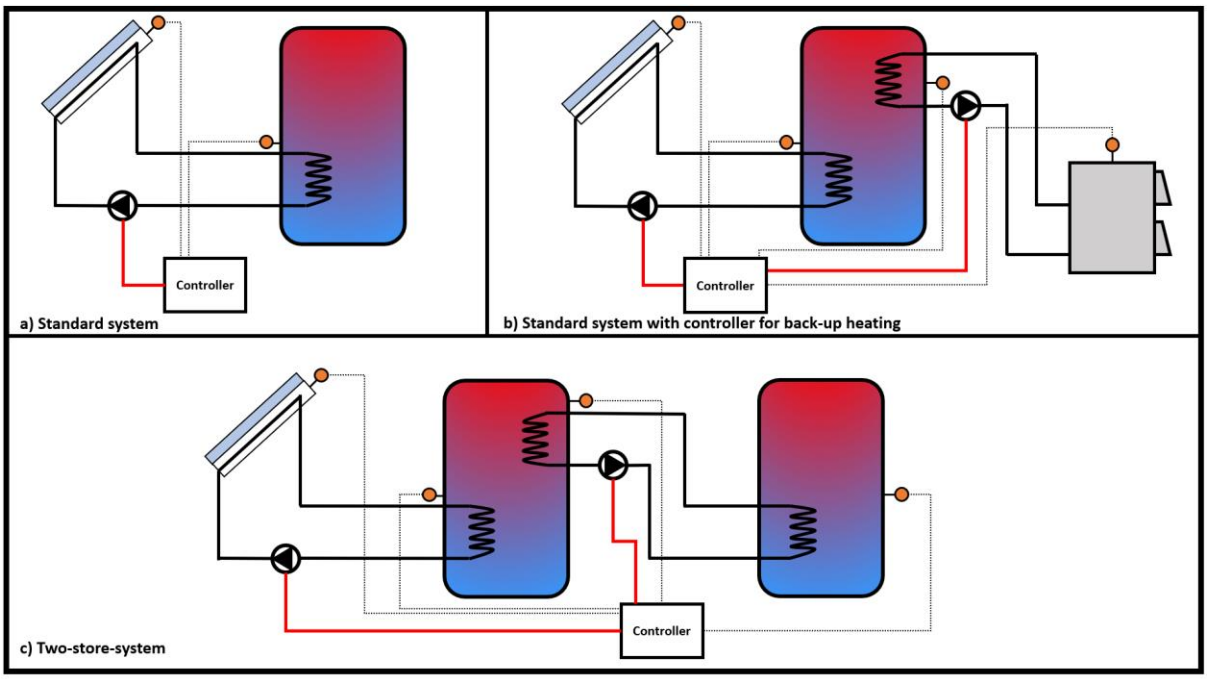

Figure 65: Examples of possible DTC systems.
Source: Based on figures by (DSG, 2010)

7.5 Important system considerations

7.5.1 Drain-back systems

As previously mentioned, all of the heat transfer fluid is resting inside the drain-back vessel when the pump is not operating in drain-back systems. According to (Viridian Solar, n.d.), during periods with adequate amounts of global solar irradiance, the circulation pump will start to push the transfer fluid out of the resting position inside the drain-back.

When the solar conditions become unfavorable, and the temperature difference between the solar collectors and the storage unit becomes small enough, the circulation pump is switched off, and gravity pulls the heat transfer fluid until it reaches a resting fill level (see Figure 66). This protects the heat transfer fluid from freezing, and in some cases from overheating, when the ambient temperature is too low, or the pump stagnates.

(Viridian Solar, n.d.) mentions three main benefits with drain-back systems:

- They are relatively easy to install.
- The heat transfer fluid is protected against freezing.
- The solar collectors and circuit are protected against overheating during pump stagnation.

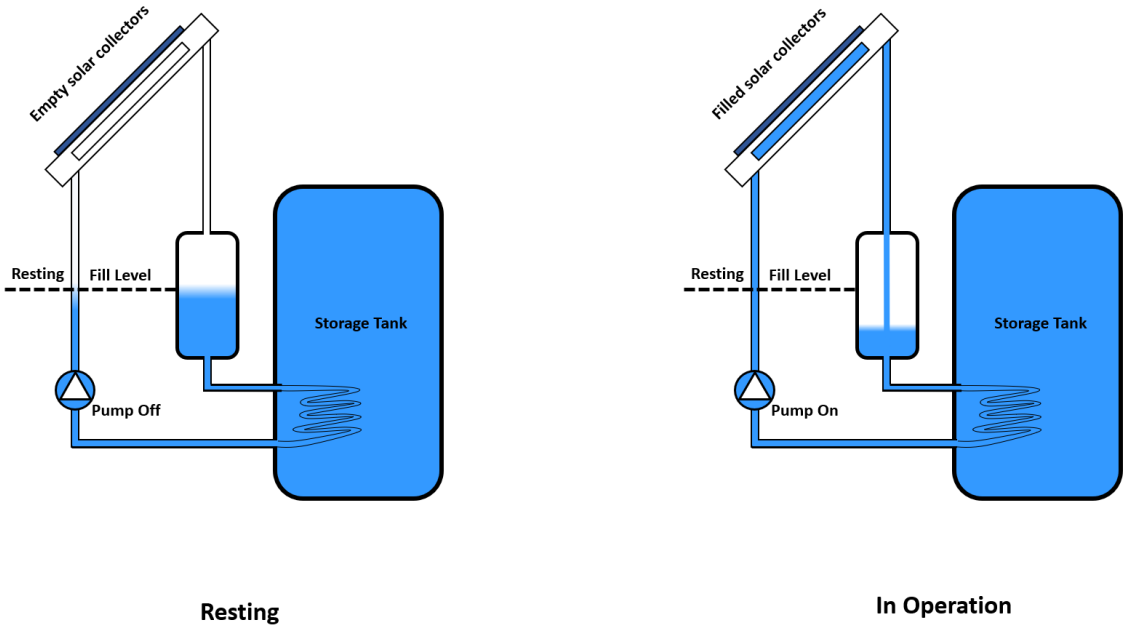

Figure 66: Drain-back system during operation and resting fill level.
Source: Based on a figure by (Viridian Solar, n.d.)

7.5.2 Overheating in non-draining systems

According to (Zijdemans, 2014), overheating is a phenomenon in non-draining solar water-heating systems, that occurs when the storage tank does not absorb sufficient thermal energy carried from solar collectors. The temperature of the fluid inside the solar circuit may then reach the boiling point and start to evaporate. These high temperatures may cause complications or permanently damage the solar collectors and circuit.

(Zijdemans, 2014) explains that the four most common techniques for dealing with overheating are:

- Dumping excess heat
- Reducing system performance
- Controlling the boiling
- Installing a high-pressure system

Dumping excess heat

(Zijdemans, 2014) mentions that there are four primary methods for dumping excess heat from the solar water-heating system. The first method is to use automatic drainage of hot tap water. Here, a temperature sensor measures the temperature of the tap water, and if it is above a predetermined temperature, a valve opens, and the hot water is lead to a drain until the sensor measures a low enough temperature. In the second method, known as night cooling, when the storage tank reaches above the desired temperature level, the circulation pump is forced to operate during the night, cooling the temperature of the liquid in the solar circuit through the solar collectors. It should be noted that this only works for flat plate collectors as evacuated tube collectors are more insulated.

The third method, which is also explained by (Zijdemans, 2014), is to dump the excess heat through an outdoor located convector. Should the return temperature from the solar circuit be too high, a three-way valve will open, leading the heat transfer medium to the outdoor installed convector, cooling the fluid with ambient air. The last method dictates that the storage tank is attached to either a seawater or a ground-source heat pump. The excess heat is then carried from the storage unit to the heat source of the heat pump, increasing the temperature of the heat source, resulting in a higher COP for the heat pump.

Reduced system performance

According to (Zijdemans, 2014), this technique entails using a circulation pump control mode known as "Inefficient operation". When the desired temperature of the storage tank has been reached, the circulation pump enters this mode, where the flow in the solar circuit is reduced or stopped for short periods, forcing the temperature of the fluid inside the solar collectors to rise. With the increased temperature inside the solar collectors, the heat loss increases, lowering the system performance, but making it possible to utilize more of the solar energy.

Controlled boiling

(Zijdemans, 2014) explains that for this method the pressure inside the solar water-heating system should be as low as possible, so that the boiling point inside the solar collectors does not exceed 120 ^{o}C, as boiling increases the pressure, forcing the heat transfer fluid into the expansion vessel. It is then possible to use a small container, connected in series to the expansion vessel, to cool down the fluid before it enters the vessel.

Installing a high-pressure system

The last technique mentioned by (Zijdemans, 2014) is to utilize high-pressure systems. Similar to before, the circulation pump stops when the desired temperature inside the storage tank is reached. Due to the high system pressure, the boiling point of the heat transfer fluid is way above the stagnation temperature, meaning that the heat transfer fluid will not start to boil. It is essential that all components in the system can withstand the high pressures, typically up to 9-10 bar.

(Zijdemans, 2014) explains that this technique works best for flat plane solar collectors as they have lower stagnation temperatures than evacuated tube collectors.

7.5.3 Inspection and maintenance of solar water-heating systems

There is never any guarantee that a solar water-heating system is going to run smoothly throughout the whole lifespan of the system. According to (Energy.Gov, n.d.-c), all solar water-heating systems require periodic inspections and maintenance of the system components, to ensure optimal system efficiency and to avoid situations which could lead to permanent damage to the system.

(Energy.Gov, n.d.-c) provides an extensive list of possible ways to inspect the different components of the solar water-heating system. These include:

- Visually checking for dust and soil on the solar collectors, and if this is a routine occurrence, then periodic cleaning may be necessary.
- Tighten the nuts and bolts of the support structure to the solar collectors.
- Inspect the pipelines for leaks, especially in connection points between pipes.
- Visually check for damage or degradation of the insulation used to cover the pipes.
- Inspect if the circulation pumps are operating. After mid-morning, in a day with favorable solar conditions, listen to if the pump is running. If this is not the case, it is possible that either the pump or the monitoring equipment malfunctions.
- The antifreeze solution in the solar collector must be periodically replaced to avoid blocking or damaging the pipes.
- The storage unit(s) should be inspected for cracks, leaks or rust.

8 Methodology

In this chapter, the methodology for studying and solving the central research question of this master thesis is explained. As introduced in Chapter 1: *Introduction*, the purpose of this paper is to study the possible effect an increased utilization of active solar energy may have on the greenhouse gas emissions related to energy consumption in Norwegian agriculture.

The adopted approach for studying this potential effect is to design and create corresponding simulation models for a possible photovoltaic system and solar water-heating system for the milk barn at Mære Agricultural School. The results from the simulations are then generalized and adapted to several similar farm buildings as the milk barn, to study the total potential reduction in greenhouse gas emissions.

The method can be summarized in three steps:

1. Perform an extensive literature review to get a better understanding of the two solar energy systems, and to obtain relevant information regarding input parameters necessary for creating simulation models.
2. Through software simulations, identify and evaluate the expected performance of each of the solar energy systems.
3. Generalize the results from the simulations and use them to determine the potential reduction in greenhouse gas emissions from Norwegian agriculture.

8.1 Literature review

As mentioned in the first step, a literature review was performed to get a better understanding of the solar energy systems and to try to determine relevant parameters for the simulation models. The journal articles have been collected from the period 2004 to 2020, but the majority of the papers are from 2010 to 2020. Large quantities of information have also been obtained through the Internet, with the purpose to fill the gaps left by the journal articles. It was sometimes difficult to determine the publishing year of the information found online, and in the cases where this was not obtained, n.d. has been used to denote "no date".

There are some inherent uncertainties with the literature provided from studies made in other nations, as some conditions and environmental factors may vary from country to country.

8.2 Simulation software

To be able to investigate the potential performance of the designed solar energy systems, a simulation model of the photovoltaic system and solar water-heating system, as well as their system variations, was created in Polysun.

Polysun was chosen as the simulation software for this master thesis, mainly due to the simple program interface and its comprehensive library of photovoltaic and solar water-heating components. A student-license for the software Polysun Designer was obtained from Vela Solaris on January 29th, 2020.

The whole process of designing and implementing the simulation models is further described in Chapter 9: *Polysun simulations*.

8.2.1 Evaluation of system performance

There are several ways to estimate the performance of different solar energy systems. In the case of the photovoltaic systems, the central indicator of system performance is the amount of energy consumption that it is possible to replace with electricity generated from solar energy, and also the performance ratio of the system.

The photovoltaic systems will also be evaluated with economic indicators, where the most central indicator will be payback time. This is the amount of time it takes before the initial investment cost and potential energy cost savings break-even. Net Present Value (NPV) will also be used to evaluate the photovoltaic systems, and can be calculated with:

$$NPV = -I_0 + \sum_{t=1}^{n} \frac{B_t - C_t}{(1+r)^t} \quad \textbf{[8.1]}$$

Where I_0 is the initial investment cost [NOK], n is the number of time periods, B_t is the net cash inflow during a period t [NOK], C_t is the net cash outflow during the period t [NOK], and r is the discount rate [-].

The performance of the solar water-heating system can be determined by using two indicators. The first is the solar fraction, as this shows the relationship between the solar energy supplied to the storage unit and the heat supplied from an auxiliary heat source. The solar fraction can be determined by:

$$Solar\ fraction = \frac{Supplied\ solar\ energy}{Supplied\ solar\ energy + auxiliary\ thermal\ energy} \quad \textbf{[8.2]}$$

The second indicator is the potential electricity savings by utilizing solar collectors in the hot water system. For this case, a simulation model of the existing hot water system at the milk barn is designed, and the electricity consumption of this system is compared with the solar collector systems.

8.3 Generalizing the results

The results from this study can be generalized by multiplying the potential amount of current electricity consumption that it is possible to replace with solar energy, with the number of similar agriculture buildings found in Norway, and an emission factor (introduced in Chapter 2: *Energy usage and CO2 emissions in agriculture*).

As it is difficult to determine the electricity mix associated with the consumption of agriculture in 2019, the potential reduction of greenhouse gas emission will therefore be studied for three different assumptions:

- *Low emissions:* The current electricity consumption is covered by the Norwegian electricity mix
- *Substantial emissions:* The current electricity consumption is covered by the Nordic electricity mix
- *Moderate emissions:* The current electricity consumption is covered by 50 % Norwegian and 50 % Nordic electricity mix

It will be assumed that all milk farms have similar electricity consumption and hot water demand as the milk barn at Mære Agricultural School. This means that in Norway, only a maximum of 7 600 farms can adopt this specific photovoltaic system and solar water-heating system (see Chapter 2.1: *Norwegian agriculture*).

9 Polysun simulations

9.1 Software description

Polysun is a simulation software designed by the Swiss company Vela Solaris, which makes it possible to plan and design energy systems, as well as study potential optimizing strategies for already existing energy systems.

The software has different limitations and privileges based on which version that is bought from Vela Solaris. The three main versions are:

- Standard
- Designer
- Premium

Common for all three versions is that they come with over 1 000 preconstructed energy system templates.

The Standard version limits the user's freedom of creativity, as the user cannot design new energy systems but has to select one from the premade templates. This version does also only allow limited amounts of configuration for control logic. The Designer version, on the other hand, allows the user to design energy systems from scratch, and it is also possible to somewhat freely configure the control logic. The Premium version stands out from the previously mentioned versions, as it in addition to the designer features also allow for support through the Polysun web service and also include plug-in controllers.

According to (Vela Solaris, 2018), the general design procedure in Polysun consists of the following steps:

1. Selecting the system location, local weather data and designing the horizon profile.
2. Choosing either a predefined system template, based on accessible system components, or outlining an energy system from scratch.
3. This step may vary based on what the user did in Step 2, but usually the hot water demand, building dimensions and the energy consumption are to be defined in this step.
4. Dimensioning and modifying the system components.
5. Simulate the energy system model.
6. Evaluate the results.

To clarify, Polysun Designer was used in this master thesis.

9.1.1 Weather database

According to (Vela Solaris, 2018), Polysun comes with a predefined weather database with reliable yield forecasts for more than 8 400 locations all across the globe. Still, should the desired location not be found in the existing database, it would be possible to upload the weather information from one of the user's data files. If no such file is available, then the user can choose the desired location manually, and Polysun will generate a weather forecast for this area based on interpolation of parameters from the surrounding areas that has already been mapped out.

The necessary weather data for running through a single simulation are global and diffuse radiation [Wh/m^2], longwave irradiation [Wh/m^2], ambient temperature [°C], wind speed [m/s] and humidity [%].

9.1.2 Horizon editor

Included in the Polysun Software is the Horizon editor, which (Vela Solaris, 2018) explains is a designer tool that makes it possible to implement surrounding topography and obstacles into the simulation model. As can be seen in Figure 67, the horizon line is edited by inputting the distance, height and azimuth angle of the nearby obstruction. The red line in the figure illustrates the hills, trees and buildings nearby that obstructs the sunlight from reaching the system's location, while the yellow line indicates the position of the sun on a specific day.

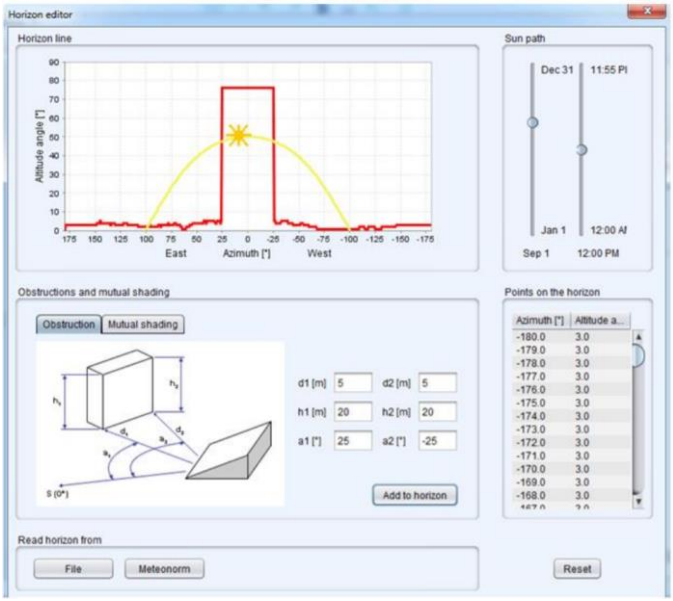

Figure 67: The Horizon Editor in Polysun Designer.
Source: (Vela Solaris, 2018)

9.2 Metrological data for the milk barn

9.2.1 Building location

There was no area located near Mære Agricultural School available on the weather database in Polysun. The location of the school was therefore chosen manually through the Open Street Map option (see Figure 68), meaning that Polysun interpolates the weather data for the school based on other locations in Trøndelag.

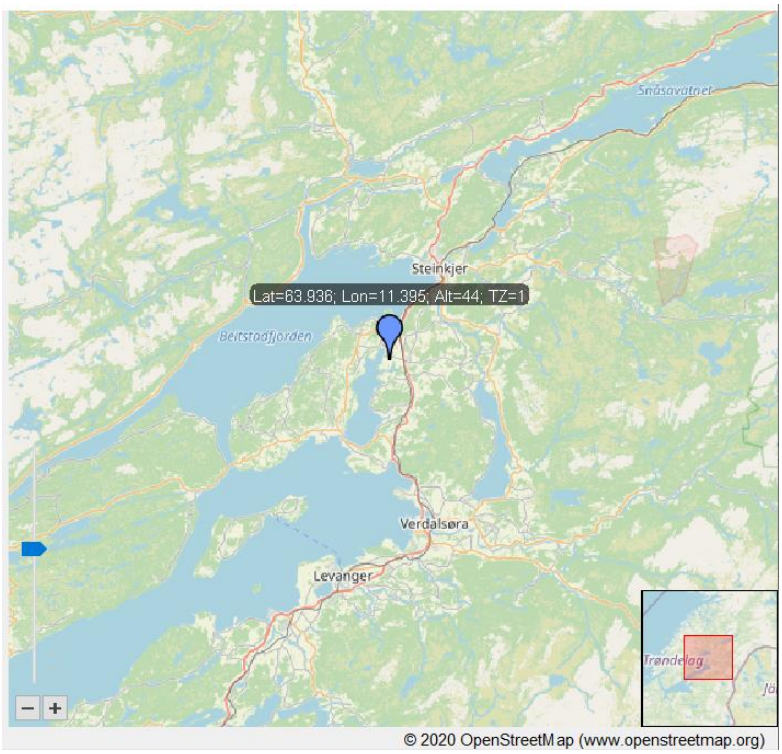

Figure 68: Polysun Open Street Map: Mære Agricultural School.

9.2.2 Horizon profile

As already mentioned in Chapter 5: *The milk barn at Mære Agricultural School*, the only real shading obstruction for the milk barn is the neighboring hilltop and also some trees (see Figure 69). By using the Horizon editor, the hill was successfully added to the simulation model, but the trees were not included.

The relevant parameters for implementing the hilltop was found by using the information provided by Google Maps, (Den Norske Turistforening, n.d.) and (Yr.no, 2020). The inputted values can be seen in Figure 70, and the corresponding horizon profile can be seen in Figure 71.

Figure 69: The hilltop located south of the milk barn.
Pictures: Dan Remi Antonsen, 11.11.2019

Parameters	Values
Distance 1 (d_1)	120.5 m
Distance 2 (d_2)	205.7 m
Height 1 (h_1)	23.7 m
Height 2 (h_2)	23.7 m
Azimuth angle 1 (a_1)	0°
Azimuth angle 2 (a_2)	- 37.5°

Figure 70: Horizon editor - Inputted values.
Source: Google Maps

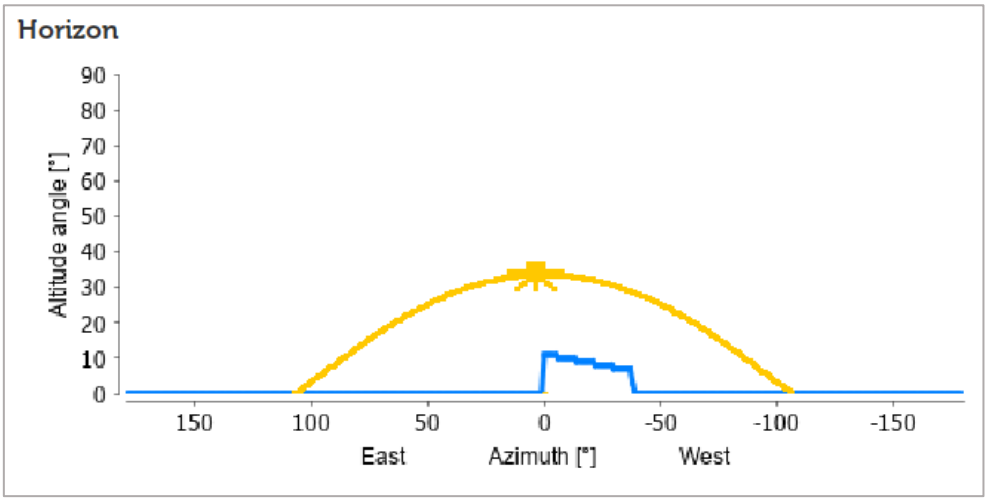

Figure 71: The implemented horizon profile in Polysun.

9.3 Implementing the photovoltaic systems in Polysun

Figure 72 shows the different systems components added to the simulation model of the photovoltaic system at the milk barn. The only necessary elements that have to be implemented into the Polysun energy system diagram is the photovoltaic modules, inverters and the power grid.

The following subchapters will provide an overview of the necessary input parameters for each of these components. Also, a couple of assumptions are going to be presented, which has mostly been based on the earlier literature review.

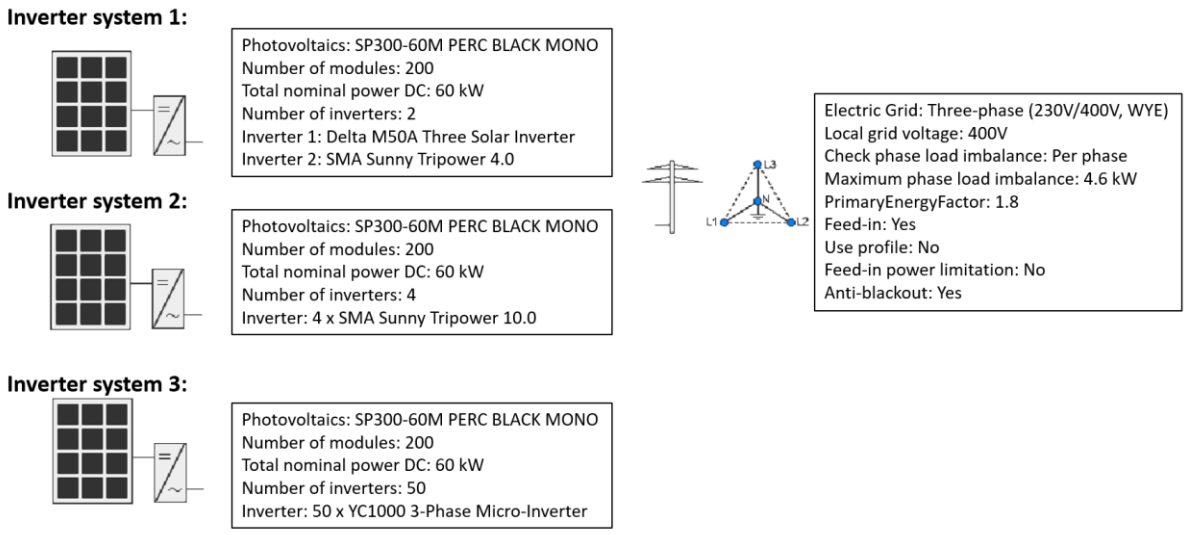

Figure 72: The photovoltaic system created in Polysun.

9.3.1 Photovoltaic modules

Table 33 provides an overview of the various parameters inserted into the simulation model for the photovoltaic modules. All of these values are collected from Attachment A.5 and has previously been introduced in Chapter 6.1.6: *Photovoltaic modules for the milk barn*.

In addition to the table showing the input parameters for the photovoltaic modules, Table 34 displays the various necessary assumptions influencing the electricity production of the photovoltaic modules.

Table 33: An overview of the inputted photovoltaic module parameters.

Photovoltaic Module	
Product Specification	
Type:	SP300-60M PERC BLACK MONO
Max power (P_{Max})	300 W
Max power voltage (V_{MPP})	32.6 V
Max power current (I_{MPP})	9.19 A
Open-circuit voltage (V_{OC})	39.9 V
Short-circuit current (I_{SC})	9.64 A
Module efficiency (η)	18.3 %
Max system voltage	DC 1000 V (TUV)
Maximum Series Fuse Rating	15 A
Mechanical Data	
Dimensions	1640x992x35 mm
Weight	18 kg
Cell type	Mono Crystalline Silicon PERC
Gross area	1.627 m²
Temperature characteristics	
Temperature coefficient of I_{SC}	0.495 %/K
Temperature coefficient of V_{OC}	- 0.2893 %/K
Temperature coefficient of P_{Max}	- 0.40 %/K
System description	
Number of modules	200
Total gross area	325.38 m^2
Inclination angle (Hor. = 0°, Vert. = 90°)	26 °
Orientation (East = 90°, South = 0°, West = -90°)	0 °

Table 34: Energy loss assumptions inputted into the simulation model.

Parameters	Definition in Polysun	Default Polysun input	Chosen input	Source for chosen input
Wind fraction	Wind fraction is the fraction of the local wind speed which pertains over the module area.	50 %	50 %	None
Rear ventilation	The rear ventilation of the photovoltaic modules.	Medium	Medium	None
Soiling	Reduction of radiation onto the photovoltaic module due to soiling.	2 %	4.4 %	Chapter 6.7.2
Degradation	Reduction of efficiency of the solar cells due to aging.	0.5 %	1.5 %	Chapter 6.7.1
Cable losses	Loss factor for DC cable losses at nominal power.	2 %	2 %	Chapter 6.7.1
Mismatching	Losses due to deviations of voltage/current characteristics of modules.	4 %	• 2 % for inverter system 1 & 2 • 0 % for inverter system 3	Chapter 6.7.1

9.3.2 Inverters

Table 36 shows an overview of the inputted parameters for the four different inverters implemented into the simulation model. The assumptions made regarding the inverters are on how the photovoltaic modules are connected to them. This has already been described in detail in Chapter 6.2.3: *Choosing solar inverters for the milk barn*, but a brief summarization can be seen in Table 35.

Table 35: Summarization of the connection from the photovoltaic modules to the inverters.

Inverter system	Inverter type	Inclination angle [°]	Azimuth angle [°]	Number of MPPT	Number of inputs per MPPT	Number of strings per MPPT		Number of modules per string	
1	Delta M50A	26	0	2	5	4		22	
	Sunny Tripower 4.0	26	0	2	1	1		12	
2	Sunny Tripower 10.0	26	0	2	2 + 1	2	1	14	22
	Sunny Tripower 10.0	26	0	2	2 + 1	2	1	14	22
	Sunny Tripower 10.0	26	0	2	2 + 1	2	1	14	22
	Sunny Tripower 10.0	26	0	2	2 + 1	2	1	14	22
3	50 x YC1000 3-Phase	26	0	1	4	4		1	

Table 36: An overview of the most important inverter inputs.

Inverters				
Product Specification				
Product:	Delta M50A	Sunny Tripower 4.0	Sunny Tripower 10.0	YC1000 3-Phase
Input Side (DC)				
Max. DC input power	58 kW	8 kW	15 kW	1.24 kW
Max. DC input voltage	1 100 V	850 V	1 000 V	60 V
Start-up voltage	250 V	150 V	150 V	22 V
MPPT voltage range	200 – 1000 V	175 – 800 V	320 – 800 V	16 – 55 V
Max. input current	100 A	36 A	48 A	59.2 A
MPPT number /strings per input	2/5	2/1	2/ A:2 B:1	1/4
Output side (AC)				
Max. output power	55 kVA	4 kVA	10 kVA	1.13 kVA
AC Voltage range	230 V ± 20 % /400 V ± 20 %	180 - 280 V	180 – 280 V	149 – 278 V
Nominal AC voltage	-	3/N/PE; 230 V / 400 V	3/N/PE; 230 V / 400 V	3 x 230 V
Nominal frequency	50 Hz	50 Hz	50 Hz	50 Hz
Operation phase	3	3	3	3
Nominal current	73 A	17.4 A	43.5 A	4.32 A
Power Factor (at rated output power)	0.8	1	1	1
Efficiency				
Max. efficiency	98.6 %	98.2 %	98.3 %	95 %
EU efficiency	98.4 %	97.1 %	98.0 %	-
General Data				
Dimensions [mm]	740 x 612 x 278	435 x 470 x 176	460 x 497 x 176	259 x 242 x 36
Weight	74 kg	17 kg	20.5 kg	3.5 kg
Operating ambient temperature range	-25 to 60 °C	-25 to 60 °C	-25 to 60 °C	-40 to 65 °C

9.3.3 Power grid

The implementation of the power grid was done by using a predefined power grid model provided by Vela Solaris. All the parameter inputs for the predefined model can be seen in Table 37.

Table 37: Input parameters for the predefined power grid model.

Parameters	Input	Description from Polysun
Grid configuration:	Three-phase star (WYE)	*Topology and phase shifts of the grid.*
Nominal voltage	400 V	*Nominal voltage of the grid according to standards.*
Nominal frequency	50 Hz	*Nominal frequency of the grid according to standards (usually 50 or 60 Hz).*
Local grid voltage	400 V	-
Voltage between outer lines	400 V	-
Start voltage	230.9 V	*Voltage between one of the outer lines and the (usually neutral) star point.*
Check phase load imbalance	Per phase	-
Maximum phase load imbalance	4.6 kW	*The maximum phase load imbalance according to local standards.*
PrimaryEnergyFactor	1.8	-
Feed-in	Yes	*The electrical energy is fed into the public electricity grid.*
User profile	No	-
Feed-in power limitation	No	*Limitation of active power related to the peak power. The purpose of the power limitation is to avoid feeding-in high midday peaks.*
Anti-blackout	Yes	***Yes:** AC producers continue to run when blackouts occur.* ***No:** AC producers are curtailed when blackouts occur.*

9.4 Implementing the solar water-heating system

9.4.1 Schematic of the solar water-heating system at the milk barn

Figure 73 shows a close approximation of the actual hot water system for the milk barn. The most significant discrepancy between this figure and Figure 16, which shows the real hot water system, is that this schematic has solar collectors attached to the bottom of the storage tank, and that it does not include the heat recovery circuit from the milk storage tank.

Due to difficulties with the heat exchangers in the simulation software, all external heat exchangers had to be replaced with internal heat exchangers.

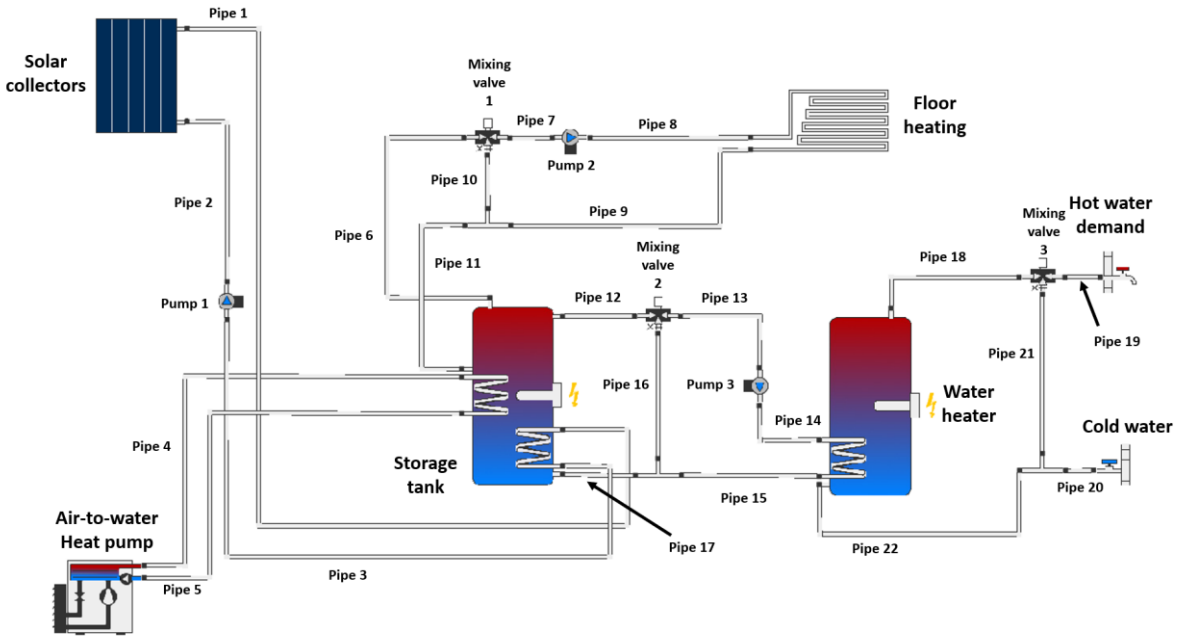

Figure 73: Schematic of the solar water-heating system for the milk barn

9.4.2 Implementing the system components

Solar collectors

Real photovoltaic modules were chosen for the photovoltaic system introduced in Chapter 6: *Designing a photovoltaic system*. The purpose of the solar water-heating system is not to design an actual system solution for the milk barn, but rather study the potential of such a system. The solar collectors are therefore chosen from the preexisting Polysun database, and the most crucial feature is that the total absorption area is equal to the area calculated in Chapter 7.1.4: *Calculating the required solar collector area*.

Polysun's "Flat-plate, good quality" was chosen to represent the flat-plate collector solution, and it was necessary to implement 14 flat-plate collectors to achieve a total absorption area of 24.99 m^2. For the evacuated tubes, Polysun's solar collector model "Vacuum tubes" were chosen. In this case, 17 evacuated tube collectors were implemented to cover a total absorption area of 22.16 m^2.

The input parameters of these two solar collector types are presented in Table 38.

Table 38: Utilized solar collectors for the solar water-heating system at the milk barn

Solar Collectors		
Polysun Specification		
Model:	Flat-plate, good quality	Vacuum tubes
General parameters		
Absorber area	1.8 m^2	1.3 m^2
Aperture area	1.8 m^2	1.4 m^2
Gross area	2 m^2	2 m^2
Eta0 (Laminar)	0.75	0.65
Eta0 (Turbulent)	0.8	0.7
a_1 (Without wind)	3.5	2
a_1 (With wind)	4	2.0999
a_2	0.02	0.01
Dynamic heat capacity	5 000 J/K	15 000 J/K
Mechanical parameters		
Volume	1.5 L	1 L
Internal pipe diameter	9 mm	6 mm
Single pipe length	18 m	3 m
Parallel piping	1	6
Pipe roughness	0.1 mm	0.1 mm
Linear form factor	1	1
Friction factor	0	0
Fluid for test	Propylene mixture	Propylene mixture

Fluid parameters		
Mixture concentration during test	36 %	36 %
Test flow rate	100 L/h	100 L/h
Max. flow rate	2 000 L/h	3 000 L/h
Max. pressure	10 Bar	10 Bar
Maximum temperature	220 °C	320 °C
Simulation model		
Number of solar collectors	14	17
Total absorption area	25.2 m^2	22.1 m^2
Total aperture area	25.2 m^2	23.8 m^2
Total gross area	28 m^2	34 m^2

In Chapter 7.3.7: *Heat transfer fluid*, several freezing point temperatures were provided for the different shares of propylene glycol in the mixture. If this information is combined with the data regarding the outdoor temperatures at Mære Agricultural School (see Figure 10), then the minimum glycol share in the heat transfer fluid mixture should be about 36 % (-18 °C).

It is assumed for both of the solar collector solutions that:

- The wind fraction is about 50 %.
- The azimuth angle is 0°
- The inclination angle is 26°.

It will also be assumed that all of the solar collectors are attached to each other in series.

Air-to-water Heat pump

Unfortunately, the information concerning the air-to-water heat pump (aroTHERM VWL 85/2) presented in Attachment A.12 is not sufficient to create an accurate simulation model of the existing heat pump at the milk barn. Inside Polysun's database is a similar air-to-water heat pump, but with less heating capacity. This pump has the model number aroTHERM VWL 85/3.

A comparison between the identified data regarding the VWL 85/2 and corresponding data for the VWL 85/3 model is presented in Table 39. All of the listed values in the table indicates that the chosen heat pump (WVL 85/3) will provide a smaller amount of heat to the hot water system than the real heat pump.

Similar to the solar collectors, it will be assumed that the heat transfer fluid running from the heat pump to the storage tank is a mixture of water and propylene glycol, where the share of glycol is 36 %, resulting in a freezing point of -18 °C.

Table 39: Differences between the real heat pump and the simulated heat pump.

	aroTherm VWL 85/2 (Actual heat pump)	aroTherm VWL 85/3 (Simulated heat pump)	Reduced heat output
A2W35	4.60 kW	4.50 kW	-2.174 %
A7W35	8.10 kW	7.70 kW	- 4.938 %
A7W45	7.80 kW	7.00 kW	-10.256 %
A7W55	7.10 kW	6.5 kW	-8.451 %

The numbers and letters on the left side of the table above have the following meaning:

- A is used for Air, while the number next to it presents the ambient outdoor temperature.
- W indicates Water, and the number next to it is the water inlet temperature.

Storage tank

The storage tank in the existing hot water system is a 300-liter Vaillant tank with 3x5 kW electric heating elements installed inside the storage unit at approximately center height. This storage tank will be used in simulations without solar collectors, but when the solar collectors are inserted into the simulation model, the existing tank will be replaced with a new tank. The dimensions of the new storage tanks are similar to the ones already calculated in Chapter 7.2.5: *Sizing the required storage tank for the milk barn*.

All three tanks were predefined by Polysun, and the input parameters can be seen in Table 40.

Table 40: Implemented Thermal Energy Storage into the solar water-heating system.

Thermal Energy Storage			
Polysun specification			
Model:	1 500 Liter combi for heat pumps	2 000 Liter combi for heat pumps	3 000 Liter combi for heat pumps

General parameters			
Volume	1 500 L	2 000 L	3 000 L
Height	2 m	2 m	2 m
Bulge Height	100 mm	100 mm	100 mm
Material	Steel	Steel	Steel
Wall thickness	2.5 mm	2.5 mm	2.5 mm
Insulation	Rigid PU Foam	Rigid PU Foam	Rigid PU Foam
Thickness of insulation	80 mm	80 mm	80 mm
Thickness at top of tank	80 mm	80 mm	80 mm
Thickness at tank base	50 mm	50 mm	50 mm
Electric heating element	16 kW	16 kW	16 kW

The 3000-liter storage tank is used as the reference tank when simulating different system solutions.

Water heater

According to Attachment A.13, the existing water heater inside the technical room has a volume of 250 liters and only one heating element, with an installed capacity of 3 kW. Table 41 shows inputted parameters for the water heater used in the simulation model of the hot water system.

Table 41: Implemented water heater into the solar water-heating system.

Water heater	
Polysun specification	
Model:	250L potable water
General parameters	
Volume	250 L
Height	1.3 m
Bulge Height	100 mm
Material	Stainless steel
Wall thickness	2.5 mm
Insulation	Rigid PU Foam

Thickness of insulation	80 mm
Thickness at top of tank	80 mm
Thickness at tank base	50 mm
Electric heating element	3 kW

Floor heating system

Attachment A.13 suggests that the floor heating system has a power of 9 kW, and according to the floor plan of the milk barn (see Figure 14), the heated floor area is roughly 130 m^2. To implement this, Polysun has a floor heating model known as "Floor heating 1500 square feet", which converted into metric units is about 139.35 m^2. By changing the model from having a heating power of 10 kW to 9 kW, and a floor area of 130 m^2 instead of 139.35 m^2, the simulation model becomes more accurate.

The parameters of the floor heating system can be seen in Table 42.

Table 42: Implemented floor heating system into the solar water-heating system.

Floor heating system	
Polysun Specification	
Heating/Cooling element:	Floor heating 1 500 square feet
General parameters	
Nominal inlet temperature	45 °C
Nominal return temperature	35 °C
Power per heating element under standard conditions	9 000 W
Heating element area	130 m^2
Flow rate per heating element under standard conditions	1 499.8 L/h
Volume	249.84 L
Inside temperature under standard conditions	20°
Number of heating/cooling modules	1

Circulation pumps

The circulation pumps come in several different sizes and variations. All three circulation pumps in the proposed solar water-heating system are assumed to have a medium size.

The input parameters for all three circulation pumps can be seen in Table 43.

Table 43: Implemented circulation pumps into the solar water-heating system

Circulation pump			
Circulation pump:	1	2	3
Polysun Specification			
Model:	Eco, Medium	Eco, Medium	Eco, Medium
Heat transfer	30 %	30 %	30 %
Flow rate-controlled	Flow rate Setting	Fixed flow Rate	Flow rate Setting
If fixed flow rate	-	1 449.8 L/h	-

Pipelines

Several parameters have to be assumed or decided for the pipelines in the hot water system model for the milk barn. Among these parameters are:

- Pipe material
- Pipe length
- Linear form factor
- Friction factor
- Insulation type and thickness

All pipes, except the ones leading to the solar collectors, were chosen to be copper pipes. These pipes have an internal and external diameter of 20 and 22 mm respectively. The pipes leading to the solar collectors are assumed to be steel pipelines, with an internal and external width of 155.4 and 165.1 mm. This pipe dimension was chosen to ensure sufficient heat transfer from the solar collectors to the storage tank.

The copper pipes have a roughness of 0.002 mm and a thermal conductivity of 394 W/m·K, while the steel pipelines have a coarseness of 0.01 mm and a thermal conductivity of 50.5 W/m·K.

The lengths of the various pipelines were determined by using estimates obtained by creating the milk barn and solar water-heating system in Sketchup. The Sketchup model can be seen in Attachment A.14, but Table 44 summarizes the relevant lengths. The pipes have been given corresponding numbers in Figure 73.

Table 44: The estimated pipeline lengths in the system.

Pipe number	1	2 & 3	4 & 5	6	7 & 8	9	10	11
Length	30.87 m	15.43 m	10.88 m	2.2 m	1.0 m	2.0 m	1.0 m	2.2 m

Pipe number	12 & 17	13 & 14	15	16	18 & 22	19 & 20	21
Length	0.5 m	0.5 m	1.0 m	2.0 m	1.0 m	10.0 m	2.0 m

The linear form factor is the pressure drop multiplier that accounts for the pipeline's bends and joints. Polysun's default value of 1 will be kept for this simulation model. The same will be done for Polysun's default friction factor, which is zero. The pipelines are insulated with "Loose glass fibers and mineral wool", which has a thermal conductivity of 0.045 W/m·K and also a heat capacity of 610 J/kg·K. The thickness of the insulation is set to 20 mm.

Control and sensors

The proposed solar water-heating system consists of several different closed- or open-loops. To easier differentiate between these, the circuits are going to be referred to as:

- *Solar circuit*: The closed-loop going from the solar collectors to the storage tank.
- *Heat pump circuit*: The closed-loop going from the heat pump to the storage tank
- *Floor heating circuit*: The open-loop going from the storage tank to the floor heating system.
- *In-between tanks circuit*: The loop going from the storage tank to the water heater.

Each of these circuits needs a control system to operate efficiently. All of the control systems used for this solar water-heating system are DTC (see Chapter 7.4.1: *Differential Temperature Controller*).

A schematic illustration of the controller system for the solar and heat pump circuit can be seen in Figure 74.

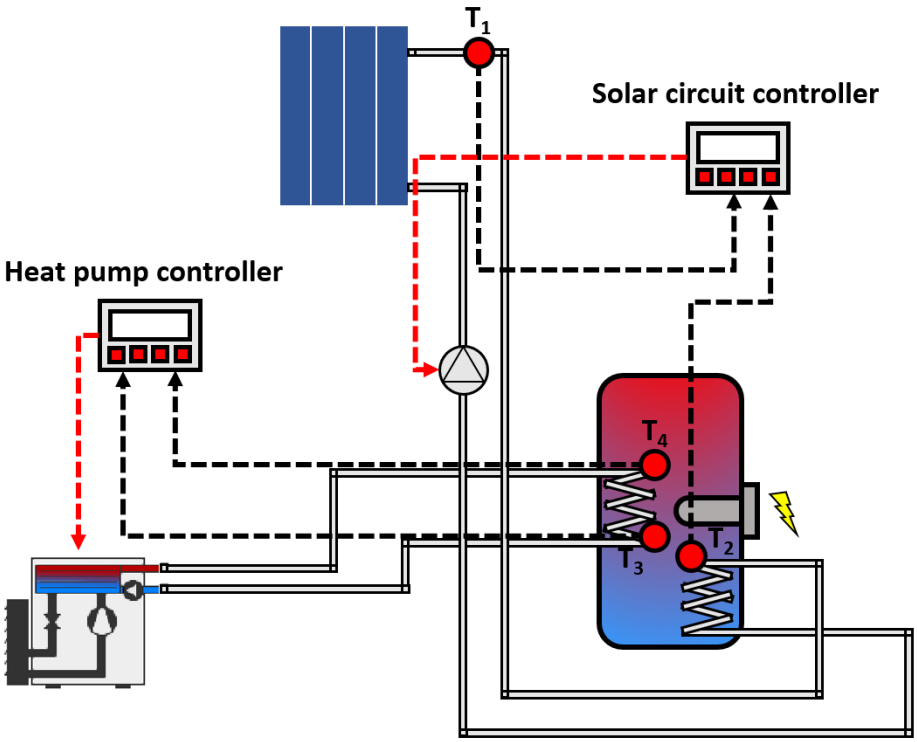

Figure 74: An illustration of the solar loop controller and auxiliary heating controller.

An overview of the input parameters for the solar loop controller can be seen in Table 45. The temperature sensors for this controller is placed at the outlet of the solar collectors (T_1) and just above the internal heat exchanger in the storage tank (T_2).

Similar to Table 45, Table 46 shows an overview of the input parameters for the auxiliary heating controller steering the heat pump. The temperature sensors for this controller is placed according to the suggestion provided by Polysun, where they both should be placed at a height equal to the height of the return pipe to the auxiliary heater or higher.

Table 45: Control inputs, outputs and Polysun parameters for the solar loop controller.

Solar loop controller	
Control inputs	
Collector temperature [T_1]	Collector: Outflow temperature [°C]
Tank temperature [T_2]	Storage tank: Layer 4 [°C]
Collector aperture area	Collector: Aperture area [m^2]
Control outputs	
On/Off pump	Pump 1: On/Off
Polysun parameters	
Maximum collector temperature	120 °C
Maximum tank temperature	90 °C
Cut-in temperature difference	6 °C
Cut-off temperature difference	2 °C
Specific flow rate	15 L/h/m^2

Table 46: Control inputs, outputs and Polysun parameters for the auxiliary heating controller.

Auxiliary heating controller – Heat pump	
Control inputs	
Layer temperature sensor on 1 [T_3]	Storage tank: Layer 4 [°C]
Layer temperature sensor off 1 [T_4]	Storage tank: Layer 7 [°C]
Control outputs	
On/Off heating device	Heat pump: On/Off
Polysun parameters	
Cut-in tank temperature 1	50 °C
Cut-off tank temperature 1	60 °C
Minimum operation time	0 min
Minimum downtime	0 min
Maximum tank temperature	140 °C

The floor heating system requires a mixing valve controller system to ensure a supply temperature of 45 °C into the floor heating module. The controller system is illustrated in Figure 75, and the input parameters are displayed in Table 47.

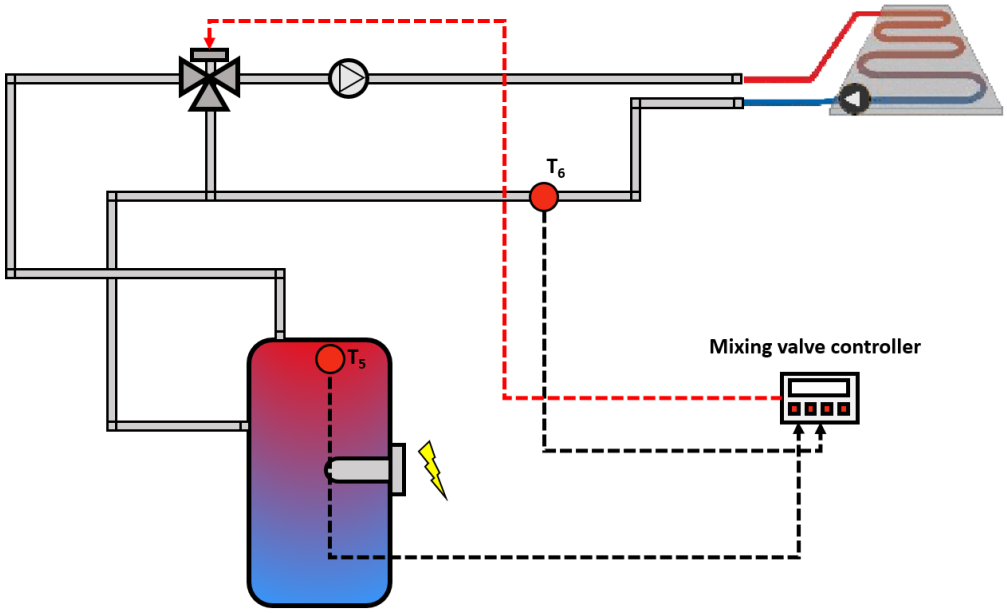

Figure 75: An illustration of the mixing valve controller for the floor heating circuit.

Table 47: Control inputs, outputs and Polysun parameters for the mixing valve controller.

Mixing valve controller	
Control inputs	
Upper temperature level [T_5]	Storage tank: Top layer [°C]
Lower temperature level [T_6]	Pipe 12: Temperature [°C]
Control outputs	
Mixing valve	Mixing valve 1: Valve position [%]
Polysun parameters	
Fixed temperature setting	47 °C

The circuit between the storage tank and the water heater should also have a control system to optimize heat transfer between the two units. In this case, the controller measures the temperature at the bottom of the water heater and the temperature at the top of the storage tank, and if there is a temperature difference, then the circulation pump begins to operate. The pump will only start if the temperature in the storage tank is above the temperature at the bottom of the water heater.

Figure 76 illustrates this control system, and all relevant input parameters are found in Table 48.

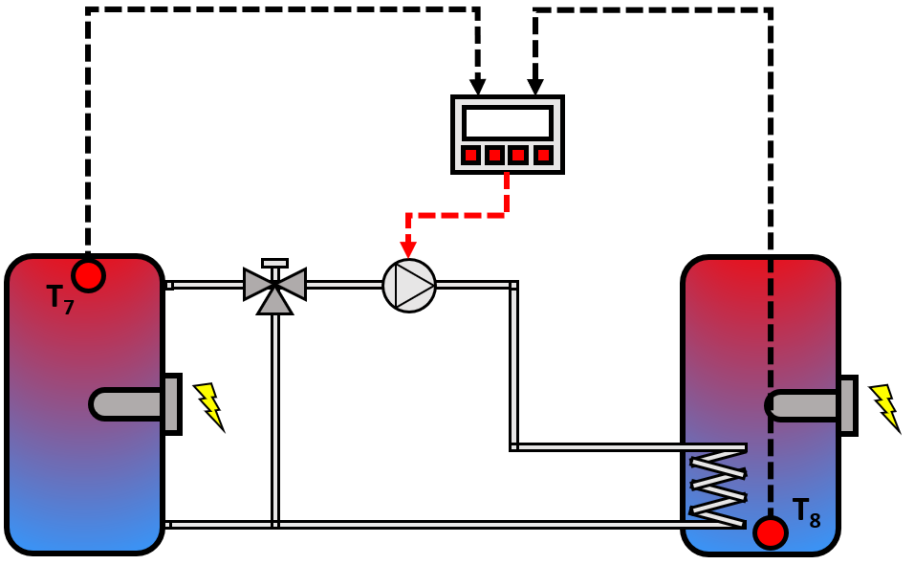

Figure 76: An illustration of the temperature controller for the circuit between the tank and water heater.

Table 48: Control inputs, outputs and Polysun parameters for the temperature controller.

Temperature controller	
Control inputs	
Temperature sensor 1 [T_7]	Storage tank: Top layer [°C]
Temperature sensor 2 [T_8]	Water heater: Bottom layer [°C]
Control outputs	
On/Off switch 1	Pump 3: On/Off
Polysun parameters	
Fixed temperature setting 1	Variable value

In addition to the controllers introduced above, two additional auxiliary heating controllers are implemented into the model. These two controllers are responsible for steering the electric heating element inside the storage tank and the water heater. Figure 77 shows the placement of the temperature sensors, and Table 49 displays the input parameters for the two auxiliary controllers.

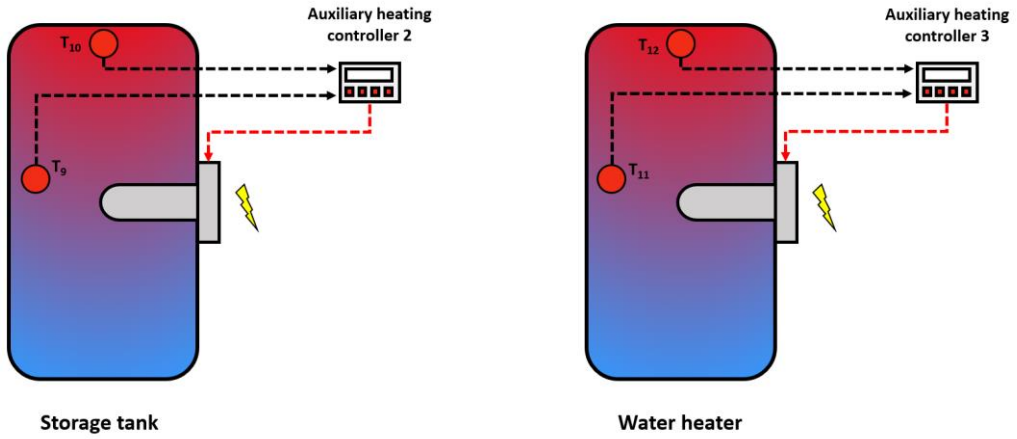

Figure 77: An illustration of the auxiliary controllers for the storage tank and water heater.

Table 49: Control inputs, outputs and Polysun parameters for auxiliary heating controller 2 & 3.

Auxiliary heating controller 2 & 3	
Control inputs	
Layer temperature sensor on 1 [T_9 & T_{11}]	Storage tank and Water heater: Layer 6 [°C]
Layer temperature sensor off 1 [T_{10} & T_{12}]	Storage tank and Water heater: Top layer [°C]
Control outputs	
On/Off heating device	Internal heater 1 & 2: On/Off
Polysun parameters	
Cut-in tank temperature 1	**Storage:** 45 °C & **Heater:** 75 °C
Cut-off tank temperature 1	**Storage:** 47 °C & **Heater:** 78 °C
Minimum operation time	0 min
Minimum downtime	0 min
Maximum tank temperature	140 °C

Hot water demand

The annual hot water consumption for the milk barn, excluding drinking water for livestock, is estimated to be about 137 240 liters. This suggests that the average daily water consumption is roughly 376 liters. The actual distribution of the hot water consumption is unknown, and a preexisting schedule known as *Daily peaks* is therefore used in the simulation model (see Figure 78).

The last step is to determine the temperature setting for the hot water withdrawal. The default value set by Polysun is 50 °C, which is kept for this simulation model.

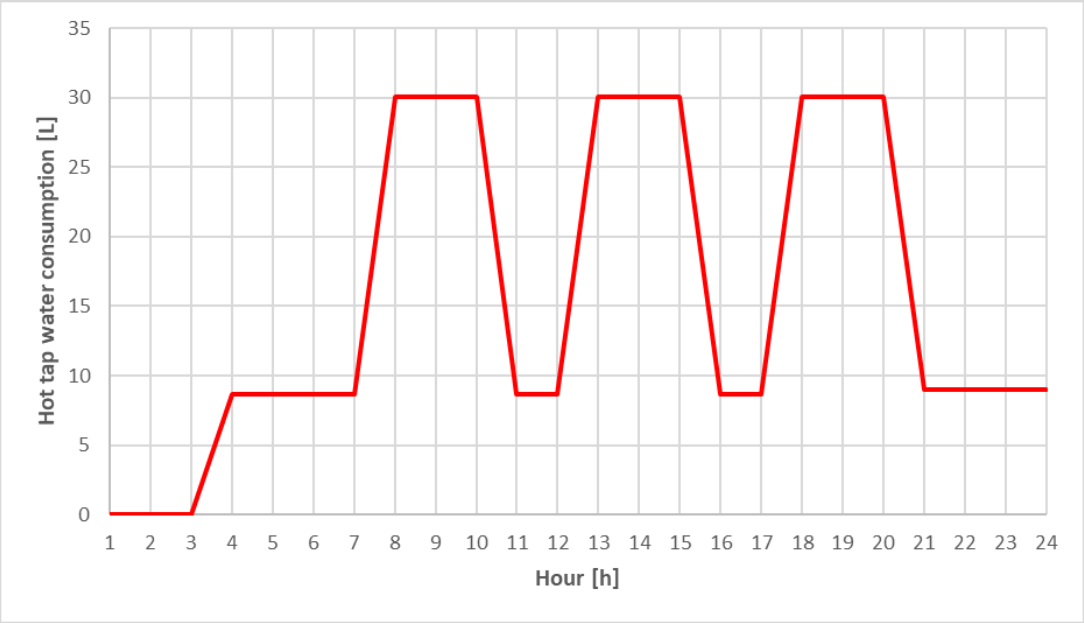

Figure 78: Distribution of hot water consumption in the milk barn.

10 Results

10.1 Results of the photovoltaic systems

As explained in Chapter 8.2.1: *Evaluation of system performance*, the performance of the three photovoltaic systems will be evaluated based on their simulated annual electricity production and performance ratio, their calculated payback time and Net Present Value, and finally their potential for greenhouse gas reduction. To try to present the results as orderly as possible, each of these indicators are separated into their own subchapter.

10.1.1 Annual electricity production

The simulated annual electricity production for each of the three photovoltaic system solutions are presented in Table 50. It should be noted that from this point on, the numbering of the photovoltaic system references the utilized inverter solution, meaning that for example, the third photovoltaic system has the inverter system that employs micro-inverters. The results in the table show that the third photovoltaic system annually generates 1.80 % more electricity than the second, and 2.05 % more than the first. All three photovoltaic systems were designed to cover about 30 % of the milk barn's annual electricity demand. Out of these three system solutions, the third system came closest to this goal, by covering roughly 26.83 %.

Table 50: Total annual energy yield for the three photovoltaic systems.

	Photovoltaic system 1	Photovoltaic system 2	Photovoltaic system 3
Total annual energy yield	52 752.8 kWh	52 879.7 kWh	53 831.9 kWh

Why the third system has the highest production can be seen in Figure 79. As shown in the figure, all losses due to environmental factors have the same size, but that the component losses diverge from each other. Out of the three system solutions, the third has the highest inverter losses, followed by the first and then the second, while the second photovoltaic system solution has the highest cable losses. It was assumed that the third system did not experience any mismatching, and this is the major contributor to the difference in annual electricity production.

The effect of the assumption concerning mismatching will be further studied in Chapter 11: *Discussion*.

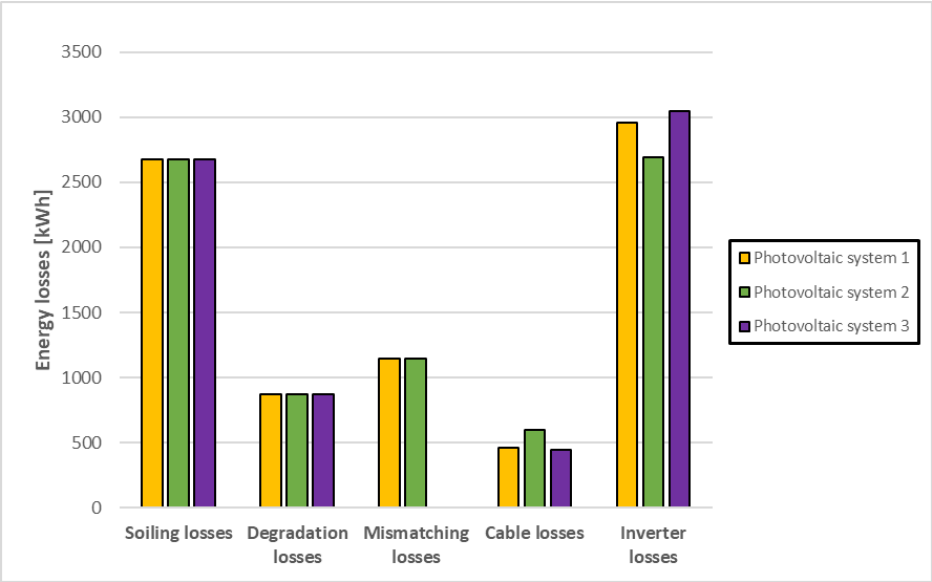

Figure 79: Energy losses for the three photovoltaic system solutions.

The hourly electricity production for each of the photovoltaic system solutions can be seen in figures presented in Attachment A.15. By comparing the results presented in these figures with the actual hourly electricity consumption at the milk barn, it is possible to estimate the size of the surplus production and also the number of hours with excess production.

Table 51 displays the estimated number of hours with surplus production if the hourly energy consumption from 2019 is used as a basis.

Table 51: Hours with excess energy production.

	Number of hours with excess production $(E_{Prod} - E_{Cons})$ > 0 kWh	Number of hours with excess production above 100 kWh	Total amount of excess energy AC production
Photovoltaic system 1	1 250 hours	0 hours	15 208.7 kWh
Photovoltaic system 2	1 251 hours	0 hours	15 156.3 kWh
Photovoltaic system 3	1 267 hours	0 hours	15 880.7 kWh

It was stated in Chapter 6.4.2: *Nord-Trøndelag Elektrisitetsverk (NTE)*, that NTE can import up to 100 kWh of generated electricity per hour from private installations, without charging additional grid costs. As none of the hours had a surplus production above 100 kWh, it should be expected that all excess electricity can be sold to NTE without having to pay additional costs.

10.1.2 Performance ratio

Figure 80 shows the monthly performance ratio for all three photovoltaic systems. The performance ratio of a photovoltaic system indicates the ratio between the effective electricity yield and the theoretical. According to the results, the performance ratio reached a peak in February, before slowly decreasing, with an additional peak in October.

For the majority of the months, the third photovoltaic system has the highest performance ratio, only surpassed by the second photovoltaic system in December and January. This could imply that the mismatching losses have less significance during these two months.

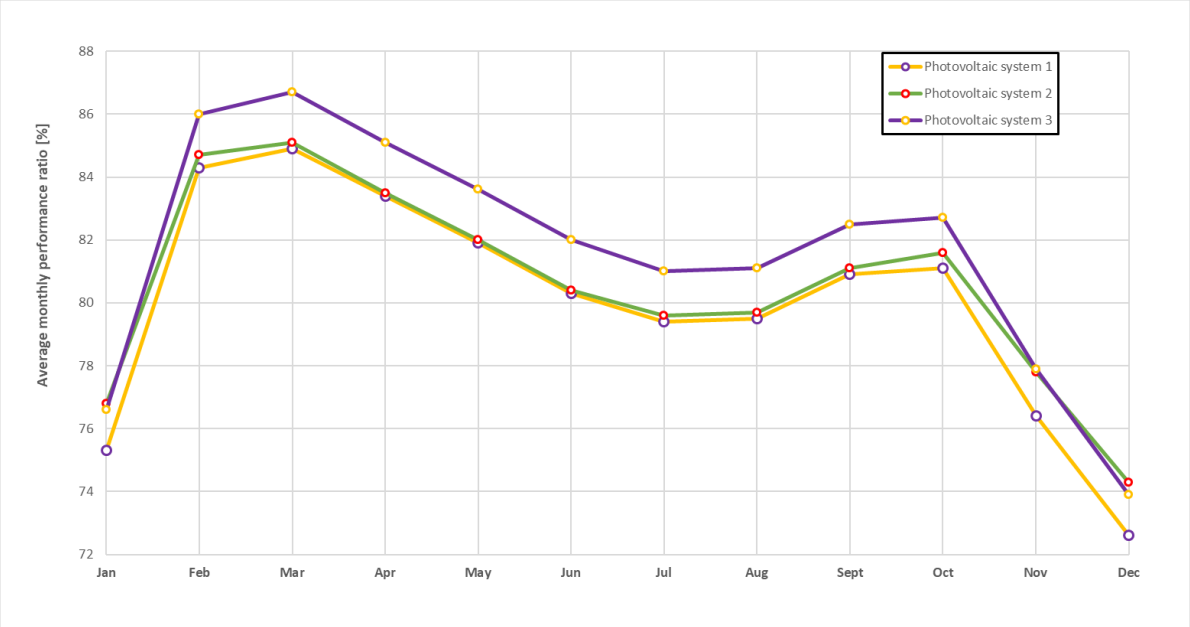

Figure 80: Average monthly performance ratio for photovoltaic system 1, 2 & 3.

10.1.3 Payback time

As mentioned in Chapter 8: *Methodology*, the photovoltaic system's payback time is the amount of time it takes before the investment cost and the potential cost savings of the investment breaks-even. For example, if a person invested 10 000 NOK in exchange for annual earnings of 5 000 NOK for three years, then the investment would break-even after the second year.

The payback time for the photovoltaic system solutions can be obtained by using the estimated investment costs for the photovoltaic systems, found in Chapter 6.8: *Estimated total cost of the photovoltaic systems*, the annual electricity production from the simulation models, and the actual electricity and grid costs for the milk barn.

Since it was initially assumed that the installation fee was equal to 10 % of the investment costs, the payback time will also be calculated with installation fees of 5 and 15 %. As most inverters have a shorter warranty than photovoltaic modules, the payback time will also be presented for a case where all inverters have to be replaced once during the lifespan of the photovoltaic systems.

It should be mentioned that the investment costs presented in this master thesis are only approximations, as they do not include the expenses related to necessary equipment such as DC and AC cables, junction boxes and required wiring plugs. The total investment costs of the real photovoltaic system should therefore be expected to be more expensive.

The highest recommended investment costs for the system solutions will be discussed in Chapter 11: *Discussion*.

Installation fees of 5, 10 and 15 %

As mentioned above, the monthly cost savings were found by using the monthly electricity productions that were obtained through simulations and combine these results with the electricity and grid costs for the milk barn in 2019 (see Table 13). The cost savings of each system solution can be seen in Table 78, Table 79 and Table 80 in Attachment A.15.

Figure 81 shows the estimated payback time for all three photovoltaic system solutions when it is assumed that the installation fee is 10 %, while Figure 122 and Figure 123 in Attachment A.15 shows the results for installation fees of 5 and 15 %, respectively.

A summarized result from all of these figures are displayed in Table 52.

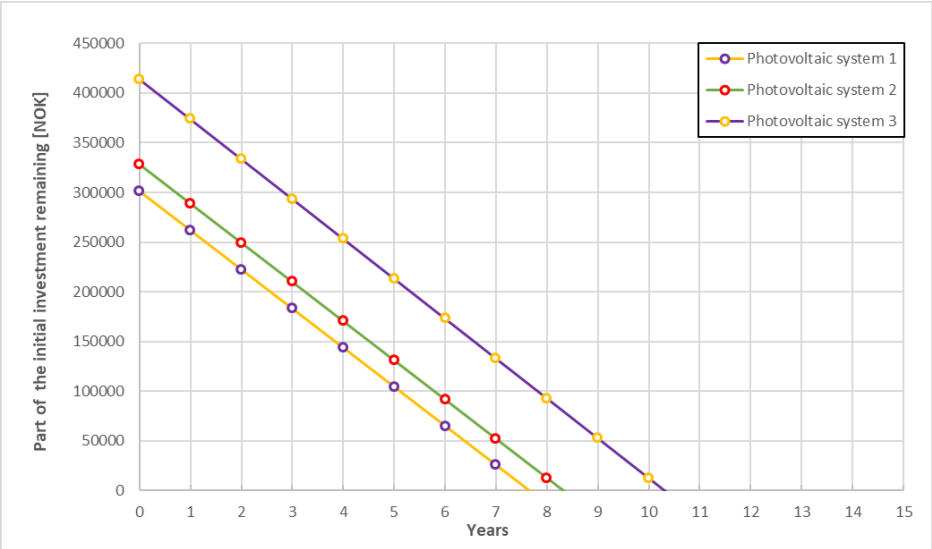

Figure 81: Payback period for photovoltaic system 1, 2 & 3 (10 % installation fee).

Table 52: Payback period for all systems and with different installation fees.

	Photovoltaic system 1	Photovoltaic system 2	Photovoltaic system 3
Payback period (5 % installation fee)	*7 years and 4 months*	*7 years and 10 months*	*9 years and 8 months*
Payback period (10 % installation fee)	*7 years and 7 months*	*8 years and 4 months*	*10 years and 4 months*
Payback period (15 % installation fee)	*8 years*	*8 years and 6 months*	*10 years and 8 months*

Replacing the inverters

Usually, most inverters do not last the entirety of the photovoltaic system's lifespan. This is often reflected in the warrant period provided by the manufacturers, as they commonly only allow for a period of either 5 or 10 years. The point of this subchapter is to see if the photovoltaic systems will remain an economically sound solution if a reinvestment in inverters becomes necessary. It is assumed that the initial installation fee is 10 % and that the additional cost of reinstalling the new inverters are 10 % of the price.

The new payback time can be seen in Figure 82, with a more detailed summarization presented in Table 53, which also includes an installation fee of 5 and 15 %.

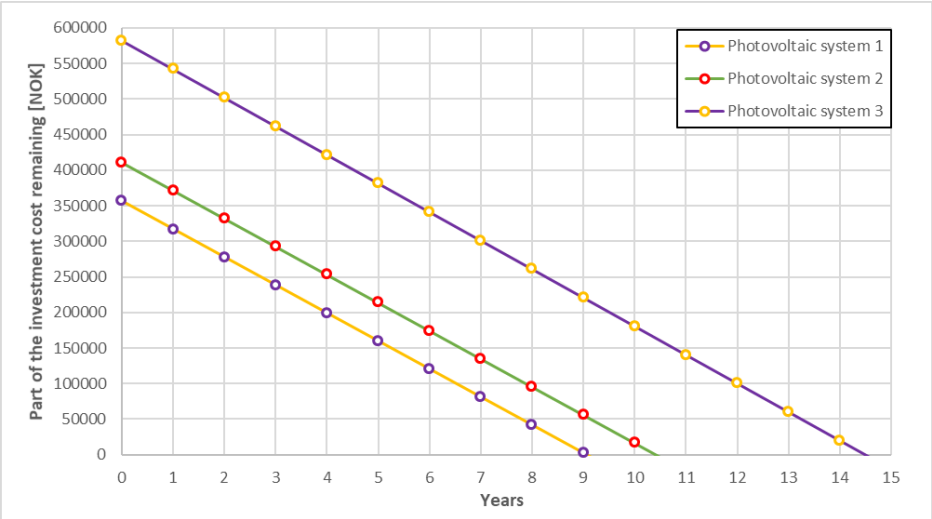

Figure 82: Payback period for photovoltaic systems, when replacing the inverters (10 % installation fee).

Table 53: Payback period for all systems, including a complete replacement of all inverters.

	Photovoltaic system 1	Photovoltaic system 2	Photovoltaic system 3
Payback period (5 % installation fee)	*8 years and 7 months*	*9 years and 10 months*	*13 years and 8 months*
Payback period (10 % installation fee)	*9 years and 2 months*	*10 years and 5 months*	*14 years and 6 months*
Payback period (15 % installation fee)	*9 years and 5 months*	*10 years and 9 months*	*15 years and 3 months*

10.1.4 Net Present Value

The payback time is a useful indicator when determining if one should expect a positive return on the investment somewhere down the line, but it does not account for the time value of money. In situations where multiple investment options are available, the Net Present Value (NPV) may be a more appropriate indicator, as it indicates the profitability of the investment by taking the present value of future cost savings and expenses into consideration. The NPV can be calculated with Equation 8.1 presented in Chapter 8.2.1: *Evaluation of system performance*.

The NPV is calculated for two cases in this master thesis:

1. The inverters last the whole lifespan of the photovoltaic system.
2. It is necessary to replace the inverters after 15 years.

In both cases, it is believed that the installation fee is 10 % and that the photovoltaic systems will have no remaining economic value after 25 years.

The results from the NPC calculations can be seen in Table 54. In the table, three different discount rates are included.

Table 54: Net Present Value for the different photovoltaic systems.

	Discount rate [%]	Photovoltaic system 1	Photovoltaic system 2	Photovoltaic system 3
NPV without replacing the inverters	2	467 394.9 NOK	441 992.2 NOK	370 129.1 NOK
	4	313 825.8 NOK	288 032.6 NOK	213 417.4 NOK
	6	202 085.7 NOK	176 008.3 NOK	99 390.7 NOK
NPV when replacing all inverters	2	426 095.9 NOK	380 366.6 NOK	244 875.3 NOK
	4	282 962.5 NOK	241 978.9 NOK	119 813.7 NOK
	6	178 892.8 NOK	141 400.3 NOK	29 050.2 NOK

10.1.5 Greenhouse gas emissions

As stated several times throughout this thesis, the main goal is to study the effect that the increased solar utilization may have on greenhouse gas emissions in Norwegian agriculture. If the annual amount of electricity generation found in Chapter 10.1.1: *Annual electricity production* is combined with the three different electricity mix assumptions introduced in Chapter 8.3: *Generalizing the results*, then it becomes possible to estimate the potential reduction in greenhouse gas emissions.

According to information presented in Chapter 2.1: *Norwegian agriculture*, there were about 7 600 milk farms in Norway at the beginning of 2019. Out of these 7 600 milk farms, about 1 500 were located in Trøndelag-county. In the same chapter, it was mentioned that the electricity consumption in Norwegian agriculture was about 0.98 TWh in 2014, excluding electricity meant for greenhouse heating, with an expected increase of 0.2 % each year until 2035. It was therefore assumed that electricity consumption in 2019 was roughly 0.988 TWh.

The electricity consumption related to milk farms in Trøndelag was about 106.1 GWh in 2017, at least according to (Andersson & Sand, 2018). Using the same 0.2 % increase assumption as above, the electricity consumption in Trøndelag agriculture for 2019 should be about 106.52 GWh.

Trøndelag agriculture

As shown in Chapter 10.1.1: *Annual electricity production*, the annual electricity generation is relatively similar for all three system solutions, with the second system generating 0.24 % more electricity than the first system, while the third produces 2.05 % more. Table 55 shows the reduction in greenhouse gas emissions for these three systems with the emission factor assumptions.

Table 55: Potential reduction of greenhouse gas emissions per photovoltaic system solution.

	Photovoltaic system 1	Photovoltaic system 2	Photovoltaic system 3
Low emissions (18.9 g CO_2/kWh)	997.03 kg CO_2	999.43 kg CO_2	1 017.42 kg CO_2
Moderate emissions (40.2 g CO_2/kWh)	2 120.66 kg CO_2	2 125.76 kg CO_2	2 164.04 kg CO_2
Substantial emissions (61.5 g CO_2/kWh)	3 244.30 kg CO_2	3 252.10 kg CO_2	3 310.66 kg CO_2

Table 56 and Table 57 shows the potential reduction in greenhouse gas emissions based on how many of the 1 500 milk farms in Trøndelag who adopt the first or second photovoltaic system solution. If all milk farms in Trøndelag installed similar photovoltaic systems, then the consumption of imported electricity should, at least according to the results and assumptions, be lowered from 106.52 GWh to either 27.39 or 27.20 GWh, depending on if system solution 1 or 2 is used.

Table 56: Reduction in greenhouse gas emissions in Trøndelag with photovoltaic system 1.

Share of milk farms in Trøndelag with photovoltaic system 1	10 %	20 %	30 %	40 %	50 %
Electricity production [kWh]	7 912 920	15 825 840	23 738 760	31 651 680	39 564 600
Low emissions [Tons of CO_2 equivalents]	149.55	299.10	448.66	598.22	747.77
Moderate emissions [Tons of CO_2 equivalents]	318.10	636.20	9 54.30	1 272.40	1 590.50
Substantial emissions [Tons of CO_2 equivalents]	486.64	973.29	1 459.93	1 946.58	2 433.22

Share of milk farms in Trøndelag with photovoltaic system 1	60 %	70 %	80 %	90 %	100 %
Electricity production [kWh]	47 477 520	55 390 440	63 303 360	71 216 280	79 129 200
Low emissions [Tons of CO_2 equivalents]	897.33	1 046.88	1 196.43	1345.99	1 495.54
Moderate emissions [Tons of CO_2 equivalents]	1 908.60	2 226.70	2 544.80	2 862.89	3 180.99
Substantial emissions [Tons of CO_2 equivalents]	2 919.87	3 406.51	3 893.16	4 379.80	4 866.45

Table 57: Reduction in greenhouse gas emissions in Trøndelag with photovoltaic system 2.

Share of milk farms in Trøndelag with photovoltaic system 2	10 %	20 %	30 %	40 %	50 %
Electricity production [kWh]	7 931 955	15 863 910	23 795 865	31 727 820	39 659 775
Low emissions [Tons of CO_2 equivalents]	149.91	299.83	449.74	599.66	749.57
Moderate emissions [Tons of CO_2 equivalents]	318.86	637.73	956.59	1 275.46	1 594.32
Substantial emissions [Tons of CO_2 equivalents]	487.82	975.63	1 463.45	1 951.26	2 439.08

Share of milk farms in Trøndelag with photovoltaic system 2	60 %	70 %	80 %	90 %	100 %
Electricity production [kWh]	47 591 730	55 523 685	63 455 640	71 387 595	79 319 550
Low emissions [Tons of CO_2 equivalents]	899.48	1 049.40	1 199.31	1 349.23	1 499.14
Moderate emissions [Tons of CO_2 equivalents]	1 913.19	2 232.05	2 550.92	2 869.78	3 188.65
Substantial emissions [Tons of CO_2 equivalents]	2 926.89	3 414.71	3 902.52	4 390.34	4 878.15

Table 58 displays the potential reduction in greenhouse gas emissions if the third system solution is installed at the milk farms in Trøndelag instead of system solution 1 or 2. If 100 % of the milk farms in Trøndelag adapted this system solution, then the consumption of imported electricity is lowered from 106.52 to 25.77 GWh.

Table 58: Reduction in greenhouse gas emissions in Trøndelag with photovoltaic system 3.

Share of milk farms in Trøndelag with photovoltaic system 3	10 %	20 %	30 %	40 %	50 %
Electricity production [kWh]	8 074 785	16 149 570	24 224 355	32 299 140	40 373 925
Low emissions [Tons of CO_2 equivalents]	152.61	305.23	457.84	610.45	763.07
Moderate emissions [Tons of CO_2 equivalents]	324.61	649.21	973.82	1 298.43	1 623.03
Substantial emissions [Tons of CO_2 equivalents]	496.60	993.20	1 489.80	1 986.40	2 483.00

Share of milk farms in Trøndelag with photovoltaic system 3	60 %	70 %	80 %	90 %	100 %
Electricity production [kWh]	48 448 710	56 523 495	64 598 280	72 673 065	80 747 850
Low emissions [Tons of CO_2 equivalents]	915.68	1 068.29	1 220.91	1 373.52	1 526.14
Moderate emissions [Tons of CO_2 equivalents]	1 947.64	2 272.24	2 596.85	2 921.46	3 246.06
Substantial emissions [Tons of CO_2 equivalents]	2 979.60	3 476.19	3 972.79	4 469.39	4 965.99

Norwegian agriculture

The results can also be expanded to include all milk farms in Norway. It has already been established that the total electricity consumption in Norwegian agriculture was roughly 0.988 TWh in 2019 and that there are 7 600 milk farms in Norway, which is all the information necessary to make the estimation.

The resulting reduction in greenhouse gas emissions for utilizing photovoltaic system 1, 2 or 3, can be seen in Table 59, Table 60 and Table 61, respectively.

Table 59: Reduction in greenhouse gas emissions in Norway with photovoltaic system 1.

Share of milk farms in Norway with photovoltaic system 1	10 %	20 %	30 %	40 %	50 %
Electricity production [kWh]	40 092 128	80 184 256	120 276 384	160 368 512	200 460 640
Low emissions [Tons of CO_2 equivalents]	757.74	1 515.48	2 273.22	3 030.96	3 788.71
Moderate emissions [Tons of CO_2 equivalents]	1 611.70	3 223.41	4 835.11	6 446.81	8 058.52
Substantial emissions [Tons of CO_2 equivalents]	2 465.67	4 931.33	7 397.00	9 862.66	12 328.33

Share of milk farms in Norway with photovoltaic system 1	60 %	70 %	80 %	90 %	100 %
Electricity production [kWh]	240 552 768	280 644 896	320 737 024	360 829 152	400 921 280
Low emissions [Tons of CO_2 equivalents]	4 546.45	5 304.19	6 061.93	6 819.67	7 577.41
Moderate emissions [Tons of CO_2 equivalents]	9 670.22	11 281.92	12 893.63	14 505.33	16 117.04
Substantial emissions [Tons of CO_2 equivalents]	14 794.00	17 259.66	19 725.33	22 190.99	24 656.66

Table 60: Reduction in greenhouse gas emissions in Norway with photovoltaic system 2.

Share of milk farms in Norway with photovoltaic system 2	10 %	20 %	30 %	40 %	50 %
Electricity production [kWh]	40 188 572	80 377 144	120 565 716	160 754 288	200 942 860
Low emissions [Tons of CO_2 equivalents]	759.56	1 519.13	2 278.69	3 038.26	3 797.82
Moderate emissions [Tons of CO_2 equivalents]	1 615.58	3 231.16	4 846.74	6 462.32	8 077.90
Substantial emissions [Tons of CO_2 equivalents]	2 471.60	4 943.19	7 414.79	9 886.39	12 357.99

Share of milk farms in Norway with photovoltaic system 2	60 %	70 %	80 %	90 %	100 %
Electricity production [kWh]	241 131 432	281 320 004	321 508 576	361 697 148	401 885 720
Low emissions [Tons of CO_2 equivalents]	4 557.38	5 316.95	6 076.51	6 836.08	7 595.64
Moderate emissions [Tons of CO_2 equivalents]	9 693.48	11 309.06	12 924.64	14 540.23	16 155.81
Substantial emissions [Tons of CO_2 equivalents]	14 829.58	17 301.18	19 772.78	22 244.37	24 715.97

Table 61: Reduction in greenhouse gas emissions in Norway with photovoltaic system 3.

Share of milk farms in Norway with photovoltaic system 3	10 %	20 %	30 %	40 %	50 %
Electricity production [kWh]	40 912 244	81 824 488	122 736 732	163 648 976	204 561 220
Low emissions [Tons of CO_2 equivalents]	773.24	1 546.48	2 319.72	3 092.97	3 866.21
Moderate emissions [Tons of CO_2 equivalents]	1 644.67	3 289.34	4 934.02	6 578.69	8 223.36
Substantial emissions [Tons of CO_2 equivalents]	2 516.10	5 032.21	7 548.31	10 064.41	12 580.52

Share of milk farms in Norway with photovoltaic system 3	60 %	70 %	80 %	90 %	100 %
Electricity production [kWh]	245 473 464	286 385 708	327 297 952	368 210 196	409 122 440
Low emissions [Tons of CO_2 equivalents]	4 639.45	5 412.69	6 185.93	6 959.17	7 732.41
Moderate emissions [Tons of CO_2 equivalents]	9 868.03	11 512.71	13 157.38	14 802.05	16 446.72
Substantial emissions [Tons of CO_2 equivalents]	15 096.62	17 612.71	20 128.82	22 644.93	25 161.03

If all Norwegian milk farms had implemented photovoltaic system 1, 2 or 3, then the imported electricity consumption should be reduced from 0.988 TWh to either 0.587, 0.586 or 0.579 TWh, depending on the system solution.

10.1.6 Summarization of photovoltaic system results

If the first photovoltaic system solution is used as a reference system, then it is possible to compare the different indicators of each photovoltaic system solution. Table 62 shows the annual energy production, average performance ratio, annual energy losses, payback time (with and without replacing the inverters) and NPV.

The table also includes the potential reduction in Norwegian greenhouse gas emissions for all three emission factor assumptions, when all 7600 milk farms in Norway install the corresponding photovoltaic systems.

All economic values presented in the table are obtained with a 10 % installation fee.

Table 62: Summarization and comparison of the most important results from the PV simulations.

	Annual energy yield	Annual performance ratio	Annual energy loss	Payback time	Payback time (with replacing inverters)
Reference system (Photovoltaic system 1)	52 752.8 kWh	81.3 %	8 116.1 kWh	7 Years 7 Months	9 Years 2 Months
Photovoltaic system 2	+ 0.241 %	+ 0.2 %	- 1.562 %	8 Years 4 Months	10 Years 5 Months
Photovoltaic system 3	+ 2.046 %	+ 1.7 %	- 13.296 %	10 Years 4 Months	14 Years 6 Months

	Net Present Value (Without replacing inverters)			Reduction in greenhouse gas emissions in Norwegian agriculture [tons of CO_2 equivalents]		
	r = 2 %	r = 4 %	r = 6 %	Low	Moderate	Substantial
Reference system (Photovoltaic system 1)	467 394.9 NOK	313 825.8 NOK	202 085.7 NOK	7 577.4	16 117.0	24 656.7
Photovoltaic system 2	- 5.435 %	- 8.219 %	-12.904 %	≈ 0 %	≈ 0 %	≈ 0 %
Photovoltaic system 3	- 20.810 %	- 31.995 %	- 50.818	+ 2.046 %	+ 2.046 %	+ 2.046 %

10.2 The solar water-heating system at the milk barn

It was mentioned in Chapter 8.2.1: *Evaluation of system performance*, that the solar fraction would be used as the principal indicator for the performance of the solar water-heating system. The problem with this indicator is that it does not allow for comparisons with hot water system solutions that do not utilize solar collectors, and therefore, in addition to the solar fraction, the electricity consumption of the different hot water system solutions will also be used as a performance indicator.

Figure 83 shows the monthly amounts of solar energy delivered to the storage tank from the solar collectors. The most prominent result displayed in the graph is that the evacuated tube collectors carry more heat monthly to the storage unit compared to the solar water-heating system with flat-plate collectors.

One of the possible reasons for this result is that the evacuated tube collectors have a relatively smaller optical efficiency compared to flat-plate collectors, but at the same time they also have more modest heat loss coefficients, suggesting that the evacuated tube collectors are less affected by the temperature difference between the heat transfer fluid and ambient outdoor air temperature.

The effect of the smaller heat losses can be seen on the average conversion efficiency for the solar collectors, found with the simulation software (see Table 63). In addition to the conversion efficiency, the lower heat losses can also be seen on the specific collector field yield per m^2 of aperture area.

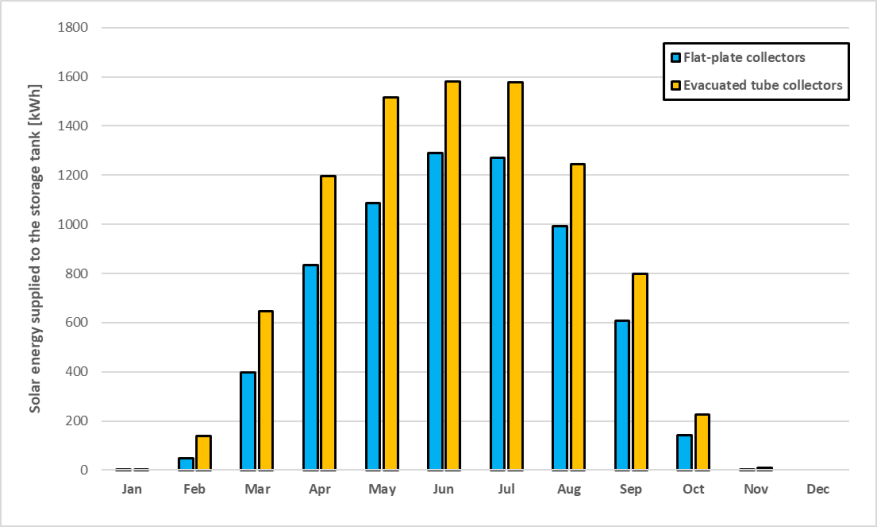

Figure 83: Monthly amount of heat carried to the storage tank from the solar collectors.

Table 63: Average solar collector efficiency and specific solar energy yield.

	Flat-plate collectors	Evacuated tube collectors
Optical efficiency (laminar flow)	75 %	65 %
Average collector efficiency	24.47 %	34.70 %
Specific collector field yield	264.64 kWh/m^2	375.25 kWh/m^2

To be able to determine the solar fraction of the two solar water-heating systems, it is also necessary to know the amount of thermal energy delivered to the storage tank from the auxiliary heat sources. The heat supplied from the electric heating elements and the heat pump is displayed in Figure 84.

By using Equation 8.2 from Chapter 8.2.1: *Evaluation of system performance*, on how to calculate the solar fraction, it becomes possible to determine the monthly average value. The calculated solar fractions for both flat-plate and evacuated tube collector systems, with different storage tank volumes, are shown in Figure 85.

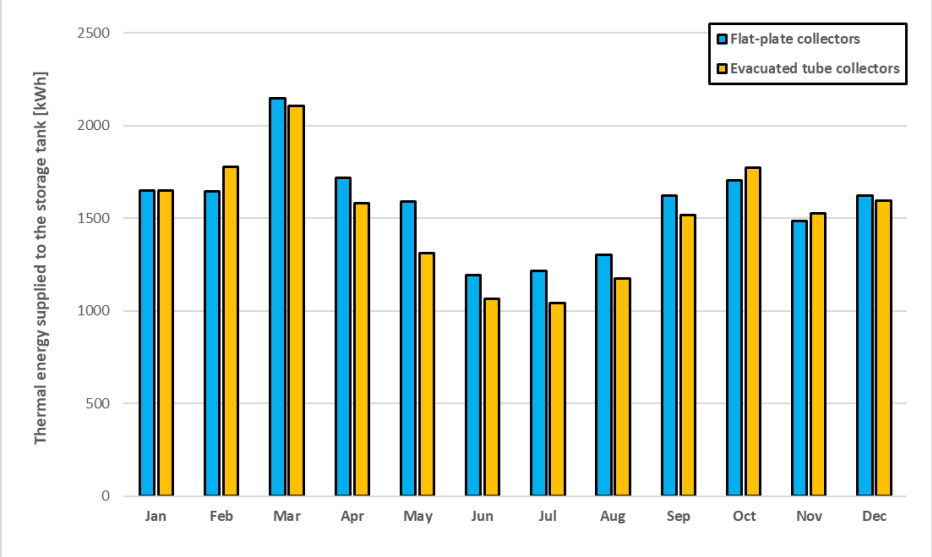

Figure 84: Amount of thermal energy delivered to the storage tank from auxiliary heat sources.

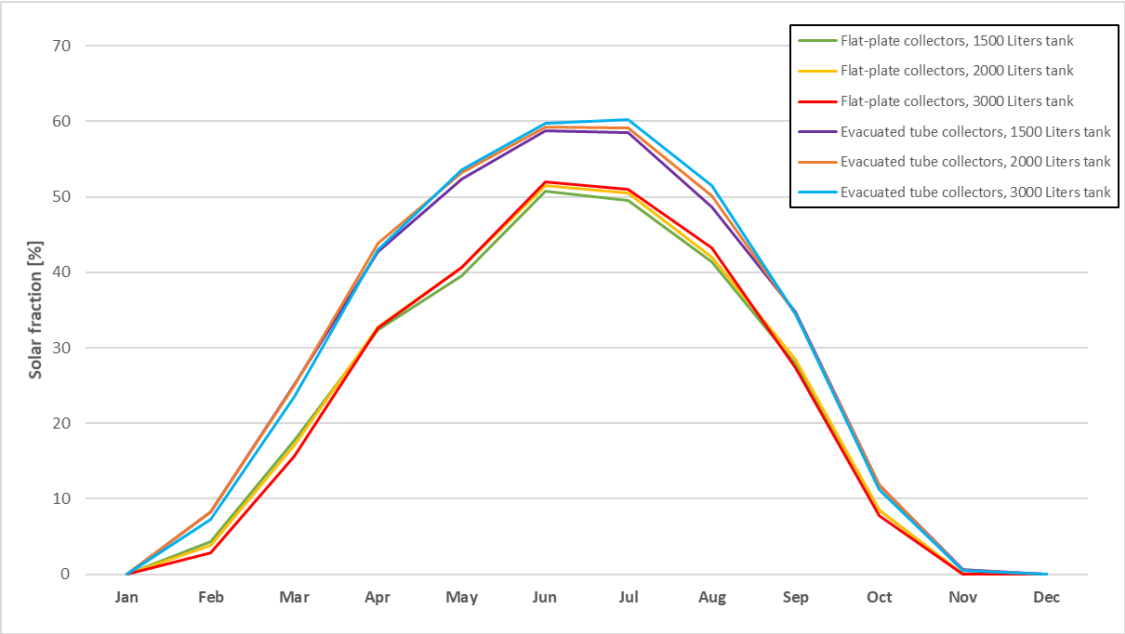

Figure 85: Monthly average solar fraction for flat-plate and evacuated tube collectors.

The figure above indicates that the volume of the storage tank has a relatively little effect on the systems solar fraction. The solar collector type, on the other hand, influences the solar fraction greatly, as the graph shows that the performance of the evacuated tube collectors is higher than for the flat-plate collectors.

In Figure 86, the monthly amount of thermal energy delivered to the storage tank is compared to the simulated energy consumption of the hot water system. In this figure, the solar collectors are removed from the solar water-heating system, and the 3000-liter storage tank is replaced with a 300-liter unit, to try to determine the amount of thermal energy delivered by the existing hot water system in the milk barn.

This new simulation model is known as the *No solar collector* in the figure.

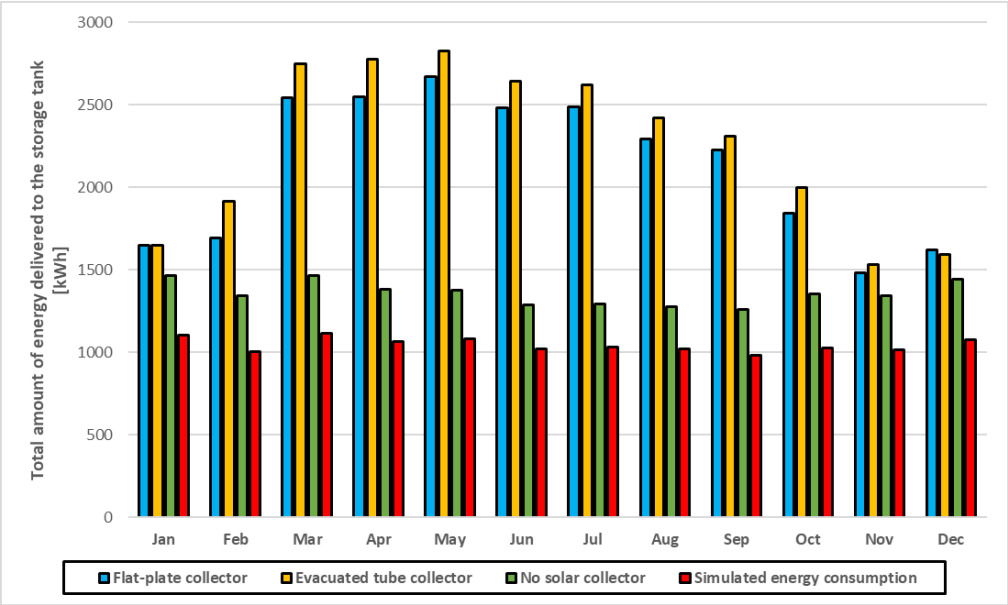

Figure 86: Total amount of energy delivered to the storage tank compared to the energy consumption.

The results displayed in the figure above implies that the solar water-heating systems produce unnecessary large amounts of thermal energy, resulting in smaller system performances, at least according to Polysun. This is not necessarily a problem as long as the electricity needed to generate this amount of heat is lower than for the *No solar collector model*.

The annual electricity consumption for each of the different hot water system solutions can be seen in Figure 87.

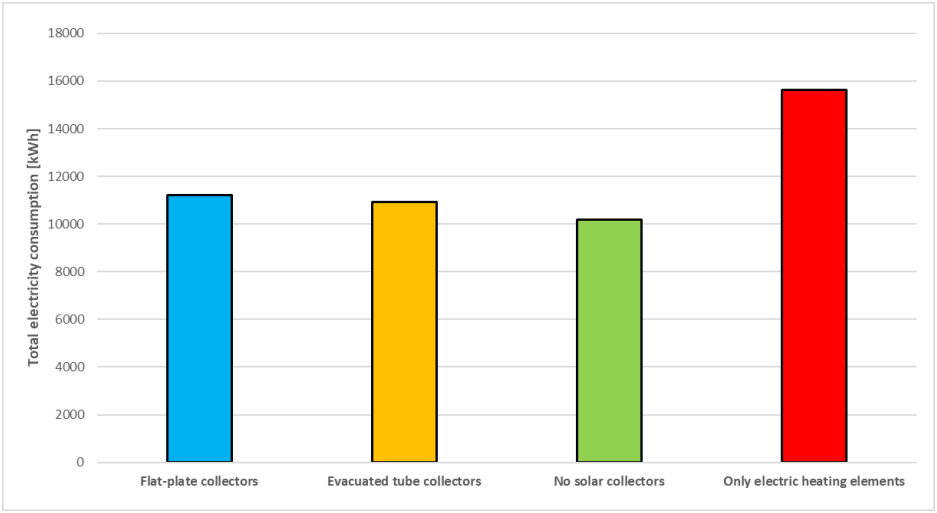

Figure 87: Electricity consumption of the hot water systems with different assumptions.

Comparing the results from Figure 86 and Figure 87, it quickly becomes apparent that the solar water-heating systems operate inefficiently, as the simulation model *No solar collector* has both lower total electricity consumption and also delivers sufficient amounts of thermal energy to the storage tank. This could imply that the heat pump and the solar collectors hinder each other from working correctly. This theory is strengthened by the fact that:

1. The controller for each component in the simulation model is not able to communicate with each other, meaning that neither the solar collectors nor the heat pump show any consideration for the other component.
2. Both components have a higher performance during summer and a more modest one during colder seasons, possibly making it unnecessary with both system components.

As the results are now, solar collectors are not a suitable addition to the hot water system at Mære Agricultural School, at least according to the simulations. The heat pump delivers sufficient amounts of "free" thermal energy, making the solar collectors unnecessary.

In Chapter 11: *Discussion*, the theory on the heat pump will be further examined, and possible changes to the existing hot water system will be suggested, with the sole purpose of reducing the electricity consumption, while at the same time deliver sufficient amount of thermal energy

Until this goal is achieved, it is little relevance in presenting the potential for reducing greenhouse gas emissions by utilizing solar collectors.

11 Discussion

In this chapter, some of the results from Chapter 10: *Results* will be discussed. In addition to the discussion, a parametric study is also performed on the simulation models. The goal of the parametric study is to examine the influence some of the assumptions made in this paper have on the final results. The parametric study will also be used to investigate the sensitivity of some of the results. In the case of the solar water-heating system, the parametric study is primarily utilized to determine the necessary conditions for optimizing the system.

It should be noted that the energy systems presented in this master thesis are sometimes very complex, and the final results presented in the previous chapter may therefore differ from actual solar energy systems. This is especially true for the solar water-heating systems, where there are several more input parameters compared to the photovoltaic systems.

11.1 Photovoltaic system solutions

11.1.1 Annual electricity production

In the case of the photovoltaic system solutions, all components were implemented with similar input parameters except for the inverter system and assumptions regarding mismatching. As presented in Chapter 10: *Results*, the overall outcome of the simulations was that the third photovoltaic system solution, which utilized micro-inverters, generated a more substantial amount of annual electricity compared to the other two system solutions.

If one does not care about the investment cost of the systems, and the main focus is to generate as much electricity as possible, then it could be argued that the third photovoltaic system solution should be installed at the milk barn. Of course, this only applies if the assumptions made in Chapter 9.3: *Implementing the photovoltaic systems in Polysun* are correct.

As mentioned, the two most prominent contributors to the different results were the assumptions regarding mismatching and the inverter systems. (Gong, 2018) claimed that when micro-inverters are being employed, then no mismatching should be implemented. If a 2 % annual mismatch is added to the third photovoltaic system, then the annual electricity production will decrease from 53 831.9 to 52 741 kWh, which is lower than the results for the first and second system solution.

The effect the mismatching assumption has on the average monthly inverter efficiency can be seen in Figure 88.

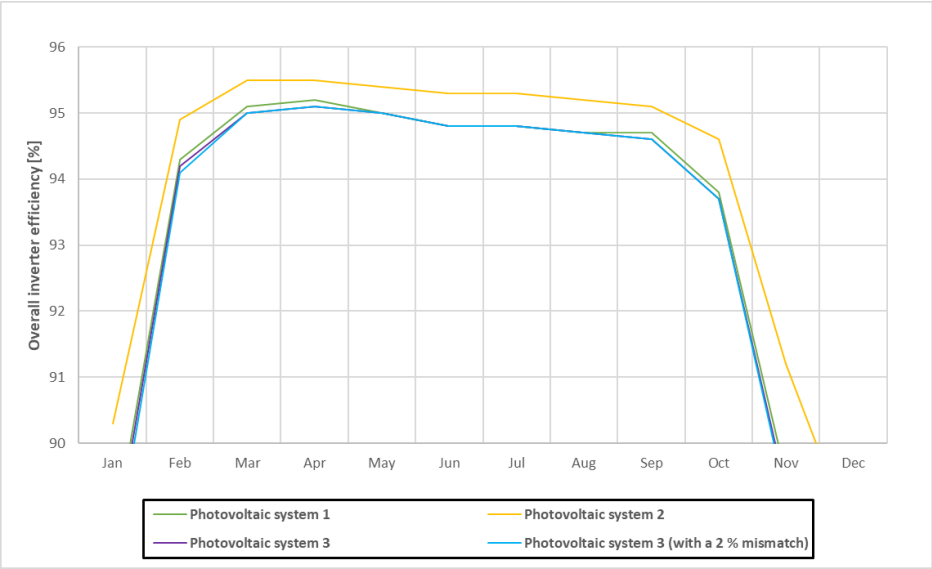

Figure 88: Monthly inverter efficiency.

The results in the figure above clearly indicate that the efficiency of the inverters is only affected in a relatively small degree by the mismatching assumption, and also that the second system solution has the highest overall inverter efficiency, regardless.

The reason for this is likely due to the power ratio of the second inverter system being 100 %, implying that the second inverter system is an excellent fit for the photovoltaic module system. The first photovoltaic system has a power ratio of 110 % for one of the string inverters and 111 % for the other, while the third system solution has a power ratio of 103 % per micro-inverter.

As can be seen in Figure 88, these different power ratios still results in very similar monthly inverter efficiencies.

Although the overall inverter efficiency is almost entirely unaffected by the mismatching assumption, the performance ratio is a little more affected. Figure 89 shows a comparison between all the original performance ratios presented in Chapter 10.1.1: *Annual electricity production* and a new performance ratio for the third photovoltaic system when 2 % mismatching is incorporated into the model.

With mismatching incorporated, the performance ratio of the third photovoltaic system solution more closely resembles the performance ratio of the first system solution.

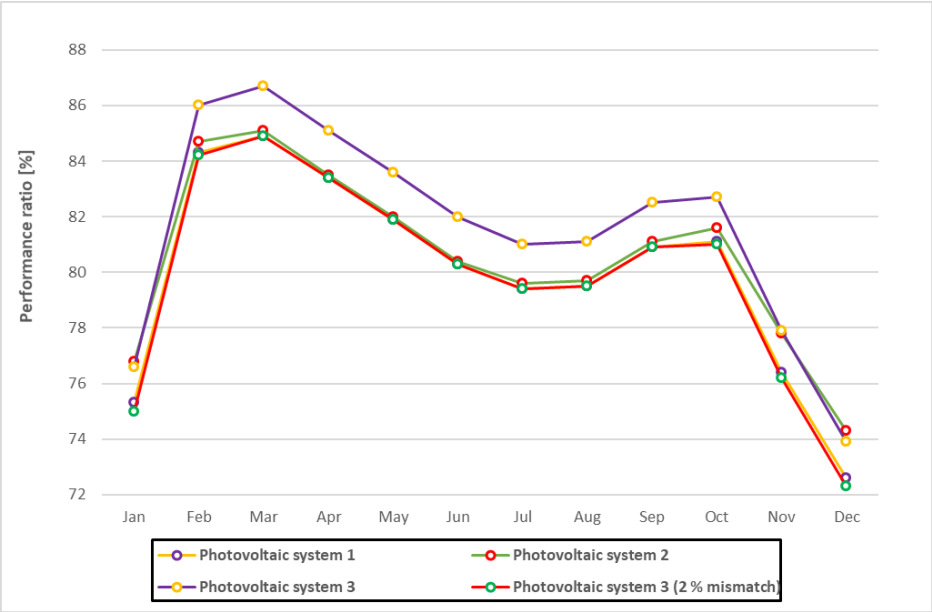

Figure 89: Average monthly performance ratio when photovoltaic system 3 has a 2 % mismatch loss.

Another approach is to see how high the annual mismatching losses for the third photovoltaic system can be before the second system solution becomes the most suitable option. Figure 90 shows the annual electricity generation for the third photovoltaic system at different mismatching percentages. The red dotted line in the graph indicates the annual electricity production for the second system, implying that the annual mismatching for the third system should not exceed 1.746 %.

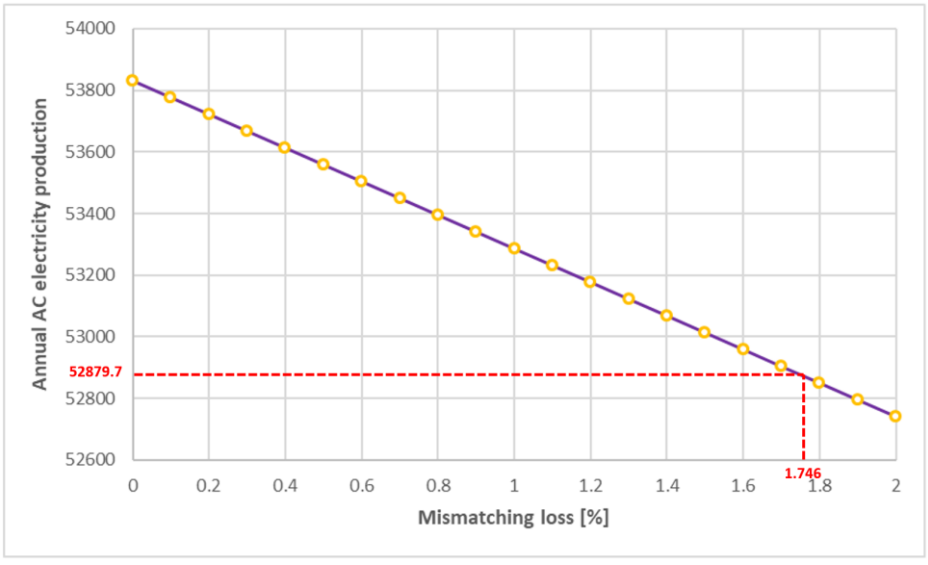

Figure 90: Annual AC electricity for Photovoltaic system 3 at different mismatching losses.

11.1.2 Cost of the photovoltaic systems

There is a high degree of uncertainty with the investment costs presented in Chapter 6.8: *Estimated total cost of the photovoltaic systems*. This is because the expenses only accounts for the photovoltaic modules, inverters and also an assumed installation fee of 10 %. Necessary components such as mounting equipment for the photovoltaic modules, cable plugs, cables, junction boxes and shipping fees are not included, resulting in the aforementioned uncertainty.

In the case of the inverters, the product cost is somewhat accurate, as it was collected from inverter stores found on the Internet. Unfortunately, the micro-inverter prices are only based on the American model of the product, as no price tag was found for the micro-inverters made for the European market.

In Chapter 10: *Results*, both the payback time and Net Present Value (NPV) were calculated for all three photovoltaic system solutions, based on the assumed total investment cost and annual estimated cost savings. Considering there is some degree of uncertainty with the investment cost of the systems, a more appropriate indicator could be to examine the highest recommended investment cost before the system become unprofitable or not an economically wise decision.

As a photovoltaic system is only expected to last 25 years, even though they sometimes last longer, the payback time should not exceed 25 years, as this means that the investment of the photovoltaic system will not break-even during its technical lifespan. In addition to the payback time, the necessary investment cost to achieve an NPV of zero should also be calculated, as an NPV of zero or lower indicates that the investment costs may not be economically sound.

If the assumption of a technical lifespan of 25 years is combined with the annual cost saving of each system solution (see Chapter 10.1.3: *Payback time*), then it is possible to determine the investment cost that would result in a break-even between the investment and annual cost savings after 25 years.

Table 64 shows the estimated highest recommended investment costs for all three system solutions before the payback time goes beyond 25 years. For all three photovoltaic systems, the highest recommended investment cost is somewhere between 600 000 to 700 000 NOK above the initial estimated investment costs in Chapter 6.8: *Estimated total cost of the photovoltaic systems*, providing much leeway for additional component costs.

Table 64: Highest recommended investment cost based on payback time.

	Photovoltaic system 1	Photovoltaic system 2	Photovoltaic system 3
Estimated investment cost (Chapter 6.8)	301 103 NOK	328 460 NOK	414 095 NOK
Highest recommended investment cost	984 070 NOK	986 572.5 NOK	1 004 207.5 NOK

The same procedure as above can be used to obtain an NPV of zero, as the annual cost savings and technical lifespan are known. The highest recommended investment costs can then be determined by assuming one or several different discount rates. The results of the calculations can be seen in Table 65. To be able to ensure the profitability of the photovoltaic systems, the real investment cost should not go above the values presented in the table.

Similar to the results of the payback time, there is still some room for the initial estimated investment costs to increase before becoming unprofitable, at least based on the assumptions in this master thesis.

Table 65: Highest recommended investment cost based on Net Present Value.

NPV = 0	Photovoltaic system 1	Photovoltaic system 2	Photovoltaic system 3
Discount rate of 2 %	768 497.9 NOK	770 452.2 NOK	784 224.1 NOK
Discount rate of 4 %	614 928.8 NOK	616 492.6 NOK	627 512.4 NOK
Discount rate of 6 %	503 188.7 NOK	504 468.1 NOK	513 485.7 NOK

It should be noted that even if the financial support scheme from Enova was introduced in Chapter 6.1.4: *The cost of PV Modules*, it has not been incorporated into any of the financial calculations. Still, they could serve to increase the potential economic gain from the systems by reducing the investment cost.

11.1.3 Potential reduction in greenhouse gas emissions

In Chapter 10.1.5: *Greenhouse gas emissions*, the potential reduction in greenhouse gas emissions was obtained by using the assumptions introduced in Chapter 8.3: *Generalizing the results* regarding the utilized electricity mix. Initially, it was assumed that the current electricity consumption at the school consisted of either 100 % Norwegian mix or 100 % Nordic mix or 50 % from both.

But, as explained by (Løvik, 2018), only about 19 % of the electricity produced in Norway is consumed in Norway, and if the building owner has no guarantee from the power company that only Norwegian generated electricity is to be imported, then the European electricity mix is used instead. This mix consists of about 16 % renewable energy, 57 % fossil heat and 27 % nuclear power, and has a much higher emission factor compared to the Norwegian and Nordic electricity mix (see Table 1).

Assuming that only 19 % of the electricity consumed at the milk barn, and the remaining milk farms in Norway, are covered by electricity produced in Norway, while the remaining 81 % is produced in other locations in Europe, then the resulting emission factor would be 243.19 g CO_2 equivalents/kWh. The reduction in greenhouse gas emissions for the three photovoltaic system solutions at the milk barn would then increase to be roughly 12 828.95, 12 859.81 and 13 091.38 kg CO_2 equivalents, respectively.

These new potential reductions in greenhouse gas emissions are a significant increase from the initial results presented in Table 55.

Because there are so many potential combinations of electricity mixes, as well as the fact that the emission factors regularly change based on the consistency of the mixture, it becomes hard to pinpoint an accurate greenhouse gas emission reduction.

Since the content of the different electricity mixtures develops over time, the potential for the photovoltaic systems to reduce the greenhouse gas emissions is not fixed. As an example, if the emission factor for the Nordic electricity mix decreases due to increased utilization of renewable energy sources in the mixture, then the potential reduction in greenhouse gas emissions for the systems are also reduced. This is because the generated electricity would replace a slightly greener energy mixture than the initial mix.

It should also be noted that the uncertainty increases with the theoretical amount of Norwegian milk farms that start to employ the photovoltaic systems. For example, if all of the milk farms utilize the first system solution, then the total reduction of greenhouse gas emissions could vary from 7 577.4 to 97 500.0 tons of CO_2 equivalents, depending on if the Norwegian electricity mix or the new mix introduced above is considered as the basis.

In the introduction of this master thesis, it was mentioned that the greenhouse gas emissions related to energy consumption in agriculture, forestry and fisheries were about 0.4 million tons of CO_2 equivalents according to (Miljødirektoratet, 2019). This suggests that if the assumption that only 19 % of the electricity used in Norway has a Norwegian origin, while the remaining originates from the European electricity mix, then considering how the situation is now, the greenhouse gas emissions could be reduced by almost ¼ of the total greenhouse gas emissions related to electricity consumption in Norwegian agriculture, forestry and fisheries in 2017.

This may seem extensive, but according to (Andersson & Sand, 2018), milk farms were responsible for about 77.85 % of agricultural electricity consumption in Trøndelag in 2017.

11.1.4 Parametric study

The simulated behavior of the photovoltaic systems depends on a large number of input parameters, each being able to affect the final result in some degree. A parametric study is introduced in this chapter, to be able to examine some of the effects of these parameters, as well as a few of the assumptions made during the design phase of the photovoltaic systems. The three photovoltaic system solutions described in Chapter 9.3: *Implementing the photovoltaic systems in Polysun* are set as reference systems, and the parametric study is performed by only changing one input parameter at a time while keeping the others constant, as this makes it possible to determine the effect that this single input parameter has on the final result.

Lastly, this parametric study will also be used to determine if the photovoltaic systems behave as expected. The principal indicator in this subchapter is the annual AC electricity production, as this is the usable or exportable electricity generated with the photovoltaic systems.

Effect of obstruction shading

There is a general consensus, both in literature and popular science, that micro-inverters provide a higher electricity production compared to traditional string inverters for areas that annually experience somewhere between moderate to large amounts of obstruction shading. Based on what has already been discussed, this could be due to the lack of mismatching, addressed in Chapter 11.1.1: *Annual electricity production*, but micro-inverters are also known to counteract the "bottleneck" effect that occurs when photovoltaic modules are partially shaded.

In this subchapter of the parametric study, the effect of varying amounts of shade is examined. This is achieved primarily by increasing the height of the nearby hilltop and studying how this affects the annual AC electricity production for each of the photovoltaic systems. Based on the literature review, it is expected that the micro-inverters are less affected by the increased shading.

Figure 91 shows how the annual AC electricity generation is affected by increased shading. The shading effect was only examined until the hilltop was twice as high as its initial height. The functions displayed on the right side of the figure indicates the estimated amount of annual AC electricity generated from each system solution, for different percentage increase in hill height, while EY1, EY2 and EY3 refer to the first, second and third system solution, respectively.

The most surprising result in the figure below is that the annual production of the third system solution is more affected by increased shading than the other two systems. This is especially unexpected as the literature on the subject suggests it should be the other way around.

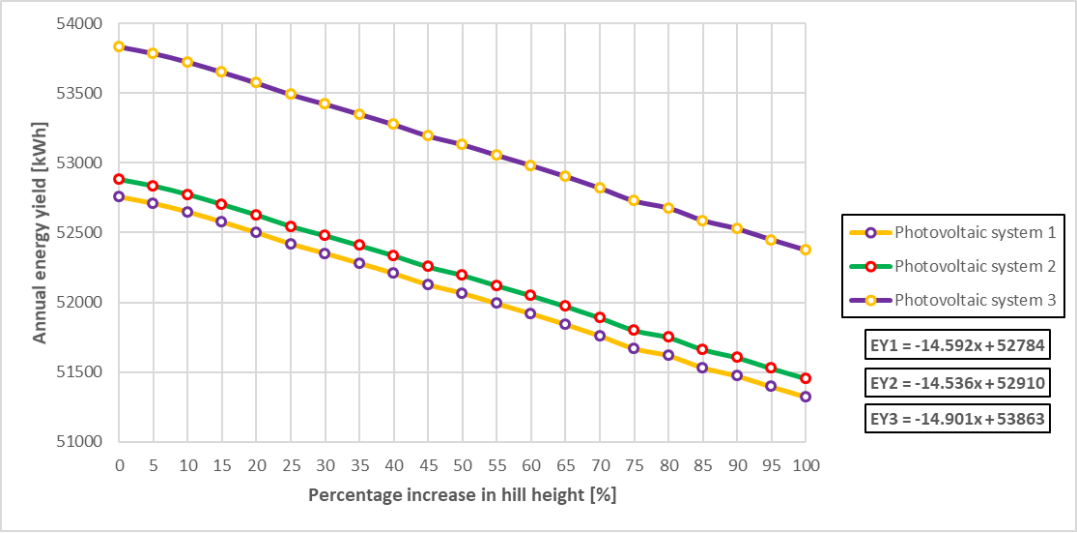

Figure 91: Annual electricity yield for increasing hill height.

There could be several various causes for this surprising result, where the micro-inverters underperforms during shade compared to the other two system solutions. Three possible reasons for this unexpected result are:

1. Poor electrical characteristics of the micro-inverters picked for the milk barn.
2. The form of the nearby obstruction.
3. Polysun may not be able to accurately represent and simulate the effect of partial shading.

When it comes to the electrical characteristics, this theory can be tested by switching out the 50 micro-inverters of the type YC1000-3 with 200 of Polysun's own 300 W micro-inverters, and attach each of the new micro-inverters to one single photovoltaic module. The new function for the third photovoltaic system can be seen in Figure 92.

The new results indicate that the altered third photovoltaic system solution is less affected by increased shading than the other two systems, though not in a considerable amount. Unfortunately, in return for the more favorable function slope, the third system solution generates a lower annual amount of electricity compared to the reference system.

Based solely on these results, the probability that Polysun is not able to accurately portray partial shading is increased. Mainly because the micro-inverters in Figure 91 and Figure 92 react to shade similar to the string-inverters.

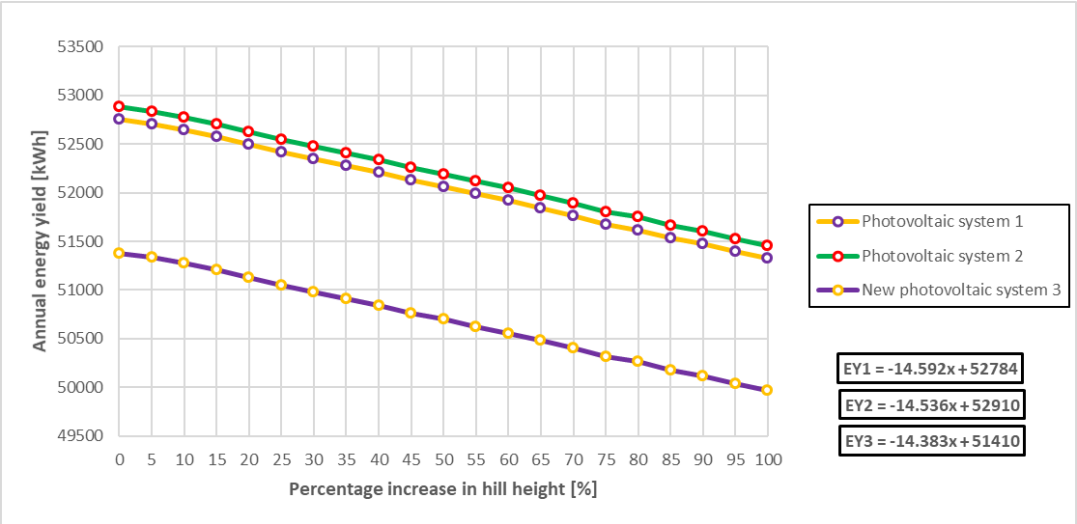

Figure 92: Annual electricity yield for increasing hill height, with an altered photovoltaic system 3.

To accurately study if it is the form of the obstruction that produces these results, the hilltop is changed into two separate towers, as these would result in more extended periods of partial shading. Each tower has a height of 20 m and is located 15 m south of the milk barn. The new obstruction form can be seen in Figure 93.

The new results, when simulating the three photovoltaic system solutions with the new obstruction form, can be seen in Table 66. In addition to the reference third photovoltaic system, the micro-inverters created by Polysun in the altered photovoltaic system are also included in the table.

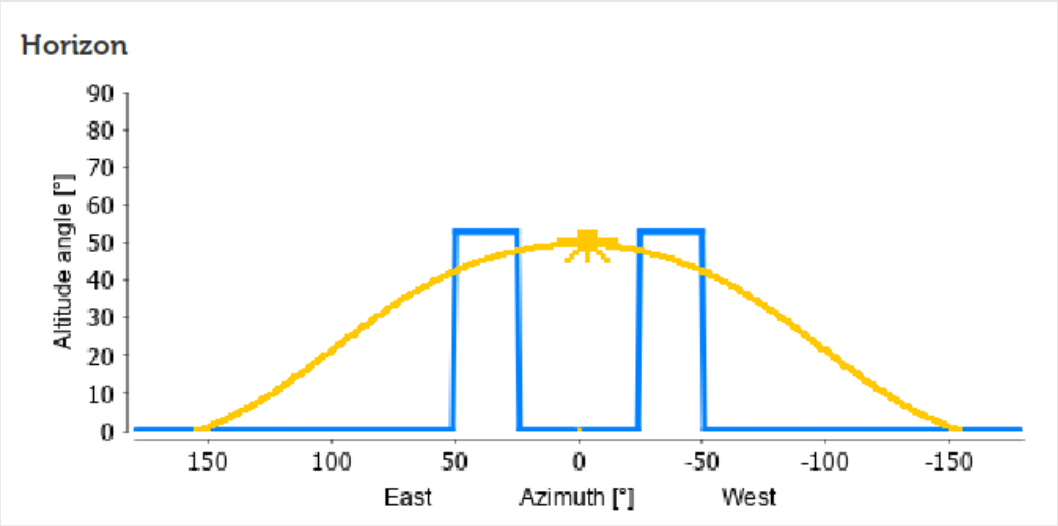

Figure 93: The new obstruction form in the horizon profile.

Table 66: Percentage reduction in electricity generation as a result of the new horizon profile.

	Photovoltaic system 1	Photovoltaic system 2	Photovoltaic system 3	Photovoltaic system with micro-inverters from Polysun
Initial results:	52 752.8 kWh	52 879.7 kWh	53 831.9 kWh	51 379.8 kWh
New results:	41 029.3 kWh	41 231.6 kWh	41 855.4 kWh	39 871.1 kWh
Change:	**- 22.22 %**	**- 22.03 %**	**- 22.25 %**	**- 22.40 %**

The new results in the table above, and the data obtained by changing the height of the hilltop, all strongly suggests that Polysun does not accurately simulate partial shading. As a result, the electricity production of the third system solution could actually be higher than what was observed during the simulations, but it is difficult to determine how much higher.

Polysun's suggested inverter systems

The simulation software Polysun comes with additional features, such as the Polysun *Wizard*. The *Wizard* can assist the system planner when designing a new photovoltaic system, and it is especially helpful if there is little prior knowledge about which type of photovoltaic modules or inverters to use. It will suggest system components that optimize the electricity production of the photovoltaic system.

The goal of this subchapter in the parametric study is to compare the annual AC electricity generation of the three photovoltaic system solutions with a couple of the recommended solutions by Polysun's *Wizard*, to examine if the inverters chosen for the photovoltaic systems in this master thesis have a performance close to what Polysun considers optimal. All previous input parameters regarding losses are kept for this study, and only the inverter and its connection to the photovoltaic modules is altered.

The recommended inverter system solutions and their corresponding annual AC electricity production are all displayed in Table 67. Examining the results in the table, it becomes apparent that the results from the inverter systems designed in this master thesis are very close to what Polysun would recommend, as only one of the recommended solutions from Polysun produce more annual AC electricity than the second inverter system.

Table 67: Comparison between implemented and recommended inverters.

	Inverter 1	Inverter 2	Power ratio	Annual electricity production
Photovoltaic system 1	Delta solar M50A Grid PV Inverter	Sunny Tripower 4.0 PV Inverter	110 % & 111 %	52 752.8 kWh
Photovoltaic system 2	4 x Sunny Tripower 10.0 PV Inverter	-	100 %	52 879.7 kWh
Photovoltaic system 3	50 x APSystems YC1000 3-Phase Micro-inverter	-	103 %	53 831.9 kWh
Suggested solution 1	Inverter 40K	-	83 %	52 878.8 kWh
Suggested solution 2	Inverter 40K	Inverter 4600	93 % & 79 %	52 927.3 kWh
Suggested solution 3	Inverter 40K	Inverter 4000	93 % & 77 %	52 605.3 kWh
Suggested solution 4	Inverter 40K	Inverter 10500T	99 % & 125 %	52 385.6 kWh
Suggested solution 5	Inverter 40K	Inverter 7000T	96 % & 103 %	52 510.3 kWh

Comparison with the boarding house system

The existing photovoltaic system at the boarding house at Mære Agricultural School was introduced in Chapter 5.5.1: *The photovoltaic system on the boarding house*. As the hourly electricity production for this system is thoroughly monitored and charted, it is possible to compare the results from the simulation software with an actual photovoltaic system. The simulation models of the three photovoltaic system solutions are in this subchapter altered to have an inclination angle of 43^{o} instead of 26^{o}, and the hilltop is removed from the model.

Unfortunately, the photovoltaic systems designed for the milk barn consists of 200 photovoltaic modules, and the boarding house system consists of 216 modules, but the total installed power is actually higher for the milk barn as it utilizes 300 W_p photovoltaic modules, while the boarding house system use 270 W_p modules.

In total, the installed peak power is 60 kW_p at the milk barn, and 58.32 kW_p for the boarding house system. Based on the 2.88 % difference in installed power, it should be assumed that the simulated results are about 2.88 % higher than the results for the actual boarding house system. A comparison between the simulated results and the actual results can be seen in Figure 94.

The graph clearly shows that the simulation software overestimates the potential electricity production in the earlier months and last month of the year. At first, it could also be assumed that the simulation model underestimates the electricity production in April, but on further examination, this can possibly be contributed to extraordinary circumstances in 2019, as the electricity production in April 2020 is much lower than the results for 2019. The electricity production from the latter half of 2018 also differs somewhat from the simulated results.

If the monthly average, presented to the right in the figure, is taken as a basis, then the simulation model of the first and second photovoltaic system would have an 11.69 % increase in AC electricity production compared to the boarding house system, while the third system solution would result in a 13.47 % increase in production.

These results should not be considered as any form of evidence that the suggested photovoltaic systems for the milk barn are a better solution for the boarding house than the one already existing, rather it should be viewed as confirmation that there are some factors that the simulation software is not able to implement, and as a result, the actual electricity production at the milk barn should be expected to be lower than what was simulated.

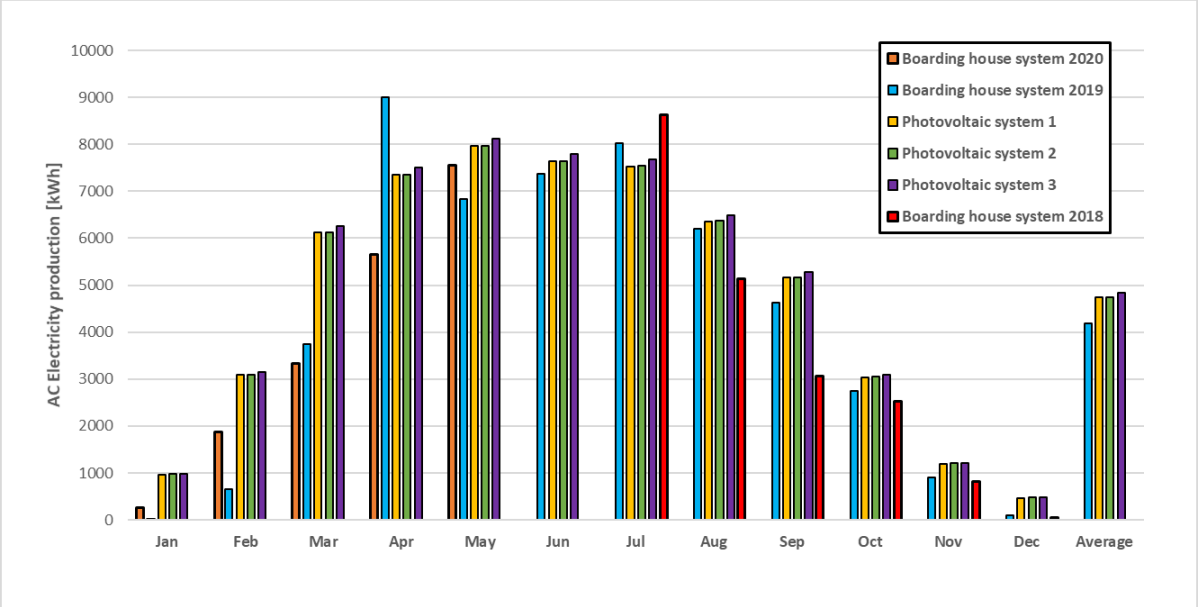

Figure 94: Comparison of simulated electricity production and real production on the boarding house.

11.2 Solar water-heating system

There was a notable and severe problem with the results from the simulated solar water-heating systems introduced in Chapter 9.4: *Implementing the solar water-heating system*. In their current form, they were clearly not more efficient than the existing hot water system at the milk barn. As solar water-heating systems can be very complicated, there may be numerous causes for the poor system performance.

It was mentioned in Chapter 7.4: *Controllers for solar water-heating systems* that faulty controllers could contribute to poor system performances, and this could likely be the case for the solar water-heating systems, as it was not possible to get the various controllers in the simulation model to communicate with each other. This resulted in the heat pump and solar collectors only operating when certain specific conditions were met, independent of the operation of the other component, and it is therefore likely that the two system components affected each other.

Optimally the solar collectors would deliver as much solar energy as possible to preheat the water, and during periods with insufficient solar irradiation, the heat pump would preheat the water instead.

The assumption that the heat pump and solar collectors affect each other can be further examined by studying the temperature evolution in the storage tank, and the ON/OFF cycle of the controllers. For these results, July 1st was chosen as the simulated day, as there is a very high possibility that both the solar collectors and the heat pump would have operated some point during the day.

The supply temperature from and the return temperature to the heat pump for both solar collector types can be seen in Figure 95, while the supply temperature from, and the return temperature to, the solar collectors can be seen in Figure 96.

Both figures also show the time of day when the heat pump and circulation pump 1 is active.

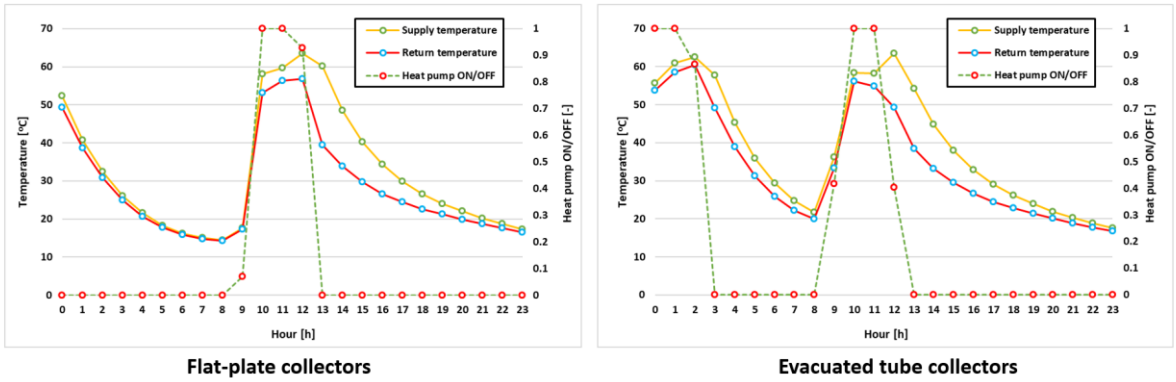

Figure 95: Supply and return temperature from and to the heat pump on July 1st.

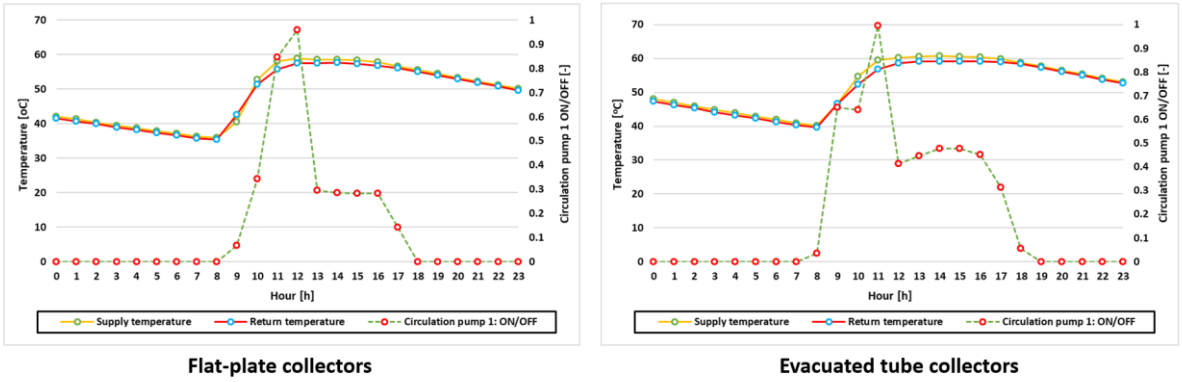

Figure 96: Supply and return temperature from and to the solar collectors on July 1st.

The first noticeable result from the figures above is that the circulation pump 1 is ON for a more extended period of the day compared to the heat pump, but at the same time, the supply and return temperature to and from the solar collector is almost constant, indicating little heat transfer. The heat pump, on the other hand, is operating less during the day, but it is possible to notice a temperature difference between the supply and return temperature.

The possible reason for the low heat transfer between the solar collector and storage tank can be seen in Figure 97, as the figure indicates that the temperature in the 4th layer of the storage tank is pretty consistent throughout the day, resulting in a very little heating need from the solar collectors. Figure 98 shows a similar result for the relationship between the temperature in the 7th layer of the storage tank and the supply temperature from the heat pump.

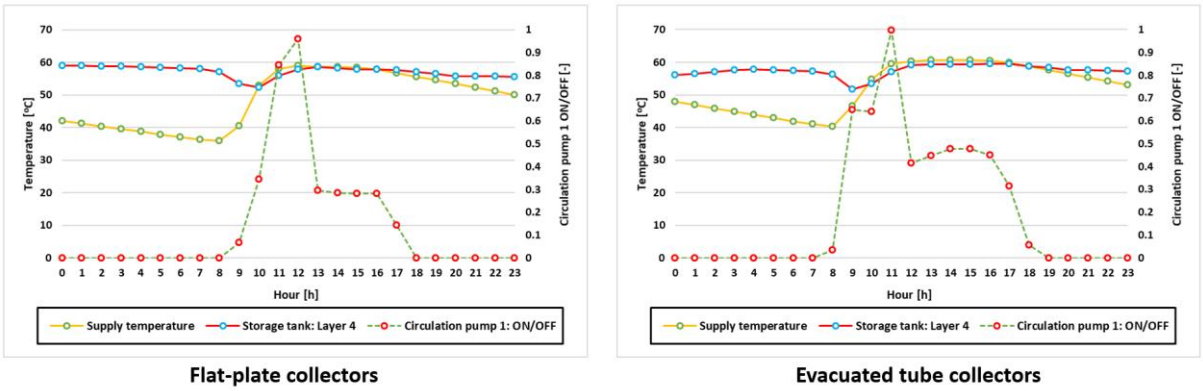

Figure 97: Supply temperature from the solar collectors to the storage tank on July 1st.

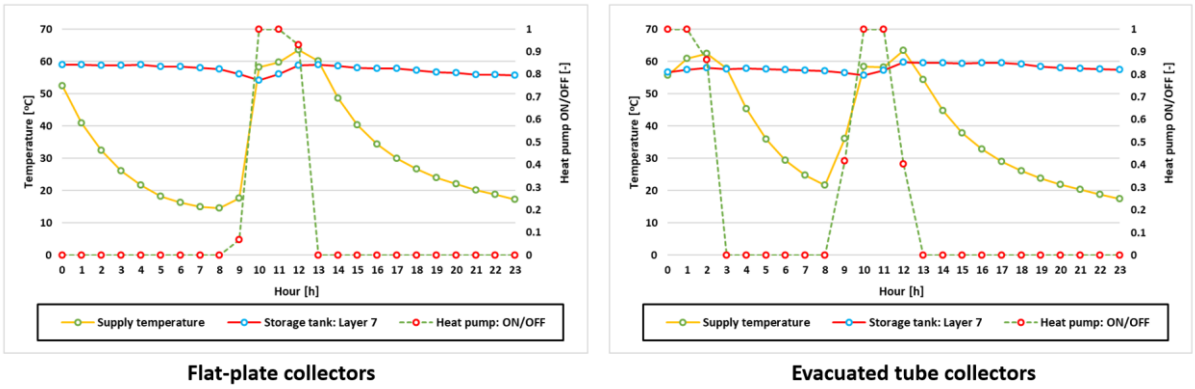

Figure 98: Supply temperature from the heat pump to the storage tank on July 1st.

Unfortunately, as Figure 99 shows, there is not nearly any time during the day where the third circulation pump is not running to some extent. This implies that either the hot water consumption has to increase so that the controller registers more low-temperature water in the water heater, or the controllers in the solar water-heating system must be made to communicate so that the solar collectors have priority when there are sufficient amounts of solar irradiance available.

Of course, none of these factors explains why the total electricity consumption of the solar water-heating systems is higher than in the systems without solar collectors. There are a couple of possible reasons for this higher consumption, all of which will be further tested in the parametric study.

The high total electricity consumption can possibly be due to considerable system inefficiency as a result of:

1. The hot water distribution profile
2. The number of solar collectors
3. The volume of the storage tank
4. The dimensions of the pipelines
5. Disagreement with the heat pump
6. The complexity of the existing hot water system

In addition to the factors mentioned above, the effect that shade has on the solar collectors, as well as the impact the inclination and azimuth angle has on the final results, will also be examined during the following parametric study.

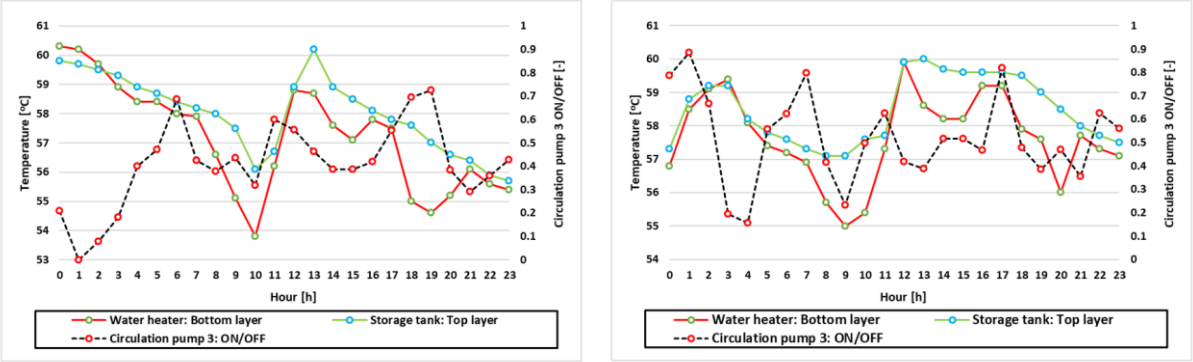

Figure 99: Temperature at the top of the storage tank and bottom of the water heater on July 1st.

11.2.1 Parametric study

Unlike the parametric study of the photovoltaic systems, where the focus was to determine the sensitivity of some of the results, this parametric study is performed to try to remodel the solar water-heating system to be more efficient. The two most prominent indicators for this study is the amount of solar energy supplied to the storage tank, and the annual total electricity consumption of the system. The goal is to reshape the simulation model to be able to provide the necessary thermal energy to cover the hot water consumption, but with as low electricity usage as possible.

The effect of shading

This subchapter is included to see if shading from the neighboring hilltop has any significant influence on the amount of solar energy supplied to the storage tank and if the shading affects the electricity consumption of the solar water-heating system.

Figure 100 and Figure 101 shows the result that increasing the height of the hilltop has on the amount of harvested solar energy and total electricity consumption. What becomes apparent is that the shade has a somewhat limited effect on the amount of solar energy delivered to the storage tank, as Figure 100 implies that the functions are approximately constant for both the flat-plate collectors and the evacuated tube collectors. The electricity consumption presented in Figure 101, on the other hand, shows a little more surprising result, as an increase in shading reduces the total electricity consumption.

This result strengthens the assumption that solar collectors in the existing hot water system will reduce the system performance, and also the assumption that the controllers in the simulation model are not functioning appropriately. This can be concluded based on the fact that as the shading increases, the solar collectors are used less during the year, and therefore the total electricity consumption is expected to increase.

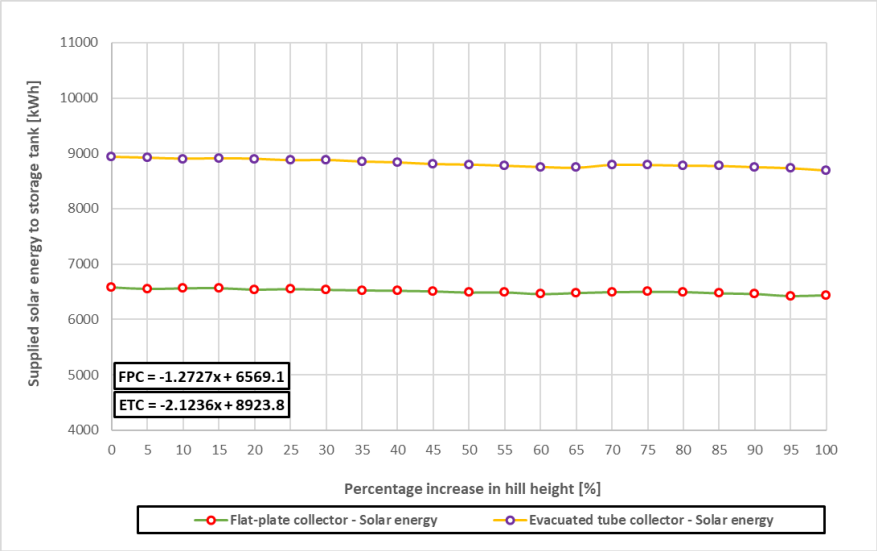

Figure 100: The total amount of solar energy delivered to the storage tank at increasing hill height.

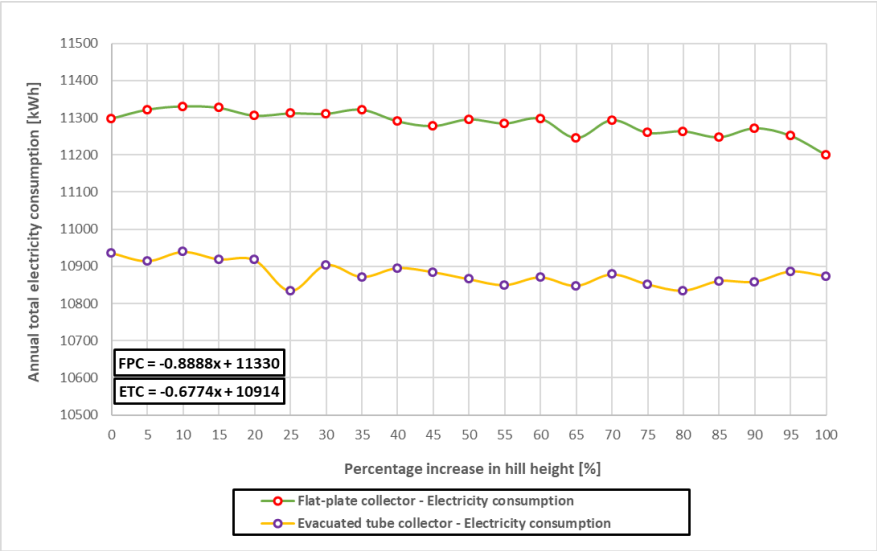

Figure 101: The total amount of annual electricity consumption at increasing hill height.

Effect of hot water distribution profiles

It has previously been assumed that the daily hot water consumption at the milk barn is similar to Polysun's schedule *Daily peaks* (see Figure 78). To be able to examine the impact of this assumption, three other Polysun schedules are introduced to the simulation model, all of which can be seen in Figure 102. Unlike *Daily peaks*, which has three hot water consumption peaks from morning to evening, the *Morning peak* has its highest consumption in the morning from 10:00 to 12:00, while *Evening peaks* have a similar schedule but with the highest peak from 18:00 to 20:00. The last distribution profile *Permanent* has constant hot water consumption during the day.

Table 68 shows the effect the hot water distribution profiles have on the final electricity consumption. The change in the result is relatively small, but out of all the schedules, the distribution profile *Permanent* requires the highest amount of annual electricity, followed by *Daily peaks* and *Morning peak*.

Table 68: Total electricity consumption for different hot water distribution profiles.

	Flat-plate collector system	Evacuated tube collector system	Heat pump and electric heating elements	Electric heating elements
Morning peak	11 252 kWh	10 848 kWh	10 100 kWh	15 462 kWh
Daily peaks	11 297 kWh	10 936 kWh	10 171 kWh	15 634 kWh
Evening peak	11 229 kWh	10 899 kWh	10 086 kWh	15 457 kWh
Permanent	11 368 kWh	10 978 kWh	10 260 kWh	15 717 kWh

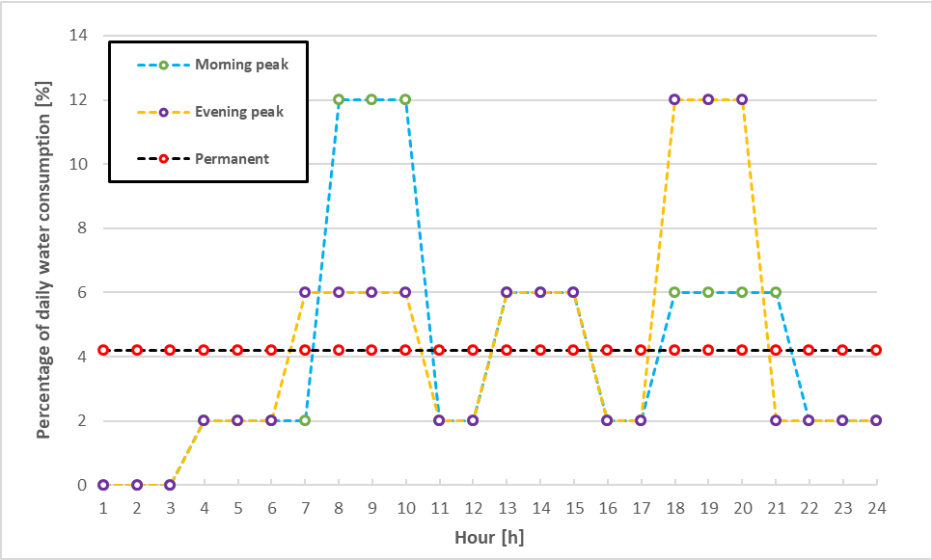

Figure 102: Different hot water consumption profiles implemented.

A possible reason for the total electricity consumption to be lower for the *Evening peak* hot water distribution profile is that both the solar collectors and heat pump have the opportunity to store sufficient amounts of thermal energy during the day, unlike if the majority of consumption was to happen in the morning.

Number of solar collectors

The original need for 14 flat-plate collectors and 17 evacuated tube collectors were determined based on simplified assumptions to obtain an annual solar fraction of 50 %. This was not achieved with the estimated number of solar collectors, as the flat-plate solar water-heating system only reached 25.8 %, while the evacuated tubes delivered an annual solar fraction of 33 %.

The goal of this subchapter in the parametric study is to determine the necessary number of solar collectors that must be implemented to achieve a solar fraction of 50 % in the solar water-heating system. Figure 103 shows the potential increase in solar fraction by adding more solar collectors to the system solution, and the graph also displays the effect that the increasing number of solar collectors have on the total electricity consumption.

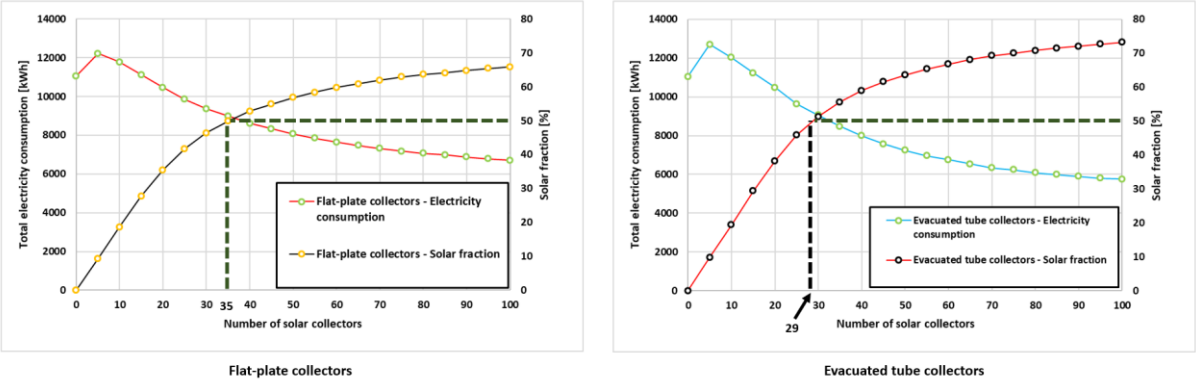

Figure 103: Annual solar fraction and electricity consumption for different number of solar collectors.

According to the graphs above, it requires roughly 35 flat-plate collectors or 29 evacuated tube collectors to achieve an annual solar fraction of 50 % with the solar water-heating system model introduced in Chapter 9.4: *Implementing the solar water-heating system*. This amount of solar collectors are significantly higher than what was required with the calculations from Chapter 7.1.4: *Calculating the required solar collector area*. The likely reason for this notable divergence is that the equations used did not consider hot water system inefficiencies, heat losses and the heat pump.

This indicates that the simplified equations that were introduced in Chapter 7.1.4: *Calculating the required solar collector area*, are not a good approximation for these kinds of large, complicated hot water systems.

Another point that is interesting in Figure 103 is that immediately after introducing solar collectors into the hot water system, the total annual electricity consumption increases, and it is not possible to go below the initial consumption before at least 15 flat-plate collectors or evacuated tube collectors are implemented. This result suggests that the significant source for the inefficiency of the solar water-heating system's performance probably is related to a component or element in the solar circuit, and not necessarily the relationship between the solar collectors and the heat pump.

This hypothesis will be examined further down in this parametric study.

The inclination and azimuth angle

As already stated and previously shown in the case of the photovoltaic systems, both the inclination angle and the azimuth angle affects the total amount of solar energy that it is possible to harvest with solar collectors. Unfortunately for the milk barn at Mære Agricultural School, the solar collectors are recommended to have an inclination angle of 26^{o} and an azimuth angle of 0^{o} to increase the possibility of the solar collectors being accepted by the Norwegian antiquities' organization. Though this is a restriction set on the milk barn, it is not likely that such limitations apply to many other milk farms in Norway.

It could therefore be interesting to study how these limitations affect the potential amount of solar energy it is possible to harvest at the milk barn.

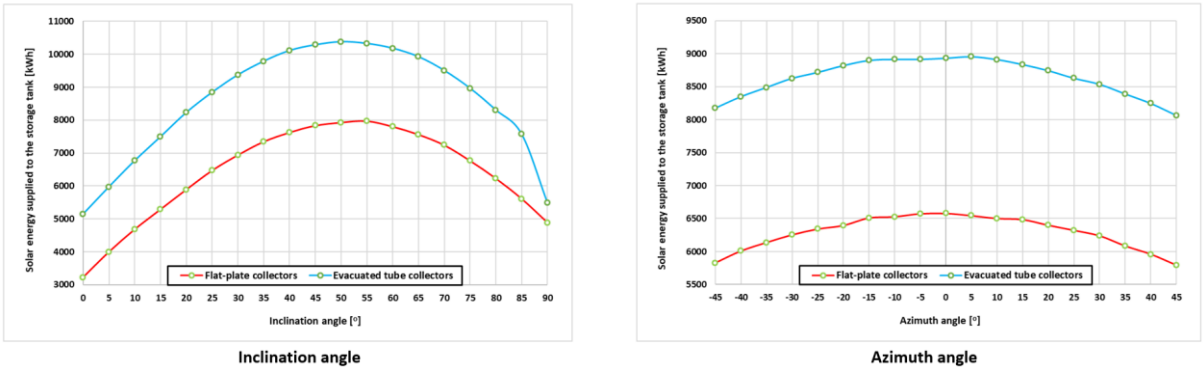

Figure 104: Solar energy delivered to the storage tank at different inclination and azimuth angles.

Figure 104 shows the inclination and azimuths angles effect on the amount of solar energy delivered to the storage. The results presented in the figure correspond well with the literature presented in Chapter 4.1: *Influence of orientation and inclination angle*, as the solar water-heating system is located in the northern hemisphere it is expected that the optimal azimuth angle is 0^{o}.

In addition to the azimuth angle, the figure above also shows that the optimal inclination angle is between 50 to 55^{o}. To determine if this is to be expected, the statement presented in Chapter 7.1.1: *Flat-plate collector* should be remembered, as it was mentioned in the chapter that the optimal inclination angle usually was equal to the latitude of the system location with rough variations up to 10 or 15^{o}. According to Google Maps, Mære Agricultural School is located at a latitude of 63.93^{o}, meaning that the results are within the expected range.

Out of the two angles, the figure clearly indicates that the solar energy generation is most sensitive to the inclination angle, which in a worst-case scenario can reduce the amount of solar energy delivered to the storage tank with roughly 60 %. The figure also shows that by forcing the solar water-heating system at the milk barn to have an inclination angle of 26°, the total amount of solar energy supplied to the storage tank is 17.5 % lower than the optimal production.

As it previously has been surprising results regarding the total electricity consumption, this is mapped out for the same inclination and azimuths angle as the figure above and can be seen in Figure 105.

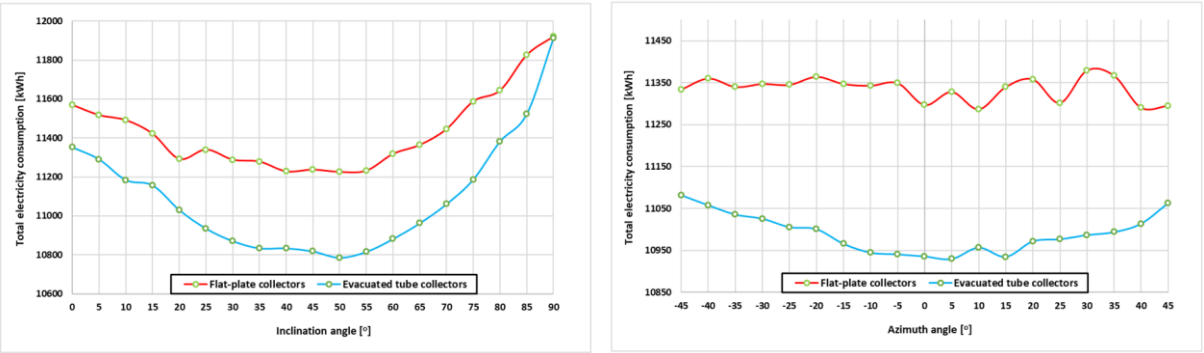

Figure 105: Total electricity consumption at different inclination and azimuth angles.

The graph in Figure 105 for the inclination angle shows a similar slope to the one presented in Figure 104, but where the amount of harvested solar energy increased from about 3 100 to 8 000 kWh when the inclination angle for the flat-plate collectors is increased from 0 to 55°, the total electricity consumption is only reduced from 11 580 to 11 220 kWh. In addition to the low reduction in total electricity consumption, the graphs also clearly contradict each other at some points. This can be seen Figure 104, where the results indicate that there is more potential for solar energy harvesting at steep solar collector angles, but Figure 105 suggests that these steep angles lead to higher electricity consumption compared to almost having a horizontal inclination angle.

Due to the complexity of the solar water-heating system, it's hard to pinpoint the exact reason for the unusual results. But, it has previously been shown in this parametric study that the total electricity consumption for the simulated models increases in varying degrees with the increased utilization of solar collectors.

Changing storage tank size

It was previously mentioned in Chapter 7.2.5: *Sizing the required storage tank for the milk barn*, that the possible size of the storage tank varies considerably with the assumptions, and that the optimal storage size should be determined with simulation software. The goal of this subchapter in the parametric study is to determine the effect that the volume of the storage tank has on the amount of solar energy supplied to the tank and also on the total electricity consumption. For the simulations, the 16-kW internal heating element in the storage tank is kept, independent on the volume of the tank, and it is also assumed that the unit will have a fixed height of 2 m.

Figure 106 and Figure 107 shows the effect that an increasing tank volume has on the amount of solar energy delivered to the storage tank for the flat-plate and the evacuated tube collector system, respectively.

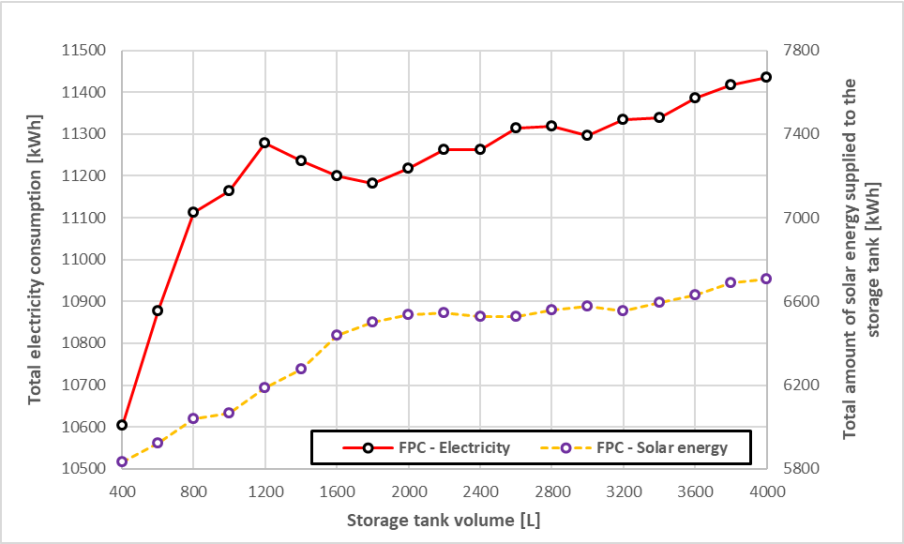

Figure 106: Total electricity consumption and amount of solar energy delivered to the storage tank from flat-plate collectors.

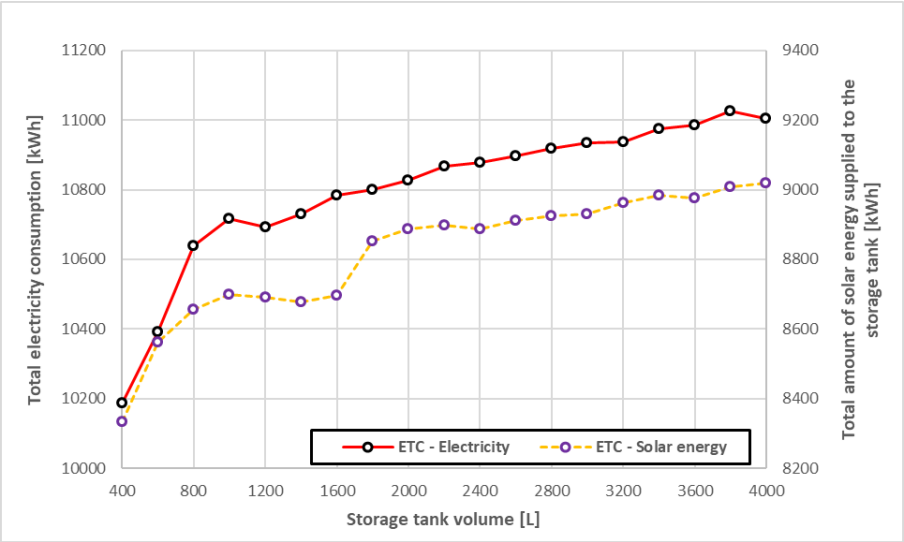

Figure 107: Total electricity consumption and amount of solar energy delivered to the storage tank from evacuated tube collectors.

Both figures indicate that the amount of solar energy delivered to the storage tank increases significantly when switching from a 400-liter storage tank to a 2 000-liters, but they also indicate that the curve of the total electricity consumption flattens at more substantial tank volumes. The same is also the case for the amount of solar energy supplied to the storage tank. The increased amount of solar energy supplied to the storage tank is likely due to the increasing capacity of the unit, and the growing need for auxiliary heating is probably due to the increased quantity of water that requires thermal energy when there are inadequate solar conditions.

The results in this subchapter suggests that a smaller storage tank could be used to reduce the total electricity consumption and still deliver a sufficient amount of hot water to the consumer.

Changing the pipe dimensions

In Chapter 9.4.2: *Implementing the system components*, it was assumed that the pipes in the solar circuit were made of steel and had an internal diameter of 155.4 mm and an external diameter of 165.1 mm, to ensure sufficient heat transfer to the storage tank. In this subchapter, the effect of such an assumption is examined. In this study, the pipes going to and from the solar collectors are switched with other preexisting pipes in the simulation software. These pipes may vary in diameters and material, and therefore thermal conductivity.

The original lengths estimated for the pipelines in Chapter 9.4.2: *Implementing the system components* are kept constant.

The results for the flat-plate and evacuated tube collectors can be seen in Figure 108 and Figure 109, respectively, where both figures show the amount of solar energy supplied to the storage tank, as well as the total electricity consumption, for a variety of Polysun's own created pipes.

Based on the result presented in both of the figures, it becomes clear that the assumption to choose a larger pipe dimension in the solar circuit has led to an increase in the amount of solar energy supplied to the storage tank, but the results also suggests that by choosing a too large pipe size, the total electricity consumption increased significantly, reducing the system performance.

According to the results in Figure 110, which displays various solar fractions for the two solar water-heating systems with different pipes, the solar fraction is actually higher with smaller pipes, even though more solar energy is delivered with a broader diameter. This indicates that a large pipe size leads to a significant heat loss that also reduces the potential efficiency of the two solar water-heating systems.

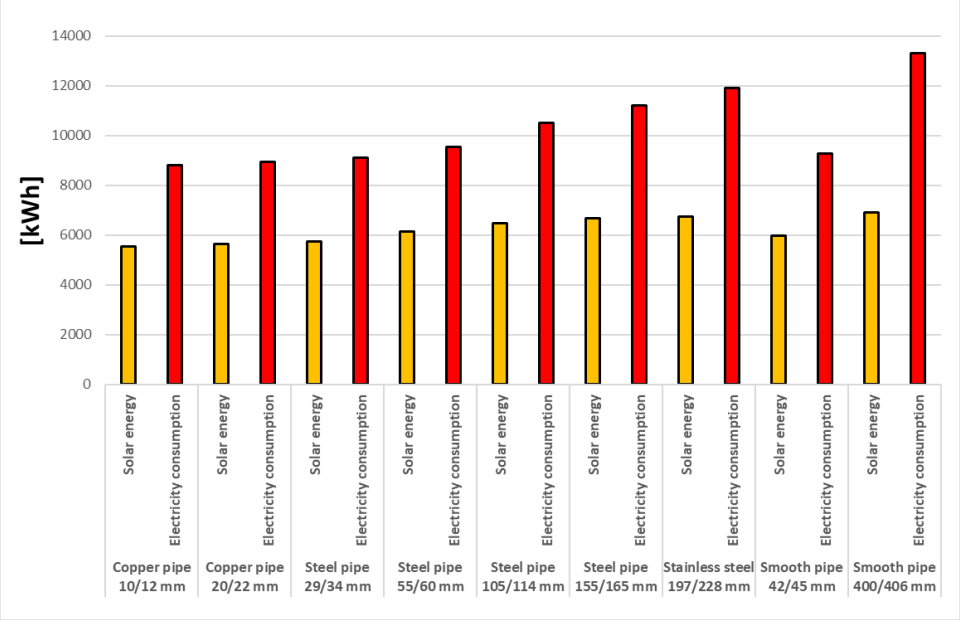

Figure 108: Solar energy supplied to the storage tank and electricity usage with varying type of pipes, for the flat-plate collectors.

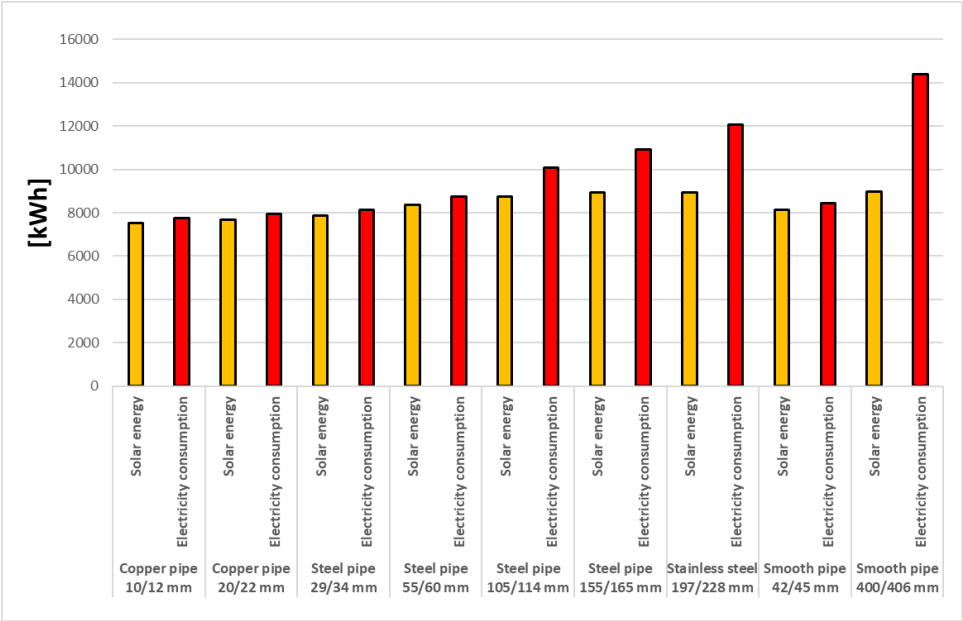

Figure 109: Solar energy supplied to the storage tank and electricity usage with varying type of pipes, for the evacuated tube collectors.

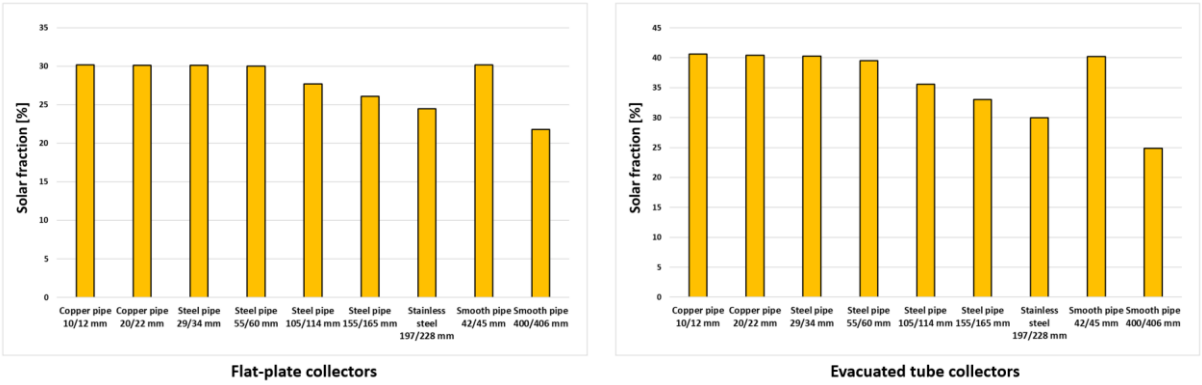

Figure 110: Solar fraction with different type of pipes.

Since the assumptions concerning the pipes influenced the final result in such a significant way, a similar study is performed in this subchapter to examine the effect the remaining pipelines in the hot water system have on the final results. It should be noted that the original steel pipes for the solar circuit are kept and that all the other pipelines in the solar water-heating system are altered.

The most important indicators for this study is the amount of solar energy supplied to the storage tank, solar fraction and total electricity consumption.

Table 69 and Table 70 shows the results for the flat-plate and evacuated tube collector systems, respectively.

Table 69: Total electricity consumption and solar energy to the FPC system, for different pipe types.

	Copper pipe 10/12 mm	Copper pipe 20/22 mm	Steel pipe 55/60 mm	Steel pipe 155/165 mm	Stainless steel 197/228 mm	Smooth pipe 400/406 mm
Total electricity consumption	11 054 kWh	11 221 kWh	11 852 kWh	13 643 kWh	14 696 kWh	18 264 kWh
Solar energy to the system	6 630 kWh	6 669 kWh	6 662 kWh	6 835 kWh	6 899 kWh	6 855 kWh
Solar fraction	26.5 %	26.1 %	24.5 %	21.4 %	20.0 %	15.9 %

Table 70: Total electricity consumption and solar energy to the ETC system, for different pipe types.

	Copper pipe 10/12 mm	Copper pipe 20/22 mm	Steel pipe 55/60 mm	Steel pipe 155/165 mm	Stainless steel 197/228 mm	Smooth pipe 400/406 mm
Total electricity consumption	10 943 kWh	11 047 kWh	11 627 kWh	13 418 kWh	14 514 kWh	18 054 kWh
Solar energy to the system	8 904 kWh	8 894 kWh	8 921 kWh	9 001 kWh	9 036 kWh	9 054 kWh
Solar fraction	33.2 %	32.8 %	31.3 %	27.1 %	25.2 %	20.3 %

The results are similar to the ones obtained by changing the pipes in the solar circuit. Also here, the smaller pipe diameters provide less solar energy to the solar water-heating system, but at the same time, it notably reduces the total electricity consumption. Similar to before, the increase in utilized solar energy is significantly smaller than the increase in total electricity consumption, indicating that the smaller pipes provide a better system performance.

Based on all the results in this subchapter, the best option could be to have pipes with as low diameters as possible, as long as they are still able to cover the space-heating need and the hot water consumption. The results also suggests that the main problem with the original solar water-heating systems introduced in Chapter 9.4: *Implementing the solar water-heating system* was not the relationship between the heat pump and the solar collectors, but rather the implemented pipe diameters in the solar circuit at the time. This new hypothesis will be tested in the subchapter below.

It should also be noted that even after reducing the pipe dimensions in the solar circuit, the system was still not able to achieve a solar fraction of 50 %, indicating that there are still some obstacles with the simulation models.

Removing the heat pump

It was theorized at the end of Chapter 10.2: *The solar water-heating system at the milk barn* that the heat pump and the solar collectors counteracted each other to some extent. This theory has been somewhat weakened during the previous subchapters of the parametric study, but this does not imply that the heat pump is not, in some degree, capable of reducing the general performance of the solar collectors. Its effect is just much lower than what was first anticipated.

This theory is further tested in this subchapter, where the heat pump is removed from the original implemented solar water-heating systems. The results from the new simulation models, concerning the amount of solar energy provided to the storage tank, solar fraction, system performance, total amount of thermal energy supplied to the storage unit and total electricity consumption, are all presented in Table 71.

Table 71: Simulated results for the simulation models without the heat pump.

	Solar energy delivered to the storage tank	Total amount of thermal energy supplied to the storage tank	Solar fraction	System performance	Total electricity consumption
Flat-plate collectors	8 006 kWh	23 808 kWh	33.6 %	0.76	16 675 kWh
Evacuated tube collectors	9 960 kWh	25 019 kWh	39.8 %	0.80	15 896 kWh

What immediately becomes apparent with the new results is that the total electricity consumption for these simulation models is higher than the total electricity consumption obtained for the simulation model, where only the electrical heating elements were utilized (see Chapter 10.2: *The solar water-heating system at the milk barn*). This finally confirms that the heat pump is not the main issue, but rather the pipe diameters of the solar circuit. This can quickly be tested by studying what would happen to the final results if the pipe diameters were reduced for these simulation models.

In the altered simulation models, the pipes were changed to Polysun's copper pipe 20/22 mm, and the result of reducing the pipe diameters can be seen in Table 72. The heat pump is still excluded in these simulation models.

Table 72: Simulated results when removing the heat pump and replacing the solar circuit pipes.

	Solar energy delivered to the storage tank	Total amount of thermal energy supplied to the storage tank	Solar fraction	System performance	Total electricity consumption
Flat-plate collectors	6 377 kWh	17 427 kWh	36.6 %	1.08	11 671 kWh
Evacuated tube collectors	8 105 kWh	17 854 kWh	45.5 %	1.22	10 305 kWh

The simulation results have improved significantly after replacing the pipes, although when comparing these new results with the results from the original simulation model without solar collectors (see Chapter 10.2: *The solar water-heating system at the milk barn*), the electricity consumption is still higher than for the simulated existing hot water system which only utilized the heat pump and the electric heating element.

In the table it is also possible to observe that by removing the heat pump and reducing the pipe diameter, the solar fraction is beginning to reach 50 %, at least for the evacuated tube collectors.

Altering the setup of the existing hot water system

As shown in the previous subchapter, even with the 20/22 mm copper pipes in the solar circuit in the solar water-heating system, both with and without the heat pump, the total electricity consumption does still not go below the results for the simulation model of the existing hot water system. This could perhaps be solved by choosing an even smaller pipe diameter, but another plausible method to reduce the consumption could be to alter the existing layout of the hot water system.

The purpose of this subchapter is to study the effect a merging of the storage tank with the water heater into one single unit would have on the solar fraction and total electricity consumption. This would of course imply that the floor heating system would have to become a closed-loop system, to avoid having the drinking water run through the floor-heating system before being consumed. A schematic of the altered solar water-heating system is presented in Figure 111.

To be able to study the potential effect that this new system solution has on the results, it will be tested for a total of six different alterations. These alteration cases are:

1. Flat-plate collectors with a heat pump and a 16-kW electric heating element inside the storage tank.

2. Evacuated tube collectors with a heat pump and a 16-kW electric heating element inside the storage tank.
3. Flat-plate collectors with a 16-kW electric heating element inside the storage tank.
4. Evacuated tube collectors with a 16-kW electric heating element inside the storage tank.
5. Heat pump and a 16-kW electric heating element inside the storage tank.
6. Only a 16-kW electric heating element inside the storage tank.

All of these new system layouts would require an updated controller system and in some cases a new storage tank. For all design alterations, the controller system to the solar circuit and its placement of the temperature sensors is left unaltered. The only change done to the heat pump controller is that the cut-off temperature is increased from 60 to 70 ^{o}C. The lower temperature sensor connected to the controller of the electric heating element inside the storage tank is moved from the 6th layer to the 9th layer, and the cut-in and cut-off temperature difference are switched from 45 and 47 ^{o}C to 75 and 77 ^{o}C, respectively.

For Case 6, the temperature sensor for the electric heater is moved down from the 9th layer of the storage tank to the 5th layer. This is to ensure sufficient hot water for the floor heating system and tap water.

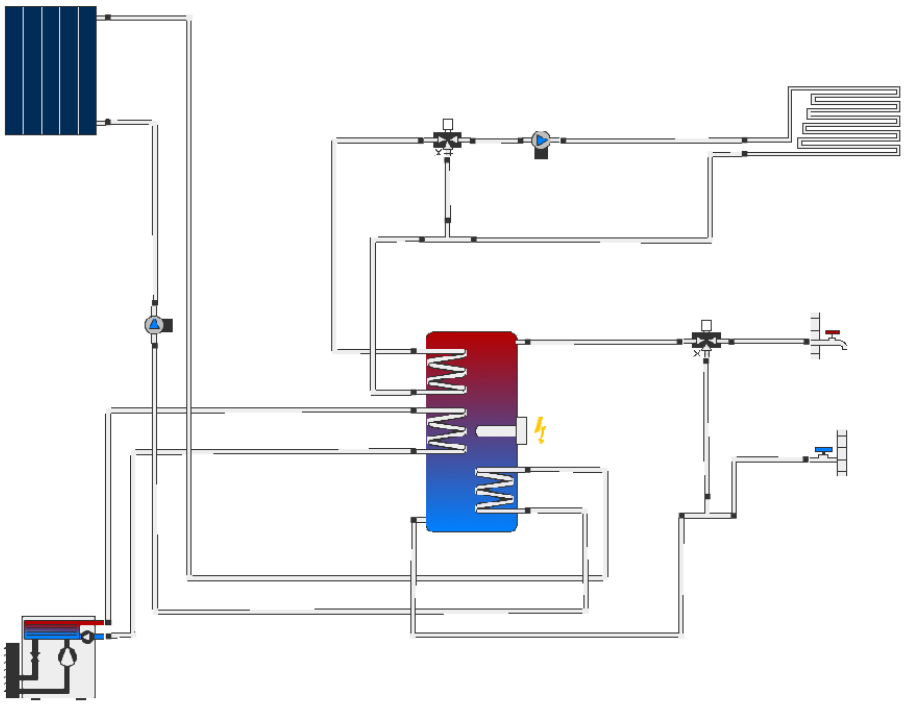

Figure 111: Alternative solar water-heating system.

For Case 1 to 4, the storage tank is the same 3000-liter tank introduced in Chapter 9.4: *Implementing the solar water-heating system*, while for Case 5 & 6, the storage unit is replaced with a similar tank but with a volume of 550 liters, which is the combined volume of the real storage tank and water heater.

The new system performances and total electricity consumptions of all the new system layouts can be seen in Figure 112. In the figure, FPC stands for Flat-Plate Collector, ETC stands for Evacuated Tube Collector, HP stands for heat pump, and EL references the 16-kW electric heating element.

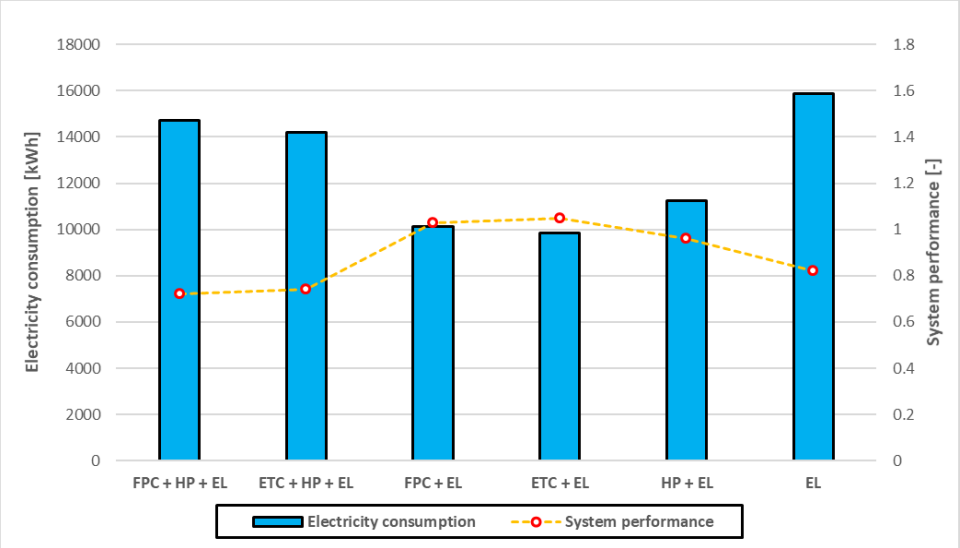

Figure 112: System performance and electricity consumption for the altered hot water systems.

The results presented in Figure 112 for the electricity consumption for the new system layouts are more agreeable with the original assumption that without the heat pump, the solar water-heating system is a more efficient solution, than simply combining both the heat pump and solar collectors in the same hot water system. Also, the system performance is highest for the solar water-heating systems without the heat pump.

The solar fractions for the new solar water-heating systems can be seen in Figure 113, which reveals that had the existing hot water system had a similar layout to the one introduced in this subchapter, then the solar fractions for the solar water-heating systems without the heat pump would be above 50 %.

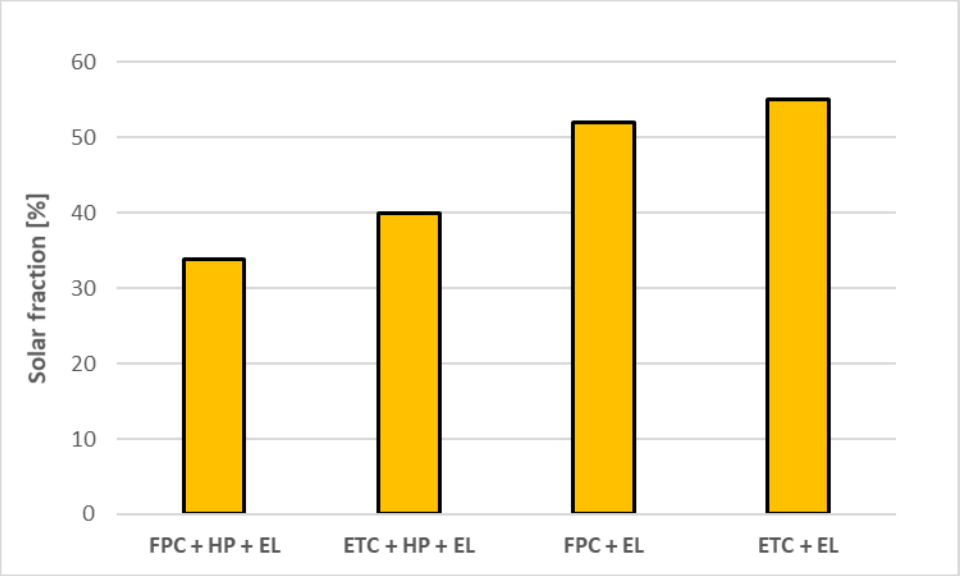

Figure 113: Annual solar fractions for the simplified systems.

As already mentioned, the results from these new system layouts more closely resemble what was initially expected from the simulation model introduced in Chapter 9.4: *Implementing the solar water-heating system*, and the model also suggest that it is more inefficient to have both the solar collectors and the heat pump in the hot water system, rather than only having one of them.

11.2.2 Attempt at optimizing the solar water-heating system models

Some of the parameters studied during the parametric study have a larger impact on the results than others. Of these input parameters, arguably the three input assumptions that affected the outcome the most were the inclination angle, type of solar circuit pipes and the merging of the storage tank and water heater into one single unit.

Unfortunately, as there are certain limitations with the inclination angle, due to the aesthetic requirements of the milk barn, it will not be changed for the solar collectors but rather still be kept at 26^{o}. In addition to the inclination angle, it is assumed that we can only replace the pipes in the solar circuit, as the remaining pipelines in the solar water-heating system should be similar to the ones in the original simulation model for the existing hot water system.

Based on the results from the parametric study and the assumptions above, the two most prominent parameters that are going to be changed for optimizing the initial solar water-heating systems are the system layout and the pipes in the solar circuit.

In the end, the final results from this subchapter will be compared with the results from the original existing hot water system, referred to as *No solar collector* in Chapter 10.2: *The solar water-heating system at the milk barn*. This is done because it is assumed that the model is somewhat similar to the existing hot water system at the milk barn, and therefore simulates a total electricity consumption close the real electricity consumption.

As a summarization, the most relevant results from the initial *No solar collector* model are shown in Table 73.

Table 73: Results for the existing hot water system in the milk barn.

	Heat supplied to the system	Total electricity consumption
No solar collectors	16 287 kWh	10 171 kWh

By using the altered solar water-heating system schematic presented in Figure 111 as a basis, the pipes in the solar circuit are changed from the steel 155/165 mm pipes to the copper 20/22 mm pipes, while at the same time, the control system is kept the same as presented in the previous subchapter for all of the system alterations.

Figure 114 shows the resulting electricity consumptions and solar fractions when both the pipes and the system layout have been changed.

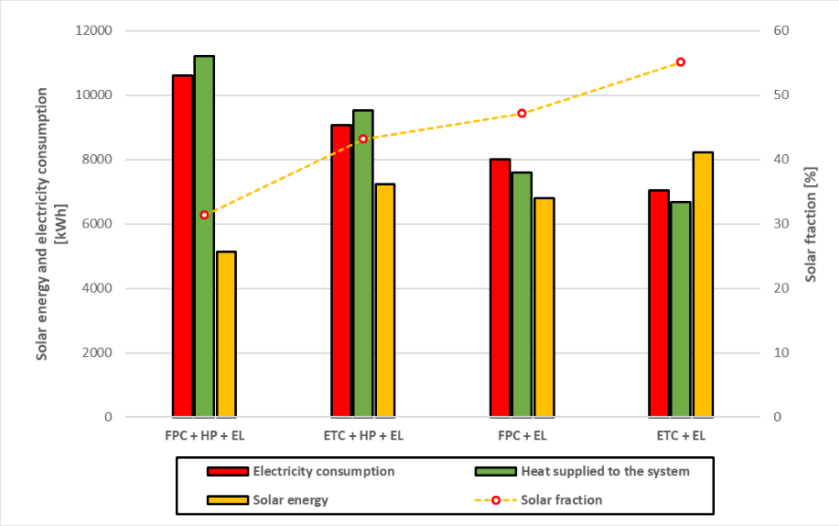

Figure 114: Altered system layout and different pipes in the solar circuit.

To avoid having to write long and hard-to-read sentences each time one of the system solutions in the figure above is referenced, they will from this point on be referred to as:

- *System solution 1*: FPC + HP + EL
- *System solution 2*: ETC + HP + EL
- *System solution 3*: FPC + EL
- *System solution 4*: ETC + EL

By comparing the new results with the results for the existing hot water system presented in Table 73, it becomes apparent that by replacing the current hot water system with system solution 2, the annual electricity consumption would probably be reduced by 1 113 kWh. Unfortunately, system solution 1 has a higher electricity consumption than the existing hot water system, indicating that this system should not be adopted.

Out of the system solutions presented in Figure 114, it is the 3rd and 4th that has the highest potential for reducing the total electricity consumption, as they could potentially save 2 170 kWh or 3 123 kWh annually, depending on which of the solutions that are employed.

It should be noted that some of the models with the initial system layout, when the copper pipes were used, would result in a lower total electricity consumption than the *No solar collector* model, but not in a significant way. These results therefore suggest that to be able to achieve an efficient solar water-heating system, it may be necessary to not only remove the heat pump from the system, but also change the existing hot water system layout altogether, though this should be studied further.

Since this is merely a feasibility study on the potential for solar harvesting with a solar water-heating system at the milk barn, the financial sides of system solutions have not been mapped out. As such, it is difficult to say if the alteration of the existing hot water system, or even investing in a solar water-heating system, would be an economically sound decision. Based on the electricity cost at the milk barn in 2019 (see Table 13), the annual cost saving would be about 928.2, 1 809.8 and 2 604.6 NOK for system solution 2, 3 and 4, respectively.

Lastly, it should be mentioned that both system solution 3 and 4 are able to either achieve an annual solar fraction of roughly 50 % or that they at least are very close it.

Greenhouse gas emission reduction

With the reduction in electricity consumption obtained for the solar water-heating systems in the previous section, it is now possible to estimate the potential reduction in greenhouse gas emissions. The same three emission factors introduced in Chapter 8.3: *Generalizing the results* are again used in this subchapter, but in addition to these factors, the new circumstance introduced in Chapter 11.1.3: *Potential reduction in greenhouse gas emissions* for the photovoltaic systems will also be used. For this new emission factor, only 19 % of all electricity consumed in Norway has a Norwegian origin, while the remaining 81 % is imported from other locations in Europe, resulting in an emission factor of 243.19 g CO_2 equivalents per kWh. This emission factor will now be referred to as the *NOR-EU* mix.

Table 74 shows the potential reduction in greenhouse gas emissions if one of the solar water-heating systems that have lower electricity consumption than the existing hot water system is adopted.

Table 74: Potential reduction in greenhouse gas emissions at the milk barn by adopting a solar water-heating system.

	System solution 2	System solution 3	System solution 4
Amount of electricity consumption replaced with renewable energy [kWh]	1 113	2 170	3 123
Low emissions [kg of CO_2 equivalents]	21.0	41.0	59.0
Moderate emissions [kg of CO_2 equivalents]	44.7	87.2	125.5
Substantial emissions [kg of CO_2 equivalents]	68.4	133.5	192.1
NOR-EU emissions [kg of CO_2 equivalents]	270.7	527.7	759.5

Table 75 displays the potential reduction in total electricity consumption in Trøndelag if a varying number of milk farms located in Trøndelag adopt system solution 4. Similar studies have been performed for Trøndelag if the 2nd or 3rd system solution is utilized, but these studies can be seen in Table 81 and Table 82 in Attachment A.16.

Table 75: Reduction in greenhouse gas emissions in Trøndelag with solar water-heating system 4.

Percentage of milk farms in Trøndelag with system solution 4	10 %	20 %	30 %	40 %	50 %
Amount of electricity consumption replaced with renewable energy [kWh]	468 450	936 900	1 405 350	1 873 800	2 342 250
Low emissions [Tons of CO_2 equivalents]	8.85	17.71	26.56	35.41	44.27
Moderate emissions [Tons of CO_2 equivalents]	18.83	37.66	56.50	75.33	94.16
Substantial emissions [Tons of CO_2 equivalents]	28.81	57.62	86.43	115.24	144.05
NOR-EU emissions [Tons of CO_2 equivalents]	113.92	227.84	341.77	455.69	569.61

Percentage of milk farms in Trøndelag with system solution 4	60 %	70 %	80 %	90 %	100 %
Amount of electricity consumption replaced with renewable energy [kWh]	2 810 700	3 279 150	3 747 600	4 216 050	4 684 500
Low emissions [Tons of CO_2 equivalents]	53.12	61.98	70.83	79.68	88.54
Moderate emissions [Tons of CO_2 equivalents]	112.99	131.82	150.65	169.49	188.32
Substantial emissions [Tons of CO_2 equivalents]	172.86	201.67	230.48	259.29	288.10
NOR-EU emissions [Tons of CO_2 equivalents]	683.53	797.45	911.38	1 025.30	1 139.22

The same method as above can be used to determine the potential reduction in greenhouse gas emissions for all 7 600 milk farms in Norway if they should choose to adopt one of the solar water-heating solutions, and if they already have a heat pump. Similar to the results above, Table 76 shows the potential reduction if the 4th system solution is implemented, while Table 83 and Table 84 in Attachment A.16 shows the results for the two other system solutions.

The results from the table above and below, as well as the ones presented in Attachment A.16, all indicate that even though the solar water-heating systems do not have the same potential for reduction in greenhouse gas emissions as the photovoltaic systems, they still reduce a reasonable amount.

Supposing that probably only some of the milk farms in Norwegian agriculture have already adopted heat pumps into their systems, it could be possible that the potential reduction would be higher for the majority of the milk farms. By comparing the results in Figure 87 for the simulation model with only internal electric heaters, with the results presented in Figure 114, it becomes apparent that the total electricity consumption could be reduced by 5 018, 6 577, 7 634 or 8 587 kWh, depending on if the implemented system is either system solution 1, 2, 3 or 4, respectively, and if no heat pump has already been installed.

These new results would of course lead to a more prominent decrease in greenhouse gas emissions, as can be seen in Table 77.

Table 76: Reduction in greenhouse gas emissions in Norway with solar water-heating system 4.

Percentage of milk farms in Norway with system solution 4	10 %	20 %	30 %	40 %	50 %
Amount of electricity consumption replaced with renewable energy [kWh]	2 373 480	4 746 960	7 120 440	9 493920	11 867 400
Low emissions [Tons of CO_2 equivalents]	44.86	89.72	134.58	179.44	224.29
Moderate emissions [Tons of CO_2 equivalents]	95.41	190.83	286.24	381.66	477.07
Substantial emissions [Tons of CO_2 equivalents]	145.97	291.94	437.91	583.88	729.85
NOR-EU emissions [Tons of CO_2 equivalents]	577.20	1 154.41	1 731.61	2 308.82	2 886.02

Percentage of milk farms in Norway with system solution 4	60 %	70 %	80 %	90 %	100 %
Amount of electricity consumption replaced with renewable energy [kWh]	14 240 880	16 614 360	18 987 840	21 361 320	23 734 800
Low emissions [Tons of CO_2 equivalents]	269.15	314.01	358.87	403.73	448.59
Moderate emissions [Tons of CO_2 equivalents]	572.48	667.90	763.11	858.73	954.14
Substantial emissions [Tons of CO_2 equivalents]	875.81	1 021.78	1167.75	1 313.72	1 459.69
NOR-EU emissions [Tons of CO_2 equivalents]	3 463.23	4 040.43	4 617.63	5 194.84	5 772.04

Table 77: Potential reduction in greenhouse gas emissions at the milk farms in Norway by adopting a solar water-heating system solution (without existing heat pumps).

	System solution 1	System solution 2	System solution 3	System solution 4
Amount of electricity consumption replaced with renewable energy [kWh]	5 018	6 577	7 634	8 587
Low emissions [kg of CO_2 equivalents]	94.84	124.31	144.28	162.29
Moderate emissions [kg of CO_2 equivalents]	201.72	264.40	306.87	345.20
Substantial emissions [kg of CO_2 equivalents]	308.61	404.49	469.49	528.10
NOR-EU emissions [kg of CO_2 equivalents]	1 220.32	1 599.45	1 856.50	2 088.26

General comments

As initially mentioned in Chapter 11.1.3 *Potential reduction in greenhouse gas emissions*, the potential for reduction in greenhouse gas emissions are not a fixed value, but rather depends on the greenhouse gas emissions linked to the electricity that would be used to cover the demand if no renewable energy were to be utilized. As several electricity producers incorporate more renewable energy sources or "cleaner" sources into their electricity mixture, the potential would be reduced.

All this suggests that even though the system solutions may have a high potential for greenhouse gas emission reduction right now, it will probably not always remain so. Also, by comparing the results from Table 74 and Table 77, it comes as no surprise that the highest potential for reduction in greenhouse gas emissions is when the solar water-heating systems are incorporated into existing hot water systems without already implemented heat pumps.

One last comparison between the initial simulation models introduced in Chapter 9.4: *Implementing the solar water-heating system*, also with the initial model without the heat pump, and the altered solar water-heating system solutions 1 to 4 is presented in Figure 115. The figure shows the total electricity consumption of each simulation model, as well as the solar fraction. Figure 116 shows a similar comparison, but in this figure, the solar circuit pipes in the initial models presented in Chapter 9.4:*Implementing the solar water-heating system* are altered to copper 20/22 mm pipes.

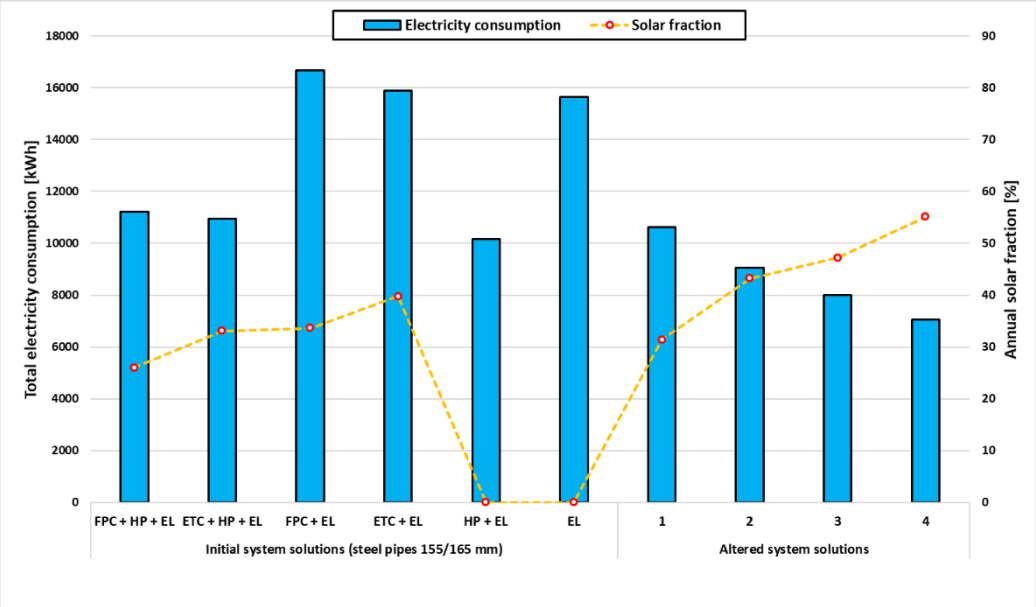

Figure 115: Comparison between the electricity consumption and solar fraction of all simulation models.

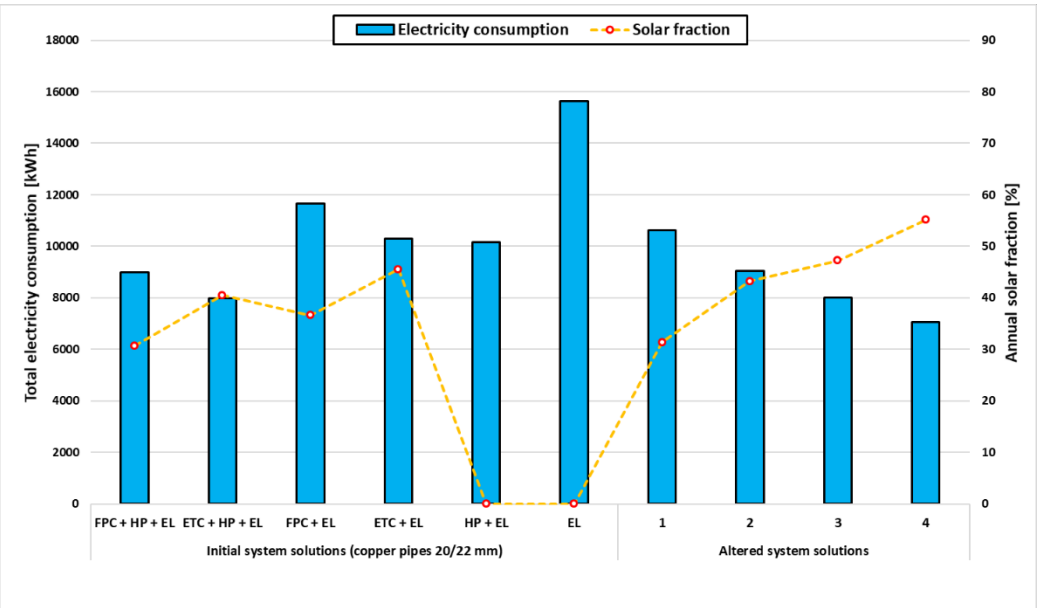

Figure 116: Comparison between the electricity consumption and solar fraction of all simulation models (copper pipes in solar circuit).

Comparing the results in Figure 115 and Figure 116, it becomes evident that it is not necessary with a completely new system layout to achieve a reduction in the total electricity consumption below the existing hot water system model, but on the other hand, it is required to be able to obtain a solar fraction of roughly 50 %.

Lastly, it should be mentioned that an additional parametric study should be performed on the altered system solutions, as it is unsure how some of the input parameters tested in Chapter 11.2.1: *Parametric study* could affect the new results.

12 Conclusion

The simulated results concerning the photovoltaic systems revealed a vast potential for electricity production, as the proposed system was able to generate roughly between 26.4 to 26.9 % of the annual electricity consumption at the milk barn. Based on the consistency of the used electricity mix at the milk barn, the photovoltaic systems could be able to reduce the greenhouse gas emissions related to the annual electricity consumption at the milk barn with an amount of somewhere between 997 to 13 091.4 kg CO_2 equivalents.

Although close, the total amount of generated electricity was not able to reach the planned coverage ratio of 30 %. According to the results from the parametric study, this was likely due to a combination of the shade from the neighboring hilltop and the system component inefficiencies, as both factors were not included in the calculations of the required number of photovoltaic modules. Based on the electricity generation and potential reduction for greenhouse gas emissions, the third photovoltaic system solution with micro-inverters appears to be the best option for the milk barn with given and assumed parameters, but all cost studies suggest that the most optimal economic solution is the first photovoltaic system solution.

The results for the solar water-heating systems instantly showed that the systems were more sensitive to input assumptions than the photovoltaic systems, as none of the initial solar water-heating systems were able to achieve a solar fraction of 50 % nor reduce the total electricity consumption below the consumption for the already existing hot water system. Only by reducing the pipe diameters in the solar circuit and changing the system layout did the solar water-heating system become more efficient than the existing system. These new system solutions were able to reduce the total electricity consumption with about 1 113 to 3 123 kWh and at the same time provide a solar fraction close to or above 50 %. The potential solar water-heating system would only be able to reduce the current electricity consumption at the milk barn, which was 199 672 kWh in 2019, with between 0.8 to 1.6 %, and reduce the current greenhouse gas emissions at the barn with about 21.0 to 759.5 kg CO_2 equivalents.

Concerning the milk barn at Mære Agricultural School, the photovoltaic systems have the most prominent potential for reducing both the total electricity consumption and the greenhouse gas emissions at the barn, and if only one of the presented solar energy systems where to be prioritized, any of the photovoltaic systems should be chosen before the solar water-heating systems.

Conclusion

The main objective of this master thesis was to study the effect that increased solar energy utilization could have on greenhouse gas emissions in Norwegian agriculture, and by combining the results from the photovoltaic system solution that achieved the highest reduction in greenhouse gas emissions, with the best solar water-heating system, each of the 7 600 milk farms in Norway would be able to reduce their greenhouse gas emissions with an amount of somewhere between 1 076.4 to 13 850.9 kg CO_2 equivalents, and in the rare occasion where all 7 600 implements both solutions, the reduction would be somewhere between 8 180.6 to 105 266.8 tons of CO_2 equivalents.

Depending on what the actual reduction would be, it could in the best-case scenario reduce the 2017 greenhouse gas emissions of 0.4 million tons of CO_2 equivalents, which are related to electricity consumption in agriculture, forestry and fisheries, with more than ¼ of the emissions. In the worst-case scenario, it would only reduce the same greenhouse gas emissions by 2.1 %. Independent on the actual size of the reduction, the solar water-heating system solution would only account for 5.5 % of the total reduction, and if the milk farms do not have heat pumps installed beforehand, the solar water-heating system would still only account for 13.8 %.

The results of this study all suggest that it is possible to reduce greenhouse gas emissions in Norwegian agriculture with solar energy, but that the potential is heavily dependent on the milk farms currently used electricity's country of origin, and that the potential reduction is not a fixed value but rather a function of the greenhouse gas emissions related to the electricity mix.

13 Further work

Out of the two solar energy systems described in this master thesis, the most detailed design was presented for the photovoltaic systems. Before any of the photovoltaic systems suggested in this master thesis is constructed, special care should be given to the compatibility of the different electrical components presented throughout Chapter 6: *Designing a photovoltaic system*, as their compatibility has only been assumed in this paper. Also, possibly due to limitations with the simulation software, it is not clear if the micro-inverters responded correctly to obstruction shading, and these results should therefore be compared with results from another simulation software.

Optimally this additional software should be able to simulate power optimizers as well, taking into consideration that Polysun could not simulate these components, and it would be interesting to see how they would affect the final results.

In regard to the solar water-heating system, an independent study on the potential for solar collectors should be performed on the existing hot water system at the milk barn. In that study, the existing piping and components should be thoroughly mapped out and analyzed, as almost all parameters in this master thesis were either assumed or based on small amounts of information and data. There was some difficulty with getting the control systems in Polysun to work together, resulting in a high degree of uncertainty surrounding the final results. Also, seeing as this study on solar water-heating systems only focused on the potential for the harvesting of solar energy and reduction in electricity consumption, no economic analysis was performed for the systems in this report. It could therefore be interesting to see a comparison between the possible annual cost savings and the investment costs, to determine if the solar water-heating system is financially sustainable.

In addition to the subjects touched upon in this master thesis, a more detailed study on building-integrated products should also be performed, before any solar water-heating or photovoltaic system is built on the milk barn, as these products could help to ensure that these new systems are accepted by the Norwegian antiquities' organization.

14 References

A1 Solar Store. (2020). *APS YC1000 Microinverter portrait orientation 4 modules*. Inverters. Available at: https://a1solarstore.com/aps-yc1000-micro-inverter-portrait-orientation.html (accessed: 13.05.2020).

Afework, B., Hanania, J., Stenhouse, K., Yyelland, B. & Donev, J. (2018). *Photovoltaic cell*. Encyclopedia: University of Calgary. Available at: https://energyeducation.ca/encyclopedia/Photovoltaic_cell (accessed: 26.02.2020).

Alibaba.com. (2020). *Solar Collector*. Electrical Equipment and Supplies - Solar Energy Products. Available at: https://www.alibaba.com/products/solar_collector/CID100704.html?IndexArea=product_en (accessed: 29.05.2020).

altE Store. (n.d.). *What is a solar charge controller*. Available at: https://www.altestore.com/store/info/solar-charge-controller/ (accessed: 04.03.2020).

Andersson, A. M. & Sand, R. (2018). Landbruket i Trøndelag som energikonsument- og produsent. *TFoU-rapport*, Volume 15.

APSystems. (2020). *About APsystems*. AP Systems - Altenergy Power. Available at: https://emea.apsystems.com/about/ (accessed: 12.05.2020).

Aurora Solar. (2019). A Solar Designer's Guide for More Accurate Energy Production Estimates. *The Ultimate Guide To PV System Losses*.

AWEA. (n.d.). *Agriculture*. Wind 101. Available at: https://www.awea.org/wind-101/benefits-of-wind/wind-in-my-community/agriculture (accessed: 04.02.2020).

Bondelaget. (2017). *Norwegian Agriculture*. Available at: https://www.bondelaget.no/getfile.php/13894650-1550654949/MMA/Bilder%20NB/Illustrasjoner/Norwegian%20Agriculture%20EN.pdf (accessed: 28.01.2020).

Bondelaget. (n.d.). *Fornybar energi*. Miljø og klima. Available at: https://www.bondelaget.no/miljoogklima/fornybar-energi/ (accessed: 04.02.202).

Breeze, P. (2016). Chapter 9 - Types of Solar Cells. *Solar Power Generation*: Pages 57-70.

Britannica. (2009). *Continental subarctic climate*. METEOROLOGY. Available at: https://www.britannica.com/science/continental-subarctic-climate (accessed: 09.03.2020).

Brown, G. (2018a). *How Solar Irradiance Is Calculated – and How We Made It 30 Times Faster*. Aurora Solar Blog - Solar Design. Available at: https://blog.aurorasolar.com/how-solar-irradiance-is-calculated-and-how-we-made-it-30-times-faster (accessed: 16.03.2020).

Brown, G. (2018b). *Module-Level Power Electronics (MLPE) for Solar Design: A Primer*. Aurora Solar Blog - Solar Design. Available at: https://blog.aurorasolar.com/module-level-power-electronics-mlpe-for-solar-design-a-primer (accessed: 28.04.2020).

Brown, G. (2019). *Solar panel wiring basics: An intro to how to string solar panels*. Solar Power World. Available at: https://www.solarpowerworldonline.com/2019/10/solar-panel-wiring-basics-an-intro-to-how-to-string-solar-panels/ (accessed: 20.03.2020).

Brownson, J. (n.d.). *Collector Orientation*. Solar Resource Assessment and Economics - Tools for Time and Space Relationships. Available at: https://www.e-education.psu.edu/eme810/node/576 (accessed: 05.02.2020).

Bushong, S. (2015). *What are solar meters?* Solar Power World. Available at: https://www.solarpowerworldonline.com/2015/11/what-are-solar-meters/ (accessed: 06.04.2020).

Byggteknisk forskrift. (2017). §15-5. Innvendig vanninstallasjon. *Kapittel 15 Installasjoner og anlegg*.

Chel, A. & Kaushik, G. (2011). Renewable energy for sustainable agriculture. *Agronomy for Sustainable Development*, Volume 31: Pages 91-118.

Chen, G., Maraseni, T., Banhazi, T. & Bundschuh, J. (2015). Benchmarking Energy Use on Farm. *National Rural Issues - Independent analysis*.

Chena, X., Shuaib, C., Zhangc, Y. & Wud, Y. (2020). Decomposition of energy consumption and its decoupling with economic growth in the global agricultural industry. *Environmental Impact Assessment Review*, Volume 81.

Clean Green Energy Zone. (2016). *Advantages of a Micro Hydro-Power Plant*. Green Energy Blog. Available at: https://cleangreenenergyzone.com/advantages-of-a-micro-hydro-power-plant/ (accessed: 15.03.2020).

Climate-Data.org. (n.d.). *Steinkjer Climate*. Norway. Available at: https://en.climate-data.org/europe/norway/nord-tr%C3%B8ndelag-1191/ (accessed: 09.03.2020).

Climates to travel. (n.d.). *Norway*. World climate guide. Available at: https://www.climatestotravel.com/climate/norway (accessed: 05.02.2020).

Contrino, A. (n.d.). *Where does my solar inverter get installed?* Green Power Energy. Available at: https://greenpowerenergy.com/where-does-my-solar-inverter-get-installed/ (accessed: 17.04.2020).

Dannevig, P. (2019). *Trøndelag - klima*. Store norske leksikon. Available at: https://snl.no/Tr%C3%B8ndelag_-_klima (accessed: 29.03.2020).

Deline, C. (2010). *Characterizing shading losses on partially shaded PV systems*. National Renewable Energy Laboratory - PV Performance Modeling Workshop. Available at: https://www.nrel.gov/docs/fy10osti/49504.pdf (accessed: 11.05.2020).

Delta Solar Solutions. (2020). *About Delta Solar Solutions Business*. Available at: https://solarsolutions.delta-emea.com/en/About-Delta-Solar-Solutions-Business-1742.htm (accessed: 05.05.2020).

Den Norske Turistforening. (n.d.). *Mære kirke*. Available at: https://ut.no/sted/141845/mre-kirke (accessed: 15.04.2020).

Detjen, B. (2018). *How does maximum power point tracking (MPPT) work?* Solar Choice - Blog. Available at: https://www.solarchoice.net.au/blog/how-does-maximum-power-tracking-work (accessed: 17.04.2020).

DSG. (2010). Solar Thermal Systems - A guide for installers, architects and engineers. *Deutsche Gesellshaft für Sonnenenergie - Planning and Installing* (2. Edition).

Dutta, S. (2018). *Standard Test Conditions (STC) in Solar PV*. Available at: https://solarpvanalytics.com/standard-test-conditions-stc-in-solar-pv/ (accessed: 26.02.2020).

EEA. (2018). *Overview of electricity production and use in Europe*. European Environment Agency. Available at: https://www.eea.europa.eu/data-and-maps/indicators/overview-of-the-electricity-production-2/assessment-4 (accessed: 01.05.2020).

EESI. (n.d.). *Bioenergy (Biofuels and Biomass)*. Environmental and Energy Study Institute - Topics. Available at: https://www.eesi.org/topics/bioenergy-biofuels-biomass/description (accessed: 18.05.2020).

EIA. (2019). *Biofuels explained - Ethanol and biodiesel*. U.S. Energy Information Administration Available at: https://www.eia.gov/energyexplained/biofuels/ (accessed: 15.03.2020).

Ekici, S. & Kopru, M. A. (2017). Investigation of PV System Cable Losses. *International Journal of Renewable Energy Research*, Volume 7 (Issue 2): Pages 807-815.

Energy.Gov. (n.d.-a). *Advantages and Challenges of Wind Energy*. Energy Basics. Available at: https://www.energy.gov/eere/wind/advantages-and-challenges-wind-energy (accessed: 04.02.2020).

Energy.Gov. (n.d.-b). *Geothermal FAQs*. Information Resources. Available at: https://www.energy.gov/eere/geothermal/geothermal-faqs (accessed: 04.02.2020).

Energy.Gov. (n.d.-c). *Solar Water Heating System: Maintenance and Repair*. Energy Saver. Available at: https://www.energy.gov/energysaver/solar-water-heating-system-maintenance-and-repair (accessed: 03.06.2020).

EnergyInformative. (2015). *Wind Energy Pros and Cons*. Available at: https://energyinformative.org/wind-energy-pros-and-cons/ (accessed: 13.03.2020).

EnergyInformative. (n.d.-a). *Grid-Tied, Off-Grid and Hybrid Solar Systems*. Available at: https://energyinformative.org/grid-tied-off-grid-and-hybrid-solar-systems/ (accessed: 30.03.2020).

EnergyInformative. (n.d.-b). *Labor Costs of Installing Solar Panels*. Available at: https://energyinformative.org/labor-costs-solar-panels (accessed: 22.03.2020).

EnergySage. (2019). *Solar hot water: What you need to know*. Green heating and cooling. Available at: https://www.energysage.com/green-heating-and-cooling/solar-hot-water/ (accessed: 12.02.20202).

EnergySage. (2020a). *How to choose the best battery for a solar energy system*. Solar Batteries - What is the Best Battery for a Solar Panel System? Available at: https://www.energysage.com/solar/solar-energy-storage/what-are-the-best-batteries-for-solar-panels/ (accessed: 31.03.2020).

EnergySage. (2020b). *String inverters vs. power optimizers vs. microinverters*. Solar 101 - What Are Solar Panels? Available at: https://www.energysage.com/solar/101/string-inverters-microinverters-power-optimizers/ (accessed: 24.03.2020).

ENF Solar. (2020). *Solar Panel Directory*. Product Directory. Available at: https://www.enfsolar.com/pv/panel/2 (accessed: 22.03.2020).

Enova. (2020a). *Akkumulatortank*. Privat - Alle Energitiltak Available at: https://www.enova.no/privat/alle-energitiltak/akkumulatortank/ (accessed: 31.05.2020).

Enova. (2020b). *El-produksjon*. Privat - Solenergi. Available at: https://www.enova.no/privat/alle-energitiltak/solenergi/el-produksjon-/ (accessed: 28.04.2020).

Enova. (2020c). *Solfanger*. Privat - Solenergi. Available at: https://www.enova.no/privat/alle-energitiltak/solenergi/solfanger-/ (accessed: 29.05.2020).

Europe - Solar Store. (2020a). *LG Chem RESU 10H - 400V lithium-ion storage batter*. Batteries. Available at: https://www.europe-solarstore.com/lg-chem-resu-10h-400v-lithium-ion-storage-battery.html (accessed: 16.05.2020).

Europe - Solar Store. (2020b). *SMA Sunny Tripower 4.0 - STP4.0-3AV-40*. SMA Sunny Tripower. Available at: https://www.europe-solarstore.com/sma-sunny-tripower-4-0-stp4-0-3av-40.html.

Europe - Solar Store. (2020c). *SMA Sunny Tripower 10.0 - STP10.0-3AV-40*. Solar Inverters. Available at: https://www.europe-solarstore.com/sma-sunny-tripower-10-0-stp10-0-3av-40.html?gclid=Cj0KCQjw17n1BRDEARIsAFDHFezhbRfaZDaVck9GKEuGL6Lihg-GlJjKcH-RnawqBTpk_OZEoumS7CcaAtNgEALw_wcB (accessed: 29.04.2020).

European Commission. (2020). *Interactive tools*. Photovoltaic Geographical Information System. Available at: https://re.jrc.ec.europa.eu/pvg_tools/en/tools.html#MR (accessed: 10.03.2020).

Eurostat. (2019). *Analysis at EU and country level*. Agri-environmental indicator - energy use. Available at: https://ec.europa.eu/eurostat/statistics-explained/index.php/Agri-environmental_indicator_-_energy_use#Analysis_at_EU_and_country_level (accessed: 28.01.2020).

Evangelisti, L., Vollaro, R. D. L. & Asdrubali, F. (2019). Latest advances on solar thermal collectors: A comprehensive review. *Renewable and Sustainable Energy Reviews*, Volume 114.

Eyecular. (n.d.). *Thermal Stratification*. What is Stratification? Available at: http://eyecular.com/what-is-stratification/ (accessed: 08.05.2020).

Fan, J., Chen, Z., Furbo, S., Perers, B. & Karlsson, B. (2009). *Efficiency and lifetime of solar collectors for solar heating plants*. Proceedings of the ISES Solar World Congress 2009: Renewable Energy Shaping Our Future.

Fan, J. & Furbo, S. (2009). *Thermal stratification in a hot water tank established by heat loss from the tank*. Proceedings of the ISES Solar World Congress 2009: Renewable Energy Shaping Our Future.

Glatzmaier, G. (2011). *Developing a Cost Model and Methodology to Estimate Capital Costs for Thermal Energy Storage*. Technical Report: NREL/TP-5500-53066. Available at: https://www.nrel.gov/docs/fy12osti/53066.pdf (accessed: 31.05.2020).

Glunz, S. W., Preu, R. & Biro, D. (2012). 1.16 - Crystalline Silicon Solar Cells: State-of-the-Art and Future Developments. *Comprehensive Renewable Energy*, Volume 1: Pages 353-387.

Gong, A. (2018). *Understanding PV System Losses, Part 1: Nameplate, Mismatch, and LID Losses*. Aurora blog - PV system losses 101. Available at: https://blog.aurorasolar.com/understanding-pv-system-losses-part-1 (accessed: 24.03.2020).

Greenmatch. (2019). *All That You Need to Know about Solar Water Heating*. Solar Energy. Available at: https://www.greenmatch.co.uk/solar-energy/solar-water-heating#solar-heater-benefits (accessed: 20.04.2020).

Guyer, J. P. (2019). An Introduction to Central Solar Water Heating Systems.

Han, Y. M., Wang, R. Z. & Dai, Y. J. (2009). Thermal stratification within the water tank. *Renewable and Sustainable Energy Reviews*, Volume 13 (Issue 5): Pages 1014-1026.

Hauer, A. (2011). *Storage Technology Issues and Opportunities* CERT Energy Storage Workshop, February 15 2011, Paris.

Heidari, N., Gwamuri, J., Townsend, T. & Pearce, J. M. (2015). Impact of Snow and Ground Interference on Photovoltaic Electric System Performance. *IEEE Journal of Photovoltaics*, Volume 5.

Herbert, S., Hashemi, M., Chickering-Sears, C., Weis, S., Carlevale, J. & Campbell-Nelson, K. (2009). *Renewable Energy Production on Farms*. UMass Extension Crops, Dairy, Livestock, Equine. Available at: https://ag.umass.edu/sites/ag.umass.edu/files/fact-sheets/pdf/RenewableEnergyProd.onFarms09-54.pdf (accessed: 18.02.2020).

Honsberg, C. & Bowden, S. (n.d.-a). *Properties of Sunlight - Average Solar Radiation*. PVEducation.org. Available at: https://www.pveducation.org/pvcdrom/properties-of-sunlight/average-solar-radiation (accessed: 16.03.2020).

Honsberg, C. & Bowden, S. (n.d.-b). *Properties of Sunlight - Azimuth Angle*. PVEducation.org. Available at: https://www.pveducation.org/pvcdrom/properties-of-sunlight/azimuth-angle (accessed: 05.02.2020).

Honsberg, C. & Bowden, S. (n.d.-c). *Solar Cell Operation - Fill factor*. PVEducation.org. Available at: https://www.pveducation.org/pvcdrom/solar-cell-operation/fill-factor (accessed: 28.02.2020).

Honsberg, C. & Bowden, S. (n.d.-d). *Solar Cell Operation - IV Curve*. PVEducation.org. Available at: https://www.pveducation.org/pvcdrom/solar-cell-operation/iv-curve (accessed: 26.02.2020).

Honsberg, C. & Bowden, S. (n.d.-e). *Solar Cell Operation - Open-Circuit Voltage*. PVEducation.org. Available at: https://www.pveducation.org/pvcdrom/solar-cell-operation/open-circuit-voltage (accessed: 28.02.2020).

Honsberg, C. & Bowden, S. (n.d.-f). *Solar Cell Operation - Short-Circuit Current*. PVEducation.org. Available at: https://www.pveducation.org/pvcdrom/solar-cell-operation/short-circuit-current (accessed: 28.02.2020).

Honsberg, C. & Bowden, S. (n.d.-g). *Solar Cell Operation - Solar Cell Efficiency*. PVEducation.org. Available at: https://www.pveducation.org/pvcdrom/solar-cell-operation/solar-cell-efficiency (accessed: 18.03.2020).

Infinite Energy. (2019). *What's the difference between Bi-directional Energy Meters, Smart Meters and Online Monitoring?* Solar Blog. Available at: https://www.infiniteenergy.com.au/whats-the-difference-between-bi-directional-energy-meters-smart-meters-and-online-monitoring/ (accessed: 10.05.2020).

IRENA. (2013). *Thermal Energy Storage*. IEA-ETSAP and IRENA © Technology-Policy Brief E17 – January 2013. Available at: https://iea-etsap.org/E-TechDS/PDF/E17IR%20ThEnergy%20Stor_AH_Jan2013_final_GSOK.pdf (accessed: 30.05.2020).

Kalogirou, S. A. (2004). Solar thermal collectors and applications. *Progress in Energy and Combustion Science*, Volume 30: Pages 231–295.

Kalogirou, S. A. (2014a). Chapter 3 - Solar Energy Collectors. *Solar Energy Engineering (Second Edition)*: Pages 125-220.

Kalogirou, S. A. (2014b). Chapter 5 - Solar Water-Heating Systems. *Solar Energy Engineering (Second Edition)*: Pages 257-321.

Kansagara, R. (2018). *Introduction to Different Types of Inverters*. Circuit Digest. Available at: https://circuitdigest.com/tutorial/different-types-of-inverters (accessed: 17.03.2020).

Klimasmart Landbruk. (2017). *Fornybar energi i landbruket*. Klima og landbruk. Available at: https://klimasmartlandbruk.no/fornybar-energi-i-landbruket/category859.html (accessed: 05.02.2020).

Koirala, B. P., Sahan, B. & Henze, N. (2014). *Study on MPP mismatch losses in photovoltaic applications*. Conference paper: Fraunhofer IWES, At Hamburg.

Lehman, C. & Selin, N. E. (2008). *Biofuel*. Encyclopædia Britannica. Available at: https://www.britannica.com/technology/biofuel (accessed: 15.03.2020).

Lien, S. K., Spilde, D. & Ericson, T. (2018). Dokumentasjon av NVEs energibruksframskrivinger 2016-2035. *RAPPORT*, Nr 89.

Lindroos, J. & Savin, H. (2016). Review of light-induced degradation in crystalline silicon solar cells. *Solar Energy Materials and Solar Cells*, Volume 147: Pages 115-126.

Lopez-Garcia, J. & Sample, T. (2018). Evolution of measured module characteristics versus labelled module characteristics of crystalline silicon based PV modules. *Solar Energy*, Volume 160: Pages 252-259.

Løvik, H. (2018). *Norge produserer 98 prosent fornybar kraft, men bruker 46 prosent fossil varmekraft fra Europa*. Vannkraft. Available at: https://www.tu.no/artikler/i-norge-produserer-vi-98-prosent-fornybar-kraft-men-vi-bruker-hele-57-prosent-fossil-varmekraft-fra-europa/441422 (accessed: 15.06.2020).

Maghami, M. R., Hizam, H., Gomes, C., Radzi, M. A., Rezadad, M. I. & Hajighorbani, S. (2016). Power loss due to soiling on solar panel: A review. *Renewable and Sustainable Energy Reviews*, Volume 59: Pages 1307-1316.

Marsh, J. (2019). *What is a solar charge controller? Do you need one?* EnergySage - Environment and Clean Technology. Available at: https://news.energysage.com/what-are-solar-charge-controllers-do-you-need-one/ (accessed: 30.03.2020).

Masters, G. M. (2004). Shading impacts on I–V curves. *Renewable and Efficient Electric Power Systems*: Pages 477-485.

McFarland, K. (2017). *Biomass Advantages and Disadvantages*. SynTech Bioenergy. Available at: https://www.syntechbioenergy.com/blog/biomass-advantages-disadvantages (accessed: 05.02.2020).

Melk.no. (2019). *Statistikk for meieriprodukter fra 2007*. Statistikk. Available at: https://www.melk.no/Statistikk (accessed: 11.03.2020).

Menon, E. S. (2015). Chapter Twelve - Meters and Valves. *Transmission Pipeline Calculations and Simulations Manual*: Pages 431-471.

Mertens, K. (2014). Photovoltaics: Fundamentals, Technology and Practice.

Miljødirektoratet. (2019). *Jordbruksrelaterte klimagassutslipp*. Rapport fra partssammensatt arbeidsgruppe. Available at:

https://www.regjeringen.no/contentassets/0f1af0ca7efe493e8e48b46b6fba5ffd/rapport-tbu-jordbruk_siste.pdf (accessed: 01.05.2020).

Miljøstatus. (2019). *Klimagassutslipp fra jordbruk*. Norske utlispp av klimagasser. Available at: https://miljostatus.miljodirektoratet.no/tema/klima/norske-utslipp-av-klimagasser/klimagassutslipp-fra-jordbruk/ (accessed: 31.03.2020).

Naked Solar. (2020). *Solar Batteries & Storage*. Storage. Available at: https://nakedsolar.co.uk/storage/ (accessed: 15.05.2020).

Nguyen, M. V., Arason, S., Gissurarson, M. & Pálsson, P. G. (2015). Opportunities for developing countries. *Uses of geothermal energy in food and agriculture*.

Norsk Solenergiforening. (n.d.-a). *Hvorfor solenergi?* Om solenergi. Available at: https://www.solenergi.no/hvorfor-solenergi (accessed: 05.02.2020).

Norsk Solenergiforening. (n.d.-b). *Norske solforhold*. Om solenergi. Available at: https://www.solenergi.no/norske-solforhold (accessed: 29.01.2020).

Norsk Solenergiforening. (n.d.-c). *Solceller*. Om solenergi. Available at: https://www.solenergi.no/solstrm (accessed: 26.02.2020).

Norton, B., Eames, P. C., Mallick, T. K., Huang, M. J., McCormack, S. J., Mondol, J. D. & Yohanis, Y. G. (2011). Enhancing the performance of building integrated photovoltaics. *Solar Energy*, Volume 85: Pages 1629-1664.

NPRO. (2018). *Carbon accounting report 2017*. Norwegian Property. Available at: https://www.norwegianproperty.no/wp-content/uploads/2018/12/NPRO-Carbon-Accounting-report.pdf (accessed: 17.05.2020).

NTE. (2020). *Om NTE*. NTE - Privat. Available at: https://nte.no/privat/om-nte (accessed: 10.05.2020).

NVE. (2018). *Endringer i regelverket om anleggsbidrag styrker vernet av kundene*. Nyheter - Reguleringsmyndigheten for energi. Available at: https://www.nve.no/reguleringsmyndigheten/nytt-fra-rme/nyheter-reguleringsmyndigheten-for-energi/endringer-i-regelverket-om-anleggsbidrag-styrker-vernet-av-kundene/ (accessed: 10.05.2020).

NVE. (2019). *Electricity disclosure 2018*. Norwegian Energy Regulatory Authority. Available at: https://www.nve.no/norwegian-energy-regulatory-authority/retail-market/electricity-disclosure-2018/ (accessed: 01.05.2020).

O'Neill, B. (2018). *Solar Meters Explained*. Canstar Blue - Solar Energy Providers. Available at: https://www.canstarblue.com.au/solar-power/solar-meters-explained/ (accessed: 06.04.2020).

Olje- og energidepartementet. (n.d.). *Strømnettet*. Energifakta Norge - Norsk energiforsyning. Available at: https://energifaktanorge.no/norsk-energiforsyning/kraftnett/ (accessed: 15.04.2020).

Orlund, K. (2018). *The Norwegian agricultural Policy – Rural Development*. Norwegian Ministry of Agriculture and Food. Available at: https://www.regjeringen.no/contentassets/3946c69018db423899edcf1736785a61/the-norwegian-agricultureal-policy--rural-development---kristin-orlund.pdf (accessed: 18.02.2020).

Osborn, B., Weiner, C. & Anderson, S. (2017). *Agricultural Hydropower Generation: On-Farm* Natural Resources Series: Water. Available at: https://extension.colostate.edu/docs/pubs/natres/06708.pdf (accessed: 15.03.2020).

Øvrebø, O. A. (2020). *Norges utslipp*. Energi og Klima - Klimavakten. Available at: https://energiogklima.no/klimavakten/norges-utslipp/ (accessed: 01.05.2020).

Parked In Paradise. (2020). *Solar Panels Basics*. Parked In Paradise - Best Solar Panels For RV Or Camper Van. Available at: https://www.parkedinparadise.com/solar-panel-basics/ (accessed: 22.03.2020).

Pawluk, R. E., Chen, Y. & She, Y. (2019). Photovoltaic electricity generation loss due to snow – A literature review on influence factors, estimation, and mitigation. *Renewable and Sustainable Energy Reviews*, Volume 107: Pages 171-182.

Pearsall, N. M. (2017). 1 - Introduction to photovoltaic system performance. *The Performance of Photovoltaic (PV) Systems - Modelling, Measurement and Assessment*: Pages 1-19.

Perlin, J. (2013). *Seven of the Greatest Solar Stories Over the Millennia*. Great Energy Challenge. Available at: https://www.nationalgeographic.com/environment/great-energy-challenge/2013/seven-of-the-greatest-solar-stories-over-the-millennia/ (accessed: 22.04.2020).

Piliougine, M., Carretero, J., Sidrach-de-Cardona, M., Montiel, D. & Sánchez-Friera, P. (2008). *Comperative analysis of the dust losses in photovoltaic modules with different cover glasses*. 23rd European Photovoltaic Solar Energy Conference and Exhibition - Spain.

Pop, L. (n.d.). *The Definitive Guide to Solar Inverters For Off-Grid and Grid-Tied Systems*. SolarPanelsVenue - What is solar inverters. Available at: https://solarpanelsvenue.com/what-is-solar-inverter/ (accessed: 20.03.2020).

Powers, L., Newmiller, J. & Townsend, T. (2010). Measuring and modeling the effect of snow on photovoltaic system performance.

PVPerformance. (n.d.). *Modeling steps - DC Wiring Losses*. An Industry and National Laboratory collaborative to Improve Photovoltaic Performance Modeling. Available at: https://pvpmc.sandia.gov/modeling-steps/3-dc-array-iv/dc-wiring-losses/ (accessed: 06.05.2020).

Qazi, S. (2017). Chapter 2 - Fundamentals of Standalone Photovoltaic Systems. *Standalone Photovoltaic (PV) Systems for Disaster Relief and Remote Areas*: Pages 31-82.

Renewable Resources Co. (2016). *The Disadvantages of Solar Energy*. Solar Energy. Available at: https://www.renewableresourcescoalition.org/solar-energy-disadvantages/ (accessed: 15.03.2020).

Renogy. (n.d.). *Learn series and parallel*. Renogy - Your Guide To Series Vs Parallel Connections. Available at: https://www.renogy.com/learn-series-and-parallel/ (accessed: 22.03.2020).

RenuGen. (2020). *Delta RPI M50A 50kW Three Phase Solar PV Grid Inverter*. Power Inverters - Delta Energy Systems. Available at: https://www.renugen.co.uk/delta-rpi-m50a-50kw-three-phase-solar-pv-grid-inverter/ (accessed: 12.05.2020).

Reynolds, L. & Wenzlau, S. (2012). *Working Hand-in-Hand toward Climate Mitigation*. Climate-Friendly Agriculture and Renewable Energy. Available at: https://www.renewableenergyworld.com/2012/12/21/climate-friendly-agriculture-and-

renewable-energy-working-hand-in-hand-toward-climate-mitigation/#gref (accessed: 18.02.2020).

Rogers, S. (2018). *Solar Panel Maximum Voltage Calculator – Why it's important*. Gold Coast Solar Power Solutions. Available at: https://gold-coast-solar-power-solutions.com.au/solar_power/solar-panel-maximum-voltage-calculator/ (accessed: 20.03.2020).

Rossing, N. K. (2011). *Praktisk solcelleteknologi for skolen*. Skolelaboratoriet ved NTNU. Available at: https://www.ntnu.no/documents/2004699/64e6deb0-41cd-48a8-8fa9-6c15a04ff7ea (accessed: 20.03.2020).

Rosvold, K. A. (2018). *Nettsystem*. Store Norske Leksikon (SNL) - Kraftnett og installasjon. Available at: https://snl.no/nettsystem (accessed: 10.05.2020).

Rosvold, K. A. (2019). *NTE*. Store norske leksikon - Kraftselskaper og kraftverk. Available at: https://snl.no/NTE (accessed: 10.05.2020).

Sabri, L. & Benzirar, M. (2014). Effect of Ambient Conditions on Thermal Properties of Photovoltaic Cells: Crystalline and Amorphous Silicon. *International Journal of Innovative Research in Science, Engineering and Technology*, Volume 3 (Issue 12).

Sarbu, I. & Sebarchievici, C. (2018). A Comprehensive Review of Thermal Energy Storage. *Sustainability*, Volume 10: Pages 191-222.

Saunders, C., Barber, A. & Taylor, G. (2006). Comparative Energy/Emissions Performance of New Zealand's Agriculture Industry. *Food Miles*.

Schachinger, M. (2020). *Module Price Index - March 2020: The coronavirus wake-up call*. pvXchange - pv magazine. Available at: https://www.pv-magazine.com/module-price-index/ (accessed: 22.03.2020).

SEIA. (2018). *Solar Energy Technologies - Solutions for Today's Energy Needs*. Solar Energy Industries Association. Available at: https://www.seia.org/sites/default/files/inline-files/SEIA-Solar-Energy-Technologies-Factsheet-2018-April.pdf (accessed: 15.03.2020).

Sendy, A. (n.d.-a). *Pros and cons of string inverters vs microinverters*. SolarReviews - Solar Inverters. Available at: https://www.solarreviews.com/blog/pros-and-cons-of-string-inverter-vs-microinverter#whatIsAStringInverter (accessed: 25.03.2020).

Sendy, A. (n.d.-b). *What are the pros and cons of Monocrystalline, Polycrystalline and Thin Film solar panels?* SolarReviews - Solar Panels. Available at: https://www.solarreviews.com/blog/pros-and-cons-of-monocrystalline-vs-polycrystalline-solar-panels (accessed: 18.03.2020).

Sheir.org. (n.d.). *How Solar or Photovoltaic (PV) Cell Works*. Solar Cells. Available at: https://sheir.org/edu/how-solar-cell-works/ (accessed: 27.02.2020).

Skaugen, A. & Romundstad, R. M. (2017). *Veileder - Solcelleanlegg i større boenheter i Oslo*. Ressurs og Miljø AS. Available at: https://static1.squarespace.com/static/597512eb579fb3d3de0207aa/t/5aaef268352f533ca574fa8e/1521414770785/Veileder-solcelleanlegg-borettslag-og-sameier-Oslo-2017.pdf (accessed: 18.03.2020).

Smets, A., Jäger, K., Isabella, O., Swaaij, R. v. & Zeman, M. (2016). 9. Solar Cell Parameters and Equivalent Circuit. *Solar Energy*: Pages 113-121.

Smith, A. (2018). *How to Calculate the Heat Loss in a Pipe*. Sciencing - Fluid Available at: https://sciencing.com/calculate-heat-loss-during-pipeline-depressurization-11383637.html (accessed: 20.05.2020).

Solar365. (n.d.). *Pipe Size and Fluid Volume in Solar Thermal Systems*. Green homes - Plumbing. Available at: http://www.solar365.com/solar/thermal/pipe-size-and-fluid-volume-solar-thermal-systems?page=0,0 (accessed: 08.06.2020).

Solar Reviews. (2018). *Wiring solar panels: Do you wire solar panels in series or parallel?* Solar Power World. Available at: https://www.solarpowerworldonline.com/2018/10/wiring-solar-panels-do-you-wire-solar-panels-in-series-or-parallel/ (accessed: 20.03.2020).

Solar Tribune. (n.d.). *Best Solar Inverters: String vs. Micro vs. Power Optimizers*. Available at: https://solartribune.com/your-home/inverters/ (accessed: 25.03.2020).

SolarEdge. (n.d.). Three Phase System with SetApp Configuration. *Installation Guide For Europe and APAC Version 1.2*.

Sopori, B., Basnyat, P., Shet, S., Mehta, V., Binns, J. & Appel, J. (2012). *Understanding Light-Induced Degradation of c-Si Solar Cells*. IEEE Photovoltaic Specialists Conference, Austin, Texas.

Sørensen, Å. L., Torp, C. B. & Nylund, H. K. (2017). Solvarme - I kombinasjon med andre varmekilder. *Norsk Solenergiforening - Håndbok*.

Spiers, D. (2012). Chapter IIB-2 - Batteries in PV Systems. *Practical Handbook of Photovoltaics (Second Edition)*: Pages 721-776.

SSB. (n.d.). *Forbruk av elektrisk energi i jordbruk. Ekskl.veksthus.* Tabell. Available at: https://www.ssb.no/294445/forbruk-av-elektrisk-energi-i-jordbruk.ekskl.veksthus (accessed: 18.05.2020).

Statnett. (2018). *Slik fungerer kraftsystemet*. Bli bedre kjent med Statnett. Available at: https://www.statnett.no/om-statnett/bli-bedre-kjent-med-statnett/slik-fungerer-kraftsystemet/ (accessed: 10.05.2020).

Steinkjer Kommune. (2015). *Kulturarven i Steinkjer*. Kulturminneplan for Steinkjer Kommune 2014-2019. Available at: https://www.riksantikvaren.no/wp-content/uploads/2019/10/steinkjerkommune.kulturminneplan.pdf (accessed: 01.04.2020).

Steinkjerleksikonet. (n.d.). *Mære landbruksskole*. Available at: https://www.steinkjerleksikonet.no/maere_landbruksskole (accessed: 02.04.2020).

Streicher, W. (2016). Solar thermal technologies for domestic hot water preparation and space heating. *Renewable Heating and Cooling*: Pages 9-39.

SunPower. (n.d.). *How Many Solar Panels Do You Need: Panel Size and Output Factors*. Available at: https://us.sunpower.com/how-many-solar-panels-do-you-need-panel-size-and-output-factors (accessed: 22.03.2020).

Taylor-Parker, P. (2019). *How to Add Battery Backup to an Existing Grid-Tied Solar System*. Wholesale Solar. Available at: https://www.wholesalesolar.com/blog/add-battery-backup-to-grid-tied-solar-system (accessed: 14.04.2020).

Tensio. (2020). *Produser din egen strøm - bli plusskunde*. Plusskunde. Available at: https://ts.tensio.no/tjenester/plusskunde (accessed: 10.05.2020).

Townsend, T. & Powers, L. (2011). Photovoltaics and snow: An update from two winters of measurments in the Sierra.

UnderstandSolar. (2017). *Understand the difference between wiring your solar panels in series vs parallel*. Wiring Solar Panels in Series vs Parallel: Which Is Better? Available at: https://understandsolar.com/solar-panels-in-series-vs-parallel/ (accessed: 20.03.2020).

Union of Concerned Scientists. (2008). *Renewable Energy and Agriculture: A Natural Fit*. Available at: https://www.ucsusa.org/resources/renewable-energy-and-agriculture (accessed: 05.02.2020).

USDA. (n.d.). *Bioenergy*. United States Department of Agriculture - National Institute of Food and Agriculture. Available at: https://nifa.usda.gov/topic/bioenergy (accessed: 15.03.2020).

USGS. (n.d.). *Hydroelectric Power Water Use*. Water Science School. Available at: https://www.usgs.gov/special-topic/water-science-school/science/hydroelectric-power-water-use?qt-science_center_objects=0#qt-science_center_objects (accessed: 15.03.2020).

Vekony, A. T. (2019). *Photovoltaic System*. Solar Energy. Greenmatch. Available at: https://www.greenmatch.co.uk/solar-energy/photovoltaics/photovoltaic-system (accessed: 26.02.2020).

Vekony, A. T. (2020). *How Much Does a Solar Battery Storage System Cost (And Is It Worth It?)*. Greenmatch UK. Available at: https://www.greenmatch.co.uk/blog/2018/07/solar-battery-storage-system-cost (accessed: 14.04.2020).

Vela Solaris. (2018). *User Manual*. Polysun simulation software Available at: https://www.velasolaris.com/wp-content/uploads/2019/02/Tutorial_EN.pdf (accessed: 15.04.2020).

Viridian Solar. (n.d.). *3.6 Solar Thermal Plumbing*. All About Solar Energy. Available at: https://www.viridiansolar.co.uk/resources-3-6-solar-thermal-plumbing.html (accessed: 20.05.2020).

Wholesale Solar. (2018). How to choose the right batteries for your solar system. *Solar Battery Guide*.

Wholesale Solar. (2020a). *AGM (Absorbent Glass Mat)*. Batteries. Available at: https://www.wholesalesolar.com/shop/battery-banks/agm-absorbent-glass-mat-batteries (accessed: 16.05.2020).

Wholesale Solar. (2020b). *Charge controllers*. Shop. Available at: https://www.wholesalesolar.com/shop/charge-controllers (accessed: 16.05.2020).

Wholesale Solar. (2020c). *Flooded Lead Acid*. Batteries. Available at: https://www.wholesalesolar.com/shop/battery-banks/flooded-lead-acid-batteries (accessed: 16.05.2020).

Wholesale Solar. (2020d). *Lithium Ferro Phosphate*. Batteries. Available at: https://www.wholesalesolar.com/shop/battery-banks/lithium-ferro-phosphate-batteries (accessed: 16.05.2020).

WVIC. (n.d.). *How Hydropower Works*. Wisconsin Valley Improvement Company. Available at: http://www.wvic.com/content/how_hydropower_works.cfm (accessed: 15.03.2020).

Yr.no. (2020). *Værvarsel for Mære landbruksskole, Steinkjer (Trøndelag)*. Available at: https://www.yr.no/sted/Norge/Tr%C3%B8ndelag/Steinkjer/M%C3%A6re_landbruksskole/ (accessed: 15.05.2020).

Zijdemans, D. (2014). Vannbaserte oppvarmings- og kjølesystemer (2. Edition).

Zipp, K. (2013). *What Are The Advantages Of String Inverters In Solar?* Solar Power World. Available at: https://www.solarpowerworldonline.com/2013/04/what-are-the-advantages-of-string-inverters-in-solar/ (accessed: 19.04.2020).

Zorrilla-Casanova, J., Piliougine, M., Carretero, J., Bernaola, P., Carpena, P., Mora-López, L. & Sidrach-de-Cardona, M. (2011). *Analysis of dust losses in photovoltaic modules*. World Renewable Energy Congress 2011 - Sweden.

15 Attachments

A.1: Extract from the report on Mære Agricultural school

mære

UTDANNER DE SOM
UTVIKLER DISTRIKTENE

Rapport fra arbeidsgruppe om anlegg for fornybar energi på Mære landbruksskole

1

investering for Mære på kr. 3 448 573. Det er også trukket fra støtte som gis til behandling av husdyrgjødsel i biogassanlegg. Pris pr. kWh uten støtte fra Innovasjon Norge er beregnet til kr. 1,08. Med støtte er prisen beregnet til 0,75 kr. Pr. kWh. Investeringen er beregnet nedbetalt innen 5 år.

Finansiering

Innovasjon Norge kan gi støtte til biogassanlegg i landbruket med inntil 45 % av kostnadene. Vi har i løpet av prosjektperioden ikke fått på plass finansiering av biogassanlegg. Dette vil det bli jobbet videre med.

Anbefaling

Bygging av biogassanlegg for reaktering av husdyrgjødsel er et godt klimatiltak. Metan som slippes ut fra husdyrgjødsel har 25 ganger sterkere effekt på drivhuseffekten enn tilsvarende mengde utslipp av karbondioksid, slik at klimagassutslippene fra landbruket vil minke dersom det bygges biogassanlegg. Det er et uttrykt mål fra myndighetene om at 30 % av all husdyrgjødsel skal reakteres i biogassanlegg innen utgangen av 2020. Dette er et ambisiøs mål, og det må skje mye på denne fronten dersom vi skal komme i nærheten av dette målet innen de tre årene som er igjen til 2020.

Det utføres mye grunnleggende biogassforskning i Norge. Dette skjer for det meste i laboratoriet på små forsøksanlegg. Det er behov for forskning og utprøving av ulike teknikker og substrater på større anlegg, og behov for demonstrasjonsanlegg flere steder i Norge. Bygging av biogassanlegg på Mære vil være et viktig bidrag til dette, og et viktig element i oppbyggingen av et klima- og energisenter på Mære. Prosjektgruppa anbefaler at det jobbes videre med planer om å bygge biogassanlegg på Mære.

Utnyttelse av solenergi til varme- og strømproduksjon.

Driftsbygningene i landbruket har til sammen store flater med takareal. Det ligger et stort potensiale i å utnytte dette til strøm- eller varmeproduksjon ved å montere solcelleanlegg eller solfangere. Produksjon av elektrisk energi i solcelleanlegg kan gi strøm til eget forbruk som kan måle seg i pris med det som leveres via el-nettet. Kombineres dette med batteriteknologi kan energien også lagres til senere forbruk. Salg av solcellestrøm på el-nettet er pr. i dag ulønnsomt. Selger du strømmen på nettet må du kjøpe den tilbake og betale for strømmen + nettleien. Prisen pr. kWh du selger er lav sammenlignet med det du må betale. Mære har i samarbeid med Nord-Trøndelag Elektrisitetsverk, NTE, og Norsk landbruksrådgivning, NLR, utredet muligheter for å montere solcelleanlegg på noen av takflatene på driftsbygningene. Det er nå lagt ny takstein med integrerte solceller på delar av taket på den gamle driftsbygningen. Strømmen fra anlegget skal bl.a. brukes i veksthuset, som har stort behov for strøm til vekstlys. Det blir videre vurdert også å legge solceller på deler av taket på den nye driftsbygningen.

I en *solfanger* kan vatn varmes opp av solvarmen. Vatnet kan benyttes til vaskevann i driftsbygninger eller i bolighus. For nyfjøset på Mære er det gjort beregninger som viser varmebehovet for oppvarming av vatn til vasking og drikkevatn for dyra.

Energiberegning oppvarming vann, nytt kufjøs Mære landbruksskole

Drikkevann dyr

Dyreslag	Alder	Antall	Vekt	l dyr/dag	l pr dag	Pr. år
Kalver	1-7 uker	9	65	5	45	16 425
Kalver	8-12 uker	9	100	10	90	32 850
Kalver	4-6 mnd	9	150	15	135	49 275
Kviger	7-9 mnd	9	225	20	180	65 700
Kviger	10-12 mnd	9	300	30	270	98 550
Kviger	13-15 mnd	9	375	35	315	114 975
Kviger	16-18 mnd	9	425	60	540	197 100
Kviger	19-21 mnd	9	475	70	630	229 950
Kviger	21-24 mnd	9	525	80	720	262 800
Kyr	Årskyr	55		100	5 500	2 007 500
				425	8 425	3 075 125

		Sp.vk. (C)	Mengde (m)	Temp.diff(K)	kWh pr år
Drikkevann dyr		4,18	3 075 125	10	35 706
Tappevann melkerobot		4,18	98 550	75	8 582
Tappevann tankrom		4,18	9 490	75	826
Tappevann sanitærrom		4,18	29 200	75	2 543
Oppvarming serviceareal 151 m^2					16 610
Totalt energibehov oppvarming vann					**64 267**
Varmegjenvinning melketank	(fradrag)	4,18	200 000	75	17 417
Varmepumpe luft - vann					16 000
Netto energibehov oppvarming vann					**30 850**

Tabellen viser totalt energibehov for oppvarming av vatn, med fratrekk for varmegjenvinningsanlegg som er montert på melketanken, og fratrekk for luft-til vann- varmepumpe som er montert for å varme opp garderober og andre fellesareal. Netto energibehov for oppvarming av vatn (30 850 kWh) kan dekkes gjennom bruk av solcellestrøm, eller solfangere, eller en kombinasjon av disse. Det er av hensyn til demonstrasjonseffekten ønskelig å montere solfangere i tillegg til solcellepaneler.

Det er stor interesse i landbruket for å utnytte solenergien direkte til strøm- eller varmeproduksjon. Et seminar om solenergi som ble arrangert på Mære i mars samlet om lag 80 deltakere. NTE, som er

en stor aktør i energimarkedet i Trøndelag, er veldig interessert i å samle kunnskap om hvilke muligheter dette «nye» markedet vil bringe. Ikke minst på bakgrunn av sterkt fokus på smarte løsninger som kan styre forbruket av strøm over strømnettet, og i beredskapsmessig sammenheng.

Trøndelag fylkeskommune vil sammen med Mære vurdere hvordan et anlegg på melkefjøset som kombinerer solfangere, solceller og batteriteknologi. Det vurderes sammen med midt-norske teknologimiljøer å bygge dette som et testanlegg også for forskningsprosjekter. Arbeidet igangsettes november 2017 med mål om investering i 2018. Det er også aktuelt å fase inn vindmøller i prosjektet.

Biovarmeanlegg med flis, halm eller ved som energibærer finnes det nå mange av i landbruket. Ved å kombinere biovarmeanlegg med strøm fra solcelleanlegg tar man enda et skritt for å forsyne gården med kortreist og miljøvennlig energi. Det er nå også åpnet muligheter for å søke Innovasjon Norge om tilskott til slike kombinerte løsninger.

Flisanlegg

Det er bygd mange flisanlegg i landet de siste årene, og det gjelder også for Nord-Trøndelag. Mære har vært sterkt involvert i dette gjennom mange år ved at vi har gjennomført mange kurs om etablering av gårdsvarmeanlegg. Innovasjon Norge har vært en sentral samarbeidspartner i dette arbeidet. Vi har hørt utsagn som «det starta med et kurs på Mære, og nå har vi flisfyringa på plass».

Det ble installert et pelletsanlegg på 300 kW for å varme opp skolebygningene i 2005. Dette er nå demontert. Anlegget var i kjelleren på det gamle internatet som nå er revet. Det settes nå opp nytt hybelbygg som skal varmes opp fra varmeanlegget. Bygget har passivhus-standard og det blir også lagt solceller på taket.

Vi har i dette prosjektet vurdert muligheter for å bygge flisanlegg til erstatning for pelletsanlegget som nå blir demontert. Flis som energibærer er den vanligste form for bioenergi i landbruket, og et flisanlegg på Mære vil derfor ha en viktig misjon som demonstrasjonsanlegg. Sett på bakgrunn av følgende, er det derimot lite aktuelt å investere i flisanlegg nå:

- Varmelagret forventes å gi så mye energi at det ser ut til å kunne dekke varmebehovet på Mære
- Vi får ikke anledning til å bygge anlegg som kun er beregnet på demonstrasjon. Det må være behov for anlegget utover det.
- Det er bygd flere flisanlegg i skolens nærhet som kan benyttes som demonstrasjonsanlegg.
- Vi har tilgang på mini-flisanlegg montert på bilhenger som kan benyttes for å demonstrere hvordan et anlegg virker.

A.2: Extract from: *Fram mot nullutslippsgården*

Foto: Thomas Thomas Jergel, Camerat.

Nytt melkefjøs stod ferdig i 2016. Det er bygd for 50 årskyr med påsett. Det er satt inn melkerobot, og fjøset inneholder forøvrig mye teknisk utstyr til fôrhandtering som bl.a. gir muligheter for å blande ulike typer grovfôr i en og samme fôrrasjon.

Byggematerialer

Fjøset er bygd i tre, noe som binder mye CO_2 sammenligna med bygg i betong. Veggene er i massivtre og det er ikke lagt inn ekstra isolasjon utover treets egen isolasjonsevne. Det er naturlig ventilasjon i bygget.

Varmegjenvinning

Når melka kommer fra kua holder den en temperatur på ca 38°C. Når den kjøles ned i melketanken avgis mye varme. Det er montert varmeveksler på melketanken slik at varmen som avgis brukes til å varme opp vannet i varmtvannstanken, eller gis som temperert drikkevann til dyra.

Varmepumpe

Det er installert varmepumpe (luft til luft) som skaffer varme til oppvarming av garderober og andre fellesrom.

3

Solceller på ammekufjøset

Solceller

På ammekufjøset er det montert solceller på et takareal på 192 m². Dette er et takintegrert anlegg som har en total ytelse på 34,8 kWp, og er beregnet å gi en årlig strømproduksjon på 34 500 kWh. Antall paneler er 120.

Solceller omdanner solenergi direkte til elektrisk energi. Den elektriske energien kan brukes direkte i et elektrisk apparat, den kan lagres i batterier, eller transporteres til forbruker via overføringsnettet. Lokal produksjon av elektrisk energi har blitt mer interessant etter hvert som energibehovet øker og overføringsnettet ikke er utbygd for å ta de energitoppene som kommer. Innenlands produksjon av elektrisk energi kan også i perioder bli for lavt i forhold til forbruket.

I perioder importeres det allerede en god del strøm til Norge. Lokal produksjon av elektrisk energi fra sola er et godt klimatiltak framfor import av strøm som kan være produsert i kullfyrte eller oljefyrte kraftanlegg i utlandet.

Slik virker en solcelle

Kilde: www.ndla.no

En solcelle er bygget opp av to lag med halvledermetaller, for eksempel silisium. Fotoner i lys blir absorbert i halvlederne og slår løs elektroner som på grunn av halvlederegenskapene bare kan bevege seg i én retning. Vi har dermed grunnlaget for elektrisk strøm.

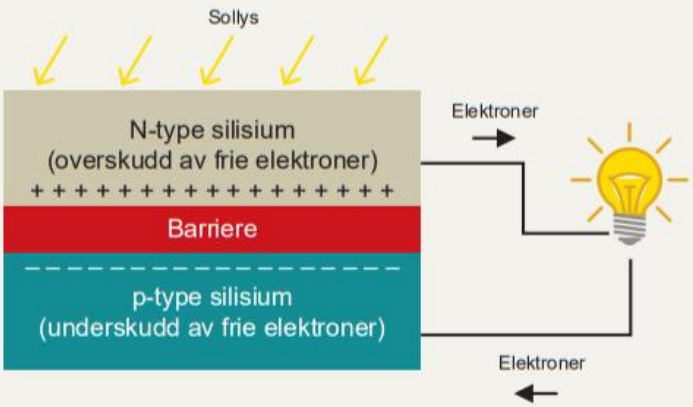

11

Hybelbygget

Hybelbygget skal gi minst mulig utslipp i løpet av sin levetid. Bygget er et passivhus med lite behov for oppvarming, det er bygd i tre som gir lite karbonavtrykk og solcellene på taket produserer strøm som også går til kjøkken og undervisningsbygg.

Solceller

På taket som vender mot sør er det lagt solceller oppå eksisterende tak. Det er i alt 216 paneler som dekker et takareal på 300m^2. Taket har en ideell takvinkel for solceller. Best effekt får vi når solstrålene treffer mest mulig vinkelrett på solcellen. Anlegget har en effekt på 58 kWp, og er beregnet å gi en årlig strømproduksjon på 55 000 kWh.

Til sammen kan de to takene med solceller (hybelbygg og ammekufjøs) gi en årlig strømproduksjon på omlag 90 000 kWh (tilsvarer totalt energibehov i om lag 4 husstander). Mye av strømmen vil gå til direkte forbruk ved skolen. Det som ikke forbrukes direkte transporteres inn i overføringsnettet. Det er ønskelig i framtida å kunne lagre overskuddet i batterier i nærheten av solcellene.

Passivhus

Hybelhuset er basert på passivhusstandard NS 3700 – 13. Et passivhus er et bygg som bruker lite energi til oppvarming sammenlignet med vanlige hus.

Grunnen til at det kalles passivhus, er at man bruker passive tiltak for å redusere energibehovet:

- yttervegger, tak og gulv mot grunn som er ekstra godt isolert
- ekstra godt isolerte vinduer
- godt tetthet og dermed svært få luftlekkasjer

For å få til god luftkvalitet og et godt inneklima i et passivhus bør man ha et ventilasjonssystem med mulighet for varmegjenvinning.

Videre er det lagt vannbåren varme i golv. Varmen kommer fra energilagret i veksthuset. Det er en ambisjon om at bygget skal produsere like mye energi som blir brukt over året.

13

A.3: Details on the existing photovoltaic systems on the school

Hei,

1. Det er to anlegg på Mære LS. Ammekufjøset har et integrert anlegg på 34,8kW og hybelhuset har et parallell-montert anlegg på 58,3kW.
   Det vil si en samlet installert effekt på 93,1kW. Dette gir en beregnet strømproduksjon på ca80 000kWh pr år.

2. På ammekufjøset hvor det er et «integrert» system, erstatter solcellematrisen konvensjonelt tak, da solcellepanelene utgjør selve yttertaket. På Hybelhuset så er det et ordinært utenpåliggende anlegg, so mer montert utenpå eksisterende tak.

   Begge anleggene er bygd på samme system, som er litt mer avansert enn tradisjonelt streng-anlegg. Det er montert et system fra SolarEdge – også omtalt som SolarEdge solution – hvor det sitter effektregulatorer under panelene som optimaliserer effektproduksjonen på panelnivå, i stedet for en hel streng. Disse modulene kalles optimizere. Her er det koblet to panel per optimizer. Fordelene med dette er at ytre påvirkninger gir mindre konsekvenser for energiproduksjonen enn hva det ville gjort på et ordinert streng-anlegg.
   Du kan se hvordan dette oppfører seg om du klikker på denne linken:
   https://youtu.be/-Bsq7umcffg

3. Mære LS har fått opprettet en EOS (Energi Overvåkings System)fra NTE, som er et produkt hvor kundene kan holde god oversikt over energiforbruket sitt, og utviklingen av dette over tid. Det er pr i dag ikke montert noe aktiv styring av laster opp mot egen produksjon. Men anleggene er satt inn i en elektrisk infrastruktur som gjør at de har veldig og utnyttelse av egenprodusert energi uten bruk av aktive styringssystemer.

4. Potensialet for videre utbygging på Mære LS er ganske stort. De har store takarealer og et høyt strømforbruk, som gjør at det er en meget bra utgangspunkt til å produsere mye mer av strømmen de trenger selv. Pr i dag er det planlagt et nytt solcelleanlegg på den nye stallen som snart skal bygges, samt enda et eksisterende bygg hvor solenergi er under utreding for mulig utbygging, dog på et tidlig stadium.

Med vennlig hilsen / Best Regards,

Håvard Lutdal | Prosjektleder - Solenergi | havard.lutdal@nte.no
NTE Marked AS | Telefon 74 15 02 00 | Mobil 907 16 179 | www.nte.no

A.4: Energy consumption at Mære Agricultural School provided by NTE

Energi på Mære

- Totalforbruk av energi forholdsvis stabilt over de siste 10 år, omkring 3,4 GWh (3,4 millioner kWh) pr år
- Oppvarming utgjør omkring 1,4 GWh – Lys og annet 2,0 GWh
- Propan, olje, pellets og elkjel er erstattet av varmelageret, altså de samme 1,4 GWh – men da er 0,4 elkraft og 1,0 GWh lagret varme
- Om vi trekker ut veksthuset med 0,9 GWh og melkefjøset med 0,2 GWh, bruker skolen i vid forstand (alle undervisningsbygg, kontor, internat, kjøkken, anleggshall, verksted, smie, ammekufjøs, saufjøs, stall og grisefjøs) 0,9 GWh strøm til lys, kontorutstyr,, ventilasjon, og varmtvann hvert år. Dette har vært stabilt de siste 5 år

Strøm – vi antar at tall fra NTE er riktige og da er forbruk fordelt slik

År	Skole	Kjel skole	Teknisk veksthus	Lys og Mære 1	Grishuset	Mære 2	Melkefjøset	Sum kWh
2009	1 061 759	203 929	102 192	819 252	80 341			2 267 473
2010	1 057 475	210 916	96 864	746 357	90 836			2 202 448
2011	1 043 748	131 441	232 682	457 788	86 369			1 952 029
2012	990 382	211 504	171 042	740 501	88 931			2 202 359
2013	881 035	207 635	106 074	443 026	88 076			1 725 846
2014	821 956	224 379	113 972	744 946	87 868			1 993 120
2015	812 906	252 910	109 516	964 026	93 170	68 141		2 300 669
2016	826 892	151 341	101 447	999 732	93 067	211 646	123 040	2 507 164
2017	801 652	119 328	95 693	747 890	97 467	277 594	179 101	2 318 725
2 018	796 247	20 077	137 353	895 252	94 985	301 118	200 647	2 445 680

- Skolebygg nedgang fra over 1 000 000 til ca 800 000
- Elkjel gikk stabilt omkring 200 000 kWh, men lite i 2018

Totalt forbruk kWh Mære 2009-2018

År	Sum strøm kWh	Bio kwh	Propan/Olje kwh	Varmelager ut kwh	Tot energi-forbruk
2009	2 267 473	361 600	996 648		3 625 721
2010	2 202 448	541 560	1 103 980		3 847 988
2011	1 952 029	470 296	667 536	335 274	3 425 135
2012	2 202 359	518 168	612 480	313 878	3 646 885
2013	1 725 846	465 224	602 388	238 994	3 032 452
2014	1 993 120	438 920	728 172	160 697	3 320 909
2015	2 300 669	318 560	445 716	393 526	3 458 471
2016	2 507 164	219 560	-	649 948	3 376 672
2017	2 318 725			879 916	3 198 641
2018	2 445 680			963 203	3 408 883

•Vi ser det er rimelig stabilt over år – men bio og fosilt er byttet med energi fra varmelager

Solceller hybelhus 20.juni-31.des
18 22,32 MWh = 22 320 kWh

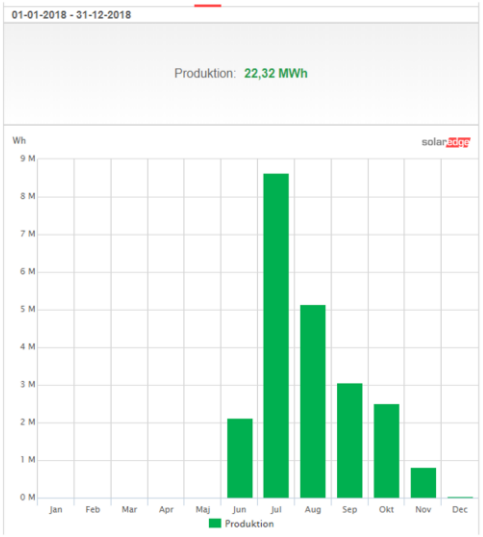

Solceller ammekufjøs 24,34 MWh = 24 340 kWh
(litt under beregning på forrige side 30 000 kWh)

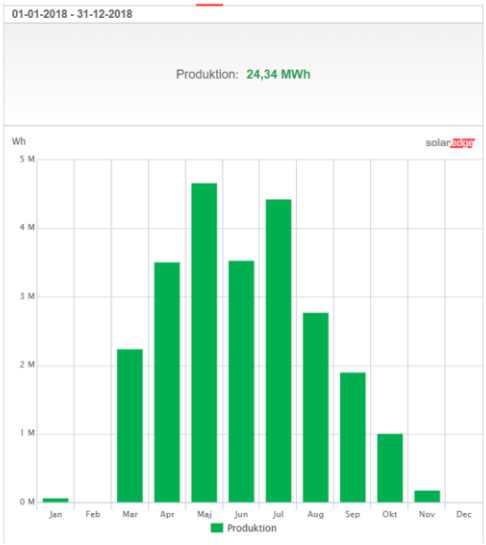

A.5: Datasheet for the photovoltaic module (PERC 300W 60 CELLS)

SUNPRO POWER CO.,LTD

SP315-60M PERC BLACK MONO

280W/290W/300W/310W/315W

Mono-Crystalline Photovoltaic Module

Power tolerance
0~±3%

Withstand strong snow load
5400 Pa / wind load 2400 Pa

Excellent low light performance
3.5% relative eff.reduction at low-irradiance(200W/m²)

100% EL online Inspection
Better module reliability

AMMONIA & SALT RESISTANCE
PID FREE

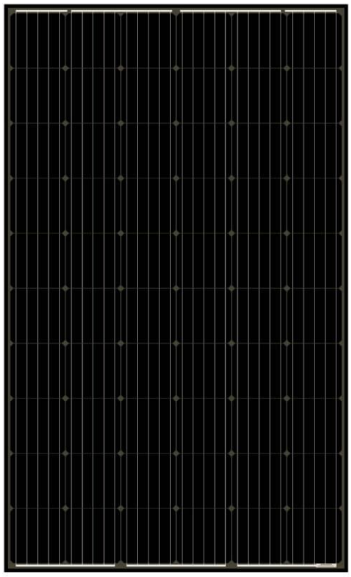

Reliability & Certification

Product Guarantee: 10-year
Linear Performance Warranty
10-year : 90.7% power output
25-year : 80.2% power output

ISO 14001 ISO 9001 OHSAS 18001

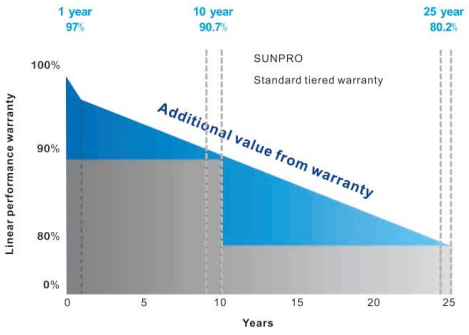

Product Specification

Electrical parameters at standard test conditions
(STC:AM=1.5,1000W/m^2,Cells Temperature 25°C)

Typical type	280W	290W	300W	310W	315W
Max power(Pmax)	280	290	300	310	315
Max power voltage(Vmp)	31. 72	32.44	32.6	32.55	33.2
Max power current(Imp)	8. 83	8.94	9. 19	9.56	9.49
Open circuit voltage(Voc)	38. 11	39.11	39.9	40.0	40.7
Short circuit current(Isc)	9. 38	9.54	9.64	9.81	10.04
Module Efficiency(%)	17. 21	17.82	18. 3	19.1	19.2
Max system voltage	DC 1500V(TUV) / DC 1000V(TUV)				
Maximum Series Fuse Rating	15A				

Mechanical Data

Item	Specification
Dimensions	1640x992x35mm
Weight	18kgs
Front glass	3.2mm tempered glass
Output cables	4mm^2 symmetrical lengths 900mm
Connectors	MC4 compatible IP67
Cell type	Mono Crystalline Silicon PERC 156.75mm x 156.75mm
Number of cells	60 cells in series

Temperature Characteristics

Item	Specification
Temp.Coeff.of Isc(TK Isc)	0.495%/°C
Temp.Coeff.of Voc(TK Voc)	-0.2893%/°C
Temp.Coeff.of Pmax(TK Pmax)	-0.40%/°C
Operating temperature	-40~+85°C
Normal operating cell temperature	45±2°C

Packing Configuration

Item	Specification		
Container	20'GP	40'GP	40'HQ
Pieces per pallet	60	52	64
Pallets per container	6	14	14
Pieces per container	360	728	896

Tests, Certifications and Warranties

Item	Specification
Standard tests	IEC 61215, IEC 61730
System certs	ISO 9001, ISO14001, OHSAS 18001
Certifications	TUV, AMMONIA AND SALT MIST CORROSION, ANTI-PID, CE, WEEE, INMERTRO
Extreme wind and snow loads testing	Withstand extreme wind(2400 Pascal) and snow loads(5400 Pascal)
Power tolerance	0~±3%
Junction box	IP67
Warranties	10 years product warranty and 25 years 80% of power

Dimensions and Structure

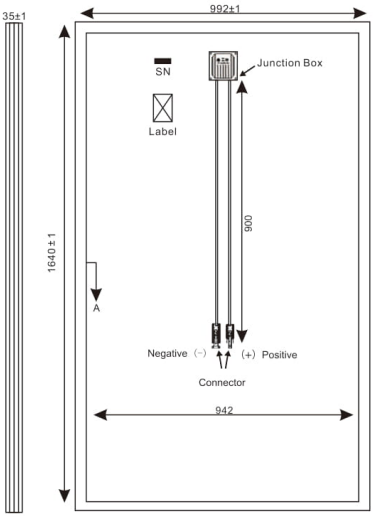

I-V Curve

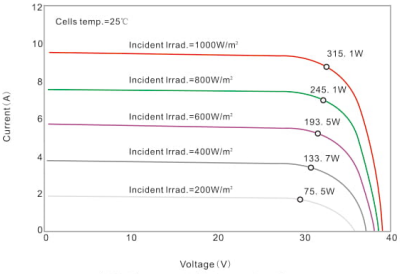

I-V Curves at different irradiance

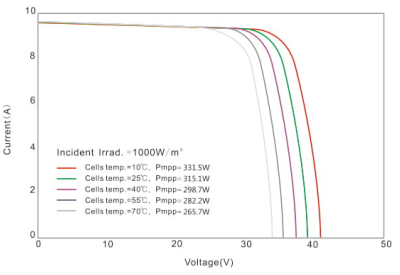

I-V Curves at different temperature

A.6: Datasheets for the inverters used in *Inverter System 1*

Delta Solar M50A Grid PV Inverter

RPI M50A

High efficiency 3-phase solar inverters for the European market - Perfect choice for large-scale solar PV systems, such as those used in the commercial or agricultural sectors.

Versatile applications

- Aluminium housing ensures long lasting protection against moisture and corrosion
- Wide input voltage range
- Suitable for indoor and outdoor applications (IP65)
- Compact design for simplified installation – exceptional power density-to-size ratio

Maximum profitability

- Peak efficiency of 98.6 %
- Built-in and replaceable AC and DC-side Type 2 SPDs (surge protection devices) and string fuses [4)]
- 2 MPP trackers - symmetrical and asymmetrical loading possible (40/60 % or 60/40 %)
- Nominal apparent power 50 kVA (55 kVA max. apparent power possible [8)])

www.solar-inverter.com

50 kVA transformerless solar inverters

Technical data RPI M50A

INPUT (DC)	RPI M50A
Max. recommended PV power	70 kW_p 1)
Max. input power	58 kW
Nominal power	52 kW 2)
Voltage range	200 ... 1100 V 3)
MPP operating voltage range	200 ... 1000 V
Startup voltage	250 V
Voltage range for maximum power	520 ... 800 V symmetrical load (50/50 %)
Max. current	100 A (50 A per MPP tracker)
Max. number of MPP trackers	Parallel inputs: 1 MPP tracker Separate inputs: 2 MPP trackers
Input load	≤ 34.8 kW per MPPT, symmetrical and asymmetrical
String Fuse Protection	15 A 4)
Surge Protection Devices 5)	Type 2
OUTPUT (AC)	
Max. apparent power	55 kVA 6) 8)
Nominal apparent power	50 kVA 6)
Voltage range	230 ± 20% / 400 V ± 20% 7) 3 phase + PE or 3 phase + N + PE
Nominal current	73 A 8)
Nominal frequency	50 / 60 Hz
Frequency range	50 / 60 Hz ± 5 Hz 7)
Power factor adjustable	0.8 cap ... 0.8 ind
Total harmonic distortion (THD)	< 3 % @ nominal apparent power
Surge Protection Devices 5)	Type 2
GENERAL SPECIFICATION	
Model name	RPI M50A
Part numbers Delta 5)	RPI M50A_120 Model: RPI503FA0E0000 RPI M50A_122 Model: RPI503FA0E0200
Max. efficiency	98.6 %
Efficiency EU	98.4 %
Operating temperature	-25 ... +60 °C
Full power without derating	-25 ... +40 °C
Storage temperature	-25 ... +60 °C
Humidity	0 ... 100 % non-condensing
Max. operating altitude	2000 m (above sea level)
Standard guarantee	5 years (guarantee extension is possible)
MECHANICAL DESIGN	
Size (L x W x D)	740 × 612 × 278 mm
Weight	74 kg
Cooling	Fans
AC connector	China Aviation Optical-Electrical Technology Co. PVE5T125KE36 (included)
DC connector	10 pairs of Multi-Contact MC4 (included)
Communication interfaces	2 x RS485, 2 x Dry contacts, 1 x EPO, 6 x Digital inputs
DC disconnector	Integrated
Display	2 LEDs, 4-line LCD

www.solar-inverter.com

May 20, 2015 - All information and specifications are subject to change without notice

SAFETY / STANDARDS	RPI M50A
Protection degree	IP65
Safety class	I
Configurable trip parameters	Yes
Insulation monitoring	Yes
Overload behavior	Current limitation; power limitation
Anti-islanding protection / Grid regulation	VDE 0126-1-1/A1; UTE C15-712-1 VDE 16 1-1 A1 VFR 2013/VFR 2014; UTE C15-712 MV; French Islands (50 Hz/60 Hz); G59/3 LV; VDE-AR-N 4105; BDEW; ÖNORM E8001-4-712 + A1: 04/2014; TOR D4
EMC	EN61000-6-2; EN61000-6-3; EN61000-3-11; EN61000-3-12
Safety	IEC62109-1 / -2; CE compliance

1) When operated with balanced DC inputs (50/50 %)
2) Max. 34.8 kW per DC input with asymmetrical load (60/40 %)
3) For some firmware versions limited to 1000 V
4) The value when internal temperature of the inverter is 25 °C. At higher internal temperatures, the value may drop to 10 A.
5) RPI M50_120 model has integrated AC & DC-side Type 2 SPDs
RPI M50_122 model without SPDs
6) Cos Phi = 1 (VA = W)
7) AC voltage and frequency range will be programmed according to the individual country requirements.
8) 55 kVA / 80A AC is possible under the following conditions: DC input voltage 600 V with symmetrical load and ambient temp. is < 34 °C.

	DC SPDs	AC SPDs	String Fuses
RPI M50A_120	X	X	X
RPI M50A_122			X

The M50A is available with (M50A_120) and without (M50A_122) AC and DC surge protection devices (SPDs). Important: The model RPI M50A_122 contains no sockets for SPDs.

United Kingdom
Email: sales.uk@solar-inverter.com
Tel: 0800 051 4280 (Free Call)

International
Email: sales.europe@solar-inverter.com
Tel: +49 7641 455 547

SMA Sunny Tripower 4.0 PV Inverter

SUNNY TRIPOWER 3.0 / 4.0 / 5.0 / 6.0
With SMA SMART CONNECTED

Compact
- One-person installation due to low weight of 17 kg
- Compact design means minimum space requirements

Easy to use
- 100% plug and play installation
- Free online monitoring via Sunny Places
- Automated service thanks to SMA Smart Connected

High yields
- Use of surplus energy through dynamic active power limitation
- Shade management with OptiTrac Global Peak or integrated TS4-R communication

Combinable
- Intelligent energy management and storage solutions can be added anytime
- Can be combined with TS4-R components for module optimization

SUNNY TRIPOWER 3.0 / 4.0 / 5.0 / 6.0

Higher yields for private homes – intelligent solar power generation

The new Sunny Tripower 3.0–6.0 ensures maximum energy yields for private homes. This inverter combines the integrated Service SMA Smart Connected service and intelligent technology for all ambient requirements. Thanks to its extremely light design, the device can be installed quickly and easily. The Sunny Tripower can be commissioned quickly via smartphone or tablet thanks to its integrated web interface. For specific requirements on the roof, such as shading, the TS4-R module optimizers can be added into the system, with all communication and monitoring facilitated through the inverter. Current communication standards make the inverter future-proof, meaning intelligent energy management solutions as well as SMA storage solutions can be flexibly added anytime.

Efficiency curve

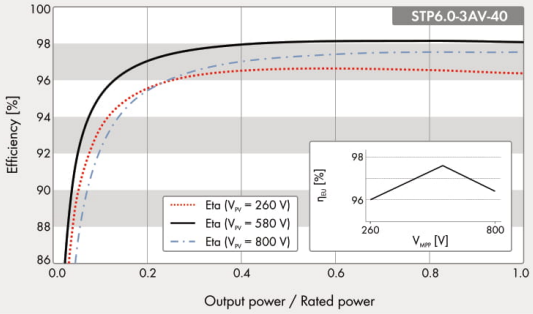

Accessories (optional)

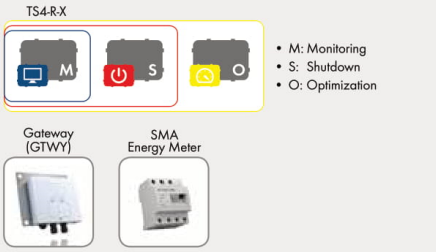

● Standard features ○ Optional features – not available
Data in nominal conditions
Last revision: August 2018

Technical data	Sunny Tripower 3.0	Sunny Tripower 4.0	Sunny Tripower 5.0	Sunny Tripower 6.0
Input (DC)				
Max. PV array power	6000 Wp	8000 Wp	9000 Wp	9000 Wp
Max. input voltage	850 V	850 V	850 V	850 V
MPP voltage range	140 V to 800 V	175 V to 800 V	215 V to 800 V	260 V to 800 V
Rated input voltage	580 V			
Min. input voltage / initial input voltage	125 V / 150 V			
Max. input current input A / input B	12 A / 12 A			
Max. DC short-circuit current input A/input B	18 A / 18 A			
Number of independent MPP inputs / strings per MPP input	2/A: 1; B: 1			
Output (AC)				
Rated power (at 230 V, 50 Hz)	3000 W	4000 W	5000 W	6000 W
Max. apparent power AC	3000 VA	4000 VA	5000 VA	6000 VA
Nominal AC voltage	3/N/PE; 220 V / 380 V 3/N/PE; 230 V / 400 V 3/N/PE; 240 V / 415 V			
AC voltage range	180 V to 280 V			
AC grid frequency / range	50 Hz / 45 Hz to 55 Hz 60 Hz / 55 Hz to 65 Hz			
Rated grid frequency / rated grid voltage	50 Hz / 230 V			
Max. output current	3 x 4.5 A	3 x 5.8 A	3 x 7.6 A	3 x 9.1 A
Power factor at rated power / Displacement power factor, adjustable	1 / 0.8 overexcited to 0.8 underexcited			
Feed-in phases / connection phases	3 / 3			
Efficiency				
Max. efficiency / European efficiency	98.2% / 96.5%	98.2% / 97.1%	98.2% / 97.4%	98.2% / 97.6%
Protective devices				
Input-side disconnection point	●			
Ground fault monitoring / grid monitoring	● / ●			
DC reverse polarity protection / AC short circuit current capability / galvanically isolated	● / ● / –			
All-pole-sensitive residual-current monitoring unit	●			
Protection class (according to IEC 62103) / surge category (according to IEC 60664-1)	I / III			
General data				
Dimensions (W / H /D)	435 mm / 470 mm / 176 mm (17.1 inches / 18.5 inches / 6.9 inches)			
Weight	17 kg (37.4 lbs)			
Operating temperature range	-25°C to +60°C (-13°F to +140°F)			
Noise emission, typical	30 dB(A)			
Self-consumption (at night)	5.0 W			
Topology / Cooling concept	Transformerless / Convection			
Degree of protection (according to IEC 60529)	IP65			
Climatic category (according to IEC 60721-3-4)	4K4H			
Max. permissible value for relative humidity (non-condensing)	100%			
Equipment				
DC connection / AC connection	SUNCLIX / AC connector			
Display via smartphone, tablet, laptop	●			
Interfaces: WLAN / Ethernet / RS485	● / ● / ●			
Communication protocols	Modbus (SMA, Sunspec), Webconnect, SMA Data, TS4-R			
Shade management: OptiTrac Global Peak / TS4-R	● / ○			
Warranty: 5 / 10 / 15 years	● / ○ / ○			
Certificates and permits (more available upon request)	AS 4777, C10/11, CE, CEI 0-21, DIN EN 62109-1/IEC 62109-1, DIN EN 62109-2/IEC 62109-2, EN 50438, G59/3, G83/2, NEN-EN 50438, ÖVE / ÖNORM E 8001-4-712, PPDS, PPC, RD 1699, SI 4777, TR 3.2.1, UTE C15-712, VDE-AR-N 4105, VDE-0126-1-1, VFR 2014			
Certificates and approvals (currently being planned)	DEWA 2016, EN 62116, IEC 61727, IE-EN 50438, NBR 16149, NRS 097-2-1			
Country availability of SMA Smart Connected	AU, AT, BE, CH, DE, ES, FR, IT, LU, NL, UK			
Type designation	STP3.0-3AV-40	STP4.0-3AV-40	STP5.0-3AV-40	STP6.0-3AV-40

A.7: Datasheets for the inverters used in *Inverter System 2*

SUNNY TRIPOWER 8.0 / 10.0
with SMA SMART CONNECTED

Compact
- One-person installation due to low weight of 20.5 kg
- Compact design means minimum space requirements

Easy to use
- 100% plug and play installation
- Free online monitoring via Sunny Places
- Automated service thanks to SMA Smart Connected

High yields
- Use of surplus energy through dynamic active power limitation
- Yield increase without installation effort due to integrated shade management SMA ShadeFix

Combinable
- Intelligent energy management and storage solutions can be added anytime
- Can be combined with TS4-R components for module optimization

SUNNY TRIPOWER 8.0 / 10.0

Higher yields for private homes – intelligent solar power generation

The new Sunny Tripower 8.0–10.0 ensures maximum energy yields for private homes. This inverter combines the integrated SMA Smart Connected service with intelligent technology for all ambient conditions. Thanks to its extremely light design, the device can be installed quickly and easily. The Sunny Tripower can be commissioned quickly via smartphone or tablet thanks to its integrated web interface. For specific requirements on the roof, such as shading, the TS4-R module optimizers can be added into the system, with all communication and monitoring facilitated through the inverter. Current communication standards make the inverter future-proof, meaning intelligent energy management solutions as well as SMA storage solutions can be flexibly added anytime.

Efficiency curve

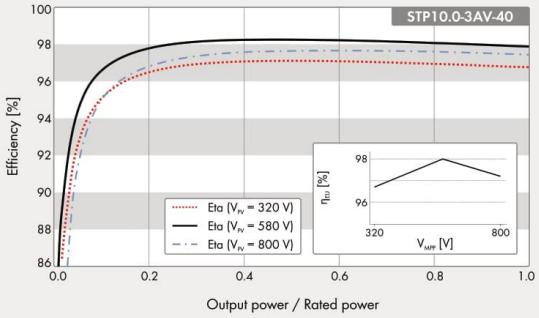

Accessories (optional)

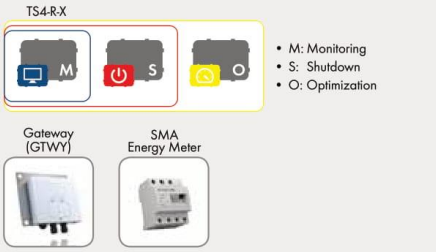

● Standard features ○ Optional features – not available
Data in nominal conditions
Last updated: 11/2019

Technical data	Sunny Tripower 8.0	Sunny Tripower 10.0
Input (DC)		
Max. PV array power	15000 Wp	15000 Wp
Max. input voltage	1000 V	1000 V
MPP voltage range	260 V to 800 V	320 V to 800 V
Rated input voltage	580 V	
Min. input voltage / initial input voltage	125 V / 150 V	
Max. input current input A / input B	20 A / 12 A	
Max. DC short-circuit current input A / input B	30 A / 18 A	
Number of independent MPP inputs / strings per MPP input	2 / A:2; B:1	
Output (AC)		
Rated power (at 230 V, 50 Hz)	8000 W	10000 W
Max. apparent AC power	8000 VA	10000 VA
Nominal AC voltage	3 / N / PE; 220 V / 380 V 3 / N / PE; 230 V / 400 V 3 / N / PE; 240 V / 415 V	
AC voltage range	180 V to 280 V	
AC grid frequency / range	50 Hz / 45 Hz to 55 Hz 60 Hz / 55 Hz to 65 Hz	
Rated grid frequency / rated grid voltage	50 Hz / 230 V	
Max. output current	3 x 12.1 A	3 x 14.5 A
Power factor at rated power / displacement power factor adjustable	1 / 0.8 overexcited to 0.8 underexcited	
Feed-in phases / connection phases	3 / 3	
Efficiency		
Max. efficiency / European efficiency	98.3 % / 97.7 %	98.3 % / 98.0 %
Protective devices		
Input-side disconnection point	●	
Ground fault monitoring / grid monitoring	● / ●	
DC reverse polarity protection / AC short circuit current capability / galvanically isolated	● / ● / –	
All-pole-sensitive residual-current monitoring unit	●	
Protection class (according to IEC 61140) / surge category (according to IEC 60664-1)	I / III	
General data		
Dimensions (W / H / D)	460 mm / 497 mm / 176 mm (18.1 inches / 19.6 inches / 6.9 inches)	
Weight	20.5 kg (45.2 lbs)	
Operating temperature range	-25 °C to +60 °C (-13 °F to +140 °F)	
Noise emission, typical	30 dB(A)	
Self-consumption (at night)	5.0 W	
Topology / cooling method	Transformerless / convection	
Degree of protection (according to IEC 60529)	IP65	
Climatic category (according to IEC 60721-3-4)	4K4H	
Max. permissible value for relative humidity (non-condensing)	100%	
Features		
DC connection / AC connection	SUNCLIX / AC connector	
Display via smartphone, tablet, laptop	●	
Interfaces: WLAN / Ethernet / RS485	● / ● / ●	
Communication protocols	Modbus (SMA, Sunspec), Webconnect, SMA Data, TS4-R	
Shade management: SMA ShadeFix (integrated) / TS4-R	● / ○	
Warranty: 5 / 10 / 15 years	● / ○ / ○	
Certificates and permits (more available upon request)	AS 4777.2, C10/11, CE, CEI 0-21, EN 50438, G59/3-4, G83/2-1, DIN EN 62109 / IEC 62109, NEN-EN50438, ÖVE/ÖNORM E 8001-4-712 & TOR D4, PPC, PPDS, RD1699, SI4777, TR3.2.1, UTE C15-712, VDE-AR-N 4105, VDE0126-1-1, VFR 2014, RfG compliant	
Certificates and approvals (planned)	DEWA, IEC 61727, IEC 62116, IE-EN50438, MEA, NBR16149, NT_Ley20.571, PEA, TR3.2.2	
Country availability of SMA Smart Connected	AU, AT, BE, CH, DE, ES, FR, IT, LU, NL, UK	
Type designation	STP8.0-3AV-40	STP10.0-3AV-40

A.8: Datasheets for the inverters used in *Inverter System 3*

APsystems

Leading the Industry in
Solar Microinverter Technology

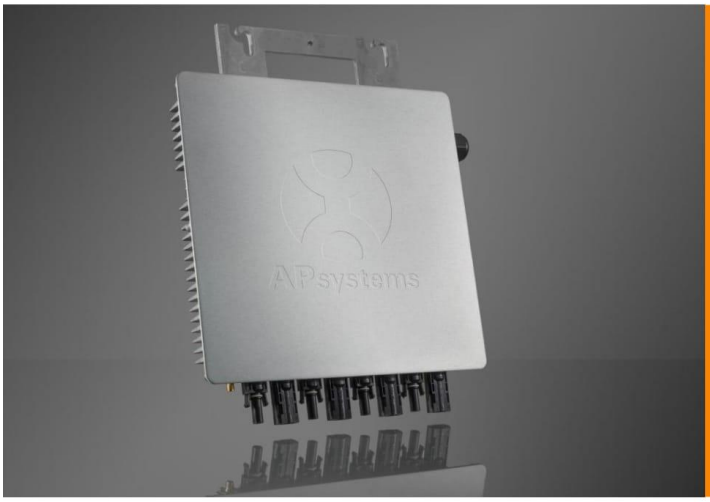

YC1000-3

3-Phase Microinverter

- Single unit connects up to four modules
- Maximum 1130W AC output
- True 3-phase output
- ZigBee wireless communication and monitoring
- Up to 48 solar modules (60 or 72-cell) can be linked in a single 20A circuit*

*Please see YC1000 user manual on specifi cs for 230/400VAC.

World's first true 3-phase microinverter – only from APsystems

WIRING SCHEMATIC

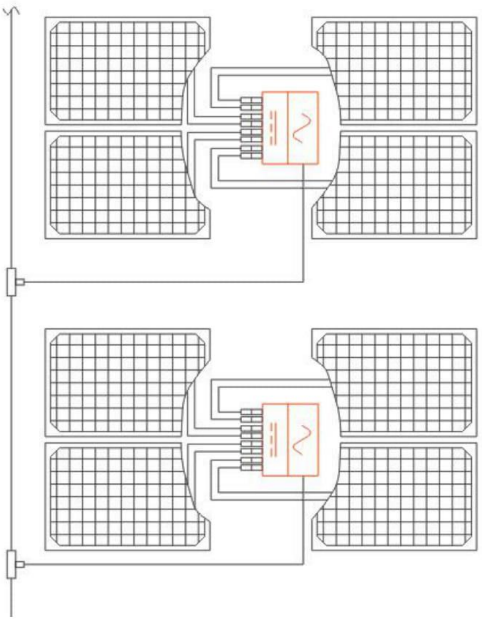

The YC1000 is the industry's first true 3-phase solar microinverter, handling commercial grid voltages of 230/400 with 1130 watts maximum output, ZigBee communication and an integrated ground. Each YC1000 supports up to 4 solar modules.

DIMENSIONS

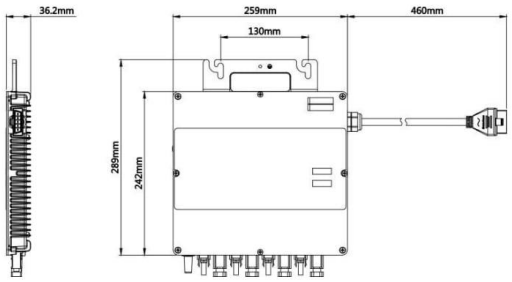

YC1000-3 3-Phase Microinverter Datasheet

Region	Netherlands,France,Portugal,Switzerland
Model	YC1000-3-EU
Input Data (DC)	
Recommended PV Module Power (STC)Range	Up to 310 Wp (4 Module configuration) Up to 360 Wp (3 Module configuration)
MPPT Voltage Range	16V-55V
Operation Voltage Range	16V-55V
Maximum Input Voltage	60V
Startup Voltage	22V
Maximum Input Current	14.8A×4
Output Data (AC)	
3-Phase Grid Type	230V/400V
Rated Output Power	900W
Maximum Output Power	1130W
Nominal Output Current	1.44A×3
Nominal Output Voltage	230V×3
Default Output Voltage Range	184V-253V*
Extended Output Voltage Range	149V-278V
Nominal Output Frequency	50Hz
Default Output Frequency Range	48Hz-51Hz*
Extended Output Frequency Range	45.1Hz-54.9 Hz
Power Factor	>0.99
Total Harmonic Distortion	<3%
Maximum Units per Branch (20 A)	12 for 20A X 3 Breaker / 48 Modules
Efficiency	
Peak Efficiency	95%
CEC Weighted Efficiency	94.5%
Nominal MPPT Efficiency	99.9%
Night Power Consumption	300mW
Mechanical Data	
Operating Ambient Temperature Range	-40°C to +65°C
Storage Temperature Range	-40°C to +85°C
Dimensions (W x H x D)	259mm × 242mm × 36mm
AC BUS Maximum Current	20A
Weight	3.5kg
Enclosure Rating	IP67
Cooling	Natural Convection - No Fans
Features & Compliance	
Communication	Zigbee
Safety and EMC Compliance	EN 62109-1; EN 62109-2;EN61000-6-1; EN61000-6-2; EN61000-6-3; EN61000-6-4;
Grid Connection Compliance	EN50438;VDE126-1-1
Transformer Design	High Frequency Transformers, Galvanically Isolated

* Programmable through ECU in field to meet customer need.

Rue des Monts dor ZAC de Folliouses Sud-Les Echets 01700 Miribel, France | +33-481 65 60 40 | **APsystems.com** | emea@APsystems.com

A.9: Battery sizing worksheet – Wholesale Solar

Battery Sizing Worksheet

1. Enter your daily amp-hour requirement.
(Divide watts per day by 12, 24, or 48, depending on your system voltage.)
AH/ Day _____

2. Enter the maximum number of consecutive cloudy weather days expected in your area, or the number of days of autonomy you would like your system to support.
(We use 3 - 5 days.)._____

3. Multiply the amp-hour requirement by the number of days. This is the amount of amps-hours your system will need to store. AH _____

4. Enter the depth of discharge for the battery you have chosen. This provides a safety factor so that you can avoid over-discharging your battery bank. This number should not exceed 0.8. We use 50% maximum or 0.5 _____

5. Divide line 3 by line 4 . AH _____

6.Select the multiplier (below,next page) that corresponds to the average winter time ambient temperature your battery bank will experience._____

7. Multiply line 5 by line 6. This calculation ensures that your battery bank will have enough capacity to overcome cold weather effects. This number represents the total battery capacity you will need. AH _____

8. Enter the amp-hour rating for the battery you have chosen._____
Click specific battery page for AH rating on batteries—
http://wholesalesolar.com/products.folder/battery-folder/concorde.html or
http://wholesalesolar.com/products.folder/battery-folder/Surretterolls.html

9. Divide the total battery capacity (#7) by the battery amp-hour rating (#8) and round off to the next highest number. This is the number of the batteries wired in parallel required._____

10. Divide the nominal system voltage (12V, 24V, or 48V) by the battery voltage and round off to the next highest number. This is the number of batteries wired in series._____

11. Multiply line 9 by line 10. This is the total number of batteries required._____

Wholesale Solar
wholesalesolar.com
1 800 472-1142

Ambient Temperature Multiplier

80F	26.7C	1.00
70F	21.2C	1.04
60F	15.6C	1.11
50F	10.0C	1.19
40F	4.4C	1.30
30F	-1.1C	1.40
20F	-6.7C	1.59

A.10: Permission to use Figure 7 in (Zijdemans, 2014) by NemiTek

Hei!

Mitt navn er Dan Remi Antonsen, og jeg skriver for tiden en masteroppgave om solcellepaneler og solfangere for NTNU Gløshaugen i Trondheim.

Grunnen til at jeg sender dere en e-post er fordi jeg kunne tenke meg å bruke en figur ifra boken "Vannbaserte oppvarmings- og kjølesystemer" (2014), skrevet av David Zijdemans, og utgitt av dere, i min masteroppgave. Den spesifikke boken jeg tenker på er 3. utgave (Opplag 2018), og figuren jeg tenker på er **Figure 3.43 midlere globalinnstråling per døgn i Norge for januar og juli måned**. Figuren viser oversiktlig de forskjellige strålingsintensivitetene i Norge, og føler at denne kan være et godt tilskudd til teksten i oppgaven min.

Jeg lurte om jeg kunne få tillatelse til å bruke denne figuren i masteroppgaven min, eller hva som eventuelt må til for at jeg skal få lov å bruke den?

Hvis dere ikke ønsker å gi meg tillatelse til å bruke figuren har jeg full forståelse for dette.

Jeg må så klart oppgi at masteroppgaver ved NTNU blir publisert, men at hvis jeg får tillatelse til å bruke figuren kommer jeg til å referere til opprinnelig eier av figuren, samt legge ved korrespondansen som viser tillatelsen i vedlegg slik at det ikke er noen tvil om hvem som har rettighetene.

Tusen takk for alt av hjelp!

Vennlig hilsen
Dan Remi Antonsen
Tel: +47 99 32 97 92
5. Klasse Energi og miljø

Hei,
Så hyggelig at du ønsker å bruke en av Davids (og våre) illustrasjoner. :-D
Du kan gjerne bruke figuren så lenge som du oppgir kilden.

Lykke til med oppgaven!

Med vennlig hilsen

Maria Rosander Hagen
Kundeservice Kompetansebiblioteket
(+47) 906 99 353
–
NemiTekAS
Besøksadr.: Hagegata 22, 0653 Oslo
Postadr.: Postboks 2843 Tøyen, 0608 Oslo
Org.nr. 915 903 037
nemitek.no

A.11: Permission to use relevant figures in Chapter 5 by the administration

Dan Remi Antonsen
I går, 15:27
Tove Jystad <tovjy@trondelagfylke.no>

Hei Tove,

Lenge siden sist! Håper alt står bra til med dere på Mære landbruksskole.

Jeg lurte på om jeg kunne få bruke noen av bildene fra konkurransegrunnlaget og systemtegningen deres i masteroppgaven min?

Tove Jystad <tovjy@trondelagfylke.no>
I dag, 08:49

Det er bare å bruke dette. Lykke til med siste runde.

Med vennlig hilsen
Tove Jystad
Tlf: 74 17 63 17 / 414 13 441
...

Dan Remi Antonsen
I går, 15:31
Tove Jystad <tovjy@trondelagfylke.no>

I tillegg lurte jeg på dette bilde fra Trøndelag fylkeskommune, hvor det står at dere eier bildet?

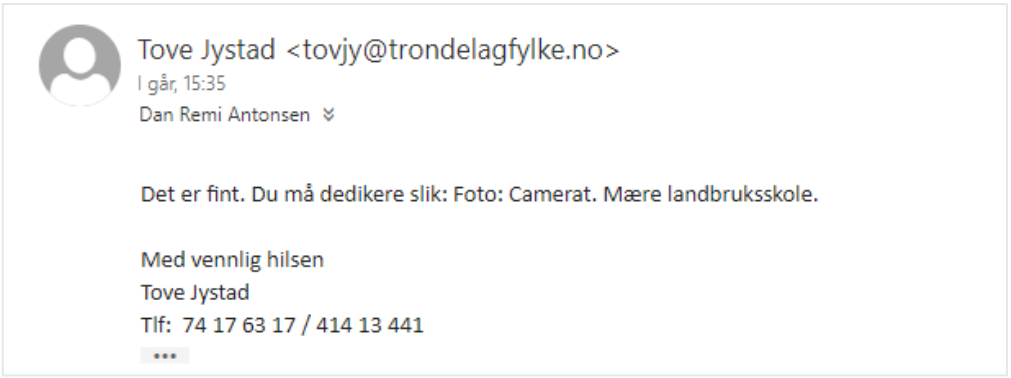

Tove Jystad <tovjy@trondelagfylke.no>
I går, 15:35
Dan Remi Antonsen

Det er fint. Du må dedikere slik: Foto: Camerat. Mære landbruksskole.

Med vennlig hilsen
Tove Jystad
Tlf: 74 17 63 17 / 414 13 441
...

A.12: Details on the air-to-water heat pump in the milk barn

VEDLEGG ELEKTROENTREPRISE – MÆRE
TEKNISKE SPESIFIKASJONER – LUFT/VANN VARMEPUMPE

aroTHERM	Enhet	VWL 55/2 A-230V	VWL 85/2 A-230V	VWL 115/2 A-230V	VWL 155/2 A-230V
Høyde x Bredde x Dybde Vekt med/uten emballasje	mm kg	834 x 970 x 408 90	973 x 1103 x 463 106	973 x 1103 x 463 126	1375 x 1103 X 463 165
Elektriske data/tilslutning		1/NP/PE~230 V, 50 Hz			
Sikring - treg Startstrøm Beskyttelsesart EN 60529	A A IP	1x16 16 25	1x16 16 25	1x20 20 25	1x25 25 25
Varmekrets Maks. driftstrykk Min./ Maks. innløpstemperatur Nominell volumstrøm dT 5 K Rest. transporthøyde dT 8 K Elektrisk ytelsesopptak	 bar °C m³ mbar W	 3 22 / 63 0,86 750 15-70	 3 22 / 63 1,4 690 15-70	 3 22 / 63 1,9 660 15-70	 3 22 / 63 2,59 686 15-70
Kjølekrets Kuldemedie Mengde	 kg	 R410 A 1,8	 R410A 1,95	 R410A 3,53	 R410A 4,4 kg
Kompressortype		Piston rotasjon inverter			
Lydeffekt ute EN 12102 -> EN 14511 LWo	dBA	58	60	65	66
Ytelsesdata Varmepumpe EN 14511					
A7W35 dT5 -> EN 14511 Varmeytelse / Ytelsesopptak Ytelsestall	 kW COP	 4,7/1,1 4,7	 8,1/1,8 4,8	 10,5/2,6 4,2	 14,6/3,4 4,5
A7W55 dT8 -> EN 14511 Varmeytelse / Ytelsesopptak Ytelsestall	 kW COP	 4,2/1,6 2,7	 7,1/2,4 3,0	 9,8/3,5 2,9	 11,2/5,0 2,3
Driftsområde	°C	-15/+46	-20/+46	-20/+46	-20/+46

aroTHERM	Enhet	VWL 115/2 A-400V	VWL 155/2 A-400V
Høyde x Bredde x Dybde Vekt med/uten emballasje	mm kg	973 x 1103 x 463 124	973 x 1103 x 463 165
Elektriske data/tilslutning		3/N/PE~400 V, 50 Hz	
Sikring - treg Startstrøm Beskyttelsesart EN 60529	A A IP	3x16 13 25	3x16 16 25
Varmekrets Maks. driftstrykk Min./ Maks. innløpstemperatur Nominell volumstrøm dT 5 K Rest. transporthøyde dT 8 K Elektrisk ytelsesopptak	 bar °C m³ mbar W	 3 22 / 63 1,8 660 15-70	 3 22 / 63 2,59 686 15-70
Kjølekrets Kuldemedie Mengde	 kg	R410A 3,53	R410A 4,4
Kompressortype		Piston rotasjon inverter	
Lydeffekt ute EN 12102 -> EN 14511 LWo	dBA	65	66
Ytelsesdata Varmepumpe EN 14511			
A7W35 dT5 -> EN 14511 Varmeytelse / Ytelsesopptak Ytelsestall	 kW COP	10,5/2,6 4,2	14,6/3,4 4,5
A7W55 dT8 -> EN 14511 Varmeytelse / Ytelsesopptak Ytelsestall	 kW COP	9,8/3,5 2,9	11,2/5,0 2,3
Driftsområde	°C	-20/+46	-20/+46

Vaillant Group Norge AS
Støttumveien 7 ▮ N-1540 Vestby ▮ Telefon +47 64 95 99 00
Telefaks +47 64 95 99 01 ▮ www.vaillant.no ▮ info@vaillant.no

A.13: Excerpt from the tender documents

Videre skal det innkalkuleres alle nødvendige utgifter i fm. opplegg og tilkobling av følgende utstyr:

- Varmtvannsbereder i tankrom, 250 l, 1 fas, 3 kW.
- Akkumulatortank for varmeanlegg i tankrom, 300 l, 1 fas, 3x5 kW.
- Sirkulasjonspumpe til drikkekar i tankrom, 16 A, 1 fas
- Gulvvarme serviceavdeling, 3 fas, 9 kW.
- Luft – vann varmepumpe i serviceavdeling, se vedlegg med tekniske spesifikasjoner.
- Gårdstank, 32 A sikring ved 400 V. Sikringen skal være treg med minimum C-karakteristikk.
- 3 stk leddheisporter ved forbrett og forsentral. Motorer leveres og monteres av annen leverandør. 1 fas, 0,5 kW på samtlige porter.
- Løfteplattform i heissjakt, 16 A sikring ved 400 V. 3 fas, 2,2 kW. Frekvensstyring for å få myk start/stopp.
- Det skal monteres et balansert ventilasjonsanlegg i serviceavdeling og tekniske spesifikasjoner for anlegget vil bli ettersendt når entreprenør er valgt.

2.7.2 Virksomhet

Herunder skal det medtas installasjoner for virksomheten som de enkelte rom omfatter.

1. Følgende antall stikkontakter tas med:
   - Serviceavdeling 1. etg
     - 1 dobbel stikk 1 fas på tankrom.
     - 1 enkel stikk 1 fas for sentral til trådløse romtermostater i tankrom
     - 2 doble stikk 1 fas på ansattegarderobe.
     - 2 doble stikk 1 fas på herregarderobe
     - 2 doble stikk 1 fas på damegarderobe
     - 1 dobbel stikk 1 fas i bøttekott
     - Egen 16 A kurs til vaskemaskin i bøttekott
     - Egen 16 A kurs til tørketrommel i bøttekott
     - 2 doble stikk i gangareal
     - 2 doble stikk i gangareal mot fjøs
     - 1 hylle med varme til støvler i huk ved akse C6
     - 2 doble stikk til HC toalett
     - 1 dobbel stikk i wc i gang mot fjøs
     - 1 enkel stikkontakt 1 fas i fordelerskap for gulvvarme på tankrom

   - Serviceavdeling 2. etg
     - 2 doble stikk 1 fas på møterom
     - 3 triple stikk 1 fas på møterom
     - 1.dobbel 1 fas i tak på møterom
     - 6 doble stikk 1 fas på kontor (Datasystem skal ha eget vern)
     - 1 dobbel stikk 1 fas på teknisk rom

A.14: SketchUp model for estimating the pipeline lengths

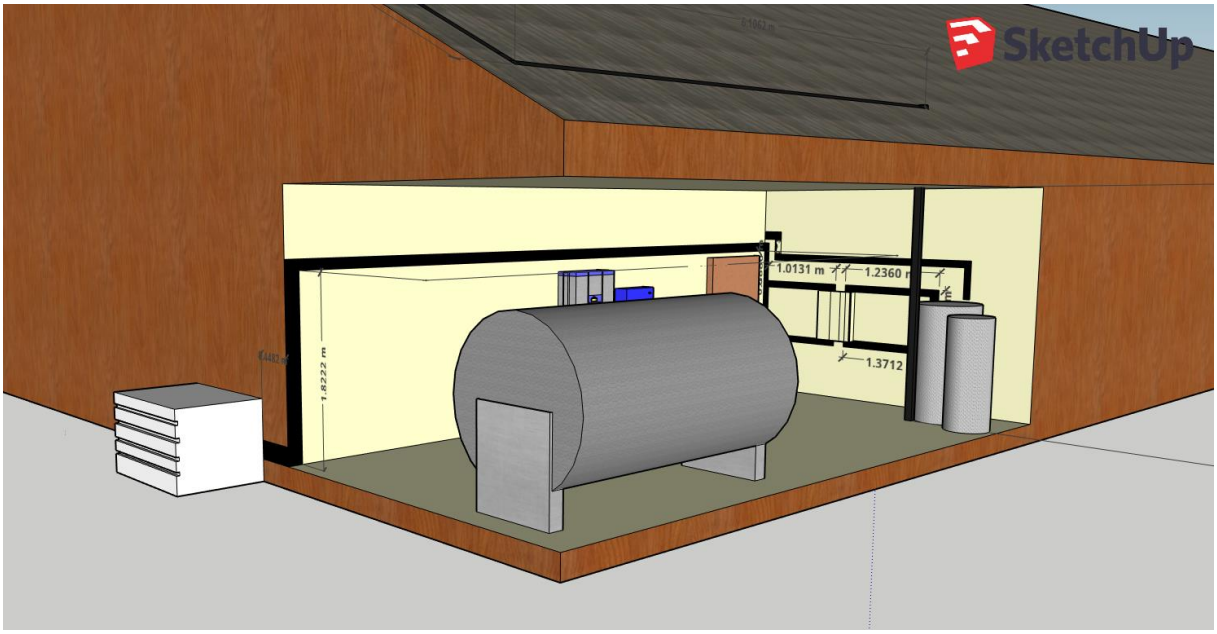

Figure 117: Technical room (with outdoor heat pump).

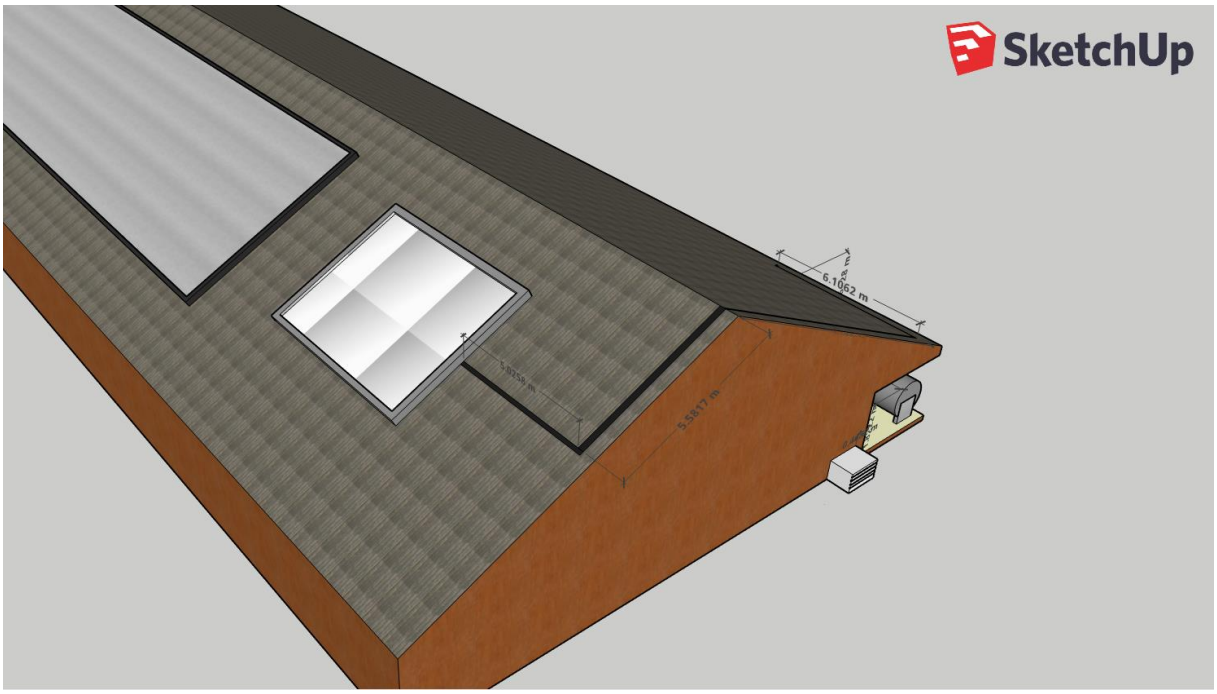

Figure 118: Solar collectors and photovoltaic modules on the roof.

A.15: Tables and figures relevant for the results of the photovoltaic system

Hourly electricity production from photovoltaic system 1, 2 & 3

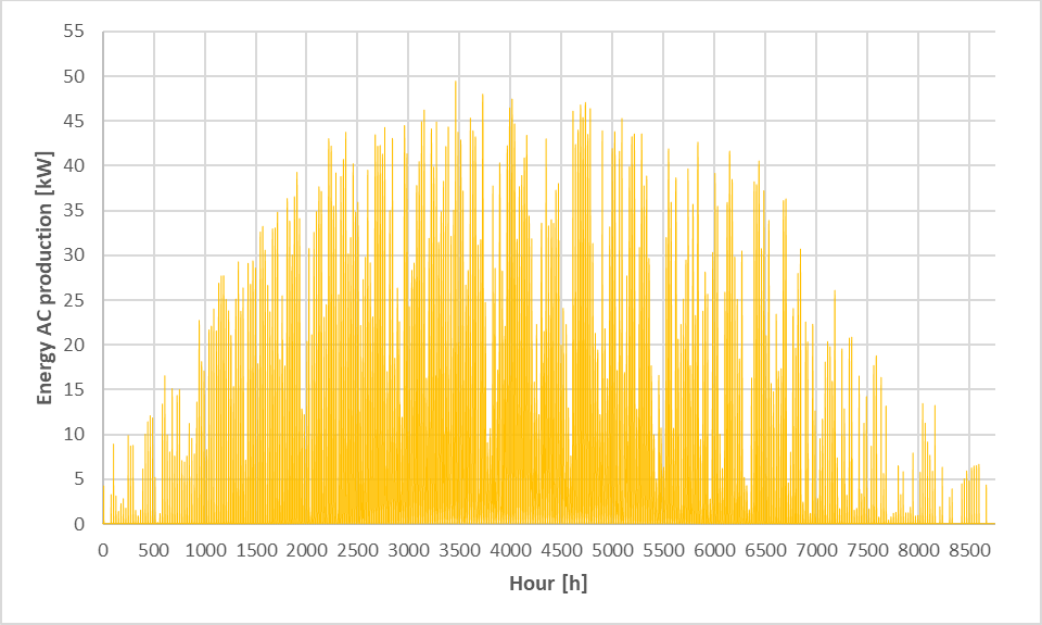

Figure 119: Hourly energy AC production for photovoltaic system 1.

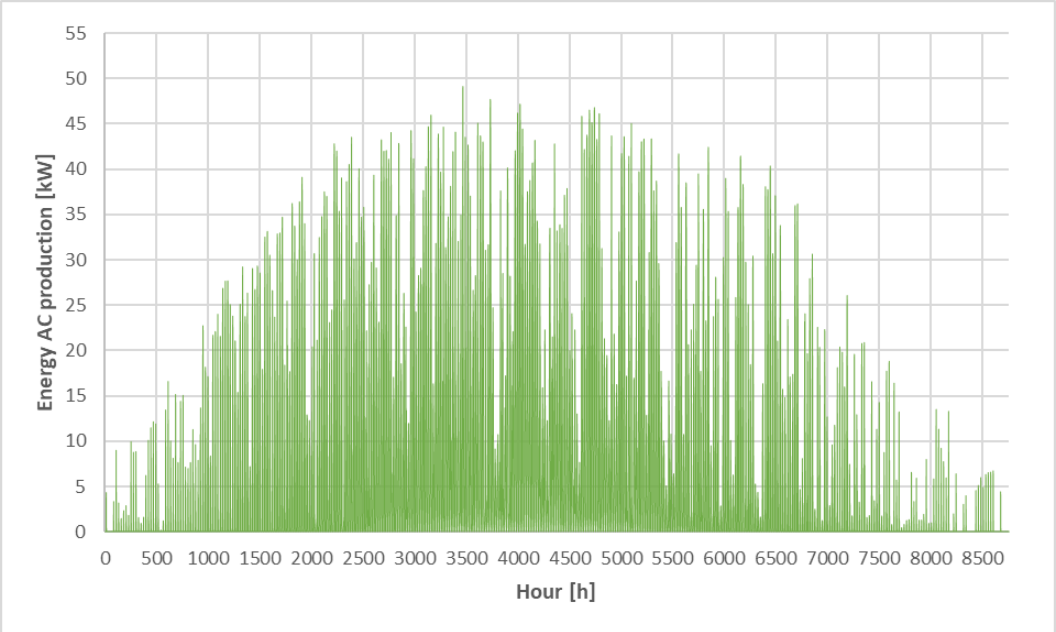

Figure 120: Hourly energy AC production for photovoltaic system 2.

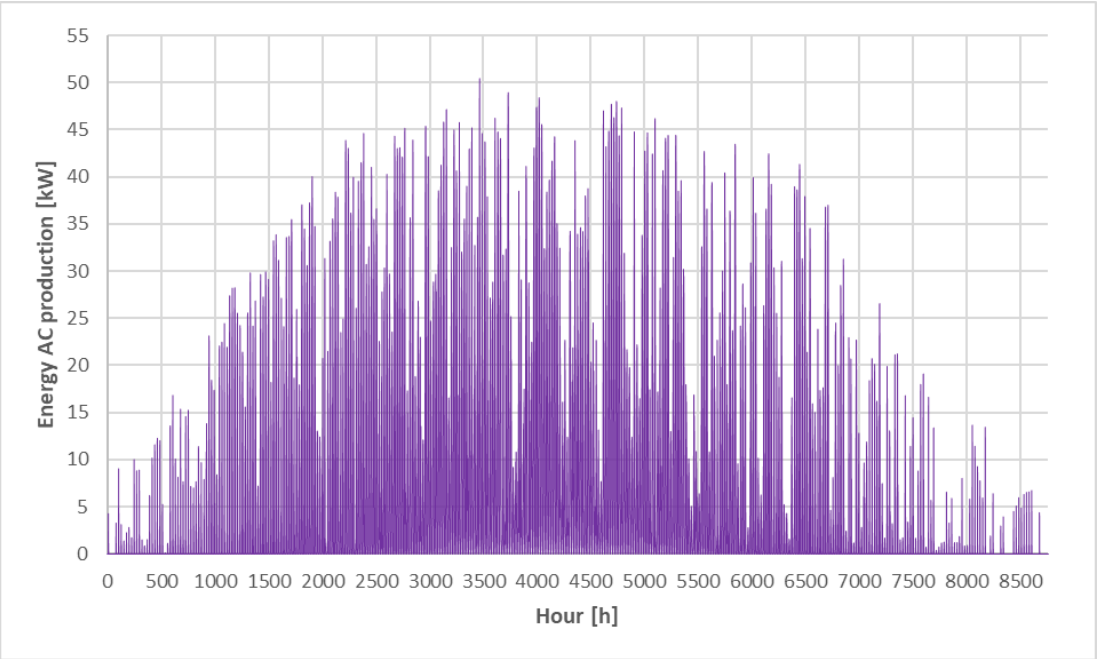

Figure 121: Hourly energy AC production for photovoltaic system 3.

Estimated monthly cost savings for the photovoltaic systems

Table 78: Monthly cost savings with photovoltaic system 1.

	Jan	Feb	Mar	Apr	May	Jun	Jul	Aug	Sept	Oct	Nov	Dec
Average electricity and grid costs [NOK/kWh]	0.990	0.979	0.949	0.951	0.665	0.621	0.638	0.660	0.643	0.867	0.896	0.857
Monthly energy yield [kWh]	395	2 259	5 211	6 959	8 116	7 951	7 758	6 255	4 618	2 480	562	188
Monthly cost savings [NOK]	391.1	2 211.6	4 945.2	6 618.0	5 397.1	4 937.6	4 949.6	4 128.3	2 969.4	2 150.2	503.6	161.1

Table 79: Monthly cost savings with photovoltaic system 2.

	Jan	Feb	Mar	Apr	May	Jun	Jul	Aug	Sept	Oct	Nov	Dec
Average electricity and grid costs [NOK/kWh]	0.990	0.979	0.949	0.951	0.665	0.621	0.638	0.660	0.643	0.867	0.896	0.857
Monthly energy yield [kWh]	403	2 271	5 221	6 965	8 126	7 962	7 772	6 270	4 630	2 495	572	192
Monthly cost savings [NOK]	399.0	2 223.3	4 954.7	6 623.7	5 403.8	4 944.4	4 958.5	4 138.2	2 977.1	2 163.2	512.5	164.5

Table 80: Monthly cost savings with photovoltaic system 3.

	Jan	Feb	Mar	Apr	May	Jun	Jul	Aug	Sept	Oct	Nov	Dec
Average electricity and grid costs [NOK/kWh]	0.990	0.979	0.949	0.951	0.665	0.621	0.638	0.660	0.643	0.867	0.896	0.857
Monthly energy yield [kWh]	402	2 305	5 318	7 103	8 283	8 114	7 917	6 383	4 713	2 530	573	191
Monthly cost savings [NOK]	398.0	2 256.6	5 046.8	6 755.0	5 508.2	5 038.8	5 051.0	4 212.8	3 030.5	2 193.5	513.4	163.7

Estimated payback time for an installation fee of 5 and 15 %

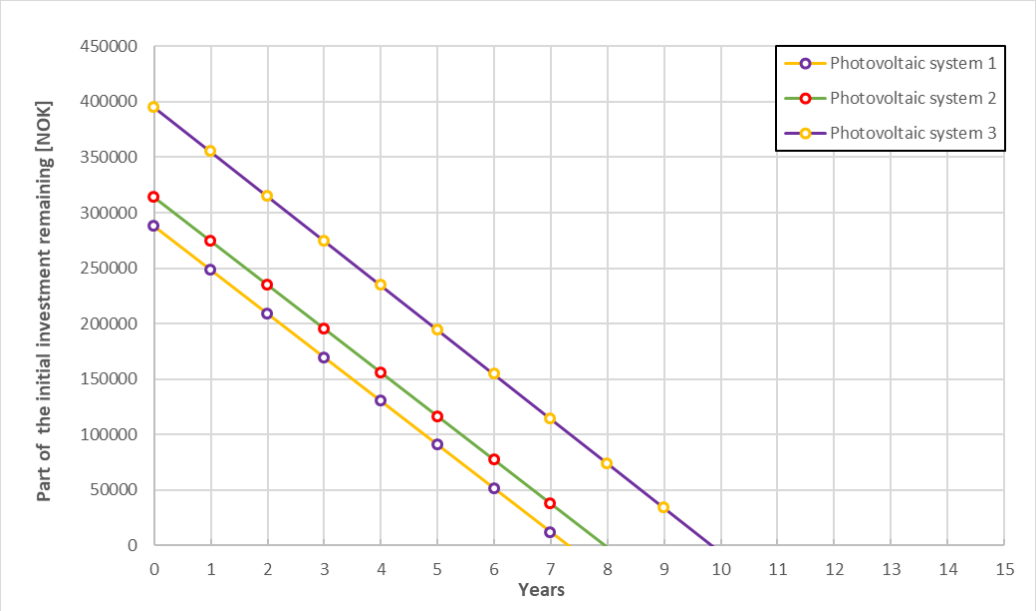

Figure 122: Payback time for photovoltaic system 1, 2 & 3 (5 % installation fee).

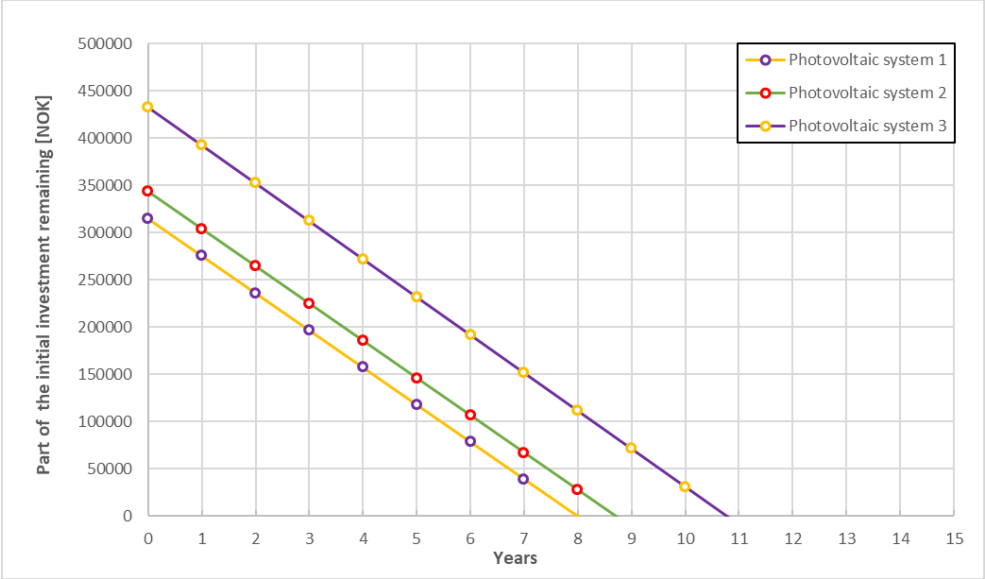

Figure 123: Payback time for photovoltaic system 1, 2 & 3 (15 % installation fee).

A.16: Tables relevant for the discussion of solar water-heating systems

Reduction of greenhouse gas emissions in Trøndelag

Table 81: Reduction in greenhouse gas emissions in Trøndelag with solar water-heating system 2.

Percentage of milk farms in Trøndelag with system solution 2	10 %	20 %	30 %	40 %	50 %
Amount of electricity consumption replaced with renewable energy [kWh]	166 950	333 900	500 850	667 800	834 750
Low emissions [Tons of CO_2 equivalents]	3.16	6.31	9.47	12.62	15.78
Moderate emissions [Tons of CO_2 equivalents]	6.71	13.42	20.13	26.85	33.56
Substantial emissions [Tons of CO_2 equivalents]	10.27	20.53	30.80	41.07	51.34
NOR-EU emissions [Tons of CO_2 equivalents]	40.60	81.20	121.80	162.40	203.00

Percentage of milk farms in Trøndelag with system solution 2	60 %	70 %	80 %	90 %	100 %
Amount of electricity consumption replaced with renewable energy [kWh]	1 001 700	1 168 650	1 335 600	1 502 550	1 669 500
Low emissions [Tons of CO_2 equivalents]	18.93	22.09	25.24	28.40	31.55
Moderate emissions [Tons of CO_2 equivalents]	40.27	46.98	53.69	60.40	67.11
Substantial emissions [Tons of CO_2 equivalents]	61.60	71.87	82.14	92.41	102.67
NOR-EU emissions [Tons of CO_2 equivalents]	243.60	284.20	324.80	365.40	406.00

Table 82: Reduction in greenhouse gas emissions in Trøndelag with solar water-heating system 3.

Percentage of milk farms in Trøndelag with system solution 3	10 %	20 %	30 %	40 %	50 %
Amount of electricity consumption replaced with renewable energy [kWh]	325 500	651 000	976 500	1 302 000	1 627 500
Low emissions [Tons of CO_2 equivalents]	6.15	12.30	18.46	24.61	30.76
Moderate emissions [Tons of CO_2 equivalents]	13.09	26.17	39.26	52.34	65.43
Substantial emissions [Tons of CO_2 equivalents]	20.02	40.04	60.05	80.07	100.09
NOR-EU emissions [Tons of CO_2 equivalents]	79.16	158.32	237.47	316.63	395.79

Percentage of milk farms in Trøndelag with system solution 3	60 %	70 %	80 %	90 %	100 %
Amount of electricity consumption replaced with renewable energy [kWh]	1 953 000	2 278 500	2 604 000	2 929 500	3 255 000
Low emissions [Tons of CO_2 equivalents]	36.91	43.06	49.22	55.37	61.52
Moderate emissions [Tons of CO_2 equivalents]	78.51	91.60	104.68	117.77	130.85
Substantial emissions [Tons of CO_2 equivalents]	120.11	140.13	160.15	180.16	200.18
NOR-EU emissions [Tons of CO_2 equivalents]	474.95	554.11	633.26	712.42	791.58

Reduction of greenhouse gas emissions in Norway

Table 83: Reduction in greenhouse gas emissions in Norway with solar water-heating system 2.

Percentage of milk farms in Norway with system solution 2	10 %	20 %	30 %	40 %	50 %
Amount of electricity consumption replaced with renewable energy [kWh]	845 880	1 691 760	2 536 640	3 383 520	4 229 400
Low emissions [Tons of CO_2 equivalents]	15.99	31.97	47.96	63.95	79.94
Moderate emissions [Tons of CO_2 equivalents]	34.00	68.01	102.01	136.02	170.02
Substantial emissions [Tons of CO_2 equivalents]	52.02	104.04	156.06	208.08	260.11
NOR-EU emissions [Tons of CO_2 equivalents]	205.71	411.42	617.13	822.83	1 028.54

Percentage of milk farms in Norway with system solution 2	60 %	70 %	80 %	90 %	100 %
Amount of electricity consumption replaced with renewable energy [kWh]	5 075 280	5 921 160	6 767 040	7 612 920	8 458 800
Low emissions [Tons of CO_2 equivalents]	95.92	111.91	127.90	143.88	159.87
Moderate emissions [Tons of CO_2 equivalents]	204.03	238.03	272.04	306.04	340.04
Substantial emissions [Tons of CO_2 equivalents]	312.13	364.15	416.17	468.19	520.22
NOR-EU emissions [Tons of CO_2 equivalents]	1 234.25	1 439.96	1 645.67	1 851.38	2 057.09

Table 84: Reduction in greenhouse gas emissions in Norway with solar water-heating system 3.

Percentage of milk farms in Norway with system solution 3	10 %	20 %	30 %	40 %	50 %
Amount of electricity consumption replaced with renewable energy [kWh]	1 649 200	3 298 400	4 947 600	6 596 800	8 246 000
Low emissions [Tons of CO_2 equivalents]	31.17	62.34	93.51	124.68	155.85
Moderate emissions [Tons of CO_2 equivalents]	66.30	132.60	198.89	265.19	331.49
Substantial emissions [Tons of CO_2 equivalents]	101.43	202.85	304.28	405.70	507.13
NOR-EU emissions [Tons of CO_2 equivalents]	401.07	802.13	1 203.20	1 604.27	2 005.34

Percentage of milk farms in Norway with system solution 3	60 %	70 %	80 %	90 %	100 %
Amount of electricity consumption replaced with renewable energy [kWh]	9 895 200	11 544 400	13 193 600	14 842 800	16 492 000
Low emissions [Tons of CO_2 equivalents]	187.02	218.19	249.36	280.53	311.70
Moderate emissions [Tons of CO_2 equivalents]	397.79	464.08	530.38	596.68	662.98
Substantial emissions [Tons of CO_2 equivalents]	608.55	709.98	811.41	912.83	1 014.26
NOR-EU emissions [Tons of CO_2 equivalents]	2 406.40	2 807.47	3 208.54	3 609.61	4 010.67

Dan Remi Antonsen

Increased solar energy utilization in Norwegian agriculture

NTNU
Norwegian University of
Science and Technology